

DETERMINISTIC AND PROBABILISTIC SIMPLE MODEL FOR SINGLE PILE
BEHAVIOR UNDER LATERAL TRUCK IMPACT

A Dissertation

by

ALIREZA MIRDAMADI

Submitted to the Office of Graduate and Professional Studies of
Texas A&M University
in partial fulfillment of the requirements for the degree of

DOCTOR OF PHILOSOPHY

Chair of Committee, Jean-Louis Briaud
Committee Members, Jose M. Roesset
J. N. Reddy
Charles Aubeny
Paolo Gardoni
Head of Department, Robin Autenrieth

August 2014

Major Subject: Civil Engineering

Copyright 2014 Alireza Mirdamadi

ABSTRACT

In this study a simple and fast method and computational code to analyze the behavior of a single post under a vehicle impact for any soil type, any vehicle mass, any truck velocity and any post size is developed. The final outcome of this research is a simple model with an estimation of each parameter. In order to contribute uncertainties in parameters and the model, a probabilistic model is also designed, and finally a fragility estimation is made by using these models. The research covers 4 main studies: Performing 13 full and medium scale tests with full investigation of soil properties by means of in-situ and lab tests, conducting 49 detailed numerical simulations with LS-DYNA with different range of parameters to build a database of results for calibrating the simple model, developing and calibrating a finite difference model for single pile subjected to impact load using dynamically modified Kelvin-Voigt model for soil behavior, modifying the simple model with Bayesian approach to build a probabilistic model and generating fragility estimates based on the probabilistic model. The outcome of the research is a probabilistic simple method to analyze a single pile under lateral impact for any soil and any geometry condition with limitation of elastic behavior of pile during the impact.

DEDICATION

To my Mom and Dad,

For their unconditional support and encouragement

ACKNOWLEDGEMENTS

I would like to thank my committee chair, Dr. Briaud, and my committee members, Dr. Roesset, Dr. Gardoni, Dr. Reddy, and Dr. Aubeny, for their guidance and support throughout the course of this research.

I would like to thank the United States Department of State, Bureau of Diplomatic Security, Physical Security Division and Sandia National Laboratories which sponsored the project and provided the support for my research studies. I also want to extend my gratitude to Dr. Dean Alberson, Mr. Gary Gerke, Mr. Dusty Arrington and other members at Texas Transportation Institute for their support and help in impact testing and in-situ soil testing.

Thanks also go to my friends and colleagues, Oswaldo Bravo, Carlos Fuentes for their help in experimental work and Armin Tabandeh, Vahid Bisadi, Maryam Mardfekri, for their help in probabilistic section. I also want to extend my gratitude to Mojdeh Asadollahi for her help in experimental part of the research and her help in proofreading the dissertation.

TABLE OF CONTENTS

	Page
ABSTRACT	ii
DEDICATION	iii
ACKNOWLEDGEMENTS	iv
TABLE OF CONTENTS	v
LIST OF FIGURES.....	viii
LIST OF TABLES	xvi
1. INTRODUCTION.....	1
2. LITERATURE REVIEW.....	3
Static behavior.....	5
Dynamic behavior	7
3. EXPERIMENTAL TESTS	15
Instruments and data analysis.....	17
String potentiometer	17
Load cell	18
Strain gauges	19
Data acquisition system.....	21
High speed camera	21
Accelerometer	22
Data analysis.....	23
Past tests	25
Soil properties	31
Soil tests	32
Loose sand.....	43
Soft clay.....	46
Hard clay	50
Very dense crushed limestone.....	54
Medium scale tests	58
Static and creep test.....	61
Constant velocity tests.....	63
Semi constant acceleration test.....	72
Full scale impact test on single post in hard clay (PU60).....	76

Static test results	78
Impact test results	80
Full scaled impact test on single post in very dense crushed limestone (M50)	88
Static test results	89
Impact test results	91
4. NUMERICAL SIMULATION	100
LS-DYNA Model	102
Materials models	102
Pile, soil and vehicle numerical models	111
Initializing	117
Hourglass	118
Simulation calibration	119
PU60 calibration	120
M50 calibration	124
Verifying simulations	127
Experimental design	127
Virtual experiment data	129
5. ANALYTICAL MODEL	131
Model theory	134
Soil material model	134
Pile-soil model	136
Model parameters	141
Output	152
Sensitivity analysis	153
Model calibration	158
PU60	161
M50	164
6. PROBABILISTIC DEMAND MODEL AND FRAGILITY ESTIMATE....	166
Probabilistic demand models	167
Prior distributions	170
Likelihood functions	171
Posterior distributions	174
Methodology for model selection	177
Rotation and load demand models	178
Rotation demand model	178
Load demand model	184
Fragility estimation	188
Capacity and demand models	189
Fragility calculation	190

7. CONCLUSION	194
Experimental tests	194
LS-DYNA Simulation.....	195
Simple analytical model	196
Probabilistic model and fragility estimate.....	196
REFERENCES	198
APPENDIX 1	208
APPENDIX 2	211
APPENDIX 3	218
APPENDIX 4	219
APPENDIX 5	220

LIST OF FIGURES

	Page
Figure 2-1: Load types schematic curve	4
Figure 2-2: Lateral Static loading test (Applied Foundation Testing 2012).	12
Figure 2-3: Limit state chart for single post (W14x106) in clay (Lim 2011).	14
Figure 3-1: String potentiometer	18
Figure 3-2: Load cell used for PU60 static test	19
Figure 3-3: Half bridge circuit	19
Figure 3-4: Installed strain gauge on the pile surface	20
Figure 3-5: Data acquisition system	21
Figure 3-6: High speed cameras	22
Figure 3-7: Accelerometer, angular rate transducer, and data acquisition on a pickup truck rear	23
Figure 3-8: Load measurement from strain	25
Figure 3-9: Plan and section of test	26
Figure 3-10: Pendulum and Bogie tests (Lim 2011)	27
Figure 3-11: Full-scale K-12 (M50) impact test on single post (Alberson et al. 2007)	29
Figure 3-12: Impact frame captured from high speed camera of K-12(M50) test (Alberson et al. 2007)	30
Figure 3-13: Acceleration and impact load based on acceleration of the truck for K-12 (M50) test at two locations (center of gravity and rear)	30
Figure 3-14: In-situ tests equipment	31
Figure 3-15: Typical preboring pressuremeter test result	33

Figure 3-16: Pencil pressuremeter equipment and the test in the field.....	35
Figure 3-17: BCD equipment and test in the field	37
Figure 3-18: DCP equipment and test in the field.....	38
Figure 3-19: PPT equipment and field test.....	39
Figure 3-20: VST equipment and field test.....	40
Figure 3-21: Triaxial set-up.....	42
Figure 3-22: Pouring sand into the test box	43
Figure 3-23: Particle-size analysis result of loose sand	44
Figure 3-24: Pressuremeter test results in loose sand	45
Figure 3-25: DCP test results in loose sand	46
Figure 3-26: Soft clay placing inside the trench box	47
Figure 3-27: Pressuremeter test result in soft clay	48
Figure 3-28: DCP test results in soft clay	49
Figure 3-29: UU test results for boring 1	51
Figure 3-30: UU test results for boring 2	51
Figure 3-31: Boring preparation for PMT in hard clay.....	53
Figure 3-32: Pressuremeter test result in hard clay.....	54
Figure 3-33: Particle size curve and sample of very dense crushed limestone (Lim 2011).....	55
Figure 3-34: Soil compaction during the post installation using a mechanical tamper.....	56
Figure 3-35: Pressuremeter test result for young and aged very dense crushed limestone	57
Figure 3-36: Pile installation in soft soil.....	60

Figure 3-37: Medium scale test plan and section (unit is meter)	60
Figure 3-38: 3D shape of excavation for medium scale test	61
Figure 3-39: Static test results in loose sand and soft clay.....	62
Figure 3-40: Creep comparison between sand and clay for different level of load ...	63
Figure 3-41: 2300 kg bogie with rigid nose	64
Figure 3-42- Medium scale test sensors location	64
Figure 3-43: Grid line on soil surface for a) loose sand and b) soft clay	65
Figure 3-44: 15 mph Bogie test in soft clay	67
Figure 3-45: Load-displacement curve for bogie tests in soft clay (load from two methods)	68
Figure 3-46: Load-displacement curve for bogie tests in loose sand (load from two methods)	69
Figure 3-47: 500 Hz Low Pass FFT filter of Soil Acceleration at 1m from the pile a) Loose sand b) Soft clay	71
Figure 3-48: Deformed soil after 15 mph bogie impact a)loose sand b)soft clay	72
Figure 3-49: Falling mass test setup.....	73
Figure 3-50: Sensor types and locations in falling mass test	73
Figure 3-51: 0.5g test in loose sand.....	74
Figure 3-52 Time-displacement for dropping mass test.....	75
Figure 3-53: Displacement-load for dropping mass test.	75
Figure 3-54: Section and plan of pickup truck impact test on single post (unit is meter)	77
Figure 3-55: Load displacement curve of static test of pile in the hard clay	79
Figure 3-56: Crack pattern and failure zone for the static test	79

Figure 3-57: Pickup truck impact test (PU60).....	81
Figure 3-58: Pickup truck and pile after the impact (PU60).....	82
Figure 3-59: Lateral displacement of impact point on post versus time in pickup truck crash test (PU60).....	82
Figure 3-60: Center of gravity (CG) and Rear acceleration of truck in x, y, and z (PU60)	84
Figure 3-61: Acceleration versus time for two points on the pickup truck (PU60) ...	85
Figure 3-62: Comparison between loads derived from acceleration and strain (PU60).....	85
Figure 3-63: Load-Displacement curve for PU60 and static tests	86
Figure 3-64: Soil surface acceleration (500 Hz FFT filtered) at 1.2m and 2.4m from the pile	87
Figure 3-65: Soil cracks and failure wedge after pickup truck impact test.....	87
Figure 3-66: Pile geometry and sensors location of M50 impact test on single post (unit is meter)	89
Figure 3-67: Load displacement curve of static test of pile in the very dense crushed limestone	90
Figure 3-68: Load rotation curve of static test of pile in the very dense crushed limestone	90
Figure 3-69: Soil deformation in static test for pile in very dense crushed limestone.....	91
Figure 3-70: Medium duty truck impact test (M50)	92
Figure 3-71: Medium duty truck and pile after the impact (M50).....	93
Figure 3-72: Lateral displacement of impact point on post versus time in medium duty truck crash test (M50)	93
Figure 3-73: Pile plastic deformation after the M50 (unit is meter)	95

Figure 3-74: Center of gravity (CG) and Rear acceleration of truck in x, y, and z (M50).....	96
Figure 3-75: Acceleration versus time for two points on the medium duty truck (M50).....	97
Figure 3-76: Comparison between loads derived from acceleration and strain (M50).....	97
Figure 3-77: Load-Displacement curve for M50 and static tests	98
Figure 3-78: Comparison of acceleration of truck in the new and old M50 tests	99
Figure 3-79: Failure wedge line on the surface in static and impact test (M50).....	99
Figure 4-1: Von Mises and Tresca yield surface comparison in 3D and 2D (Wikipedia 2014).....	104
Figure 4-2: a) 3D Drucker Prager yield surface (Potts and Zdravkovic 1999) b) Comparison of Mohr-Coulomb and Drucker Prager yield surface in 2D space (Alejano and Bobet 2012, 995-999).....	106
Figure 4-3: Soil and pile element mesh.....	113
Figure 4-4: Soil model's mesh pattern and dimension in x-y plane.....	113
Figure 4-5: Vehicle for M50 impact test and finite element model for numerical simulation.....	115
Figure 4-6: Vehicle for PU60 impact test and finite element model for numerical simulation.....	116
Figure 4-7: Geo Metro finite element model.....	117
Figure 4-8: stress in z direction for initialized soil box under gravity load	118
Figure 4-9: PU60 finite element model in LS-DYNA	120
Figure 4-10: Finite element LS-DYNA simulation versus full scale test for PU60 test	122
Figure 4-11: Pile displacement comparison between experiment and simulation ...	123

Figure 4-12: Equivalent impact load comparison between experiment and simulation	123
Figure 4-13: Load-Displacement comparison between experiment and simulation	124
Figure 4-14: M50 test numerical model	125
Figure 4-15: Shaft deformation during the impact in numerical model a) before the impact, b) after the impact	125
Figure 4-16: Broken shaft in the M50 test	126
Figure 4-17: Displacement comparison between experiment and simulation for M50 test.....	126
Figure 4-18: Load comparison between experiment and simulation for M50 test ..	127
Figure 5-1: Kelvin-Voigt and Maxwell material models	132
Figure 5-2: Material models for soil behavior under dynamic load (Deeks and Randolph 1995, 307-329).....	133
Figure 5-3: Soil model for pile-soil interaction (Randolph 2000, 3-11).....	133
Figure 5-4: Displacement result from the Maxwell and the kelvin-Voigt model and comparison with P1 test (Mirdamadi et al. 2012)	135
Figure 5-5: Acceleration result from the Maxwell and the kelvin-Voigt model and comparison with P1 test (Mirdamadi et al. 2012)	136
Figure 5-6: Pile-soil interaction model under lateral impact.....	138
Figure 5-7: Matrix form for governing equations	140
Figure 5-8: Load-displacement curve for spring element	142
Figure 5-9: Example of output result for lateral impact at impacted node	153
Figure 5-10: Sensitivity analysis center case output result	155
Figure 5-11: Sensitivity of normalized rotation results versus parameters factor....	156
Figure 5-12: Sensitivity of normalized load results versus parameters factor	156

Figure 5-13: Model sensitivity for time increment	157
Figure 5-14: Model sensitivity for number of nodes.....	158
Figure 5-15: Rotation prediction vs measured of single pile under impact	159
Figure 5-16: Dimensionless moment prediction vs measured of single pile under impact.....	160
Figure 5-17: Displacement prediction vs measured of single pile under impact	160
Figure 5-18: Equivalent impact load prediction vs measured of single pile under impact.....	161
Figure 5-19: PU60 impact displacement-time results from experiment, LS-DYNA simulation, and simple model.....	162
Figure 5-20: PU60 impact Load-time results from experiment, LS-DYNA simulation, and simple model.....	163
Figure 5-21: PU60 impact Load-displacement results from experiment, LS-DYNA simulation, simple model, and static.....	163
Figure 5-22: M50 displacement comparison between simple model and experiment.....	164
Figure 5-23: M50 load comparison between simple model and experiment	165
Figure 5-24: M50 load-displacement curve comparison between simple model and experiment	165
Figure 6-1: Stepwise deletion process for rotation demand model.....	181
Figure 6-2: Likelihood mean of σ change in stepwise deletion process	182
Figure 6-3: Comparison between measured versus predicted rotation demands: (a) deterministic model and (b) median probabilistic model.....	183
Figure 6-4: Stepwise deletion process for dimensionless moment demand model..	185
Figure 6-5: Likelihood mean of σ change in stepwise deletion process	185

Figure 6-6: Comparison between measured versus predicted dimensionless moment demands: (a) deterministic model and (b) median probabilistic model.....	187
Figure 6-7: Capacity estimation of pile under lateral impact.....	189
Figure 6-8: Fragility estimation for HSS 14×1/2 single pile with 2m embedment depth in medium clay under vehicle impact.....	192
Figure 6-9: 3D fragility surface for HSS 14×1/2 single pile with 2m embedment depth in medium clay under vehicle impact.....	192
Figure 6-10: Fragility estimate of Pickup truck impact on HSS 14×1/2 single pile with 2m embedment depth in medium clay	193

LIST OF TABLES

	Page
Table 3-1: Impact condition designations according to ASTM F2656 (ASTM Standard F2656 2007).....	16
Table 3-2: details of single pile tests (Lim 2011).....	27
Table 3-3: Soil properties of Lim’s experiments (Briaud, Lim, and Mirdamadi 2012)	28
Table 3-4: Loose sand laboratory test result	44
Table 3-5- Laboratory and in-situ tests list and results for loose sand.....	46
Table 3-6: Soft clay laboratory test results.....	47
Table 3-7: Laboratory and in-situ tests list and results for soft clay	50
Table 3-8: Pressuremeter test results in hard clay	54
Table 3-9: Lab and in-situ tests results for hard clay	54
Table 3-10: Lab and in-situ tests results for very dense crushed limestone.....	58
Table 3-11: List of medium scale tests performed.....	59
Table 3-12: Constant velocity tests on medium scale tests.....	66
Table 4-1: LS-DYNA Material card for Isotropic Elastic-Plastic with Failure (Livermore Software Technology Corporation (LSTC) 2013)..	105
Table 4-2: Variables on Isotropic Elastic-Plastic with Failure (Livermore Software Technology Corporation (LSTC) 2013).....	105
Table 4-3: Material cards for Jointed Rock model (Livermore Software Technology Corporation (LSTC) 2013).....	108
Table 4-4: Variables on Jointed Rock model (Livermore Software Technology Corporation (LSTC) 2013).....	108
Table 4-5: Material cards for Piecewise Linear Plasticity model (Livermore Software Technology Corporation (LSTC) 2013).....	110

Table 4-6: Variables in Piecewise Linear Plasticity model (Livermore Software Technology Corporation (LSTC) 2013)	111
Table 4-7: Hard clay model parameter in LS-DYNA for PU60 test.....	121
Table 4-8: PU60 experiment and simulation results comparison	121
Table 4-9: Virtual experiment parameters used in experimental design.....	128
Table 4-10: Soil strength classification and properties of each class for clay	129
Table 4-11: Soil strength classification and properties of each class for sand.....	129
Table 4-12: Virtual experiments specifications and results	130
Table 5-1: Vehicle velocity reduction factor.....	151
Table 5-2: Sensitivity analysis center case input parameters	154
Table 6-1: Posterior statistics of the parameters in the rotation demand model	183
Table 6-2: Posterior statistics of the parameters in the Dimensionless moment demand model	186

1. INTRODUCTION

Lateral loading on piles can be categorized in two types of static and dynamic. The dynamic load is also classified in transient and steady state condition. Impact load is a dynamic rapid shock load that is applied over short time period when two or more bodies collide. A number of studies have been performed on static behavior of piles under static and cyclic load (especially earthquake). Nevertheless, the studies on pile soil interaction under high strain loads are few and started recently. The cases such as piles under ship impact in offshore structure and piles under vehicles impact in transportation area are the most common cases in this category.

According to *DoD Barrier Anti-Ram Vehicle Barrier List* (U.S. Department of Defense January 2014) , most of the anti-ram barrier systems are embedded concrete footing. In some cases when the soil is strong the protective posts around the important and strategic buildings and locations can be placed in the soil. The main duty of these posts is to protect the place against intruder vehicles. The nature of loading on these structure systems is lateral impact.

The purpose of this research is to develop a simple and fast method and computational code to analyze the behavior of a single post under a vehicle impact for any soil type, as a function of vehicle mass, truck velocity and post size. The study is a part of a research project sponsored by the Department of State of the United States of America with experimental collaboration with Crashworthy Structures Program at Texas Transportation Institute at Riverside Campus.

The final outcome of this research is a simple model with an estimation of each parameter by using one of the in-situ or lab test results on soil. In order to contribute uncertainties in parameters and the model, a probabilistic model is also designed, and finally a fragility estimation is made by using these models. The simple method must be fast, easy to use, have a reasonably limited number of input parameters, be sufficiently accurate, and preferably be able to run without special software installation on the computer.

The research took 4 years to be complete and it covers 4 main studies:

- 1- Performing a series of experimental impact tests with full investigation of soil properties.
- 2- Conducting a number of numerical simulations with LS-DYNA with different range of parameters to build a database of results
- 3- Developing and calibrating an analytical simple model for single pile subjected to impact load.
- 4- Modifying the simple model with Bayesian approach to build a probabilistic model and generating fragility estimates based on the probabilistic model.

The current text contains 7 sections. The first and second sections are the introduction of the research and the review of the available literature. Sections 3 to 6 are the descriptions of the 4 above mentioned studies and the conclusions are discussed in the last section.

2. LITERATURE REVIEW

Although piles are typically designed for vertical loads and bearing capacity of structure in gravity direction, in some cases they are under lateral loads as piles in slopes or piles subjected to earthquake loads. However piles under horizontal load still have to bear the vertical loads and it is very rare that a pile or a group of piles are designed for only lateral loads. Studies on piles under vertical loads are more and earlier than studies on piles under lateral loads. The new solution and approach for analyzing piles under lateral loads back to Terzaghi's (1955, 297-326) work while the history of vertical loads is back to 1890's (Wellington and Hering 1893).

Lateral loads on piles can be categorized into two types: active and passive. The active load principally is applied on top of the pile while the passive load mainly is applied along the length of the pile as a result of soil movement. The active piles are mostly found in onshore and offshore structures (e.g. piers for ships, moorings dolphins, breasting dolphins, protecting piles against ship impact to the bridge pier, and jacket platform), transportation structures (e.g. foundation of bridge especially under approach slab, guard rails, traffic signs) and special structure (e.g. protecting posts against the intruder vehicles for important buildings, high-rise building under wind loads and wind turbines).

The existing knowledge about loading on pile, specifically lateral load on a single pile in terms of time-history, can be classified into three categories: static lateral loads, cyclic lateral loads, impact lateral loads (Figure 2-1). Static load is defined as a load that is applied during a long time without any significant change in magnitude so that the inertia effect of the resistance load is insignificant. Piles in the slopes and piles used for anchoring

offshore structures or ships are examples of static lateral loads. Cyclic load is a load with varying magnitude in a repetitive cyclic manner, either completely reversing from tension to compression or oscillating about some mean value. The pattern of load can be irregular and random. The impact load is a unidirectional sudden load with a high velocity in a short time (Babu and Sridhar 2010). The last two types of loading are related to dynamic load on piles, but with different nature of soil behavior.

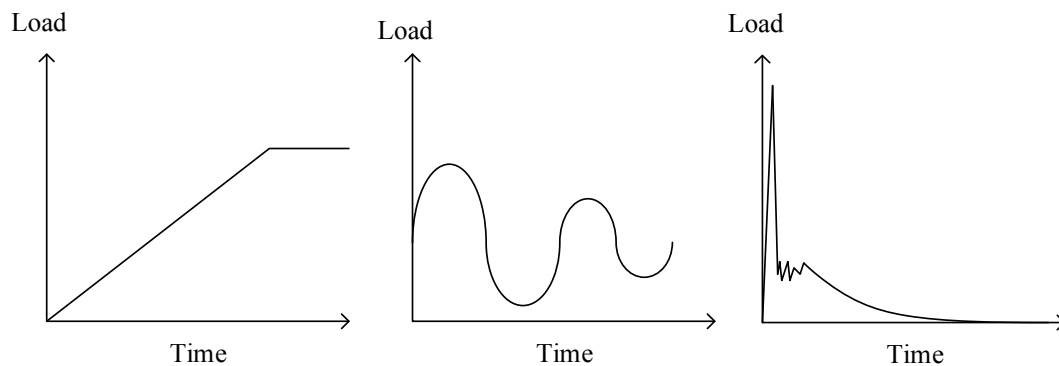


Figure 2-1: Load types schematic curve

Earthquake, wind, machine vibrations and traffic vibrations are well-known source of cyclic load containing frequency range between 100 to 0.1 Hz. While vehicle, aircraft and ship crash, explosion and extreme wind or water wave loading with the frequency range of 1000 to 0.1 Hz are the example of the impact or the impulse load (Ishihara 1996; Struck and Voggenreiter 1975, 81-87).

Static behavior

One of the well-known methods to analyze piles under lateral loads is using p-y curves. In this approach the reaction from the soil is determined from a load per unit of length versus deflection curve (p-y curve) and the problem is solved same as the ordinary equation of a beam on an elastic soil bed. Selecting a proper p-y curve is the challenging part of this method and many researches have been performed to estimate them. Other methods such as upper bound, lower bound, Characteristics Load Method (CLM) and recently 3D numerical (finite element, finite difference and discrete element) methods are also used for estimating the static capacity of a single pile under lateral load. The experimental test method to measure the lateral deflection of vertical or inclined deep foundations under lateral loading is described in ASTM D3966 (ASTM Standard D3966 2007(2013)).

The first attempt for modeling a single pile under lateral load was made by Terzaghi (1955, 297-326) suggesting values called subgrade modulus in order to solve the pile model for deflection and bending moment. The model was an elastic pile and elastic soil and has a limitation of one-half of soil bearing capacity. Poulos and his colleagues (Poulos and Davis 1980; Poulos and Hull 1989, 1578-1606) also developed different solutions with different models but with elastic behavior. The solutions have been in attention, but cannot be used for large deformation when soil behaves nonlinearly.

Broms (1964a, 27-63; 1964b, 123-156; 1965, 77-99) employed a very simple model for soil pressure on pile for a rigid pile in order to estimate the load to develop the ultimate bending moment. After defining the ultimate load, Brom derived the deflection of the pile

by assuming elastic behavior for the soil. The method is too simple to give accurate results, but it can be used for initial estimation of pile size and also check the computational methods.

Briaud (1997, 958-964) developed a simple method for lateral capacity of single piles and prediction of deflection under working loads by using pressuremeter results. Elastic behavior was assumed for the pile material and an elastic perfectly plastic model was used for the soil. In this study single piles are categorized in two types: infinitely long and rigidly short. This method has limitations for mid-length piles and linear interpolation was suggested for this case. The simple elastic perfectly plastic model for soil may cause some inaccuracy in the deflection. This approach has been developed with different assumption. For example Guo (2008, 676-697) and Motta (2012, 501-506) used nonlinear elastoplastic analysis for rigid shaft for three different cases based on plastic location of soil.

Most attempts are based on p-y curves, and providing the curve is the key parameter for all of them. Duncan et al. (1994, 1018-1033) presented the Characteristics Load Method (CLM) by implementing nonlinear behavior of soil for both sand and clay. The method outputs are 1) displacement of the ground level of pile due to lateral load and/or moment applied at the ground line for different head conditions, 2) magnitude and location of maximum moment on the pile. The method assumed uniform strength of soil in depth. Also, the CLM method is only applicable for long enough piles (minimum length should be between 6 diameters of pile for hard soil and 14 diameters of pile for soft soil).

A limit state analysis was done by Randolph and Houlsby (1984, 613-623) and modified by (Martin and Randolph 2006, 141-145) to estimate the limiting pressure on

circular pile under purely horizontal movement. Both upper and lower bound techniques with assumptions of classic plasticity theory for soil and rigidity of pile were used in this study. Different methods with different assumption have been studied since 1950's. Matlock (1970, 77-94), Poulos (1971, 711), Randolph (1981, 247-259), Evans & Duncan (1982), Reese (1984), Murff (1993, 91-107) are examples of studies that have been done on single piles subjected to lateral static load.

In the last two decades, computer programs have been developed for solving differential equations and describing the behavior of a single pile efficiently and in a use friendly fashion (Reese and Van Impe 2001). The principal advantage of using a computer program is modifying the p-y curve by using 3D models and more advanced soil models. The computer codes also can perform complicated upper bound and lower bound solutions with more detail and relative ease. Since the problem is neither plane strain nor plan stress, a 3D model is required. The necessity of using computer software may be seen in analyzing groups of piles and also for dynamic loading of piles.

Dynamic behavior

The concept of beam on elastic foundation and the elastic half-space theory were used in an approximate approach to analyze a single pile under low-amplitude surface lateral periodic vibrations (sinusoidal load). The dynamic soil response was assumed to be linear and an elastic beam with only bending stiffness was used for the pile model. The soil parameters in this study originated from vertical vibration of foundation on an elastic half-space by Reissner (1936, 381-396) which was the first attempt to solve the vertical

vibration of a massive circular base on the surface of an elastic medium. The study showed that all damping which results in energy dissipation in the elastic half-space is considered to be geometric damping. Material damping in the studied problem is insignificant. (Ghazzaly, Hwong, and O'neil 1976, 363-368)

Several approximate analytical approaches and numerical finite element analyses were done by Novak (1974, 574-598), Dobry R, et al. (1982, 439-459), Gazetas and Dobry (1984a, 20-40) to present a simplified procedure method for single piles under vibration (earthquake or machine sources) with different assumptions. In these studies stiffness and damping factor of pile were estimated and presented as a function of: soil density, shear wave velocity in the soil over, size of the pile (length and radius), soil stiffness and load frequency. Recently Taciroglu, Rha, & Wallace (2006, 1304-1314) presented a robust macro-element model for pile under cyclic loads. The model incorporates frictional forces and formation of gaps at the soil–pile interface as well as hysteretic behavior of the soil.

Boulanger W. R. et al. (1999, 750-759) at University of California Davis applied nine different earthquake motions on a single pile and a pile group supported structure modeled in a centrifuge to investigate the dynamic p-y behavior under earthquake loading. A nonlinear p-y element was developed that can model a range of desired p-y behaviors and was implemented into a finite-element program for this study. The origin of p-y curve for Bay Mud is based on Matlock's (1970, 77-94) recommendations and for sand is American Petroleum Institute (API 2007) recommendation.(Boulanger et al. 1999, 750-759) Both of these recommendations use basic soil parameters e.g. friction angle that are not sufficient to describe the p-y curve properties. In this study radiation damping was

modeled by a dashpot in the p-y element based on the recommendation of Gazetas and Dobry (1984b, 937-956). The method overestimates the peak superstructure motions on average by about 5-10%.

A pioneer study on piles under vertical impact was done by Smith (1960, 35-61). He developed a simple solution for pile-driving analysis by using the wave equation and a simple model for the soil in order to estimate the pile drivability, the pile stresses, and the pile capacity. In his method, soil resistance against impact movement is characterized as a contribution of static and damping resistance. This idea has been extensively used to estimate pile static capacity for pile driving procedure in the field. ASTM D4945 provides the procedure for applying an axial impact force with pile driving hammer or a large dropping weight (ASTM Standard D4945 2012). Statnamic load testing, a type of rapid load test, was developed by Berminghammer Foundation Equipment and The Netherlands Organization (TNO) in 1988. Statnamic Load Testing is a recognized test method by the American Society for Testing and Materials designation number ASTM D7383 (ASTM Standard D7383 2010). The Statnamic device is usually composed of a reaction mass, a piston, and a connection to the test foundation including load cells. When fuel in the piston is ignited, expanding gasses push the reaction mass away from the foundation and apply an equal and opposite thrust on the foundation (Brown 2007, 54-62).

The ranges of the Smith soil quake (static resistance) and damping from the published data were so widely scattered that it was very difficult to select reasonable values for wave equation analysis. The wave equation analysis was explored and evaluated by McVay and Kuo (1999). A set of semi-empirical equations for estimating the Smith soil parameters

were developed from the University of Florida pile database and based on classical soil properties. A total number of six theoretical (Lysmer and Richart 1966; Novak, Nogami, and Aboulella 1978, 953-959; Lee et al. 1988, 306-325; Mitwally and Novak 1988; Nguyen, Berggren, and Hansbo 1988; Liang and Sheng 1992, 111-116) and four in-situ test (Svinkin and Abe 1992, 175-182; Abou-matar et al. 1996, 163-175; Malkawi and Khalid 1996, 37-54; Paikowsky and Chernauskas 1996, 203-216) correction expressions for damping coefficient of pile tip were investigated in this study. The theoretical expression showed that the damping is mainly a function of static soil stiffness and resistance, soil density, and size of the pile; moreover, in the experimental expressions soil inertia, soil stiffness and size of the pile are the important factors. (McVay and Kuo 1999)

The current design codes for lateral impact load on structures use a simplified procedure to estimate the equivalent static load on structures due to impact. For example AASHTO 2012 provides an equation (Equation 2-1) for ship collision impact force on a pier. This equation is developed from a research by Woisin (1976, 465) and the results agreed with other research performed by International Association of Bridge and Structural Engineering (IABSE 1983).

Equation 2-1

$$P_s = 1.2 \times 10^5 V \sqrt{M}$$

where:

P_s = equivalent static vessel impact force (N)

V = vessel impact velocity (m/sec)

M = deadweight of vessel (Mg)

Although the equation is calibrated against some experimental results, the units of two sides are not compatible. The procedure is too simple and does not consider the structural behavior of both vessel and pier, while the transfer load is a function of many factors as follows (AASHTO 2012):

- Structural shape and type of the ship's bow
- Water force effects during the collision
- Size and velocity of the ship
- Collision angle and geometry
- Geometry and stiffness of pier or barrier

More studies were also done on vessel impact on piles especially on bridge substructure (McVay et al. 2009, 7-16) and fixed offshore structures (Sterndorff, Waegter, and Eilersen 1992, 149-153; Poepsel and Dowd 1995, 1227-1238) . McVay and his colleagues (2009, 7-16) performed a set of in-situ investigation, site stratigraphy, field monitoring, data reduction, and subsequent time-domain analysis of soil–structure interaction from a full scale vessel impact loading of a bridge pier at the St. George Island Causeway. The impact simulation was done with a finite element program (FB-Multipier). The software is capable of modeling a single pier or the whole bridge under linear or nonlinear static or dynamic considerations. The soil damping factor was derived from viscous dashpot parameter introduced by Smith (1960, 35-61). Although the ship impact is the most common case in the offshore collision, iceberg impact loads occur on offshore structure especially in cold weather zones. Dewoolkar at al. (2008, 1615-1626) investigated static stability against sliding of large skirted gravity structure using PLAXIS

3D validated against centrifuge test results. The load type in this study was not impact and it was applied with a slow rate (more than 2:30 min duration). A series of centrifuge model tests were carried out to study the bearing behavior of long flexible piles subjected to horizontal impact loads by Grundhoff (1997, 753-760).

For the first time in order to simulate a ship impact in the field, a lateral Statnamic testing was performed in 1998 to by the Mississippi DOT and Brown (1998, 28-30; 1999, 309-318) developed a simple method of interpretation of lateral Statnamic loading. The test method has been widely used specially by DOTs to estimate the lateral capacity of the single pile and pile group. Figure 2-2 shows a lateral Statnamic test setup.



Figure 2-2: Lateral Statnamic loading test (Applied Foundation Testing 2012).

A large scale modeling and simplified theoretical investigation were done by Zhu and his colleagues (2012) for flexible piles subjected to lateral impact. They carried out a large

static load test and three impact tests on a single pile in a silty soil. A dynamic p-y curve model with nonlinear static stiffness and constant damping factor was recommended to analyze single pile under lateral impact. They found the damping and inertia part of the soil model affect the load displacement more than the static parameter while this contribution is lower for the generated bending moment in the pile. The study shows that the amplitude of dynamic response is governed by impact energy (Zhu et al. 2012a, 86-96; Zhu et al. 2012b, 461-471). There is a little literature on piles under lateral dynamic impact. For example, Kitiyodom et al (2006, 690-699; 2007) performed some experimental tests and numerical analyses on single piles for an abutment of a highway bridge. In the dynamic horizontal load test, the pile was hit horizontally by a hammer with mass of 2140 kg and a load cell on pile measured the load. The maximum displacement of the pile was 20 mm and peak velocity was about 0.7 m/s which is lower than the magnitude that was measured in the real crash incident.

The interaction of gravel and the roadside guardrail system post was investigated through experiments and computer simulations by Wu and Thomson (2007, 883-898). A quasi-static and dynamic test series were designed and carried out and a parametric study was subsequently conducted to investigate the influence of the gravel stiffness on the soil-post interaction through computer simulations using LS-DYNA. The input parameters for the soil and concrete material model were recommended for roadside gravel in the crash analyses.

Lim (2011) at Texas A&M University developed a set of design recommendations to select the embedment of a single post or group of posts under impact of a 6800 kg truck

with three level of velocity (50 km/h, 65 km/h, and 80 km/h). The design guidelines are based on 12 medium scale impact tests with a pendulum or a bogie, 1 full scale impact test on a single post, 1 full scale impact test on a group of 8 side by side posts with a 5.2 m spacing and connected with two beams as the experimental tests. Approximately 150 3D numerical simulations of full scale impact tests using LS-DYNA, as well as fundamental theoretical concepts were also used in the design guideline. The experimental full scale tests in this study were based on “Standard Test Method for Vehicle Crash Testing of Perimeter Barriers” (ASTM Standard F2656 2007). A set of design recommendations was developed to select the embedment depth of a single post or group of posts. The design charts are only for limited types of piles and soil conditions; therefore a solution for more general cases is required. A design chart sample for single post in clay is shown in Figure 2-3.

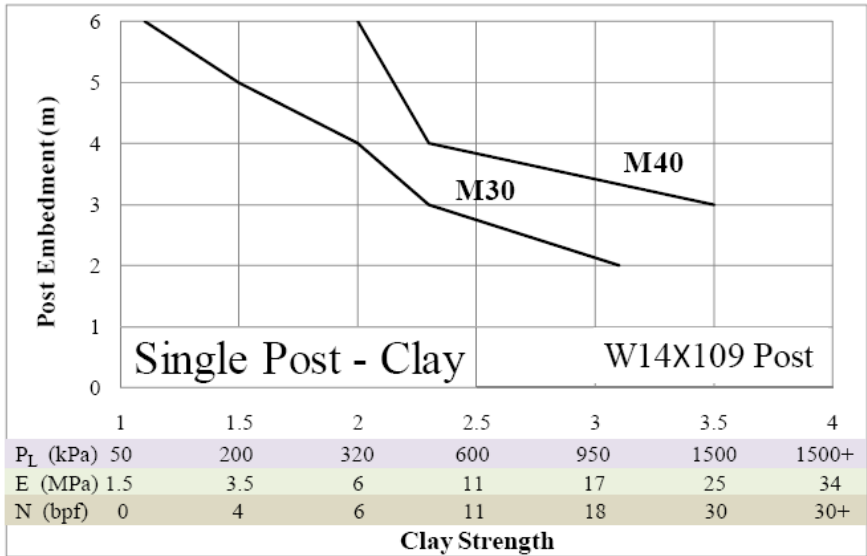


Figure 2-3: Limit state chart for single post (W14x106) in clay (Lim 2011).

3. EXPERIMENTAL TESTS

For the purpose of numerical simulation and analytical model calibration an extensive series of crash experiments including soil tests in the field and the lab were designed for this study. The experiments are classified in two types: medium and full scale tests on a single pile. A total of 13 medium scale tests with different conditions i.e. constant velocity and constant acceleration and 2 full scale tests with two truck sizes were conducted. All the experiments were performed at the Texas Transportation Institute (TTI) at the Riverside campus of Texas A&M University.

Medium scale tests were designed to investigate the soil behavior under controlled conditions of loading, soil properties, and impact conditions. A bogie with a rigid nose for the constant velocity condition and a dropping mass for the constant acceleration applied the lateral load to single piles in soft clay and loose sand. Full scale impact test with different truck sizes were performed according to ASTM F2656. Acceleration of the striking object (bogie, mass or truck) and strain on the pile in addition to high speed frame rate movie were captured in all the tests. Static lateral loading tests were conducted for each soil type to obtain the static behavior of the pile under lateral loading and the soil properties were measured with set of in-situ and lab tests.

ASTM F2656 “Standard Test Method for Vehicle Crash Testing of Perimeter Barriers” provides a range of vehicle impact conditions, designations, and penetration performance levels. Based on the standard, vehicle types are categorized in 4 major vehicles [small passenger car (C), Pickup truck (P), Medium-duty truck (M) and Heavy duty truck (H)] and each vehicle type has three specified levels of velocity. Table 3-1 lists

the impact condition designations according to ASTM F2656 and in this study PU60 and M50 are selected for full scale tests.

Table 3-1: Impact condition designations according to ASTM F2656 (ASTM Standard F2656 2007)

Test Vehicle/Minimum Test Inertial Vehicle	Mass, kg (lbm)	Nominal Minimum Test Velocity, km/h (mph)	Permissible Speed Range, km/h (mph)	Kinetic Energy, KJ (ft-kips)	Condition Designation
Small passenger car (C)	1100 (2430)	65 (40)	60.1-75.0 (38.0-46.9)	179 (131)	C40
		80 (50)	75.1-90.0 (47.0-56.9)	271 (205)	C50
		100 (60)	90.1- above (57.0-above)	424 (295)	C60
Pickup truck (P)	2300 (5070)	65 (40)	60.1-75.0 (38.0-46.9)	375 (273)	PU40
		80 (50)	75.1-90.0 (47.0-56.9)	568 (426)	PU50
		100 (60)	90.1- above (57.0-above)	887 (613)	PU60
Medium-duty truck (M)	6800 (15000)	50 (30)	45.0-60.0 (28.0-37.9)	656 (451)	M30
		65 (40)	60.1-75.0 (38.0-46.9)	1110 (802)	M40
		80 (50)	75.1-above (47.0-above)	1680 (1250)	M50
Heavy goods vehicle (H)	29500 (65000)	50 (30)	45.0-60.0 (28.0-37.9)	2850 (1950)	H30
		65 (40)	60.1-75.0 (38.0-46.9)	4810 (3470)	H40
		80 (50)	75.1-above (47.0-above)	7280 (5430)	H50

Lim (2011) also performed some medium scale and a full scale tests on single post and the results are used in this study to calibrate the simple proposed model. In this section

the instrument and data analysis of the experiments, Lim's experiments, soil in-situ and lab tests, static lateral loading, and impact tests are described.

Instruments and data analysis

In order to measure the test results data totally 6 types of sensors were used in the experimental tests. The quantities of displacement, load (or bending moment), and acceleration in static and dynamic tests are the desirable measurements. The explanation and specifications of each sensor are discussed in the following.

String potentiometer

Displacement of single pile at the point of load application (impact point location for dynamic tests) in static tests was measured by a string potentiometer model P510-50-004 with 50" range of measurement. String potentiometer is a device that measures linear position using a flexible cable and spring-loaded spool. String potentiometers are composed of four main parts: a measuring cable, spool, spring, and rotational sensor. The resolution of the string-pot is essentially infinite and sensing device is precision potentiometer. Figure 3-1 shows the string potentiometer used in this study. The string was attached to the pile with a magnet.

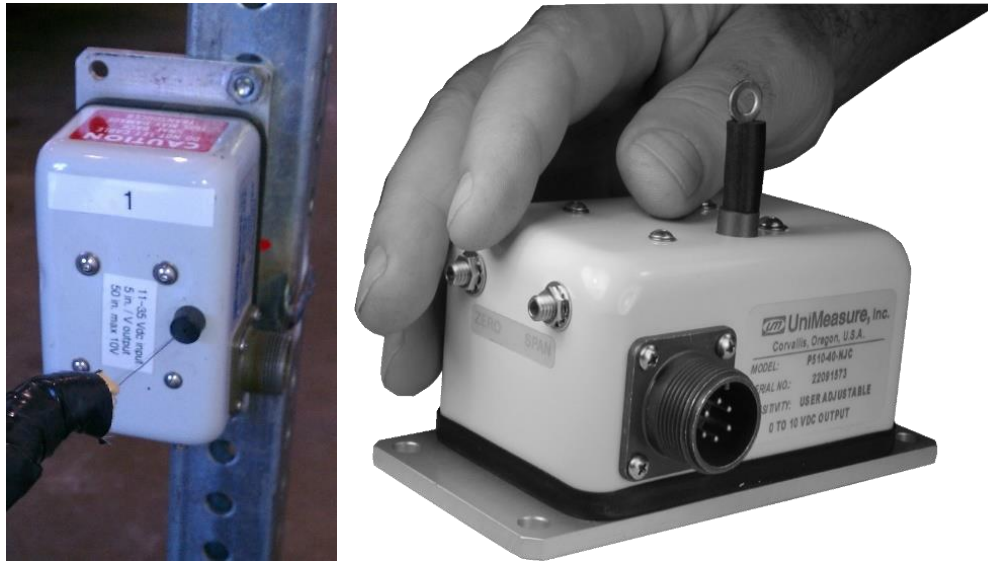


Figure 3-1: String potentiometer

Load cell

A load cell is a transducer that is used to convert a force into an electrical signal. This conversion is indirect and happens in two stages. Through a mechanical arrangement, the force being sensed deforms a strain gauge. The strain gauge measures the deformation (strain) as an electrical signal. A Honeywell model 41 load cell was used in the static test load measurement. Model 41 is a low profile “pancake” type load cells. This model is a bonded foil, strain gage load cell that is engineered to measure loads from 5 lb to 50,000 lb (22 N to 222 kN). The load cell is double diaphragm design with infinite resolution and accuracy of 0.1%. Figure 3-2 shows the load cell used in PU60 static test.



Figure 3-2: Load cell used for PU60 static test

Strain gauges

Two weldable strain gauges are installed on the pile to measure bending moment on the pile during the application of the horizontal loading (static or impact). Half bridge circuit containing two strain gauges were used in this study (Figure 3-3).

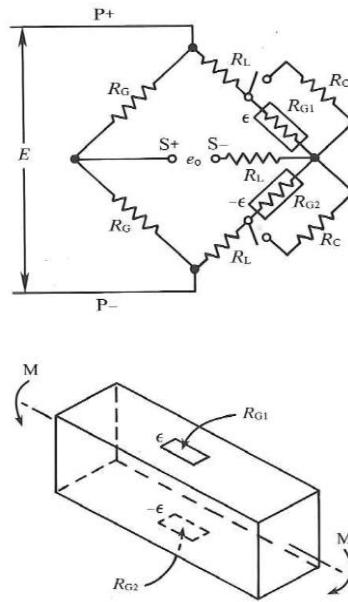


Figure 3-3: Half bridge circuit

As shown in Figure 3-4 the pile surface was smoothed in the positions where gauges need to be welded. A rotating machine with sandpaper was used for this purpose. The strain gauges were welded with a micro welding method.

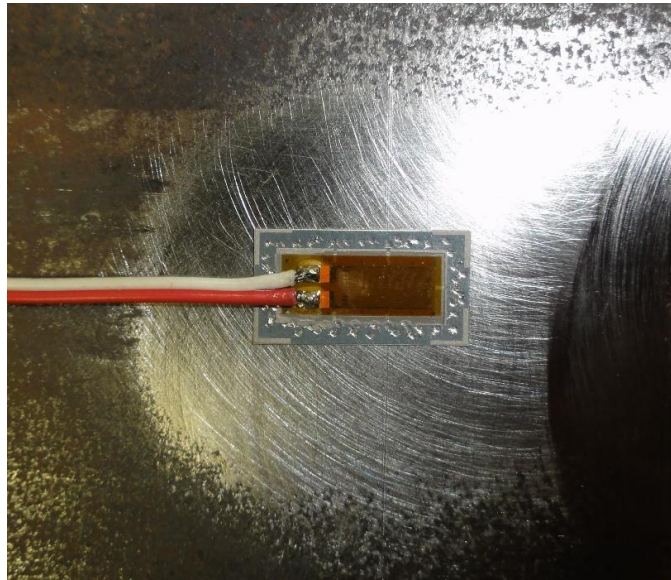


Figure 3-4: Installed strain gauge on the pile surface

A self-temperature compensation strain gauge (STC 06) from Micro-Measurements Company is chosen for this study. This type of strain gauge can compensate the temperature effects on the results. In order to connect the sensors to the data logger a 2120B Vishay model amplifier amplifies the signal and transfers it to data acquisition system.

Data acquisition system

DaqBook/2020 an Ethernet-Based, 16-Bit, 200 kHz data acquisition system collected data from sensors. The data logger has 16 differential voltage inputs and 14 single-ended analog inputs. Figure 3-5 displays the data logger system used in static and dynamic experimental tests.



Figure 3-5: Data acquisition system

High speed camera

In the impact tests the displacement were measured by tracking the reference markers on the pile using 1000 fps high speed cameras which means that time interval for displacement is 1 msec. The velocity of impactor is also measured with the same high speed cameras. The accuracy of displacement is a function of distance between the cameras and the reference target on the pile and also the resolution of the frames, however

the worst accuracy was about 1cm. the cameras took the frames from 3 spots for full scale tests (side, top and front), and 2 spots for medium scale tests (side and top). The side camera has high definition (HD) frame quality. The displacement is only obtained from side scene of the impact direction. Two models of cameras used in this study are shown in Figure 3-6.



Figure 3-6: High speed cameras

Accelerometer

Vehicles in this study are instrumented by triaxial accelerometers near the vehicle center of gravity (C.G.) and on the rear of the vehicle (Figure 3-7) to measure the three longitudinal, lateral and vertical, directions accelerations. The accelerometers are ENDEVCO Model 2262CA with a $\pm 100g$ range and 10000 sample per second. The raw

longitude acceleration is corrected for pitch rotation measured by a solid-state angular rate transducer.



Figure 3-7: Accelerometer, angular rate transducer, and data acquisition on a pickup truck rear

Data analysis

The main outputs of all the experimental tests are displacement and applied load at impact point. The displacement of the pile was determined by using a high speed camera and analyzing the movie frame by frame against a fixed target reference in the impact tests and output from the string pot in the static tests. In order to measure the load two options are available:

- 1- Multiplication of acceleration and mass of the impactor (Newton's second law: $F=m.a$) assuming the mass concentrated at the center of gravity. In order to remove the noise from the acceleration results a 50 msec average smoothing and a low-pass filter (2000 Hz) were performed on the raw acceleration records.

2- Division of bending moment on pile over the moment arm (Figure 3-8) assuming insignificance of dynamic load due to top section of pile acceleration.

Both methods have some advantages and disadvantages:

- Load from acceleration is the direct load measurement while load from strain is calculated indirectly so it contains inaccuracies
- Because of wave propagation through the impactor object, the captured acceleration on the object cannot be assumed as the lumped-mass acceleration while the strain on the pile is the original reaction of the pile and it can directly be used for pile designing
- Assumption of neglecting dynamic load from top of the pile for strain method works when the ratio of impactor mass to mass of pile is significant

For the calibration since the load prediction in numerical and analytical methods are corresponded to the strain method the impact load from the experiment has also derived from this method.

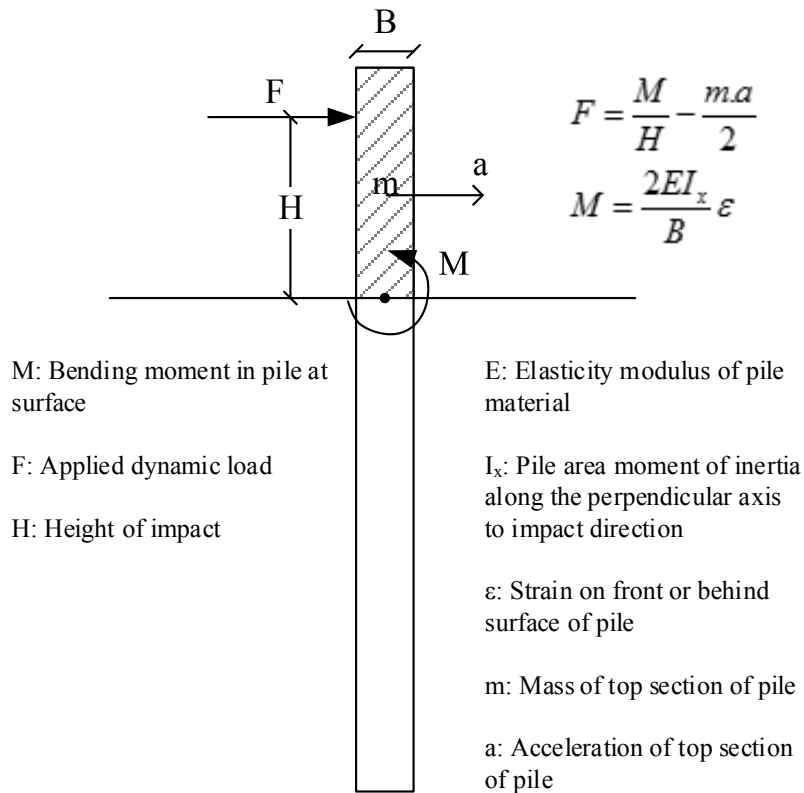


Figure 3-8: Load measurement from strain

Past tests

In a previous project (Lim 2011), eight medium scale impact tests on single pile were performed with a pendulum or a bogie. Three types of soil (loose sand, dense crushed limestone and hard clay) were prepared in a pit which was 3m by 1.5m by 1.8m deep (Figure 3-9). In these scaled tests, a rigid mass struck the pile with a specific velocity. The mass was a pendulum for the crush limestone and the sand, and a bogie for the clay. In all tests, the pile was a single 152mm×152mm×9.5mm box section embedded 1m below the ground surface.

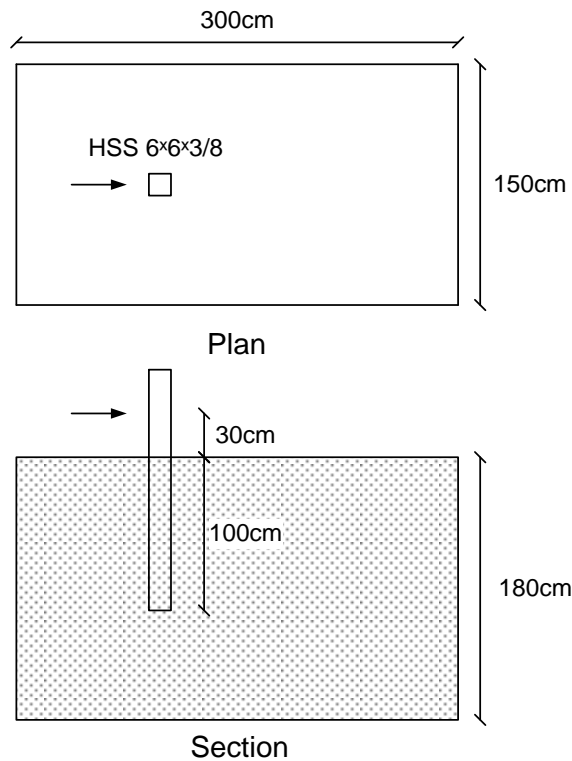


Figure 3-9: Plan and section of test

The pile was installed by either driving or backfilling, the range of velocities was between 2.5 m/s and 10 m/s and the range of masses was between 250kg and 900kg. The list of tests is presented in Table 3-2. For each test, the acceleration of the mass was measured by an accelerometer placed on the pendulum or on the bogie. A photo of tests P3 and B1 is shown in Figure 3-10. The measured properties of each soil included pressuremeter data and Standard Penetration Tests (SPT) data as in situ tests, and sieve analysis, water content, unit weight and direct shear data as laboratory tests. In addition, a series of static horizontal load tests were performed. The soil properties in this study are presented in Table 3-3. The results are presented and used for analytical simple model calibration.

Table 3-2: details of single pile tests (Lim 2011)

Test	Soil	Striking mass	Velocity (m/s)	Mass (kg)	Post installation	Kinetic energy of mass at impact (kJ)
P1	Medium Crushed limestone	Pendulum	4.65	862	Backfilled	9.3
P2	Medium Crushed limestone	Pendulum	2.41	862	Backfilled	2.5
P3	Medium Crushed limestone	Pendulum	9.97	862	Backfilled	42.8
P4	Loose Sand	Pendulum	4.94	249	Driven	3.0
P5	Loose Sand	Pendulum	2.5	249	Driven	0.8
P6	Loose Sand	Pendulum	10.1	249	Driven	12.7
P10	Loose Sand	Pendulum	9.83	249	Backfilled	12.0
B1	Clay	Bogie	4.56	903	Driven	9.4



Figure 3-10: Pendulum and Bogie tests (Lim 2011)

Table 3-3: Soil properties of Lim's experiments (Briaud, Lim, and Mirdamadi 2012)

Soil type	P _L (kPa)	E (kPa)	SPT (N) (blow/ft)	USCS	Water Content (%)	Unit weight (kN/m ³)	Compressive Strength (qu) (kPa)	Hand Vane (Su) (kPa)	Pocket Penetrometer (qu) (kPa)
very dense crushed limestone	2250	25000	>50	SP-SM	3	24	-	-	-
medium dense crushed limestone	710	5975	9.5	GM	1	23.1	-	-	-
loose sand	220	1800	1	SP	4.5	17	-	-	-
hard clay	800	13000	11	CL	17	21	360	107	402.5

In Lim's study in accordance with designation SD-STD-02.01, Revision A (2003) a full-scale impact test on a single pile in a very dense crushed limestone was performed. The test vehicle and the single pile are shown in Figure 3-11. The impact condition designation was K-12 that is identical to the impact condition designation M50 in ASTM F 2656-07. The objective of this test is to arrest a 6,800 kg vehicle travelling at 80 km/h with less than one meter of dynamic penetration.



Figure 3-11: Full-scale K-12(M50) impact test on single post (Alberson et al. 2007)

The pile was a wide flange I beam W14×109 (14 inches wide and weighing 109 lbs/ft of length) with an embedment of 3m. The truck was a 1998 Navi-Star 4700 single-unit flatbed truck. Two accelerometers were installed on the flatbed of the vehicle at the center of mass of the vehicle and near the rear axle. Two accelerometers were also placed in the back of the pile and in the soil behind the pile to measure the accelerations of the post and of the soil during the impact. (Briaud, Lim, and Mirdamadi 2012)

As it is shown in Figure 3-12, during the impact front of the truck covered the post therefore displacement could not be captured by the film analysis and acceleration of the vehicle at two spots were the only data results from the impact (Figure 3-13). The maximum impact force in this test was 1350 kN and the permanent pile leaning was 8 degree away from the impact. Unfortunately there is no static test result for this pile.



Figure 3-12: Impact frame captured from high speed camera of K-12(M50) test (Alberson et al. 2007)

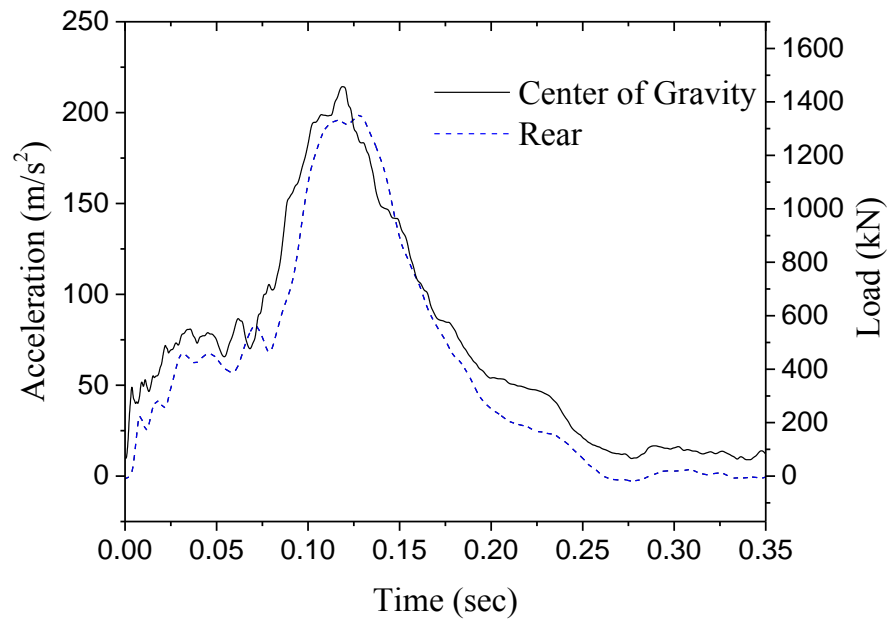


Figure 3-13: Acceleration and impact load based on acceleration of the truck for K-12 (M50) test at two locations (center of gravity and rear) (Lim 2011)

Soil properties

The soil properties investigation were done on four types of soil: loose sand, soft clay, hard clay, and very dense crushed limestone. The loose sand and the soft clay were used for medium scale (bogie and dropping mass) tests and they were placed in the trench box. Hard clay and very dense crushed limestone are a natural layer in the field and were used for PU60 and M50 tests, respectively. In order to find the soil properties, we performed more than ten different types of in-situ and lab tests. Figure 3-14 shows all the equipment used for in-situ tests except SPT. In this section soil testing in the field and lab and results of them for each type of soil will be discussed.

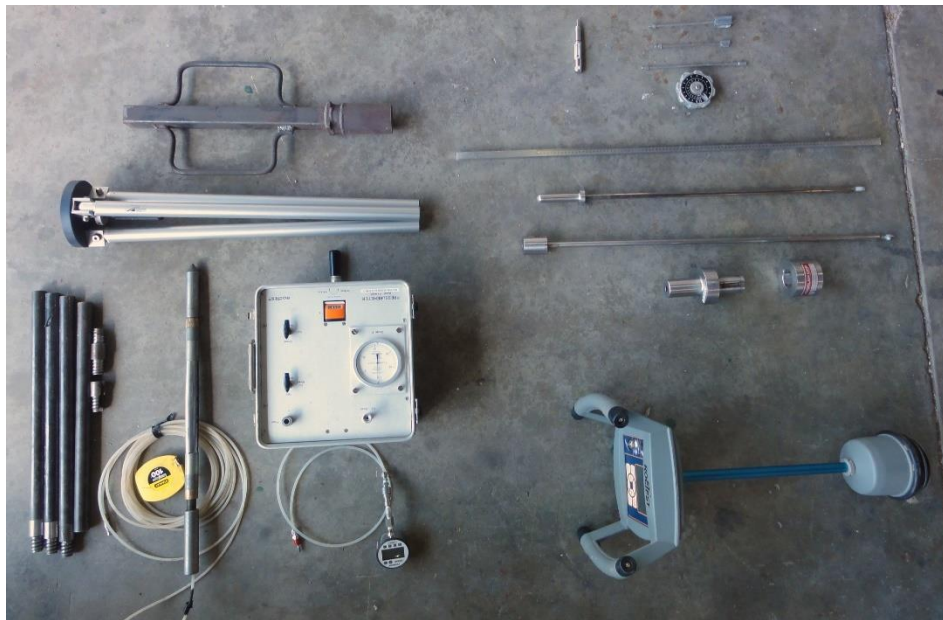


Figure 3-14: In-situ tests equipment

Soil tests

Pressuremeter Test (PMT)

The Pressuremeter Test (PMT) basically consists of placing an inflatable cylindrical probe in a predrilled hole and expanding this probe while measuring the changes in volume and pressure in the probe (ASTM Standard D4719 2007). The main in-situ test that analytical simple model is based on is PMT. The advantages of the PMT lies in its capability to be performed in most soils and rocks. Another advantage is that it represents an in situ load test in itself since different loading sequences can be duplicated such as long pressure steps for load term loading, rapid inflation for impact loading and unload reload cycles for cyclic loading. From the design aspect it is ideal for laterally loaded piles since it presents a response of the soil to the lateral loading of the membrane and hence it presents the best tool for predicting the response of this type of piles (Briaud 1992).

There are three types of pressuremeters: the preboring pressuremeter (PBPM), the self-boring pressuremeter (SBPM), and the push-in or cone pressuremeter (CPM) (Briaud 2013). The most common PMT is the preboring pressuremeter and the most commonly recommended method for preparing the borehole is the wet rotary method with bottom discharge of prepared mud (ASTM Standard D4719 2007).

4 main types of PBPM are on the market and the differences are in number of cells, pressure source, and length of the cell. The Menard pressuremeter from Bonne Esperance, the LLT (Lateral Load Test) of Oyo, the Texam from Rocrest, and the Tri-Mod from Rocrest are the examples of these four major PBPM. In the PBPM the most important part is preparation of the borehole such that disturbance of the walls of the borehole should

be slightly larger than the probe. If D_1 , D_2 , and D_3 are the drilling, deflated probe, and borehole diameter, respectively the following relationship is recommended: (Briaud 1992)

$$D_2 < D_1 < 1.03D_2$$

$$1.03D_2 < D_3 < 1.2D_2$$

A typical result from PBPMT is shown in Figure 3-15. From A to B the probe is contacting the borehole wall, from B to C the soil behaves linear, and beyond C the soil is progressively yielding (Briaud 1992). The limit pressure can be estimate by extrapolating the curve to the desirable strain in the problem.

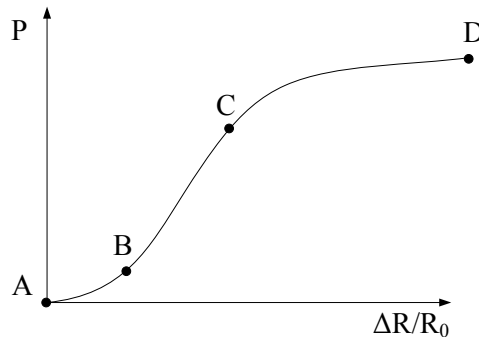


Figure 3-15: Typical preboring pressuremeter test result

There are essentially three types of SBPMT on the market. The cutting mechanism and used fluid to apply pressure are the main differences for these types. The PAF76 from the Laboratoire des Ponts et Chaussées, the Camkometer from Cambridge In Situ, and the Texam unit called the Boremac are such self-boring pressuremeter (Briaud 1992). The

SBPMT is usually the most expensive pressuremeter test method, but because the borehole is prepared fitly the result has more range of strain.

Cone pressuremeter or push-in pressuremeter test developed by implementing the idea of using cone head for probe. In CPMT the cone penetrometer test (CPT) results are recorded during the penetration and pressuremeter test results are recorded when the probe stops. The obtained curve can be similar to Figure 3-15 when the cone point diameter is larger than pressuremeter portion or similar to part B to D of same figure when the contrary is true.(Briaud 1992)

In this study a Pencil pressuremeter (Roctest), a small size of pressuremeter developed for pavement, is used for PMT in the field. The probe diameter is smaller than usual pressuremeter (33 mm) with membrane diameter of 1 inch (25.4 mm) and length of inflatable part is about 250mm. The maximum working pressure of the instrument is 2500 kPa and pressure is applied with water. The pressuremeter can be used as both pre-bored hole (for hard and stiff soils) and pushed (for soft and loose soils) down to 3m depth. The entire system fits in a small suitcase. Figure 3-16 shows the Pencil pressuremeter equipment and field setup.

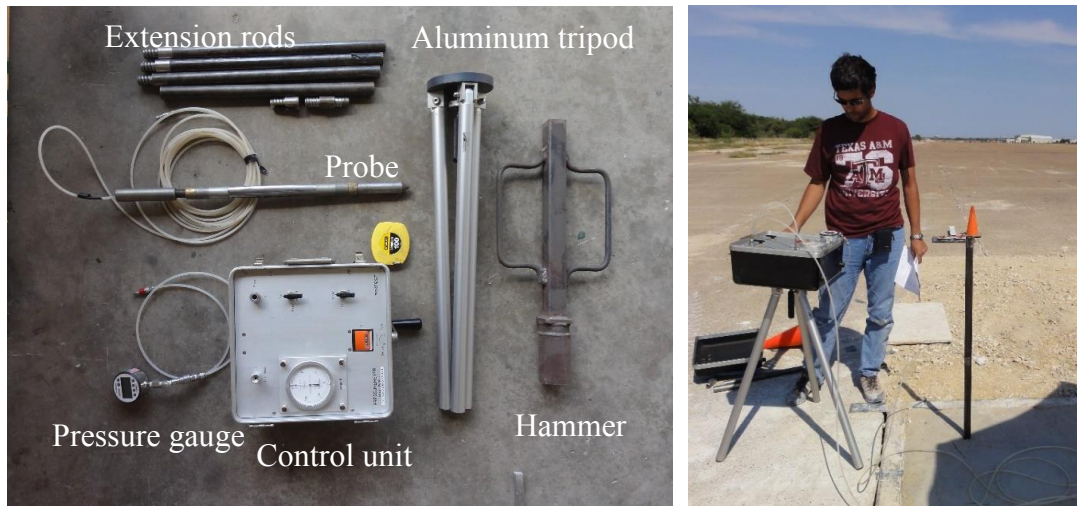


Figure 3-16: Pencil pressuremeter equipment and the test in the field

In order to correct the equipment effect on the results, two types of system compressibility calibration and membrane resistance calibration must be done before each series of tests. In system compressibility calibration (volume calibration), probe is inserted into a steel tube with the same diameter and volumes corresponding to specific pressure amounts are taken. In membrane resistance calibration (pressure calibration) the corresponding pressures to specific volumes are taken while the probe is vertical and without any confinement. The corrected volume and pressure from these volume and pressure calibration will be subtracted from the test reading, respectively.

The PMT yields at the limit pressure (p_L), the pressure against the soil such that the pressuremeter probe reaches a volume corresponding to a cavity volume equal to twice the initial volume (this value may vary for different applications). The pressuremeter modulus E is calculated by using the slope of the elastic portion of Figure 3-15 (B-C):

$$E = (1 + \nu)(p_C - p_B) \frac{\left(1 + \left(\frac{\Delta R}{R_0}\right)_C\right)^2 + \left(1 + \left(\frac{\Delta R}{R_0}\right)_B\right)^2}{\left(1 + \left(\frac{\Delta R}{R_0}\right)_C\right)^2 - \left(1 + \left(\frac{\Delta R}{R_0}\right)_B\right)^2}$$

ν : poisson's ratio (default value is 0.35)

Briaud Compaction Device (BCD)

The Briaud Compaction Device (Figure 3-17) is a device to obtain the soil modulus E . The potential for the BCD is in the field of soil compaction including that for highway subgrade, compaction of embankments and for compaction of backfills for retaining walls. The concept of test is based on measuring strain on a plate applying pressure on the soil surface. The modulus obtained with BCD corresponds to a reload modulus at an average mean stress level about 50 kPa, at an average strain level 10^{-3} , and an average loading time of 2 sec (Briaud 2013), therefore the modulus is higher than the E obtained from PMT.



Figure 3-17: BCD equipment and test in the field

Dynamic Cone Penetrometer (DCP) (ASTM Standard D6951)

The dynamic cone penetrometer (Figure 3-18) is a device to determine the stiffness of the material and is generally used for pavement applications. It consists of estimating the penetration depth of an 8 or 4.6 kg mass dropped a certain height driving a 60° cone tip with 20mm base diameter vertical into the soil and is commonly used to estimate strength properties such as the California Bearing Ratio (CBR). Other important relationships that can be obtained from this test include the relative density of the material (D_r), modulus of Elasticity (E), shear modulus (G) and the effective friction angle of the soil (ϕ').

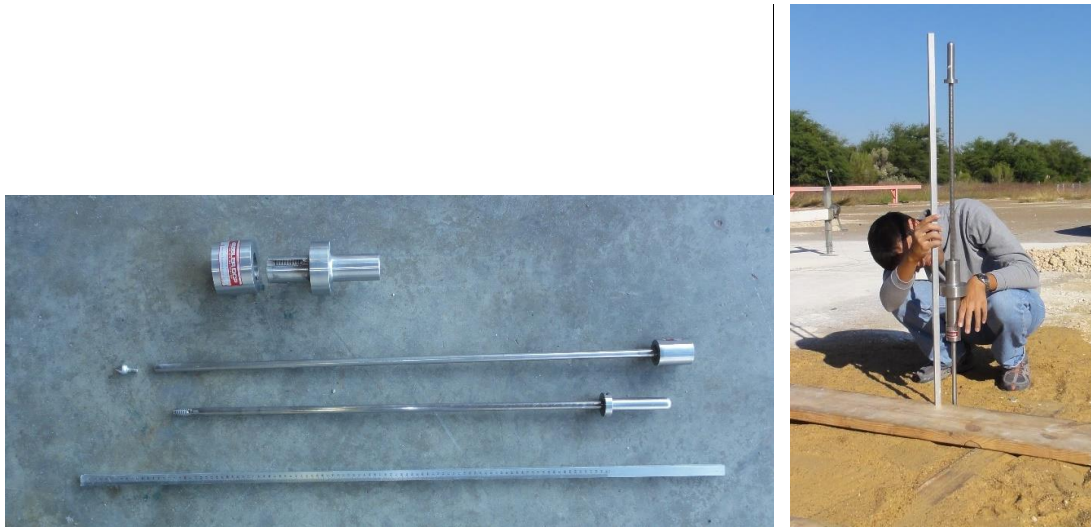


Figure 3-18: DCP equipment and test in the field

Mohammadi et al. (2008, 195-203) have presented several correlations between the Dynamic Cone Penetration (DCP) index and several parameters for sandy soils including the relative density of the sand (D_r):

$$D_r (\%) = 189.93 / (\text{DCP})^{0.53} \quad (R^2 = 0.98)$$

To obtain the modulus of the soil they suggested the following relationship from correlations from the plate load test (PLT):

$$E_{\text{PLT}} (\text{MPa}) = 53.73 / (\text{DCP})^{0.74} \quad (R^2 = 0.94)$$

While the shear modulus of the sand is approximated by:

$$G_{\text{PLT}} (\text{MPa}) = 75.74 / (\text{DCP})^{0.99} \quad (R^2 = 0.93)$$

Finally, the effective friction angle of the soil can be approximated by:

$$\phi' (^\circ) = 52.16 / (\text{DCP})^{0.13} \quad (R^2 = 0.90)$$

Pocket Penetrometer Test (PPT)

The Pocket Penetrometer (Figure 3-19) is a simple test can be performed on clay sample in the field or in the lab. The PPT consist of pushing by hand the end of a spring-loaded 6.35 mm diameter cylinder until failure of the soil. The PP gauge number is from 0 to 4.5 tsf and undrained shear strength S_u (kPa) roughly equal to 30 PP, considering that the correlation is very scatter and mass of soil tested is extremely small (Briaud 2013). The test is very fast and handy but the result must not be used in design.

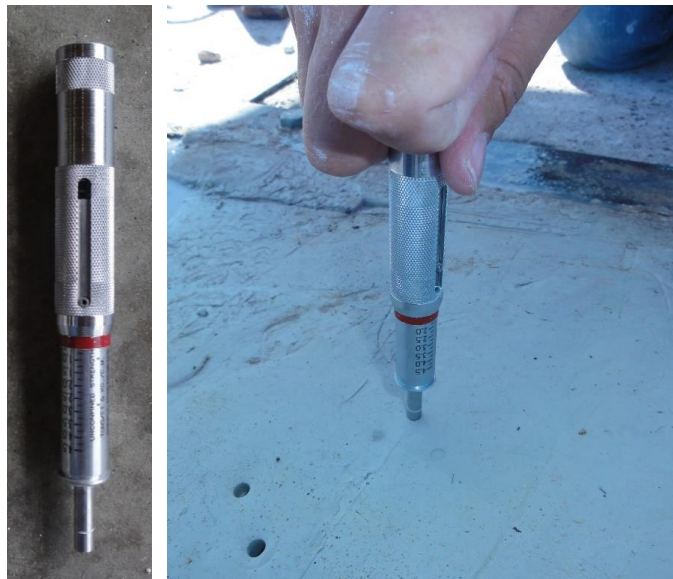


Figure 3-19: PPT equipment and field test

Vane Shear Test (VST) (ASTM Standard D4648)

The Vane Shear Test is used to determine the undrained shear strength of clays and silts. There are two types of field and mini (hand) vane available. It is made of two perpendicular blades connected to a torque gauge (Figure 3-20). The size of field vane

blades vary from 38 to 92 and 10 to 20 for mini vanes. The test consist of pushing the blades into the soil at rotating at a slow rate while measuring the torque and measuring angle. The undrained shear strength can be calculated from max measured torque from:

$$s_u = \frac{T_{\max}}{\pi D^2 \left(\frac{H}{2} + \frac{D}{6} \right)}$$

where D is the blade width, H is the blades height, and T_{\max} is maximum torque.

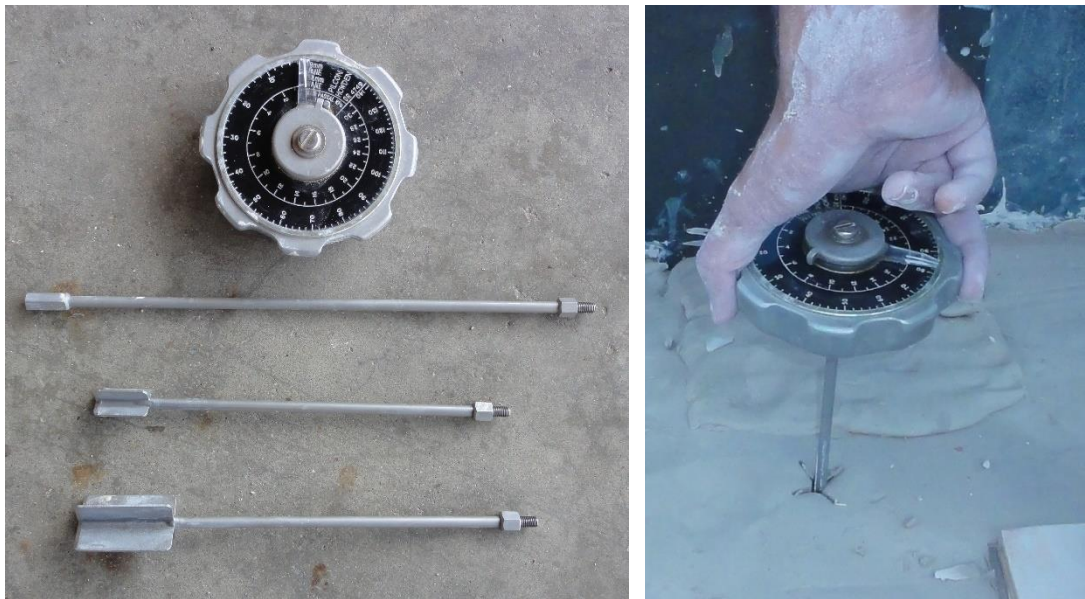


Figure 3-20: VST equipment and field test

Standard Penetration Test (SPT) (ASTM Standard D1586)

The standard Penetration Test is one of the oldest and the most well-known in situ test. The SPT consist of driving a split spoon sampler into the soil using standard 623N hammer falling from 0.76 m and counting the number of blows necessary to drive the split spoon

sampler for each 0.15 m into soil for total drive of 0.45 m. N_{SPT} is reported the sum of blows number for last two 0.15 m drive and this value is often corrected to account for influencing factors such as energy level, rod length, stress level.

The test can be done in both coarse and fine grained soil but in the United States it is not used with clays and silts because better option, taking sample, is available for them. However, some other countries, like Brazil, extend use of the SPT to silt and clay (Briaud 2013). In this study Terracon Inc. performed the SPT in the field.

Direct Shear Test (DST) (ASTM Standard D3080)

The Direct Shear Test is a simple lab test used to obtain the shear strength of a soil. The DST consist of shearing a disk soil sample placed in a steel cylinder split horizontally at mid height while a vertical load is applied on top of the sample. During the shearing process, the shear force, horizontal, and vertical displacement are measured. For the dry samples the friction angle (ϕ) is obtained directly from the shear strength envelope slope.

Unconfined Compression Test (UC) (ASTM Standard D2166)

The Unconfined Compression test is one of the simplest tests for the soil sample can stand up under its own weight. In this test a vertical load is applied to a cylinder sample with the ratio height/diameter about 2 without confinement. The vertical load and displacement are measured during the test and undrained shear strength s_u determined from the failure q_u ($s_u=q_u/2$).

Unconsolidated Undrained Triaxial Test (UU) (ASTM Standard D2850)

The triaxial test with Unconsolidated Undrained condition is similar to UC test except that a chosen confining pressure is applied to the sample during the test. Figure 3-21 shows the triaxial set-up used for this study.

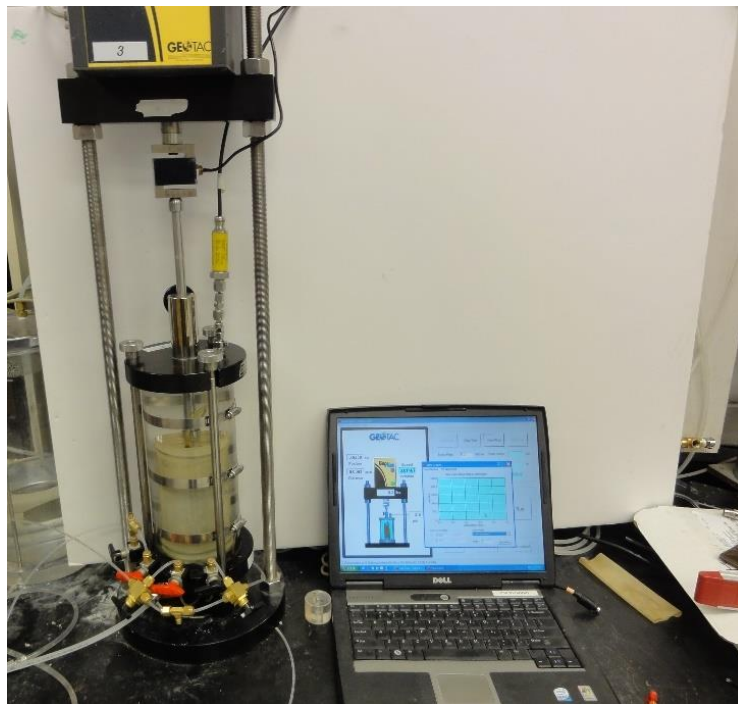


Figure 3-21: Triaxial set-up

Loose sand

A uniformed and homogenous sand was selected for the loose sand material. The sand was placed without compaction and just poured into a designed box (Figure 3-22) to having a loose behavior in the material. The soil was classified as well graded sand (SW) according to Unified Soil Classification System (USCS) based on particle-size analysis (Figure 3-23). To measure the friction angle of sand, series of direct shear tests were performed as per ASTM D3080 (2004) “*Standard test method for direct Shear test of soils under consolidated drained conditions*”. The laboratory tests results on sand are shown in Table 3-4.



Figure 3-22: Pouring sand into the test box

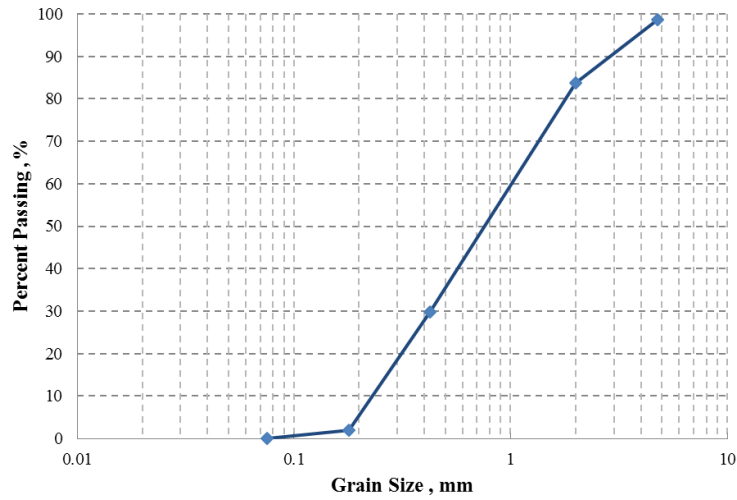


Figure 3-23: Particle-size analysis result of loose sand

Table 3-4: Loose sand laboratory test result

Parameter	Value
γ_d (kN/m ³)	17.4
G_s	2.64
e	0.49
Water content (%)	0.5
USCS Soil Classification	SW
C_u	7.5
C_c	1.2
Value of Fines (%)	<1
Friction angle (critical state)	34°

Two PMTs in different depths (0.6m and 0.8m) were conducted in the loose sand. Since the soil was so loose, probe was pushed into the soil with a hammer, as a result an initial pressure at zero volume was generated. The results of pressuremeter tests are presented in Figure 3-24. The pile in this soil has 1m embedment depth therefore for the purpose of analysis, pressuremeter results associated to 0.6m depth are selected as an average. The $p_L=70$ kPa and $E=600$ kPa are chosen for future analysis.

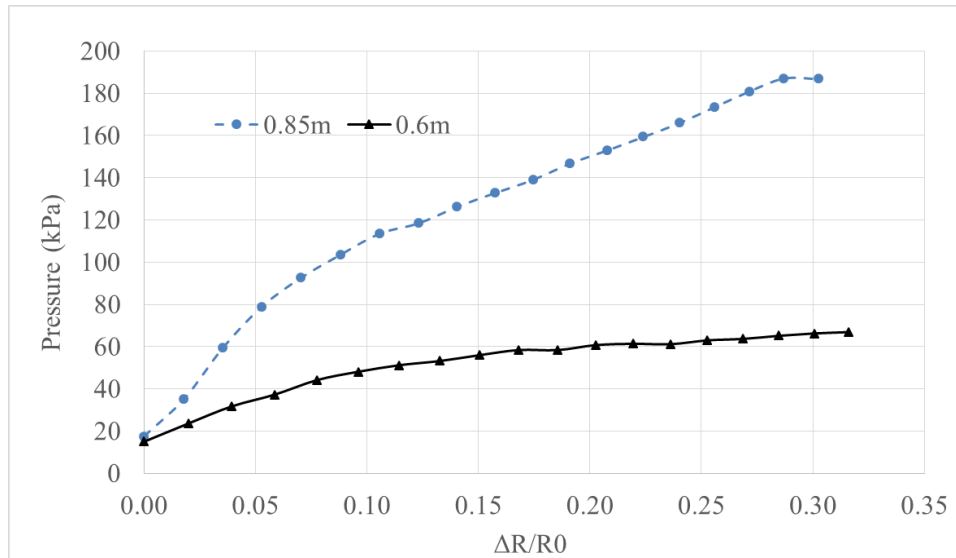


Figure 3-24: Pressuremeter test results in loose sand

A total number of 3 DCP tests were conducted in the loose sand with the 4.6 kg weight. Figure 3-25 displays the DCP index results in the soil. From the correlations presented by Mohammadi et al. (2008, 195-203) the average relative density of the sand is about 40%. The measurement of effective friction angle of the sand is consistent with that of the DST ($\approx 34^\circ$). Modulus values obtained from this test (5 MPa) should only be considered as a first estimates due to the nature of the test. Table 3-5 presents the lab and in-situ test's results for the loose sand.

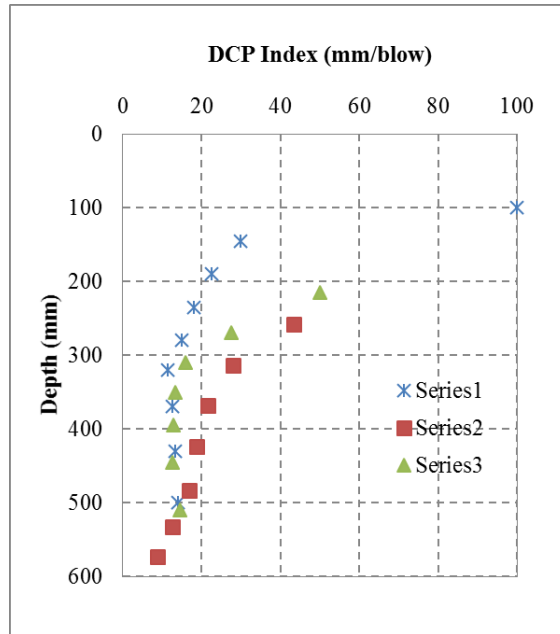


Figure 3-25: DCP test results in loose sand

Table 3-5- Laboratory and in-situ tests list and results for loose sand

Test		Result
In-situ	PMT	$p_L=70$ kPa, $E=700$ kPa
	BCD	$E=13.7$ MPa
	DCP	20 mm/blow ($\phi=35$, $E=5$ MPa, $D_r=40\%$)
Lab	Grain Size Analysis	SW
	Unit weight	17.4 kN/m ³
	Direct Shear Test	$\phi=34$

Soft clay

The clay used for this project was grayish clay denominated *porcelain clay* prepared for pottery industry and the manufacturing of the clay in vacuum takes most of the air voids out and thus the saturation of the clay is close to 100%. The soft clay came in 11 kg (25 lb), 0.15×0.15×0.22 m blocks and were placed inside the designed trench box and lightly compacted for each layer (Figure 3-26). The construction of the clay pit took two

days and to keep soil saturated a plastic blanket covered the surface. During the soil placement, material quality controlled by mini vane test.



Figure 3-26: Soft clay placing inside the trench box

A set of classical laboratory tests (Atterberg limits, Hydrometer analysis, Water content) according to ASTM were done on soft clay and the results are presented in the Table 3-6.

Table 3-6: Soft clay laboratory test results

Parameter	Value
γ_d (kN/m ³)	19
USCS Soil Classification	CL
Water Content (%)	24.5
LL	34
PL	19
PI	15
S_u (kPa)	24
D_{50} (mm)	0.013

Totally 3 Unconfined Compressive Strength tests and 3 Unconsolidated Undrained Triaxial Tests (10, 15 and 22 kPa confinement) were done on the soft clay. The results were compatible and undrained shear strength obtain from them was 24 kPa.

Two successful PMTs at the depth of 0.6m in different locations were performed in the clay trench box. Because of softness of clay, similar to loose sand the probe was driven by a hammer. The second test was done with unload-reload process to determine the E_R for the material. According to the test outcome: $E = 0.4$ MPa, $E_R = 1.8$ MPa and $p_L = 80$ kPa. Figure 3-27 present the PMT pressure vs $\Delta R/R_0$ curve in the soft clay.

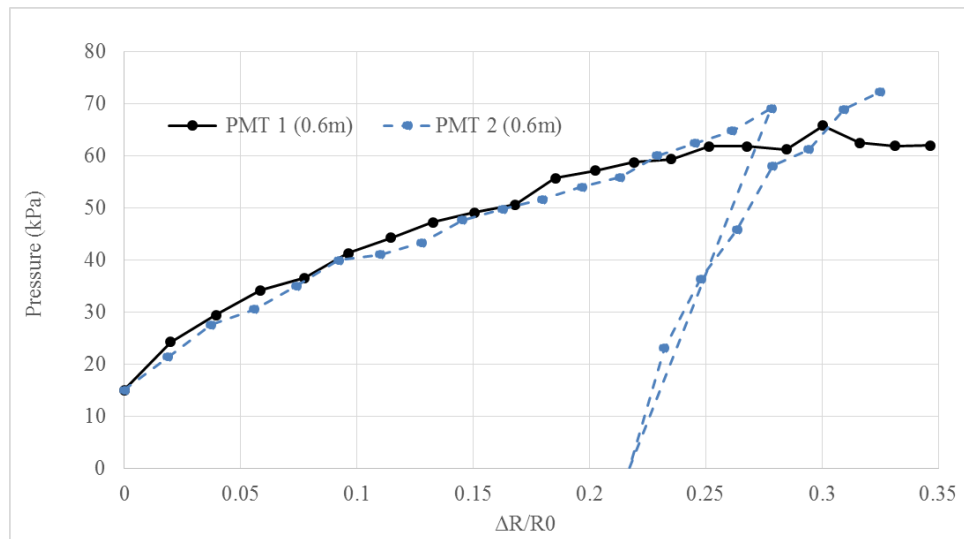


Figure 3-27: Pressuremeter test result in soft clay

A series of 22 vane shear tests were performed to determine the undrained shear strength of the soft clay at different locations and test time periods. Due to the soft nature of the clay the pocket penetrometer punctured through the clay and no clear reading was

determined from this testing device. Thus the results obtained from this test are dismissed. The BCD test was attempted at the clay site but the material was too soft and the BCD could not give an appropriate modulus since it cannot be used for E values below 3 MPa. The dynamic cone penetrometer with a mass of 4.6 kg was used at 2 locations and in both test the cone penetrate due to its weight down to 500mm so the results were taken from that depth. The plot of the DCP index vs. depth is presented in Figure 3-28. Table 3-7 presents the lab and in-situ test's results for the loose sand.

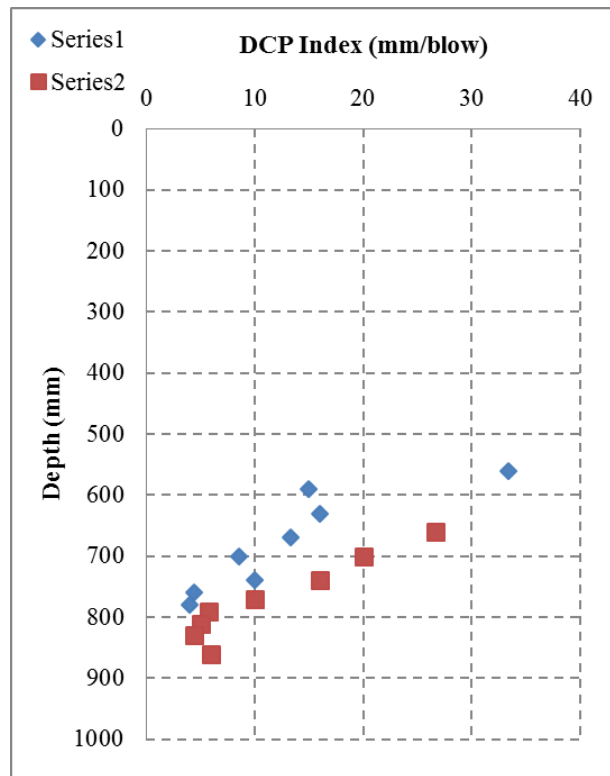


Figure 3-28: DCP test results in soft clay

Table 3-7: Laboratory and in-situ tests list and results for soft clay

Test		Result
In-situ	PMT	PL=80 kPa, E=400 kPa
	BCD	<instrument range
	DCP	15 mm/blow
	Pocket Penetrometer	<0.5 tsf
	Vane Shear Test	19 kPa
Lab	Grain Size Analysis	CL
	Unit weight	19 kN/m ³
	UU Triaxial Test	24.5 kPa
	UC	48 kPa

Hard clay

The hard clay is a dark grey sandy lean clay naturally located at TTI Riverside campus. The soil layer is about 2m deep and homogenous. Three borings were drilled and 13 Shelby tube soil samples were recovered from two borings down to 2.5m depth. The strength of all the samples was more than 4.5 tsf in the pocket penetrometer and soil was classified as CL. A total of 9 successful UU tests were conducted on samples. The deviator stress vs axial strain for two borings are presented in Figure 3-29 and Figure 3-30.

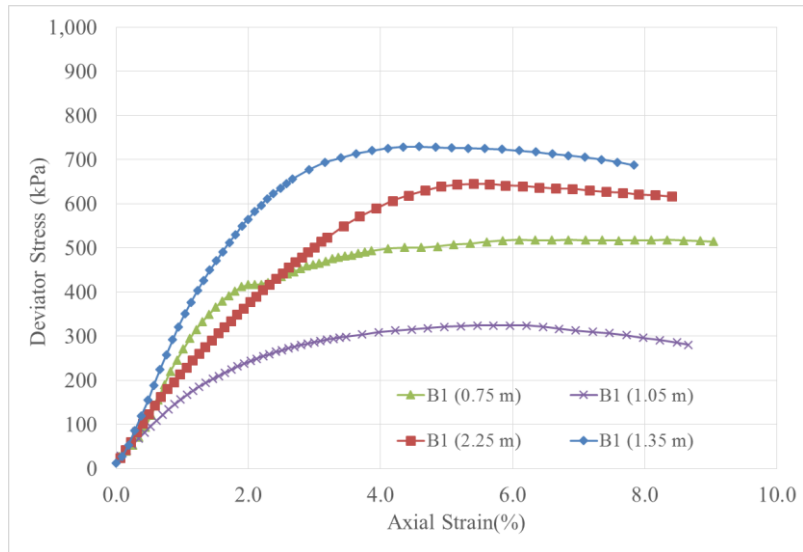


Figure 3-29: UU test results for boring 1

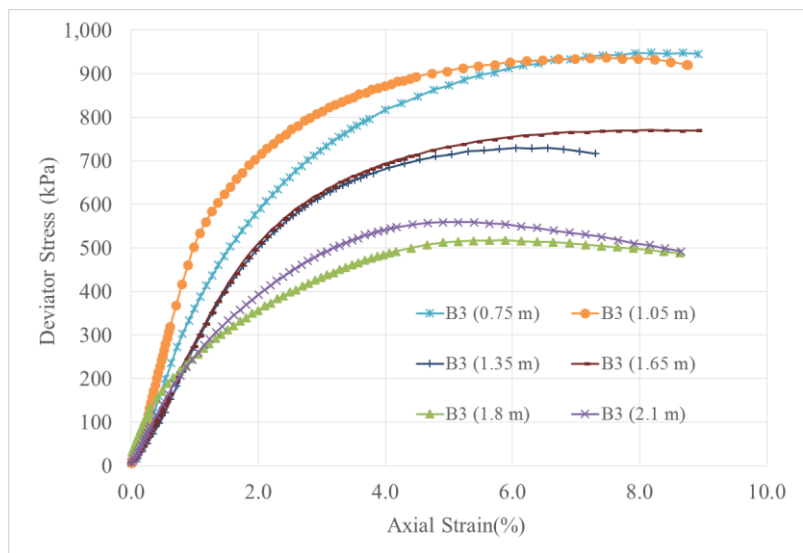


Figure 3-30: UU test results for boring 2

As it can be seen from the UU test results, in general, soil shear strength of shallow samples are greater than deeper sample and the average value of s_u was 350 kPa which is much higher than the estimate from the SPT. The modulus measured in triaxial tests averaged $E = 30$ MPa. The difference in S_u for the same similar depth is high. For example,

the B1-1.05m sample and B1-1.35 sample have about 400 kPa (200 kPa) difference in deviator (shear strength) stress. This difference and the variance between the lab test results and the field test results indicate that soil layer may have some fissures and cracks which reduce the large scale strength, therefore the bulk strength of soil cannot be estimated by small sample tests in a lab and in this situation in-situ tests would give us more realistic value.

An SPT was performed in the third boring. The SPT blow count number was consistent with depth and the average was 19 bpf which leads to an estimate of the undrained shear strength of 127 kPa using the correlation $s_u(\text{kPa}) = 6.7 \text{ N}(\text{bpf})$ (Briaud 2013). The boring logs with pocket penetrometer and SPT results are presented in Appendix 1.

Since the soil was hard, driving the pressuremeter probe was not possible and drilling with concrete driller also did not work. Two holes were prepared by pushing a #10 sharpened reinforcing rebar with a concrete block mass (Figure 3-31).



Figure 3-31: Boring preparation for PMT in hard clay

Two successful PMTs were conducted in the pre-bored holes in the hard clay, both with two unload-reload loops. Figure 3-32 and Table 3-8 show the PMT results in depths of 1m and 1.8m. The E_{R1} and E_{R2} are the elasticity modulus for first and second loop. The p_L and E at 1m depth are greater than 1.8m that is also observed in the UU test results. Table 3-9 presents the lab and in-situ test's results for the hard clay.

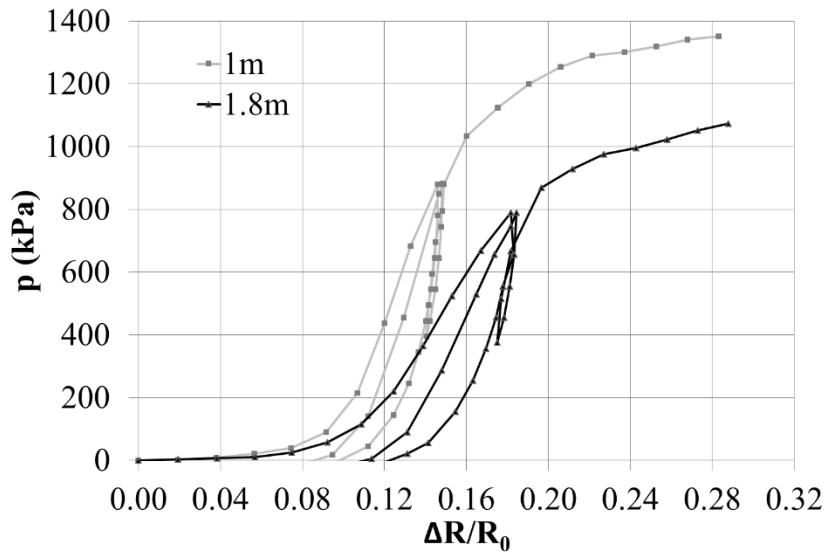


Figure 3-32: Pressuremeter test result in hard clay

Table 3-8: Pressuremeter test results in hard clay

Depth (m)	E(MPa)	E_{R1} (Mpa)	E_{R2} (Mpa)	p_L (kPa)
1	27.8	40	92	1400
1.8	16.7	27	74	1200

Table 3-9: Lab and in-situ tests results for hard clay

Test		Result
In-situ	PMT	PL=1300 kPa, E=20 MPa
	Pocket Penetrometer	>4.5 tsf
	SPT	19 bpf
Lab	Grain Size Analysis	CL
	Unit weight	21 kN/m ³
	UU Triaxial Test ⁴	$S_u=350$ kPa, E=35 MPa

Very dense crushed limestone

Very dense crushed limestone is a poorly graded sand (SP-SM) containing silt and gravel with maximum size of 30mm. The particle size analysis result and sample of crushed limestone is presented in Figure 3-33. The available ditch was prepared about a

decade ago and it gained strength during the time because of existence of the lime. Using triaxial tests, the friction angle of the material was measured as 45 degrees (Saez Barrios 2010).

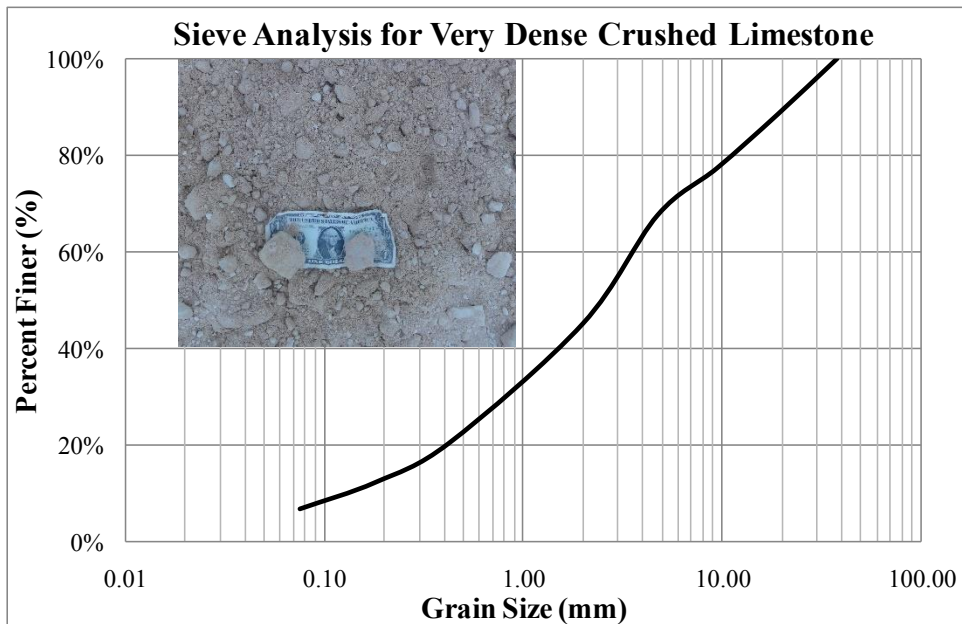


Figure 3-33: Particle size curve and sample of very dense crushed limestone (Lim 2011)

In order to place the pile in a 1m diameter hole was bored and pile was placed into it. Using hand mechanical tamper the wet material with about 10% water content was compacted consistently around the pile. Figure 3-34 shows the soil compaction around the pile in crushed limestone.



Figure 3-34: Soil compaction during the post installation using a mechanical tamper

Total number of 3 borings were drilled, two borings with pile for static and crash test and one borings without any pile to perform in-situ tests. In order to compare the young to aged soil properties two series of tests were conducted. Two SPTs and one PMT were performed in the same day of soil preparation. After 80 days, before the crash test, three SPTs (one in 80 days old soil and two in 10 years old soil) and one PMT in 10 years old soil were performed.

The SPT blow count numbers in the young soil are about the same range in depth with average of 9 and this indicates that soil was homogenously compacted. After 80 days N_{SPT} for shallow depth (0.60 m) is 19 while this value decreases to 12 in deep level (1.5 m). In the old soil the N_{SPT} value is scatter from 11 to 50 that indicates the SPT is not a suitable test method for this material however based on previous study (Lim 2011) and other test

result N_{SPT} for the aged soil is estimated 50. The boring logs with SPT results for young and aged dense crushed limestone are presented in Appendix 2.

The PMTs in young and aged crushed limestone were conducted in 0.5m depth. The holes were drilled with a concrete drill and due to difficulty in drilling a proper hole for pressuremeter test, deeper investigation was not possible. The results show a significant increase between aged and young soil which was expected (Figure 3-35). The aged soil test was incomplete because the maximum working pressure of the instrument is 2500 kPa and the resistance pressure reached more than the capacity. The pressure limit in this situation is estimated by extrapolating the pressure curve. The p_L and E for young soil are 1700 kPa and 20 Mpa, and for aged soil are estimated 3000 kPa and 45 Mpa. Table 3-10 presents the lab and in-situ test's results for very dense crushed limestone.

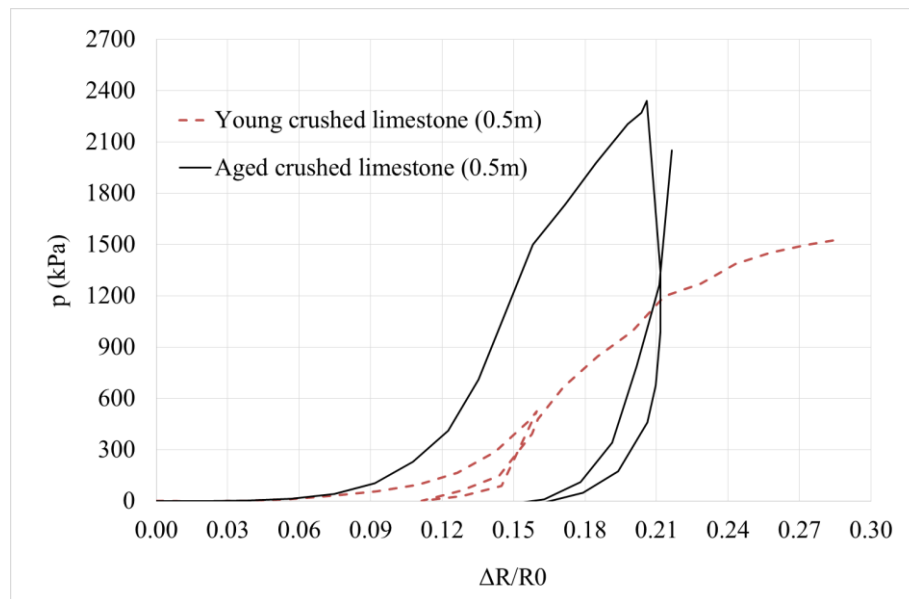


Figure 3-35: Pressuremeter test result for young and aged very dense crushed limestone

Table 3-10: Lab and in-situ tests results for very dense crushed limestone

Test		Result
In-situ	PMT	PL=3000 kPa, E=45 MPa
	SPT	>50 bpf
Lab	Grain Size Analysis	SP-SM
	Unit weight	23 kN/m ³
	Friction angle	45

Medium scale tests

A set of medium scale tests were designed to try to isolate the damping and inertia effect in order to obtain their influence on the system more directly. One set of tests would aim at keeping the velocity constant and another set of tests, the acceleration constant. By performing these tests we would isolate the dashpot and mass effects in the simple model that will be described in section 5. Indeed if the velocity is constant, the acceleration is zero, the mass effect disappears, and the damping effect is isolated. A series of scaled tests were designed to do just that. The tests were performed at the TTI Riverside campus in September and October 2011. A total of 13 tests were conducted. They included 6 impact tests, 5 static tests, and 2 creep tests and are summarized in Table 3-11.

Table 3-11: List of medium scale tests performed

Tests number	Test	Soil type	Soil condition
T1	Static	Loose sand	undisturbed
T2	Static	Loose sand	repaired
T3	Static	Loose sand	replaced
T4	Static	Soft Clay	undisturbed
T5	Static	Soft Clay	repaired

Tests number	Test	Soil type	Load levels kN(lb)
T6	Creep	Loose sand	0.45(100), 1.1(250), 1.8(400)
T7	Creep	Soft Clay	0.9(200), 2.2(500), 3.6(800)

Tests number	Test	Soil type	Velocity m/s (Mph)
T8	Bogie impact	Loose sand	2.2(5)
T9	Bogie impact	Loose sand	6.1(14)
T10	Bogie impact	Loose sand	11.2(25)
T11	Bogie impact	Soft Clay	2.2(5)
T12	Bogie impact	Soft Clay	6.7(15)
T13	Bogie impact	Soft Clay	10.3(23)

Two types of soil were used for these tests, a loose sand and a soft clay. The soft clay came in blocks and the loose sand came in a truck and was poured in place. Both soils were placed in a pre-built steel box. A 1.5m long hollow square HSS 4×4×1 steel post, 4 inches (10cm) square with 1 inch (2.5 cm) wall thickness, were pushed 1m into the soil with a big mass of concrete (Figure 3-36). The plan view and cross-section view of the box and pile location are shown in Figure 3-37 and Figure 3-38.



Figure 3-36: Pile installation in soft soil

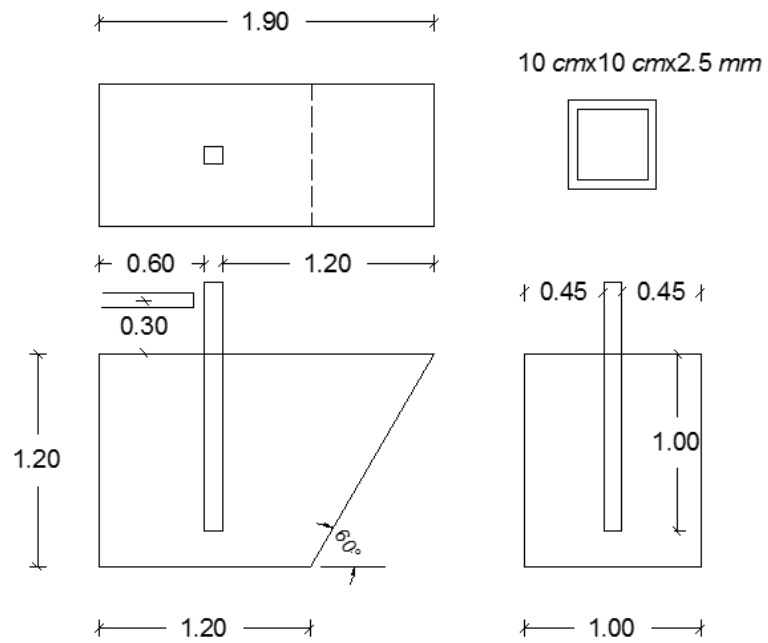


Figure 3-37: Medium scale test plan and section (unit is meter)

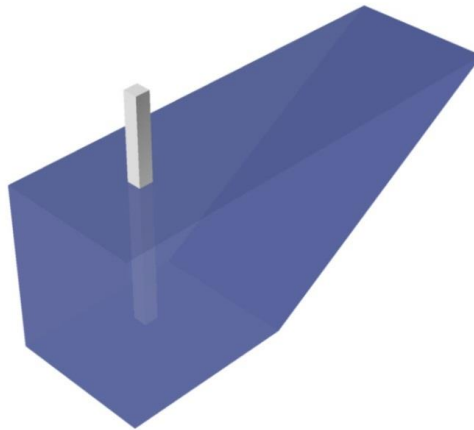


Figure 3-38: 3D shape of excavation for medium scale test

Static and creep test

In order to find the static parameters of the soil (e.g. stiffness and limit pressure) a set of static tests was done in both soils. Since after each impact test the soil was disturbed, it was necessary to repair the soil and ensure that the repaired soil would have the same properties as the first soil. Therefore for each soil type after the main static test the soil was repaired, the static test was repeated, and compared to the first test. In some cases the soil was completely excavated and replaced in the box. All static tests results are shown in Figure 3-39.

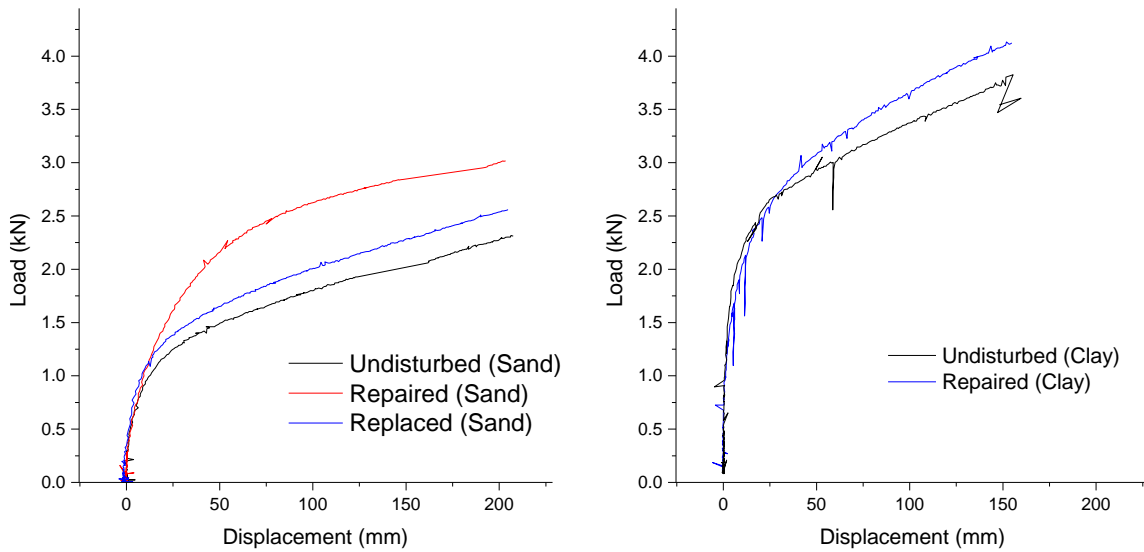


Figure 3-39: Static test results in loose sand and soft clay

After the static tests, creep tests were also performed for each soil type. Three levels of load were applied and kept constant on the post for 10 minutes for each level. During the load application, the displacement at the point of load application was measured with a string pot. For the loose sand, three load levels were selected, 100 lb (0.45 kN), 250 lb (1.1 kN), and 400 lb (1.8 kN). For soft clay the three load levels were 200 lb (0.9 kN), 500 lb (2.2 kN), and 800 lb (3.6 kN). As it was expected the sand showed a lower viscosity behavior than the clay (Figure 3-40).

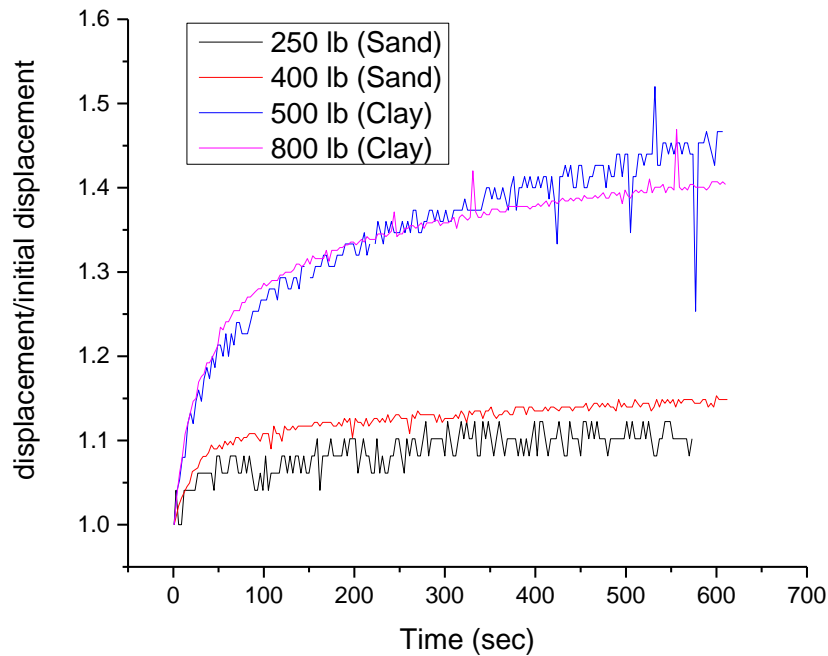


Figure 3-40: Creep comparison between sand and clay for different level of load

Constant velocity tests

In these tests, a heavy bogie impacted the pile in the soft soil at different velocities. The bogie nose is made of solid steel that impact the pile at height of 0.3m (Figure 3-41). Since the soil resistance was low, the velocity of the bogie would not change much during the impact and the constant velocity condition would be achieved; however during the initiation of impact a high amount acceleration would be generated. The location of the sensors on the post and in the soil is shown in Figure 3-42. The accelerometers behind the post were placed on the surface to measure the surface wave properties during the impact.



Figure 3-41: 2300 kg bogie with rigid nose

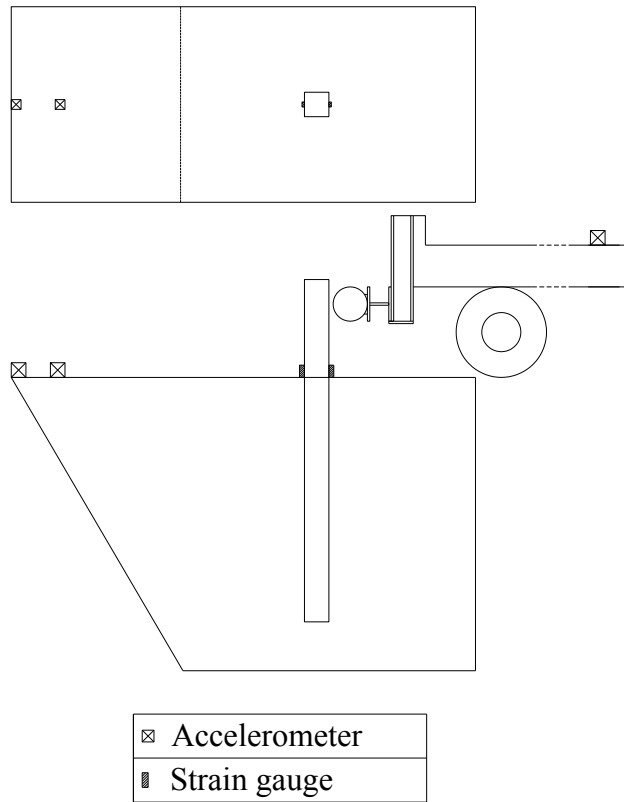


Figure 3-42- Medium scale test sensors location

In order to capture the soil deformation during and after the impact set of grid lines were drawn on the soil surface. This helps to track the soil movement on the surface and sometimes to detect the soil failure wedge for the hard material. Figure 3-43 shows the grid lines for both loose sand and soft clay tests.

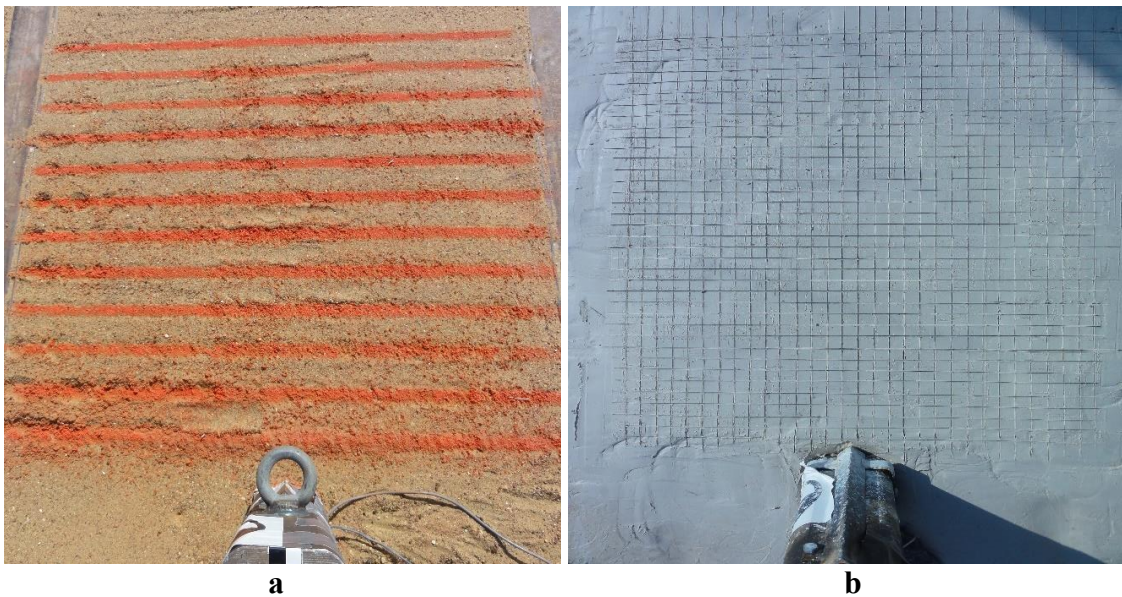


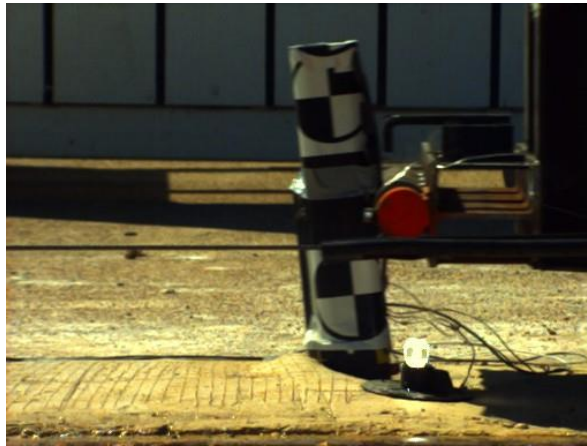
Figure 3-43: Grid line on soil surface for a) loose sand and b) soft clay

Three levels of velocity were selected for the 5000lb (2300 kg) bogie impact. The bogie is considered as a rigid mass so all the displacement comes from the post deformation. In this test the bogie is pulled by a cable connected to a truck to reach the designed velocity and at contact time a slider releases the cable from the bogie to let the bogie travel freely without external force. The constant velocity tests are listed in Table 3-12. Figure 3-44 shows photos from the bogie test at 15 mph on the post in the soft clay.

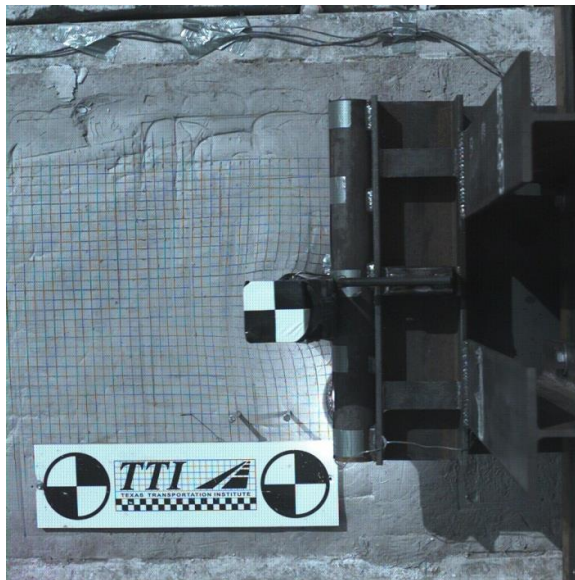
Table 3-12: Constant velocity tests on medium scale tests

Soil type	Velocity m/s (mph)
Loose sand	2.2 (5)
	6.1 (14)
	11.2 (25)
Soft Clay	2.2 (5)
	6.7 (15)
	10.3 (23)

Figure 3-45 and Figure 3-46 show the load-displacement curves for the bogie impact test on the soft clay and the loose sand. The load on the post is obtained from two measurements; acceleration on the bogie (50 msec average) multiplied by the mass of the bogie and bending strain on the post. The post was assumed to behave elastically because the maximum strain was about $500 \mu\epsilon$ which is less than $2000 \mu\epsilon$ corresponding to the yield strain of steel. The results show that the load calculated from the acceleration was higher (especially at the peak point) than the load obtained from the strain. The load calculated from the acceleration is obtained indirectly through the bogie while the load calculated from the strain is obtained directly on the post. As such the measurements from the strain on the post are considered more reliable.



Side view



Top view

Figure 3-44: 15 mph Bogie test in soft clay

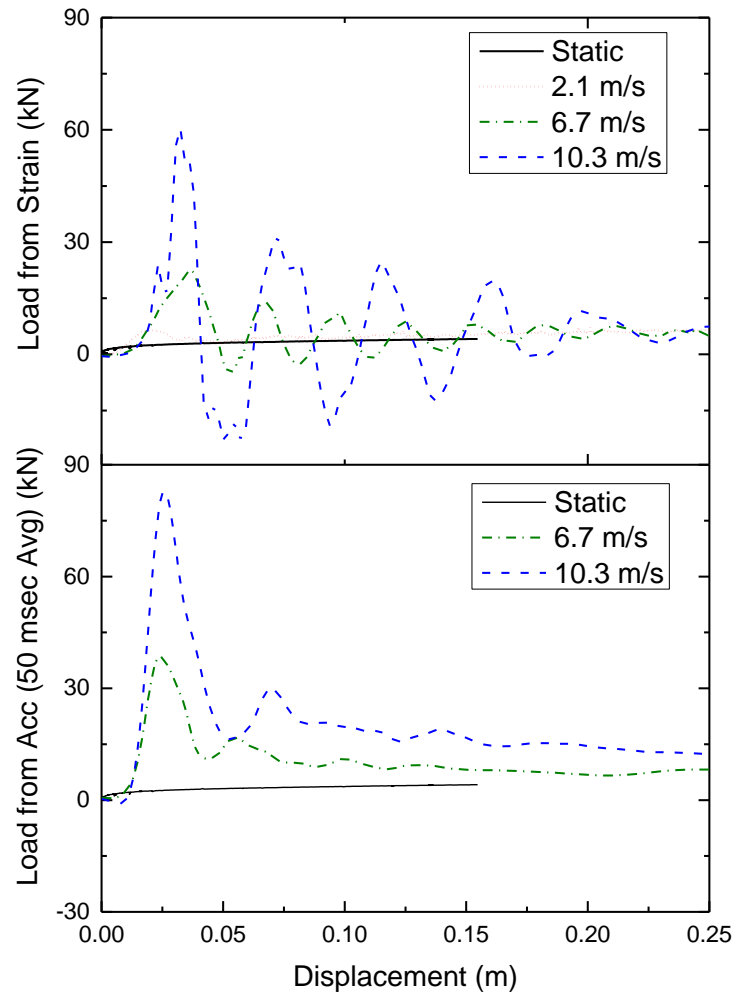


Figure 3-45: Load-displacement curve for bogie tests in soft clay (load from two methods)

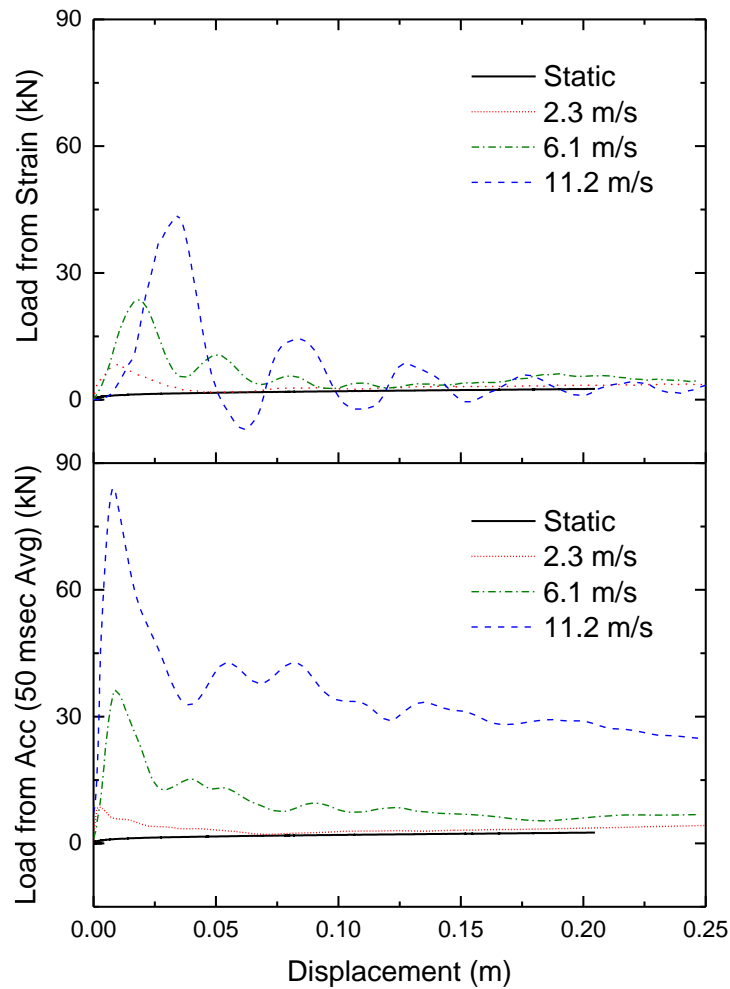


Figure 3-46: Load-displacement curve for bogie tests in loose sand (load from two methods)

Using soil surface acceleration at 1m far from the pile the first wave observed in $t=0.006$ sec for loose sand and $t=0.004$ sec for soft clay. In order to reduce the noise from the acceleration a 500 Hz low pass FFT filter is applied on the accelerometer output. Figure 3-47 shows a sample acceleration obtained from 14 mph bogie test in the loose sand and 15 mph bogie test in the clay. Considering the first observed wave is corresponding to body wave, the body (P) wave velocity is estimated 250 m/s and 167 m/s

for the soft clay and for the loose sand respectively. Having the P wave velocity, modulus of elasticity for small strain (E_0) is evaluated from the Equation 3-1, 30 MPa for the loose sand and 31 Mpa for the soft clay. The calculated modulus from this method is very sensitive to Poisson's ratio that is difficult to measure (usually assumed 0.35 for sand and 0.45-0.49 for clay); therefore the value is not very reliable.

Equation 3-1

$$c_p = \sqrt{\frac{E_0}{\rho} \frac{(1-\nu)}{(1+\nu)(1-2\nu)}}$$

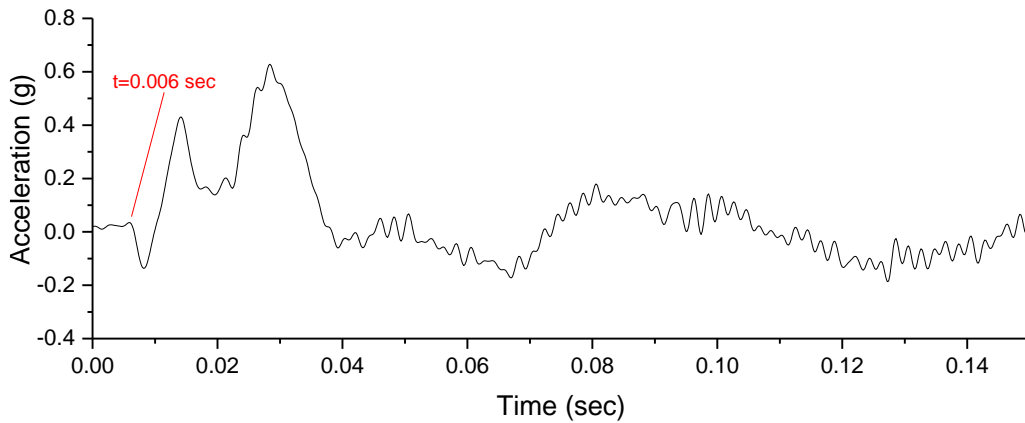
where:

c_p : P wave velocity

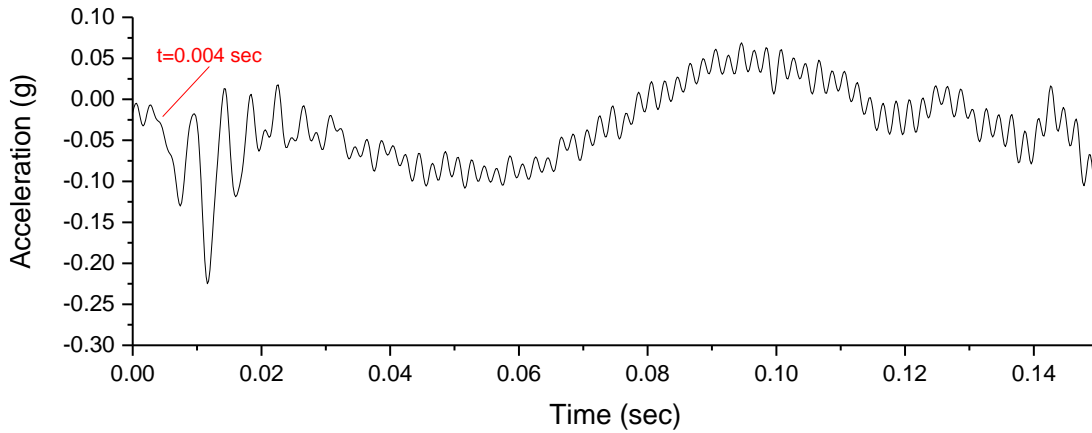
E_0 : Modulus of elasticity for small strain

ρ : Density

ν : Poisson's ratio



a



b

Figure 3-47: 500 Hz Low Pass FFT filter of Soil Acceleration at 1m from the pile a) Loose sand b) Soft clay

Post movie analysis of soft clay indicates a punching mechanism in front of the pile; however some movements of surface grid on front-side of the post is detected. In the loose sand the same mechanism with surface soil splashing is observed, yet no failure wedge is generated neither in the soft clay nor in the loose sand. Figure 3-48 shows the soil condition after the impact for 15 mph bogie test in both soils.

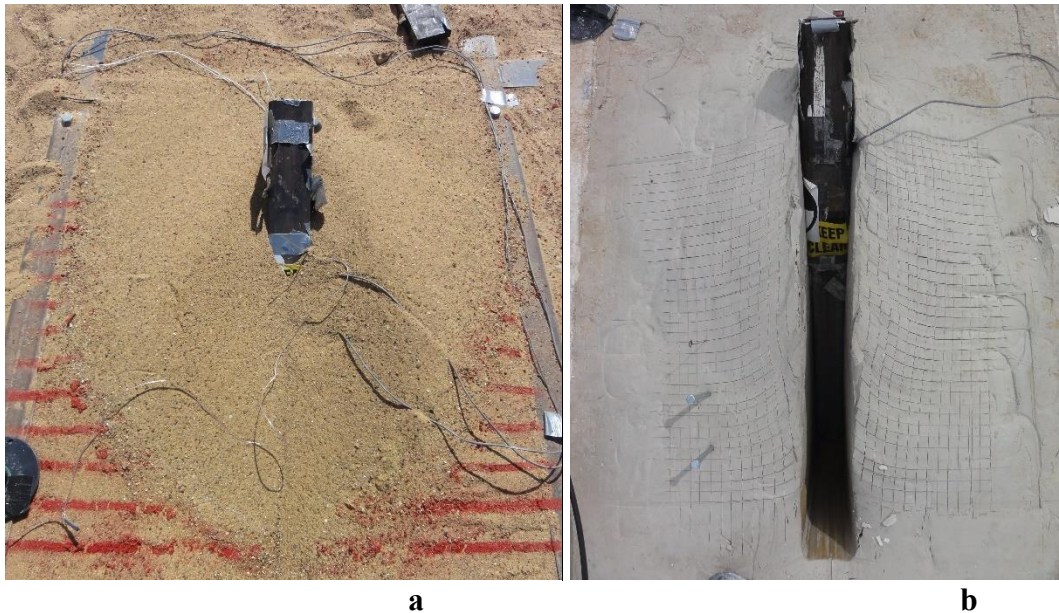


Figure 3-48: Deformed soil after 15 mph bogie impact a)loose sand b)soft clay

Semi constant acceleration test

In order to create a test where the acceleration of the post would be kept constant, gravity was used to apply the load. In this method a heavy mass falls from a chosen height under the acceleration of gravity (g) thereby generating a constant vertical load. This load is transferred into the same constant horizontal load by a cable and pulley system. By letting the same mass fall along a slope, we can reduce the value of the constant acceleration and therefore the magnitude of the constant force. The resistance from the post would vary but if the mass was large enough this resistance would be small in comparison. The test set up is shown in Figure 3-49. For these tests we used the same box as the one used for the constant velocity tests but the sensors were different (Figure 3-50). A total of 4 tests were performed with the dropping mass setup. Figure 3-51 shows a photo for the 0.5g drop test and for the loose sand.

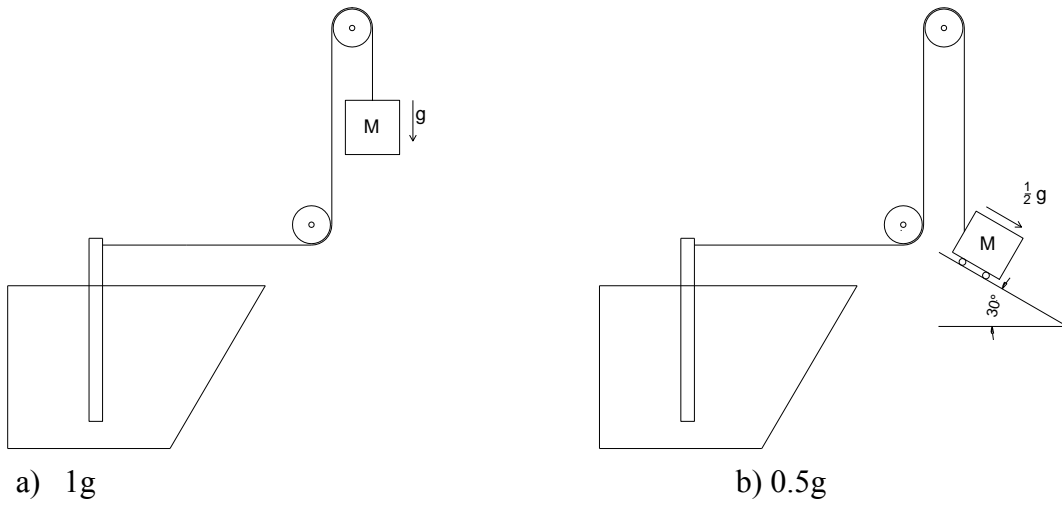


Figure 3-49: Falling mass test setup

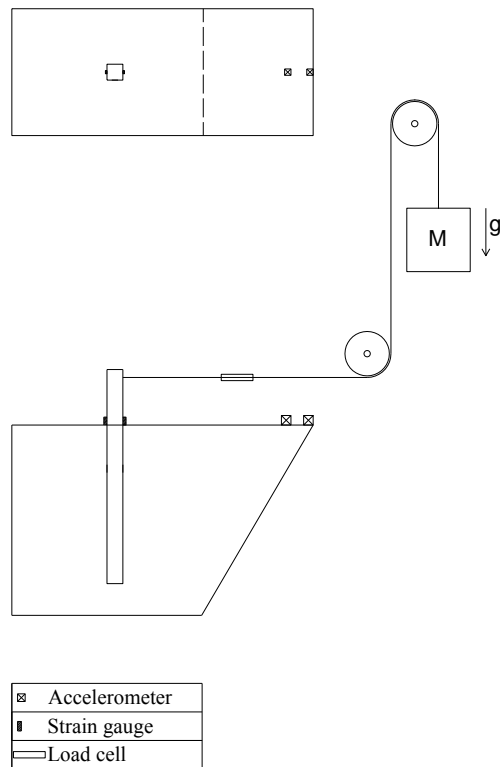


Figure 3-50: Sensor types and locations in falling mass test



Figure 3-51: 0.5g test in loose sand

Displacement-time and load-displacement results for the dropping mass tests are shown in Figure 3-52 and Figure 3-53. As can be seen from the results, the difference between the resistances of the post for the two levels of acceleration is small and indicates a small contribution of the mass to the resistance. Although the purpose of the tests were constant acceleration, the connection cable vibrated during the drop and made some acceleration in the system.

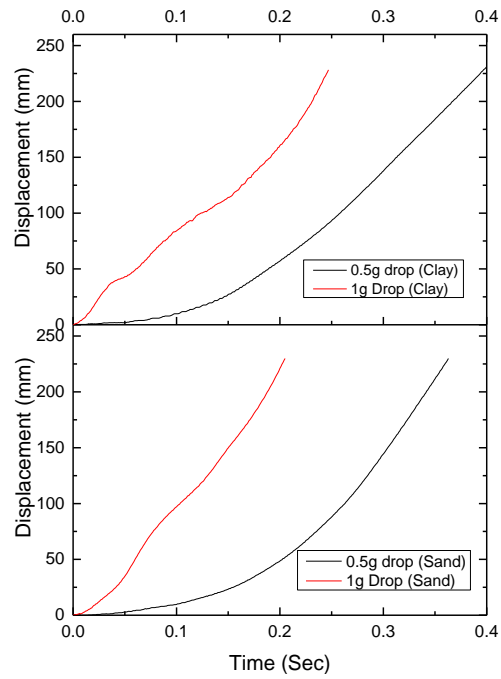


Figure 3-52 Time-displacement for dropping mass test

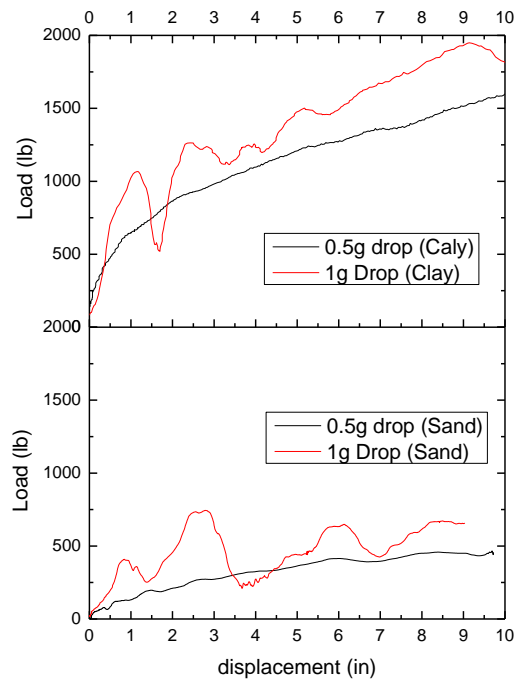


Figure 3-53: Displacement-load for dropping mass test.

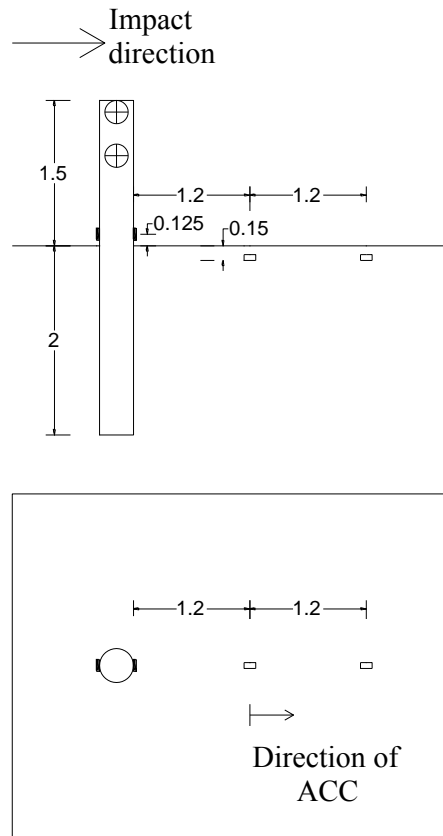
Full scale impact test on single post in hard clay (PU60)

Since we had not had enough tests and experience with strong soils and clay, the full scale test was performed in a hard clay. In order to have less complexity and less parameters for verification and simulation purposes, a single soil layer was preferable. According to the initial site investigation, the first 2 m (6.5 feet) deep layer was relatively uniform, therefore the embedded depth of the post was chosen as 2 m. A 14 inch (0.35m) diameter tube with 0.5 inch (1.27 cm) wall thickness (HSS 14×1/2) was selected to stop a 5070 lb pickup truck (Chevrolet C2500, year 2000) with a 60 mph impact velocity (PU60 test according to ASTM-F2656). The truck specification and sensors locations on the truck is presented in Appendix 3.

The initial calculations indicated that there would be no plastic deformation on the post. Since it was predicted that the truck would cover the side part of post and make the tracking of the post displacement by the camera impossible, the post was designed to stick up 1.5m above the ground. Three quantities were measured during the crash test:

- Acceleration of two points on the truck in x,y and z direction, and two locations on the soil in x direction
- Strain of the post 125 mm above the level ground with full bridge strain gauges set
- Displacement of truck and post by using four high speed cameras (two on the side, one on the top and one in the front)

The location and type of the sensors used in the test are shown in Figure 3-54.



▮ Strain Gauge ◻ Accelerometer

Figure 3-54: Section and plan of pickup truck impact test on single post (unit is meter)

Since the soil was too hard and driving the post was difficult, a 0.3m (12 inch) diameter hole was drilled with an auger first and the 0.35m (14 inch) diameter steel post was pushed into the soil. The installation of the post was done one month before the test to let the stresses created by the installation relax and dissipate.

The purpose of doing the static tests was to determine the strength of the soil-post system under low rate loading and also to observe the soil behavior at large scale. A lateral static test on the same post section was done next to the impact test location a day before

the impact test. The load was applied in steps of 8.9 kN (2 kips) and the duration of each load step was 10 minutes in order to measure the creep behavior and let the displacement occurs. The load was applied at the same height as the truck impact on the post (750 mm or 30 inch). A hydraulic pump applied the lateral load and displacement and load were measured by a string pot and a load cell respectively. A similar set of strain gauges as for the crash test was used in the static test to help calibrate the crash test strain gauges.

Static test results

The load vs. displacement curve of the static test is shown in Figure 3-55. According to the results, the failure lateral capacity of the post is 145 kN but the ultimate horizontal load H_{ou} (horizontal load at 0.1B displacement at level ground) is 115 kN. The average lateral stiffness of the pile is 1.75 MN/m while this value from the first loading curve is 2.5 MN/m and from the reloading curve is about 10 MN/m. The crack pattern around the post in the plan view and the shape of the failed soil wedge are presented in Figure 3-56.

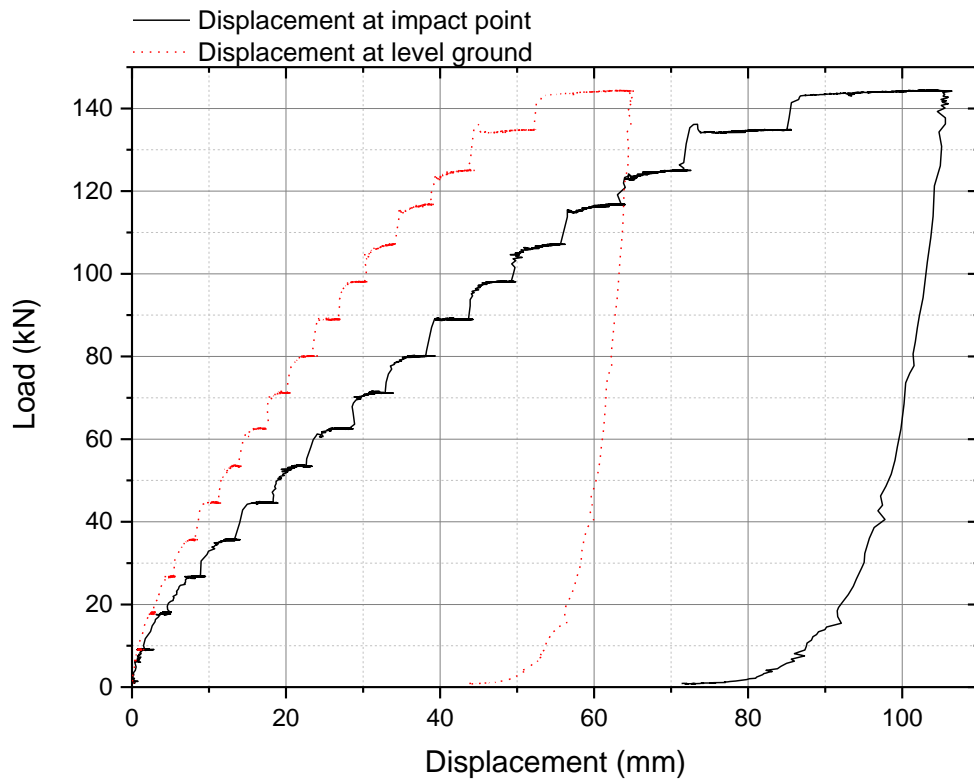


Figure 3-55: Load displacement curve of static test of pile in the hard clay

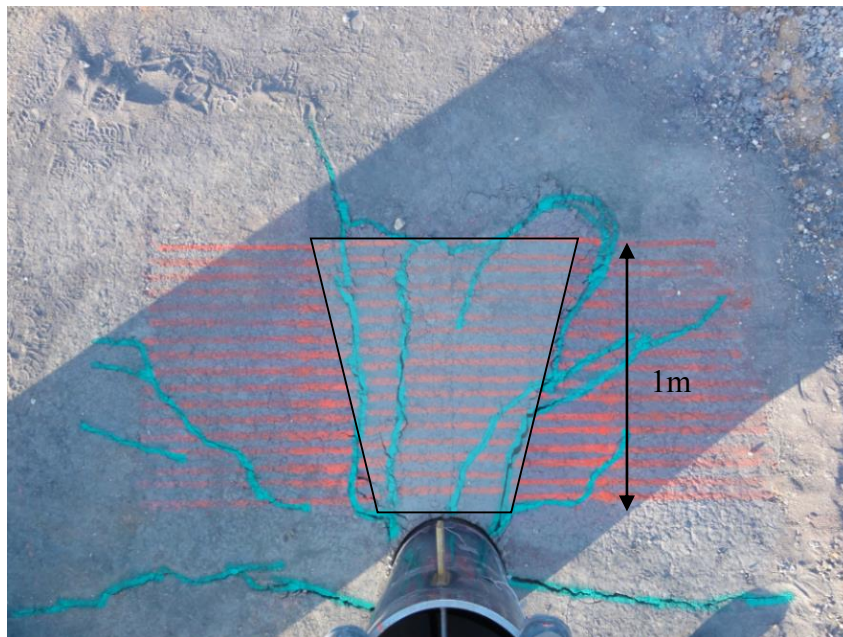


Figure 3-56: Crack pattern and failure zone for the static test

In order to reach the lateral capacity of the pile by using SALLOP method (Briaud 1997, 958-964) the p_L value is back calculated 1150 kPa for 10% displacement, so S_u should be about 150 kPa ($p_L=7.5 S_u$) while UU tests gave us $S_{u-avg}=350$ kPa. This shows that the UU triaxial tests in the lab do not give good results to estimate the capacity of the pile especially for hard soils. The p_L back calculation by SALLOP method is:

$$D_v = \frac{H_0 L^2}{3(H_0 L + 2M_0)} = \frac{H_0 \times 2^2}{3(2H_0 + 2 \times 0.75 \times H_0)} = 0.38$$

$$H = \frac{3}{4} p_L B D_v \Rightarrow p_L = \frac{4}{3} \frac{H}{B D_v}$$

$$H=115 \text{ kN} \rightarrow p_L=1150 \text{ kPa}$$

Impact test results

The full scale impact test on the single pile in the hard clay was performed in November 2012 (Figure 3-57). The truck speed was 60.4 mph (97.2 kph) and the impact angle 90.5 degrees. According to ASTM-F2656 the dynamic penetration rate (the distance between the front leading lower edge of the pickup truck bed and initial post location) was 2.2 m (88 inch) which is designated as P2 (1.01m to 7m) (Figure 3-58). During the impact, the truck rotated around the pitch axis (head of the vehicle moved upward) and stopped on the right side of the post.



1



2



3



4



5



6



7



8

Figure 3-57: Pickup truck impact test (PU60)



Figure 3-58: Pickup truck and pile after the impact (PU60)

The maximum dynamic displacement of the post at the impact point was 830 mm with rotation of 23° and the final displacement after rebound was 730 mm. The permanent pile rotation was 19.7° and the rotation point was at a depth of 1.35 m. The lateral displacement of the impact point versus time curve is shown in Figure 3-59.

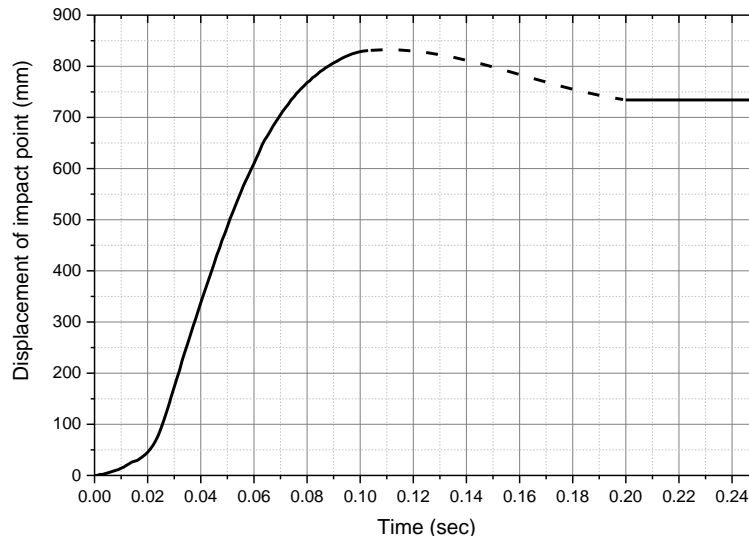


Figure 3-59: Lateral displacement of impact point on post versus time in pickup truck crash test (PU60)

Figure 3-60 presents the raw acceleration results at Center of Gravity (CG) and Rear in three direction of x, y, and z (x is the direction of impact). From the 50 msec average acceleration result, the maximum deceleration of the center of gravity of the truck and of the back of the truck were 23 g's and 19.5 g's respectively (Figure 3-61). The load calculated from the strain gages (Figure 3-62) shows a peak value of 440 kN (90 kips) while the maximum load from the acceleration data (mass times acceleration) is 520 kN (117 kips). The difference between these two values may be due to the deformation and crushing of the front of the truck. Indeed mass times acceleration assume a rigid body impact. Also the longitudinal force measured at the C.G of the vehicle separated in longitudinal and vertical forces. Figure 3-63 presents the load vs displacement curve for the impact and static tests.

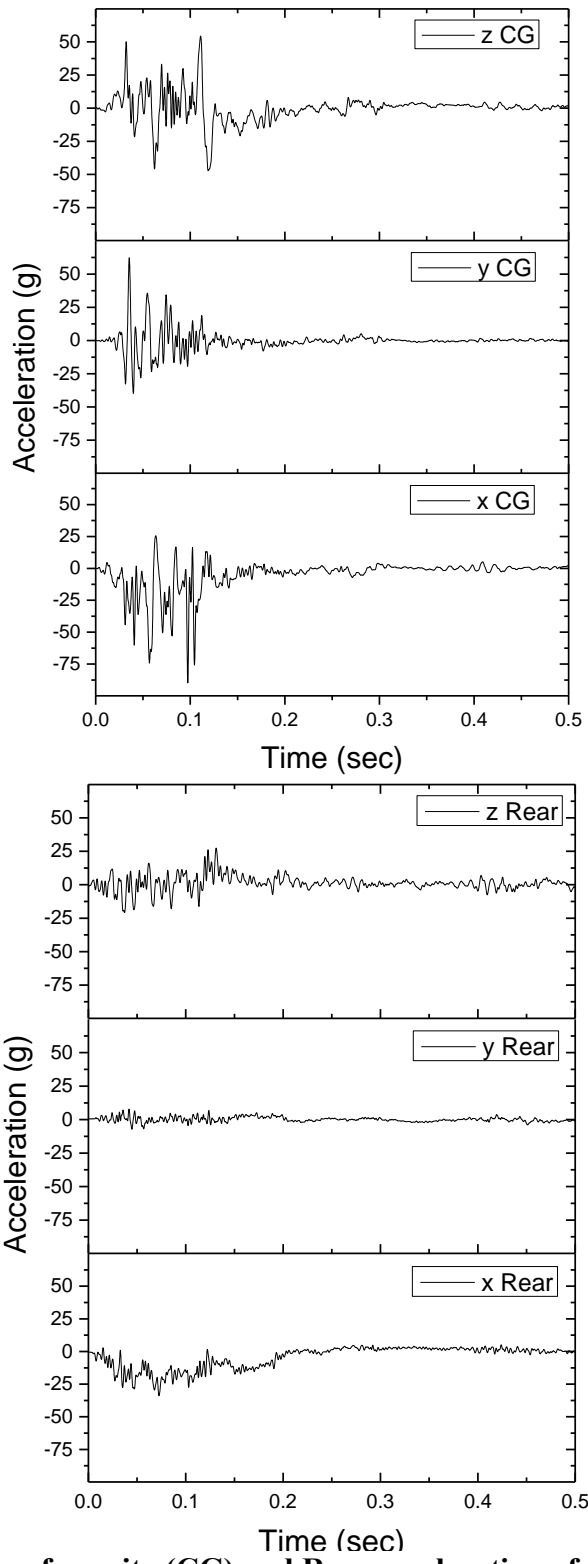


Figure 3-60: Center of gravity (CG) and Rear acceleration of truck in x, y, and z (PU60)

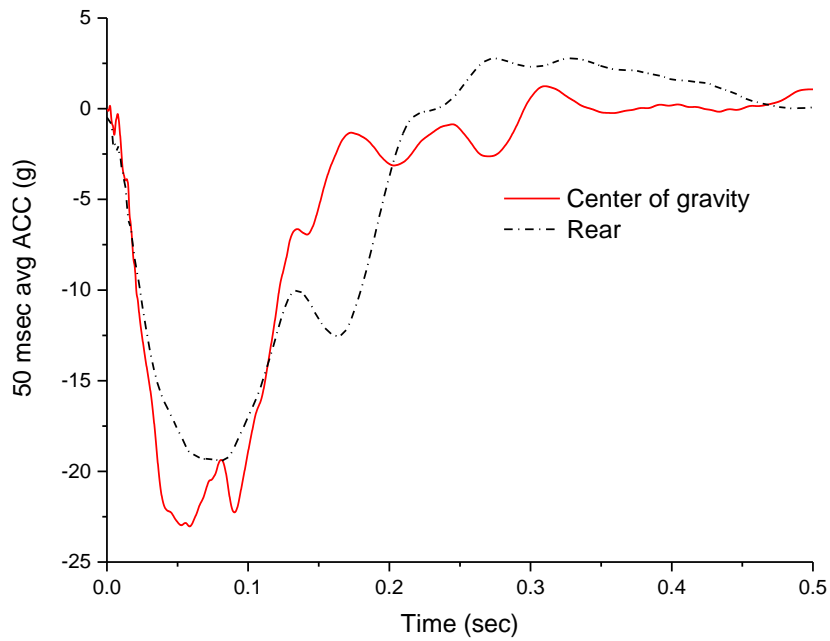


Figure 3-61: Acceleration versus time for two points on the pickup truck (PU60)

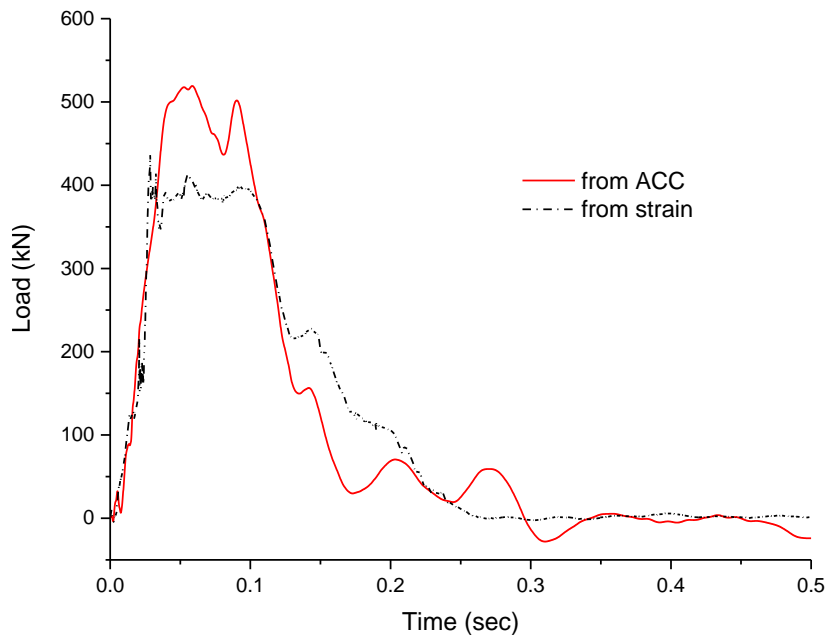


Figure 3-62: Comparison between loads derived from acceleration and strain (PU60)

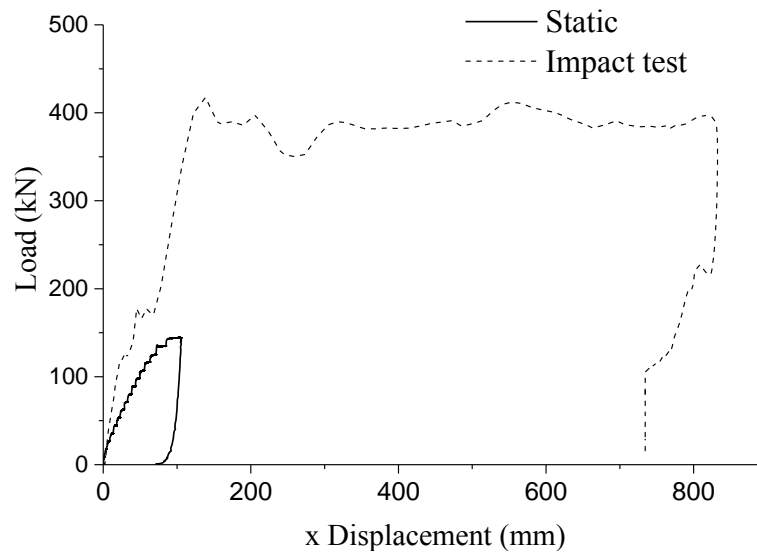


Figure 3-63: Load-Displacement curve for PU60 and static tests

The observation of the soil movement from the film analysis showed that a wedge of soil formed in front of the post with a length of 1.2 m (4 feet) while that length was 1m (3.3 feet) for the static test. The accelerometer results (Figure 3-64) on the soil at 1.2m and 2.4m from the pile were also showed a significant difference between accelerations that indicates the wedge movement of soil in 1.2m distance area. The first wave pulse in 1.2m acceleration graph happens at 0.0032 sec that results in P wave velocity of 375 m/sec. The derived E_0 from the P wave velocity is approximately about 80 MPa; however, as it was mentioned before because of difficulty of Poisson's ratio estimation the number is a rough estimation. The cracks and failure pattern in the soil after the impact test is presented in Figure 3-65.

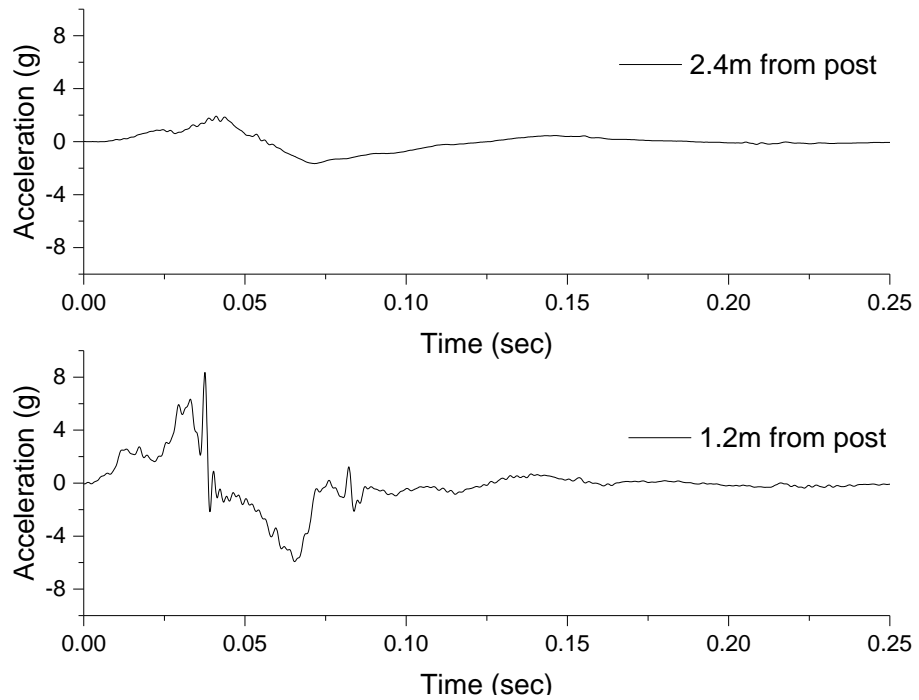


Figure 3-64: Soil surface acceleration (500 Hz FFT filtered) at 1.2m and 2.4m from the pile

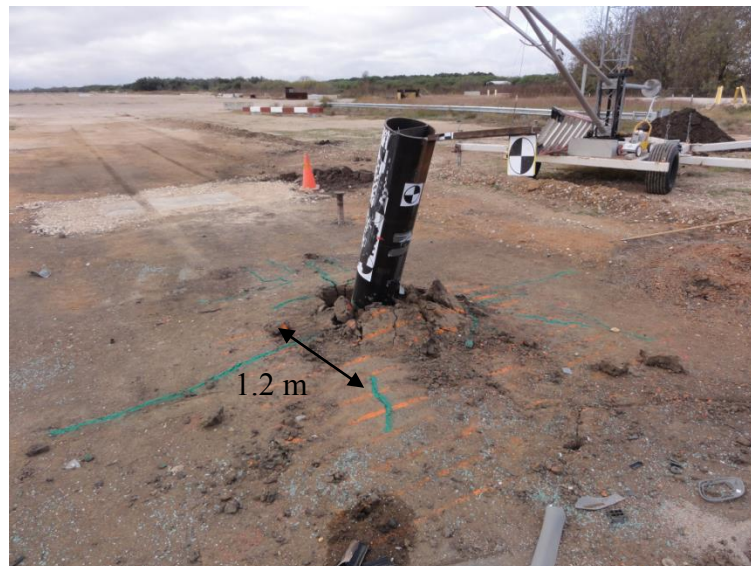


Figure 3-65: Soil cracks and failure wedge after pickup truck impact test

Full scaled impact test on single post in very dense crushed limestone (M50)

The K-12 test done by Lim (2011) was performed with some missing results like static behavior of pile, displacement of the pile during the impact, and moment result on the pile; therefore a new test was designed with same specifications but some modifications. The purpose of this test is to check the repeatability of previous test and more importantly to obtain more information from the impact for M50 impact. A The 2000 International 4700 single-unit flatbed truck with mass of 6808 kg (15010 lb), traveling at an impact speed of 50 mph (80.5 kph), impacted a 6m long W14-109 single pile with 3m embedment in the very dense crushed limestone. The pile was placed in a 1m diameter, 3m deep shaft that was drilled and backfilled with similar crushed limestone. Because the truck covers the post during the impact and hide it from cameras, the top of the pier extended 3m above the grade to let the high speed camera capture the pile displacement during the impact. The Truck specifications and sensors locations on the truck is presented in Appendix 4.

Three quantities were measured during the crash test:

- Acceleration of two points on the truck in x,y and z direction.
- Strain of the post 125 mm above the level ground with full bridge strain gauges set
- Displacement of truck and post by using four high speed cameras (two on the side, one on the top and one in the front)

In order to determine the soil-post behavior under low rate loading, a static test was performed on an identical pile placed with the same procedure in the same soil. Static loading was applied at 0.85m above ground in 11 steps, each step at 45 kN (10 kips). At each step, load was kept constant for 10 min (600 seconds) and data was read at 2 second

intervals. Forces for the static load test were transmitted to the pier via a rod and 150 kips rated hydraulic ram (Enerpac Z-Class E4 10,000 psi power unit and model RRH1508 ram) system. The load, displacement, and strain of the pile were logged during the test and the rotation of the pile was measured by hand after each load step.

The location and type of the sensors used in the impact and static tests are shown in Figure 3-66.

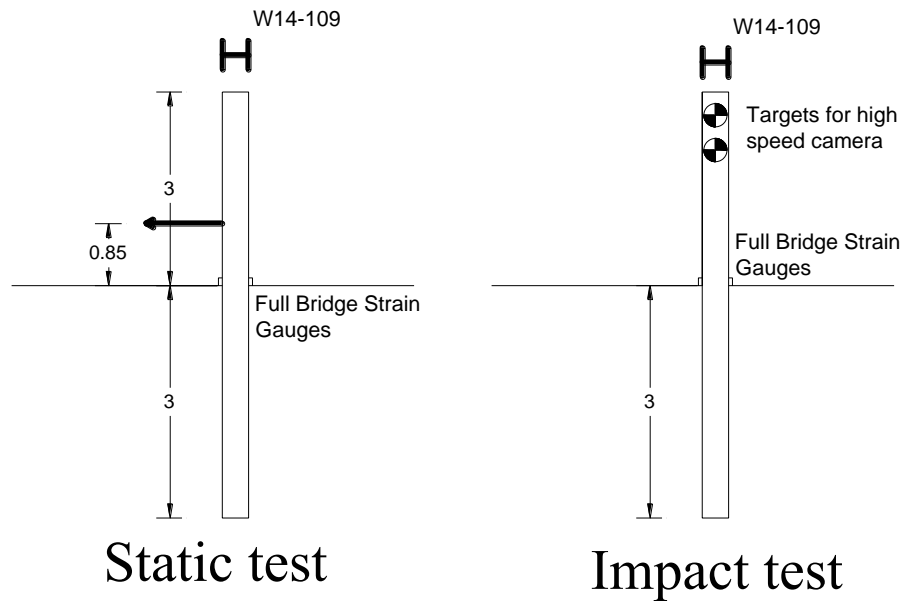


Figure 3-66: Pile geometry and sensors location of M50 impact test on single post (unit is meter)

Static test results

The load vs. displacement curve and load vs rotation of the static test is shown in Figure 3-67 and Figure 3-68. The pile static capacity is 493 kN with the maximum rotation of 3.6 degree.

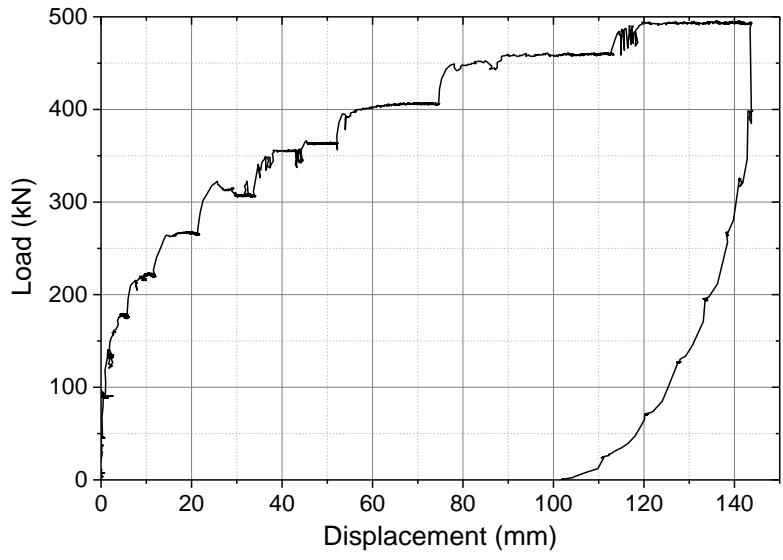


Figure 3-67: Load displacement curve of static test of pile in the very dense crushed limestone

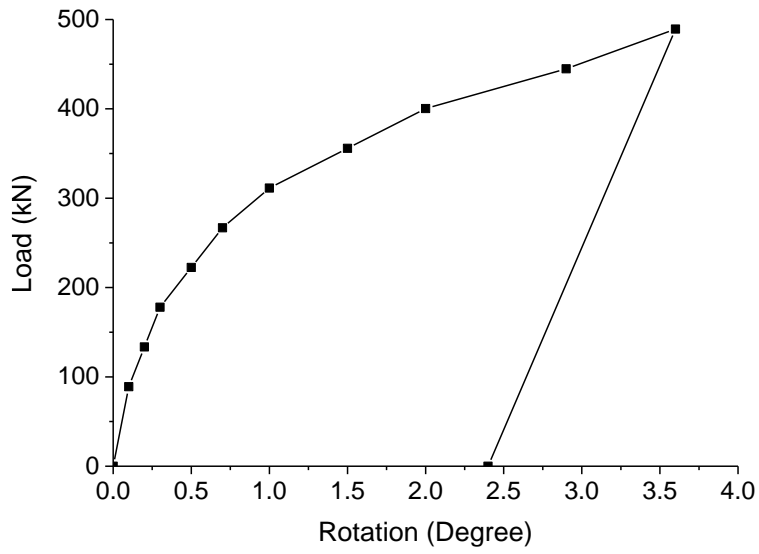


Figure 3-68: Load rotation curve of static test of pile in the very dense crushed limestone

A trapezoidal shape failure with height of 1.2m in front of the pile and circular shape failure with radius of 0.35m behind the pile were generated during the static test. Shows the soil deformation in the last step of loading in static test.



Figure 3-69: Soil deformation in static test for pile in very dense crushed limestone

Impact test results

The full scale impact test on the single pile in the very dense crushed limestone was performed in September 2013 (Figure 3-70). The medium duty truck impacted the post with 81 kph (50.2 mph) velocity at 90.5 degrees, with the centerline of the vehicle aligned with the centerline of the post. The pier brought the vehicle to a complete stop and the cargo remained onboard the vehicle (Figure 3-71). According to ASTM F2656 the pile meets the penetration rating P1, which allows penetration of less than 1m of cargo.



1



2



3



4



5



6



7



8

Figure 3-70: Medium duty truck impact test (M50)



Figure 3-71: Medium duty truck and pile after the impact (M50)

The maximum dynamic displacement of the post at impact point was 450 mm with rotation of 9° and the residual displacement after the crash was 300 mm. The permanent pile rotation was 8° at the impact point. The lateral displacement of the impact point versus time is presented in Figure 3-72.

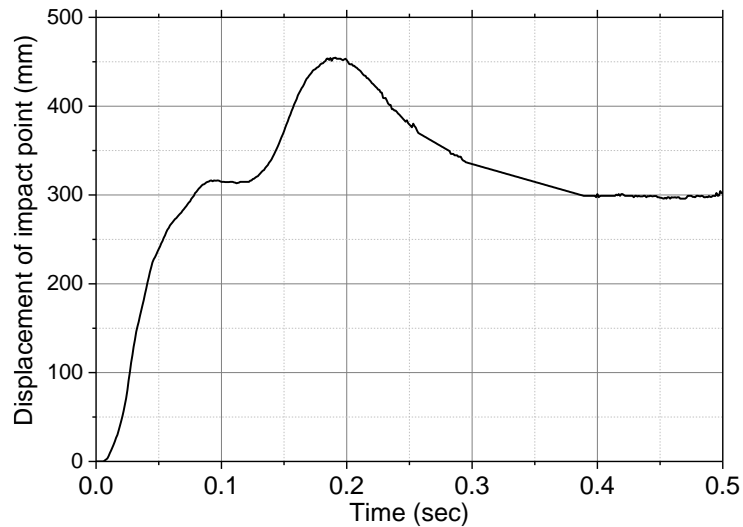


Figure 3-72: Lateral displacement of impact point on post versus time in medium duty truck crash test (M50)

The impact generated a plastic point at 1m depth of the pile that makes the displacement raises at 0.13 sec after the impact. The permanent displacement due to plastic behavior of pile, measured by post observation after the impact, was 120 mm at impact point (Figure 3-73).

Figure 3-74 presents the raw acceleration results at Center of Gravity (CG) and Rear in three direction of x, y, and z (x is the direction of impact). According to the 50 msec average acceleration result, the maximum deceleration of the center of gravity of the truck and of the back of the truck were 29 g's and 22 g's respectively (Figure 3-75). The load calculated from the strain gages shows a peak value of 1970 kN (442 kips) while the maximum load from the acceleration data (mass times acceleration) is 1600 kN (360 kips) (Figure 3-76). Since the pile at strain gages location experience a plastic deformation during the impact, a residual load at the end in load from strain curve is generated (yielding behavior happens at load 1200 kN for the strain gages location). Figure 3-77 presents the load vs displacement curve for the impact and static tests.

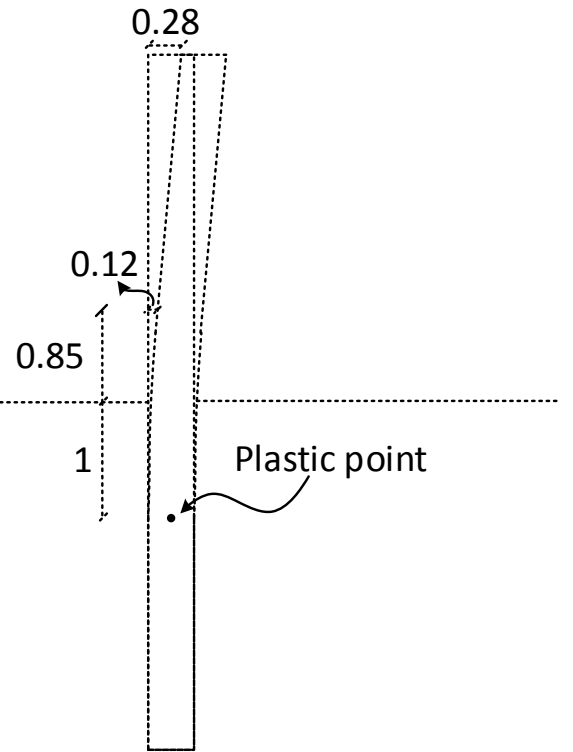


Figure 3-73: Pile plastic deformation after the M50 (unit is meter)

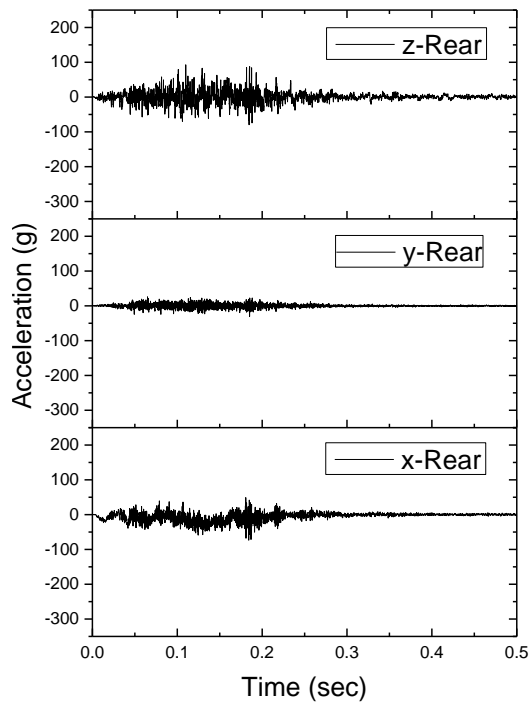
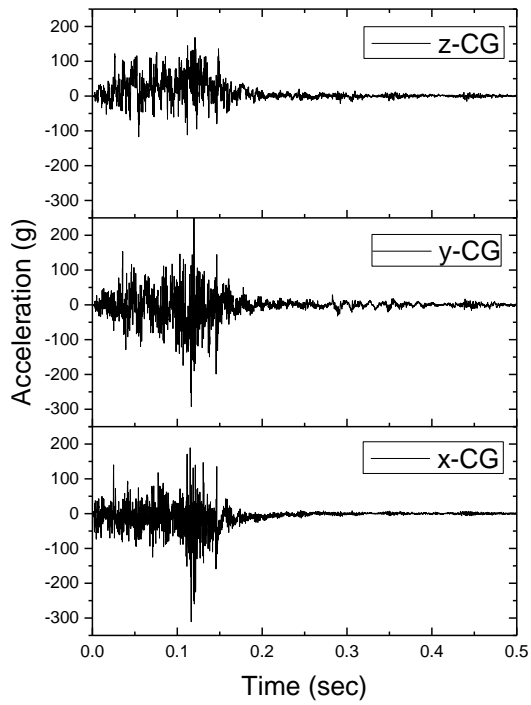


Figure 3-74: Center of gravity (CG) and Rear acceleration of truck in x, y, and z (M50)

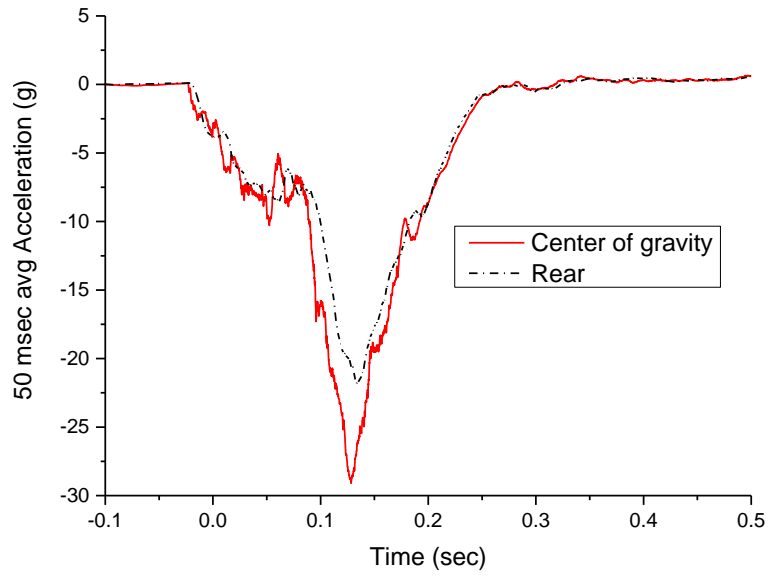


Figure 3-75: Acceleration versus time for two points on the medium duty truck (M50)

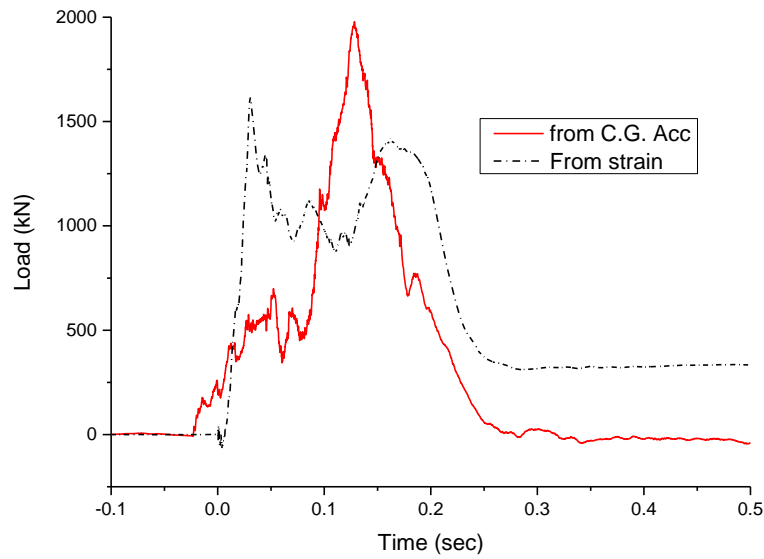


Figure 3-76: Comparison between loads derived from acceleration and strain (M50)

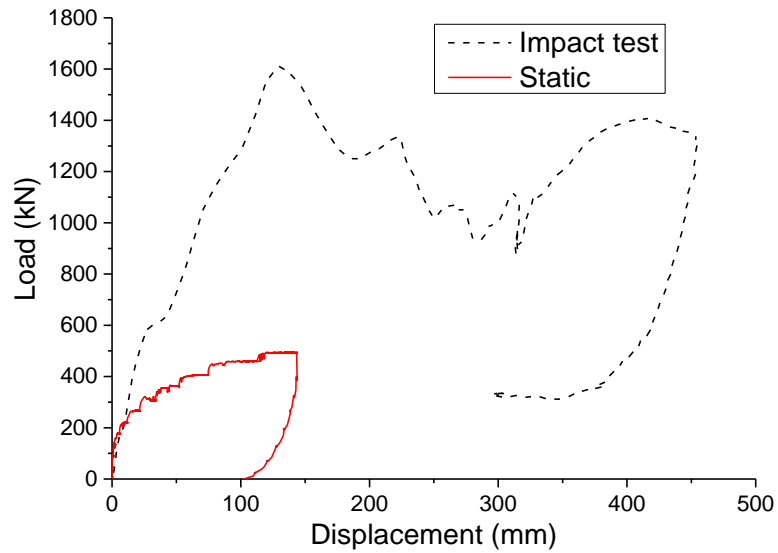


Figure 3-77: Load-Displacement curve for M50 and static tests

The comparison between the M50 test in this study and the M50 (K12) test done by Lim (2011) shows a good analogy in acceleration of truck rear and fair match in center of gravity acceleration, however the trend and range of number are close to each other and this can indicate the repeatability of the crash tests. The difference in pile height (3m in new M50 and 1m in old M50) could be the reason of the dissimilarity. Figure 3-78 shows the comparison of truck acceleration in the new and old M50 tests for two location on truck.

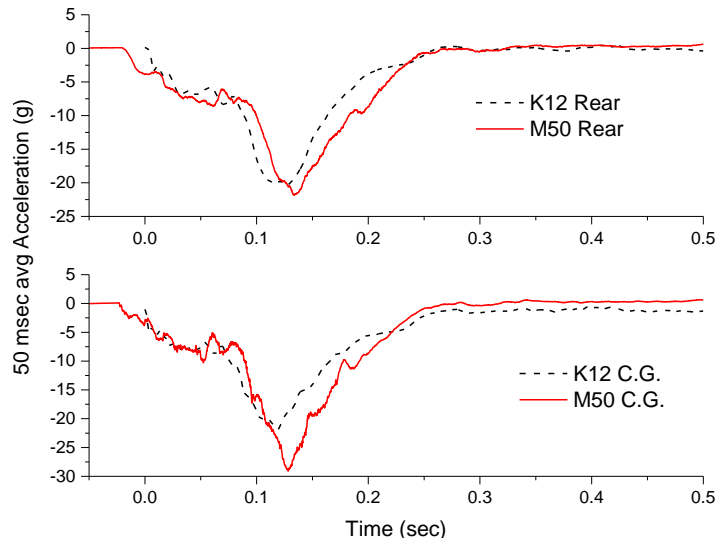


Figure 3-78: Comparison of acceleration of truck in the new and old M50 tests

Post soil inspection indicated a wedge failure on soil with length of 2m front of the pile. Figure 3-79 demonstrates the failure wedge trace on the surface for static and M50 impact tests.

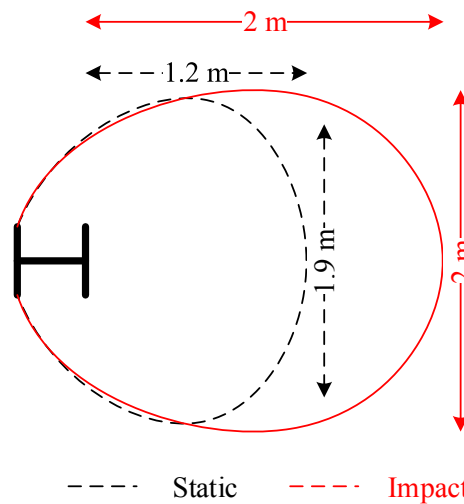


Figure 3-79: Failure wedge line on the surface in static and impact test (M50)

4. NUMERICAL SIMULATION

For the purpose of analyzing the vehicle impact an explicit numerical software is required. LS-DYNA was selected as a mean of numerical simulation for this study. A successful experience in past (Lim 2011) led us to use LS-DYNA as a software package for the simulation of vehicle crash to single pile. One of the advantages of LS-DYNA in this study is that the system including vehicle, pile, and soil can be modeled and analyzed with limited but proper plastic soil models.

Wu and Thomson (RW.ERROR - Unable to find reference:100) performed a study on the interaction between a guardrail post and soil due to vehicle accident through experimental tests and LS-DYNA computer simulations. They used a bogie for the experiments and simulation which cannot represent the deformation behavior of the vehicle during the impact. Two material models were used for the soil in LS-DYNA numerical analyses to model the gravel in their study. The results of this study showed that the soil and concrete material model can effectively capture soil–post interaction under impact loading for approximately 280mm of post deflection, while the FHWA soil behaved overly stiff relative to the soils tested.

Lim (2011) at Texas A&M University also conducted a large number of simulations with LS-DYNA for crash simulation on single pile and a group of piles. He developed design guideline for the post system directly embedded in soil based on the soil strength category. Two soil models were used in his study as a mean of modeling soil. For granular material the model was Jointed Rock model that is modified from Drucker-Prager model.

The other model was Isotropic Elastic-Plastic with Failure for clay. His results showed a good correlation between experimental and numerical results.

HyperMesh as a pre-processor and LS-PrePost as a pre and post processor were used in this study. LS-DYNA version was 971 and the analyzing process was performed on Texas A&M Supercomputing Facility. The supercomputer, named EOS, is an IBM "iDataPlex" commodity cluster with nodes based on Intel's 64-bit Nehalem & Westmere processor. The cluster is composed of 6 head nodes, 4 storage nodes, and 362 compute nodes. The storage and compute nodes have 24 GB of DDR3 1333 MHz memory while the head nodes have 48 GB of DDR3 1066 MHz memory (Texas A&M Supercomputing Facility 2014). In this study 32 cpus with 88 GB memory allocation were used for the simulations. The processing time is dependent on the model complexity, but the average cpu-hours for an ordinary simulation of a vehicle crash to single post was 400 cpu-hours. Parameters units in LS-DYNA must be consistence and in this study millimeter for length, kilogram ton (1000 kg) for mass, and second for time are selected as the main units.

In this section the numerical model and its specifications in LS-DYNA are explained and a model is calibrated with a full scale experimental test (PU60) in order to verify the model robustness. Finally, in order to generate a bank of impact test data, a set of numerical experiments with two different vehicles in sand and clay material are designed and discussed.

LS-DYNA Model

LS-DYNA is a general purpose finite element code for analyzing the large deformation static and dynamic response of structures including structures coupled to fluids. It is used by the automobile, aerospace, construction, military, manufacturing, and bioengineering industries. The code's origins lie in highly nonlinear, transient dynamic finite element analysis using explicit time integration. However the software also includes an implicit solver for somewhat limited capabilities. A contact-impact algorithm allows difficult contact problems to be easily treated. LS-DYNA currently contains more than one hundred constitutive models to cover the whole range of material behavior. (Livermore Software Technology Corporation (LSTC) 2006)

Materials models

Because of successful experience in Lim's research (2011) and based on the several examination of different material models, the same two soil models as Lim's work were used in this study.

Clay (von Mises)

"Isotropic Elastic-Plastic with Failure" (MAT 013) was used for clay material. The material model is based on von Mises yield condition with failure criterion modification. One of the simplest models for clay material under undrained loading is the Tresca model. Because of the sharpness of corners in the Tresca model (Figure 4-1), the numerical analysis has difficulties in simulations, so the von Mises criterion is generally used in this situation as a replacement of the Tresca model (Potts and Zdravkovic 1999).

Inside the yield surface material behaves elastically and beyond the surface it becomes perfectly plastic. In the model, two parameters of plastic failure strain and plastic pressure (≤ 0) are defined. When the pressure reaches the failure pressure or when the effective plastic strain reaches the failure strain, the element would not carry tension and the deviatoric stresses become zero, i.e., the material behaves such as a fluid. (Livermore Software Technology Corporation (LSTC) 2013)

Yield stress in von Mises yield criterion can be obtained using undrained compression strength of clay. The yield function is expressed as:

Equation 4-1
$$\phi = J_2 - \frac{\sigma_y^2}{3}$$

where:

ϕ : yield function

$J_2 = \frac{1}{2} S_{ij} S_{ij}$: the second deviatoric stress invariant

$$\begin{aligned} &= \frac{1}{6} [(\sigma_{11} - \sigma_{22})^2 + (\sigma_{22} - \sigma_{33})^2 + (\sigma_{33} - \sigma_{11})^2] + \sigma_{12}^2 + \sigma_{23}^2 + \sigma_{31}^2 \\ &= \frac{1}{6} [(\sigma_1 - \sigma_2)^2 + (\sigma_2 - \sigma_3)^2 + (\sigma_3 - \sigma_1)^2] \end{aligned}$$

$$s_{ij} = \sigma_{ij} - \frac{\sigma_{kk}}{3} \delta_{ij} = \begin{bmatrix} \sigma_{11} & \sigma_{12} & \sigma_{13} \\ \sigma_{21} & \sigma_{22} & \sigma_{23} \\ \sigma_{31} & \sigma_{32} & \sigma_{33} \end{bmatrix} - \frac{\sigma_{11} + \sigma_{22} + \sigma_{33}}{3} \begin{bmatrix} 1 & 0 & 0 \\ 0 & 1 & 0 \\ 0 & 0 & 1 \end{bmatrix} : \text{stress deviator tensor}$$

σ_y : yield stress

In the undrained compression test while $\sigma_1 \neq 0, \sigma_2 = \sigma_3 = 0$, Equation 4-1 is reduced to $\sigma_1 = \sigma_y$ where σ_1 is undrained compression strength. Therefore, the plastic pressure in the model for clay with undrained behavior is negative undrained compression strength.

Figure 4-1 displays a schematic comparison between von Mises and Tresca failure surfaces in 3D and 2D spaces.

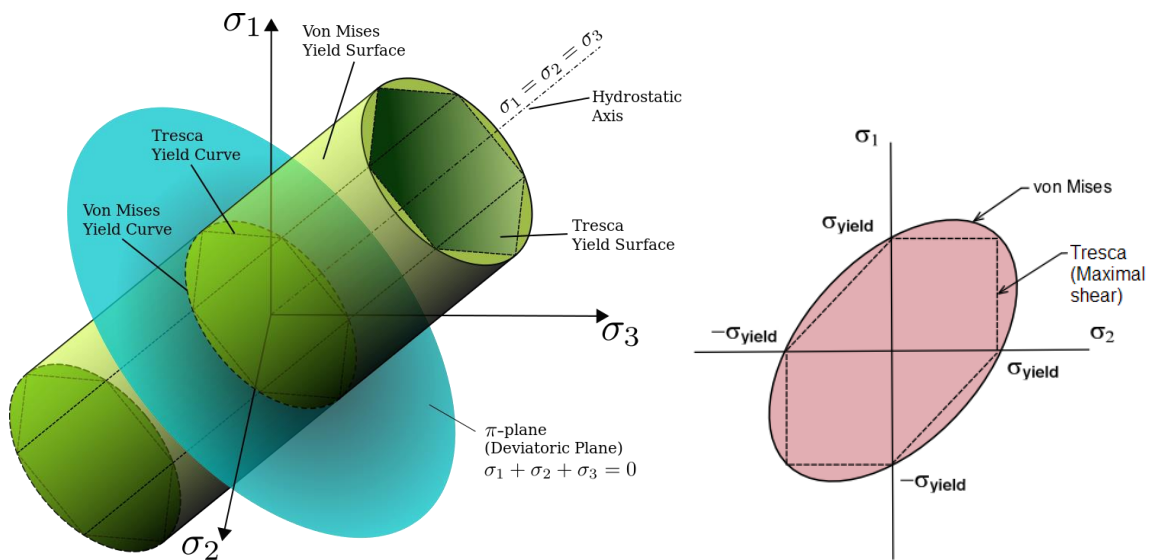


Figure 4-1: Von Mises and Tresca yield surface comparison in 3D and 2D (Wikipedia 2014)

Material card for Isotropic Elastic-Plastic with Failure model in LS-DYNA is shown in Table 4-1. The explanations of the abbreviations for the variables in the material card table are shown in Table 4-2.

Table 4-1: LS-DYNA Material card for Isotropic Elastic-Plastic with Failure (Livermore Software Technology Corporation (LSTC) 2013)

Variable	MID	RO	G	SIGY	ETAN	BULK
Default	none	none	none	none	0.0	none
Variable	EPF	PRF	REM	TREM		
Default	none	0.0	0.0	0.0		

Table 4-2: Variables on Isotropic Elastic-Plastic with Failure (Livermore Software Technology Corporation (LSTC) 2013)

Variable	Description
MID	Material identification
RO	Mass density
G	Shear modulus
SIGY	Yield stress
ETAN	Plastic hardening modulus
BULK	Bulk modulus
EPF	Plastic failure strain
PRF	Failure pressure (≤ 0.0)
REM	Element erosion option
TREM	dt for element removal

Granular soil (Drucker Prager)

For granular material, i.e, sand and crushed limestone, the Jointed Rock model (MAT 198) that is a modified version of the Drucker-Prager yield criterion. The behavior of the Drucker-Prager material model (MAT 193) in LS-DYNA version 971 was unstable with the explicit solver. Hence Jointed Pock material card was used instead of the Drucker-Prager material card (Lim 2011). In this model a correction has been made on the Drucker Prager model, in the way that the yield surface never goes against the Mohr-Coulomb criterion. This means that the model does not behave as a “pure” Drucker Prager model

(Livermore Software Technology Corporation (LSTC) 2013). The difference between the Jointed Rock and the Drucker-Prager model is that the Jointed Rock model can consider joints inside the materials with properties of dip, plane and strength. By adding zero joint as an input, the Jointed Rock model becomes the Drucker-Prager model.

The Drucker-Prager yield criterion is a pressure dependent model suitable for granular soil materials that was established as a generalization of the Mohr-Coulomb criterion. Same as von Mises model the Drucker-Prager model has the advantage of smooth surface that does not exist in the Mohr-Coulomb criterion. The sharp edges in the Mohr-Coulomb model make the numerical analysis more difficult (Figure 4-2).

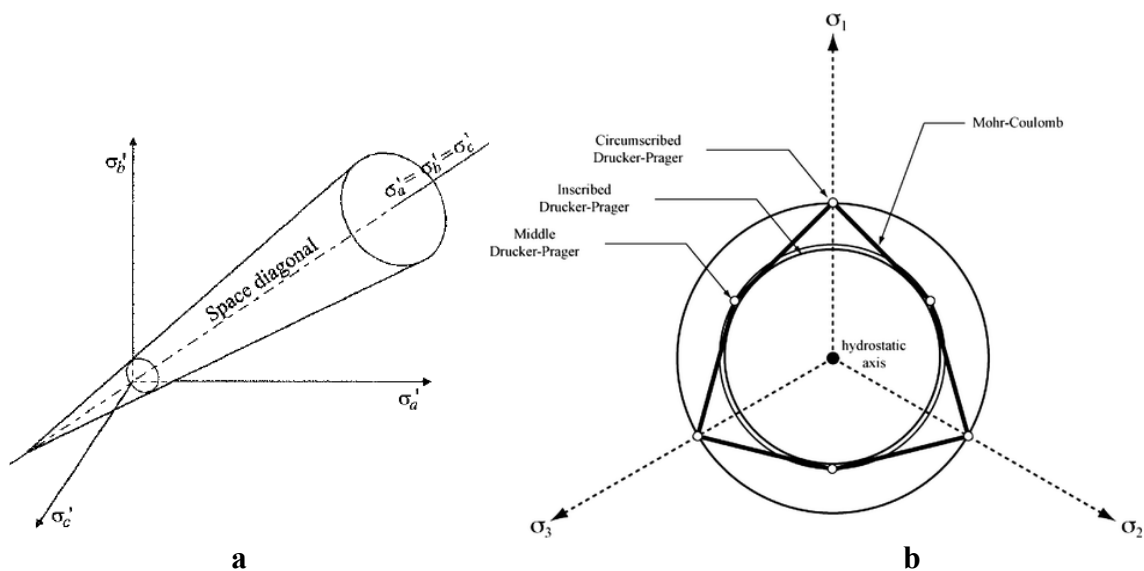


Figure 4-2: a) 3D Drucker Prager yield surface (Potts and Zdravkovic 1999) b) Comparison of Mohr-Coulomb and Drucker Prager yield surface in 2D space (Alejano and Bobet 2012, 995-999)

The yield criterion in the Drucker-Prager model has the form:

Equation 4-2

$$\phi = \sqrt{J_2} - \lambda I_1 - \kappa$$

Where:

$$I_1 = \frac{\sigma_{11} + \sigma_{22} + \sigma_{33}}{3} : \text{the first invariant of Cauchy stress}$$

$$J_2 = \frac{1}{2} S_{ij} S_{ij} = \frac{1}{6} [(\sigma_1 - \sigma_2)^2 + (\sigma_2 - \sigma_3)^2 + (\sigma_3 - \sigma_1)^2] : \text{the second deviatoric stress}$$

invariant

κ and λ : model parameter determined from experiment

The parameters κ and λ can be obtained from standard compression triaxial test and expressed in term of soil friction angle (ϕ) and cohesion stress (c):

$$\text{Circumscribed Drucker-Prager:} \quad \kappa = \frac{6c \cos \phi}{\sqrt{3}(3 + \sin \phi)}$$

$$\lambda = \frac{2 \sin \phi}{\sqrt{3}(3 + \sin \phi)}$$

$$\text{Inscribed Drucker-Prager:} \quad \kappa = \frac{6c \cos \phi}{\sqrt{3}(3 - \sin \phi)}$$

$$\lambda = \frac{2 \sin \phi}{\sqrt{3}(3 - \sin \phi)}$$

Material cards for the Jointed Rock model is shown in and Table 4-3. The explanations of the abbreviation for the variables on the material cards are shown in Table 4-4.

Table 4-3: Material cards for Jointed Rock model (Livermore Software Technology Corporation (LSTC) 2013)

Card 1	1	2	3	4	5	6	7	8
Variable	MID	RO	GMOD	RNU	RKF	PHI	CVAL	PSI
Default					1.0			0.0
Card 2	1	2	3	4	5	6	7	8
Variable	STR_LIM	NPLANES	ELASTIC	LCCPDR	LCCPT	LCCJDR	LCCJT	LCSFAC
Default	0.005	0	0	0	0	0	0	0
Card 3	1	2	3	4	5	6	7	8
Variable	GMODDP	PHIDP	CVALDP	PSIDP	GMODGR	PHIGR	CVALGR	PSIGR
Default	0.0	0.0	0.0	0.0	0.0	0.0	0.0	0.0
Card 4	1	2	3	4	5	6	7	8
Variable	DIP	STRIKE	CPLANE	FRPLANE	TPLANE	SHRMAX	LOCAL	
Default	0.0	0.0	0.0	0.0	0.0	1.0e+20	0.0	

Card 4 is repeated for each plane (maximum 3 planes)

Table 4-4: Variables on Jointed Rock model (Livermore Software Technology Corporation (LSTC) 2013)

Variable	Description
MID	Material identification
RO	Mass density
GMOD	Shear modulus
RNU	Poisson's ratio
RKF	Failure surface shape parameter
PHI	Angle of friction (radians)
CVAL	Cohesion
PSI	Dilation angle (radians)
STR_LIM	Minimum shear strength of material is given by STR_LIM*CVAL
NPLANES	Number of joint planes (maximum 3)
ELASTIC	Flag = 1 for elastic behavior only
LCCPDR	Load curve for extra cohesion for parent material (dynamic relaxation)
LCCPT	Load curve for extra cohesion for parent material (transient)
LCCJDR	Load curve for extra cohesion for joints (dynamic relaxation)
LCCJT	Load curve for extra cohesion for joints (transient)
LCSFAC	Load curve giving factor on strength vs time
GMODDP	Depth at which shear modulus is correct
PHIDP	Depth at which angle of friction is correct
CVALDP	Depth at which cohesion is correct

Table 4-4 continued

Variable	Description
PSIDP	Depth at which dilation angle is correct
GMODGR	Gradient at which shear modulus increases with depth
PHIGR	Gradient at which angle of friction increases with depth
CVALGR	Gradient at which cohesion increases with depth
PSIGR	Gradient at which dilation angle increases with depth
<i>DIP</i>	Angle of the plane in degrees below the horizontal
<i>DIPANG</i>	Plan view angle (degrees) of downhill vector drawn on the plane
<i>CPLANE</i>	Cohesion for shear behavior on plane
<i>PHPLANE</i>	Friction angle for shear behavior on plane (degrees)
<i>TPLANE</i>	Tensile strength across plane (generally zero or very small)
<i>SHRMAX</i>	Max shear stress on plane (upper limit, independent of compression)
<i>LOCAL</i>	DIP and DIPANG are with respect to the global or local axes

The elastic parameters in both models is defined from the theory of elasticity. Shear modulus and Bulk modulus are obtained from Young's modulus and poisson's ratio via Equation 4-3 and Equation 4-4. In this study, Poisson's ratios are considered 0.35 and 0.49 for granular and clay material, respectively.

Equation 4-3

$$G = \frac{E}{2(1-\nu)}$$

Equation 4-4

$$K = \frac{E}{3(1-2\nu)}$$

where:

G = Shear modulus

K = Bulk modulus

E = Young's modulus

ν = Poisson's ratio

Steel (Piecewise Linear Plasticity)

“PIECEWISE_LINEAR_PLASTICITY” (MAT 024) was used for steel material in the LS-DYNA model. The material is elasto-plastic with an arbitrary stress versus strain curve and arbitrary strain rate dependency can be defined. The yield criterion is based on von Mises in addition to capability of modeling the hardening behavior by using a hardening term in yield stress (σ_y).

$$\sigma_y = \beta[\sigma_0 + f_h(\varepsilon_{eff}^p)]$$

where the hardening function $f_h(\varepsilon_{eff}^p)$ can be specified in tabular form as an option.

Table 4-5 and Table 4-6 present the Piecewise Linear Plasticity model input parameters and description of each one.

Table 4-5: Material cards for Piecewise Linear Plasticity model (Livermore Software Technology Corporation (LSTC) 2013)

Card1	1	2	3	4	5	6	7	8
Variable	MID	RO	E	PR	SIGY	ETAN	FAIL	TDEL
Type	A8	F	F	F	F	F	F	F
Default	none	none	none	none	None	0	1.00E+21	0
Card2	1	2	3	4	5	6	7	8
Variable	C	P	LCSS	LCSR	VP	LCF		
Type	F	F	F	F	F	F		
Default	0	0	0	0	0	0		
Card3	1	2	3	4	5	6	7	8
Variable	EPS1	EPS2	EPS3	EPS4	EPS5	EPS6	EPS7	EPS8
Type	F	F	F	F	F	F	F	F
Default	0	0	0	0	0	0	0	0

Table 4-6: Variables in Piecewise Linear Plasticity model (Livermore Software Technology Corporation (LSTC) 2013)

Variable	Description
MID	Material identification
RO	Mass density
E	Young's modulus
PR	Poisson's ratio
SIGY	Yield stress
ETAN	Tangent modulus, ignored if (LCSS.GT.0) is defined.
FAIL	Failure flag. LT.0.0: User defined failure subroutine, matusr_24 in dyn21.F, is called to determine failure EQ.0.0: Failure is not considered. This option is recommended if failure is not of interest since many calculations will be saved. GT.0.0: Effective plastic strain to failure. When the plastic strain reaches this value, the element is deleted from the calculation.
TIDEL	Minimum time step size for automatic element deletion.
C	Strain rate parameter, C
P	Strain rate parameter, P
LCSS	Load curve ID defining effective stress versus effective plastic strain.
LCSR	Load curve ID defining strain rate scaling effect on yield stress.
VP	Formulation for rate effects: EQ.-1.0: Cowper-Symonds with deviatoric strain rate rather than total, EQ.0.0: Scale yield stress (default) EQ.1.0: Viscoplastic formulation
LCF	The equivalent plastic strain for failure may be specified with either a load curve or a table. (for heat affected zones)
EPS1-EPS8	Effective plastic strain values
ES1-ES9	Corresponding yield stress values to EPS1 - EPS8

Pile, soil and vehicle numerical models

Pile part

The pile in all the simulations is tubular (circular) with different diameter and wall thickness. The 4-node Belytschko-Tsay shell element, with 4 Gauss integration points

through the thickness, was selected for the pile part. This element type is appropriate for cases where the bending stiffness is negligible. The elements sizes are constant in the part with 20.8mm height and 34.3mm width. The Piecewise Linear Plasticity material model is set for the pile.

Soil part

The soil part is meshed with block constant stress solid element. The mesh size on the x-y plane varies based on the distance from the pile and remains constant in depth (z direction). The minimum size is in the neighborhood the pile with 25mm×25mm×20.8mm (xyz) and the maximum size is at the corner of the soil box with 100mm×100mm×20.8mm (xyz) dimension. The size of elements changes gradually in the model, and there is no element with dimensions ratio of more than 5. The box size differs relative to pile embedment depth, the depth of the box is 0.5 m more than the embedment depth of the pile. However, based on trial and error the width and length of the box were selected as 3600mm and 5500mm, respectively, so that the failure zone in the soil remains untouched with the boundary of the box. Figure 4-3 and Figure 4-4 display the model mesh of the soil and pile parts.

The pile is coupled with the soil by using `CONSTRAINED_LAGRANGE_IN_SOLID` card that allows coupling between the edge of a shell part or part set and one or more solid groups. In this option the user does not need to match the nodes position of the pile to the soil's nodes. One of the applications of this method is to embed steel rebars into a concrete beam in order to model reinforced

concrete elements. In order to remove the tension strength behind the post for clay a failure pressure is defined in the material model.

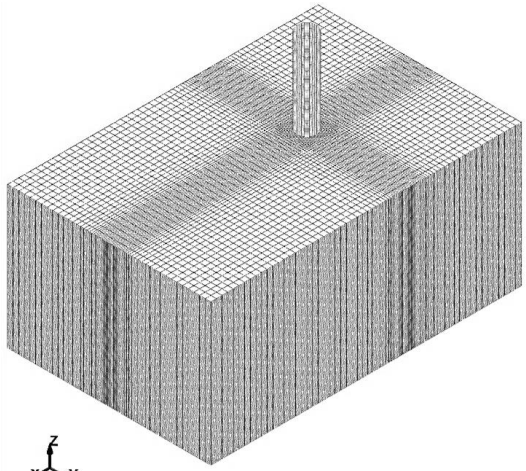


Figure 4-3: Soil and pile element mesh

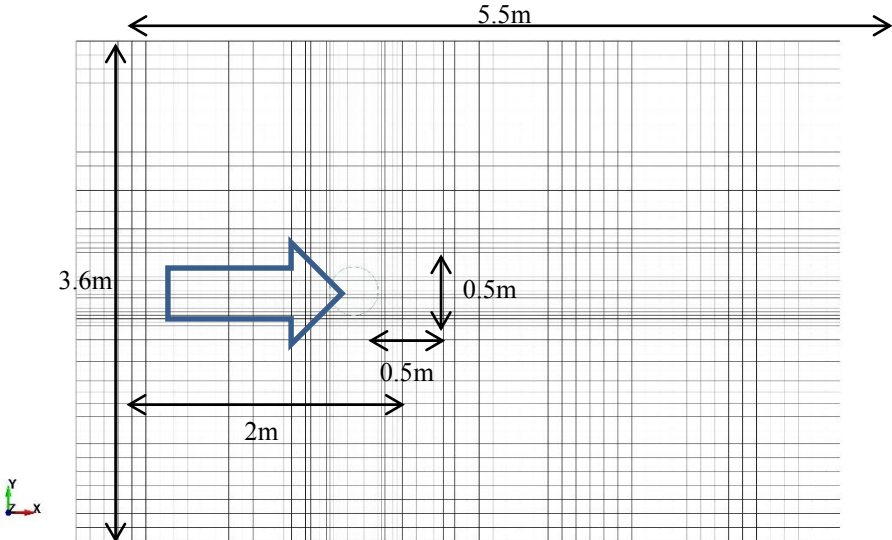


Figure 4-4: Soil model's mesh pattern and dimension in x-y plane

Vehicles models

Three types of vehicles were used in this study: Single-unit flatbed truck, Chevrolet C2500 Pickup, and Geo Metro. The single unit flatbed truck model has been built by Roadside Safety division of the Texas Transportation Institute at Texas A&M University. The Chevrolet C2500 Pickup and Geo Metro vehicle finite element models have been developed by The National Crash Analysis Center (NCAC) of The George Washington University under a contract with the FHWA and NHTSA of the US DOT.

Medium duty truck part

The medium duty truck is modeled by the single unit flatbed truck with 25123 (160 beam, 3228 mass, 20201 shell, 1534 solid) elements. Mass of the model is 6835 kg and 4 types of materials are used in the model. Some features of the original model were modified including contact properties and thickness of main frame of vehicle. The vehicle model is designed for the purpose of roadside safety and it shows some major misbehavior in large deformations and severe impacts. At the time of preparation of this research a project was ongoing to build another finite element model of the medium duty truck compatible for extreme impact with large deformations. The M50 test truck and finite element model of Medium duty truck are shown in Figure 4-5. Height of the concentrated load on the pile from this vehicle is 0.85m above the ground.

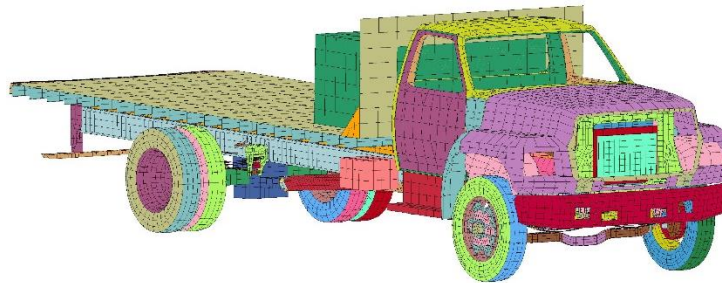


Figure 4-5: Vehicle for M50 impact test and finite element model for numerical simulation

Pickup truck part

A Chevrolet C2500 Pickup model was used as the Pickup truck (P designation in ASTM F2656). The original model has 58372 (163 beam, 83 mass, 54565 shell, and 3561 solid) elements with total mass of 2013 kg. Some features such as the mass of vehicle (to match the PU60 test truck specification) and hourglass parameters were modified in the model. The PU60 test truck and finite element model of Chevrolet C2500 Pickup are shown in Figure 4-6. Height of concentrated load on pile from this vehicle is 0.75m above the ground.

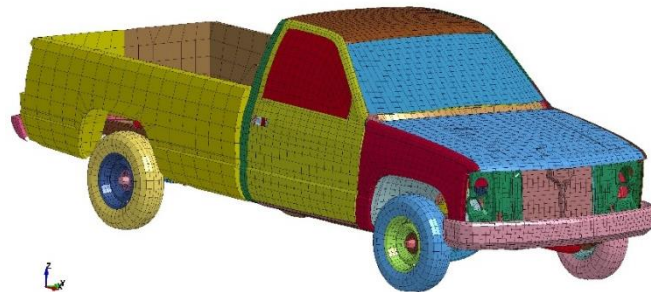


Figure 4-6: Vehicle for PU60 impact test and finite element model for numerical simulation

Very small passenger car part

A Geo Metro finite element model with 808 kg mass and 16260 (4 beam, 133 mass, 15294 shell, 820 solid) elements was used as a very small passenger car in the simulation. However, the mass is less than ASTM F2656 criterion, 1100 kg for small passenger car, for C vehicle type. Due to the significant difference between the mass of C vehicle type and the model, and because changing the mass in the model may cause instability, the original model was used in the simulations. The finite element model of Geo Metro is presented in Figure 4-7. The Height of the concentrated load on the pile from this vehicle is 0.7m above the ground.



Figure 4-7: Geo Metro finite element model

Other model features

A penalty-based contact “AUTOMATIC_NODES_TO_SURFACE” with friction factor of 0.075 was used for the contact between the vehicles and the pile. A horizontal rigid wall was designed at the level ground for the support of vehicle wheels. Boundary conditions for soil in the simulations are $x=y=0$ for perimeter area, and $x=y=z=0$ for the bottom of the soil box.

Initializing

The soil part was initially simulated under gravity loading. The initialing is necessary only for pressure dependent material. However, gravity initializing was done prior to all the simulations. In order to reduce the bouncing behavior of soil and pile a global damping was applied to the model during the gravity application. Figure 4-8 displays the vertical stress due to the gravity initializing on the soil box model. The output results of initialization were used as the input initial stress and strain in the main simulations.

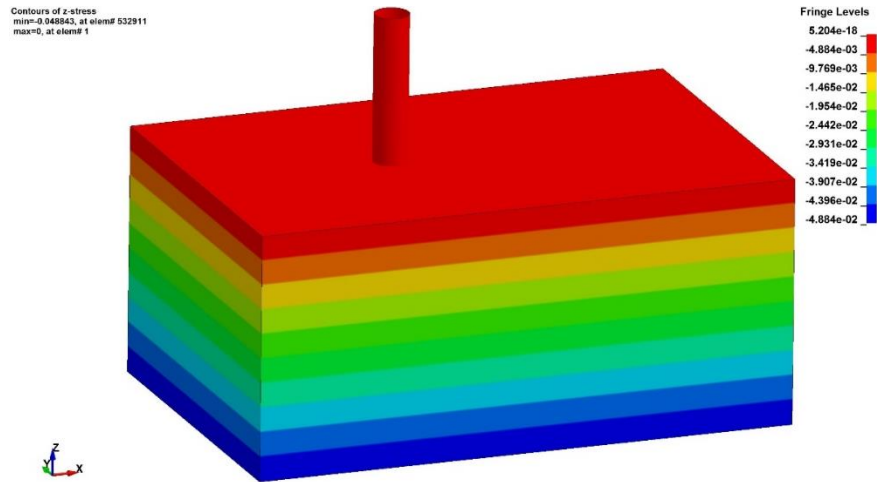


Figure 4-8: stress in z direction for initialized soil box under gravity load

Hourglass

Hourglass (HG) modes are nonphysical, zero-energy modes of deformation that produce zero strains and no stresses. Hourglass modes occur only in reduced-integrated (single integration point) solid, shell, and thick shell elements.

LS-DYNA has various algorithms for inhibiting hourglass modes. The first algorithm (type 1), while the cheapest, generally not the most effective algorithm is normally used in regular simulations (LS-DYNA support 2013).

A way to entirely eliminate hourglass concerns is to use fully-integrated element formulations with or selectively reduced (S/R) integration. There can be a downside to this approach. For example, Type 2 solids are much more computationally and timely expensive than the single point default solid. Secondly, they are much more unstable in large deformation applications due to the possibility of element distortion (negative volumes or negative Jacobian much more likely). Third, the type 2 solids may behave too

stiffly in applications where the element shape is poor because they have some tendency to 'shear-lock' (LS-DYNA support 2013).

To evaluate hourglass energy, the nonphysical HG energy must be small relative to internal energy for each part (<10% as a rule-of-thumb) (LS-DYNA support 2013). In this study the option of “Flanagan-Belytschko stiffness form with exact volume integration for solid elements” was used for Hourglass control. In addition to Hourglass energy control, other controls including sliding energy and contact time steps are also needed to be checked for each simulation.

Simulation calibration

The purpose of the calibration is to find the soil properties correlation and use the correlation to perform extra numerical simulations. The correlation is based on pressuremeter test results and soil density as soil properties, however the correlation can be made for the other in-situ or lab tests through the PMT relationship to the particular soil test. In order to calibrate the finite element model against the experiments, a set of a simulations for PU60 and M50 tests were conducted. Due to the numerical difficulty in finite element analysis for very large deformations and unavailability of proper finite element model for the used bogie in the experiments, we could not calibrate the model against medium scaled tests. The pile displacement and bending moment on pile at the level ground from the experiments were used in LS-DYNA model calibration.

PU60 calibration

The PU60 test was performed with the Pickup truck vehicle with speed of 60 mph (97 kph) hit single pile with 2m embedment in hard clay. 16 full simulations were initially conducted to calibrate the finite element model and material parameters. Several features including material strength, failure pressure, modulus of elasticity, contact friction factor, soil density, and size of soil box were investigated in the simulations. The finite element model of the PU60 test is shown in Figure 4-9.

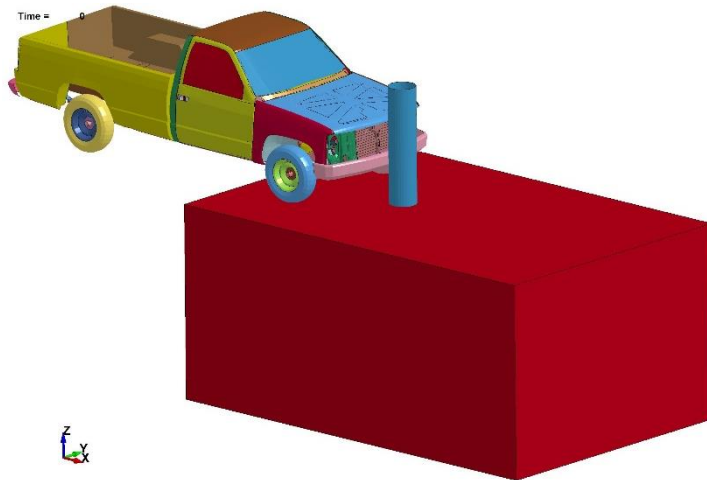


Figure 4-9: PU60 finite element model in LS-DYNA

After the trial simulations the final model parameters were selected according to Table 4-7. The units in the table are 1000kg/mm^3 for mass density and MPa for stresses. The yield stress parameter in the material model for soil is calculated from limit pressure in PMT by Equation 4-5 (Briaud 1992). Shear modulus and bulk modulus are obtained from modulus (E) in the PMT, assuming $\nu=0.49$ and using Equation 4-3 and Equation 4-4.

According to calibration simulations and Lim's (2011) study, the failure pressure is estimated $-0.5\sigma_y$.

Equation 4-5

$$\sigma_y = 2s_u = 2 \times 0.67(p_L)^{0.75}$$

Table 4-7: Hard clay model parameter in LS-DYNA for PU60 test

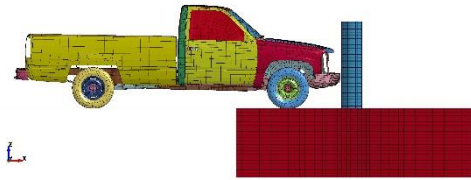
Variable	Mass density	Shear modulus	Yield stress	Plastic hardening modulus	Bulk modulus
Default	2.1E-9	6.71	0.29	0	333.33
Variable	Failure pressure	Element erosion option	dt for element removal		
Default	-0.145	1	0.0		

32 CPUs with 88 Gigabit allocated Ram were used to simulate the model. The initial time step for the simulation was $7E-7$ sec and 550 cpu-hours were spent for simulating 0.5 sec of the impact. Figure 4-10 compares the PU60 simulation result with the full scaled test result for different times. Table 4-8 presents the important results comparison between test and simulation. Figure 4-11, Figure 4-12, and Figure 4-13 show the displacement-time, Load-time, and Load-displacement comparison curves for experiment and LS-DYNA simulation.

Table 4-8: PU60 experiment and simulation results comparison

Quantities	Experiment	Simulation	Difference
Displacement (mm)	830	778	-6.2%
Rotation (degree)	23	20	-13%
Equivalent load (kN)	440	490	11.4%

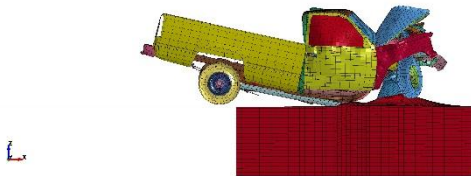
LS-DYNA keyword deck by LS-PrePost
Time = 0.000



t= 0 sec



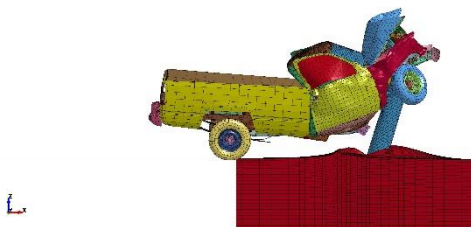
LS-DYNA keyword deck by LS-PrePost
Time = 0.125



t= 0.125 sec



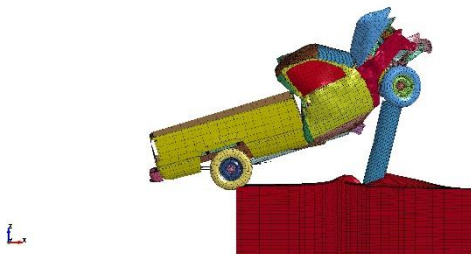
LS-DYNA keyword deck by LS-PrePost
Time = 0.250



t= 0.25 sec



LS-DYNA keyword deck by LS-PrePost
Time = 0.375



t= 0.375 sec



Figure 4-10: Finite element LS-DYNA simulation versus full scale test for PU60 test

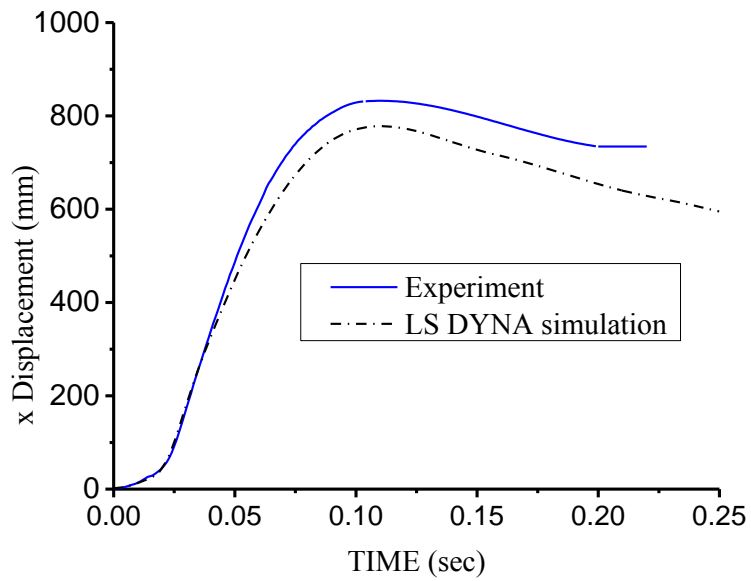


Figure 4-11: Pile displacement comparison between experiment and simulation

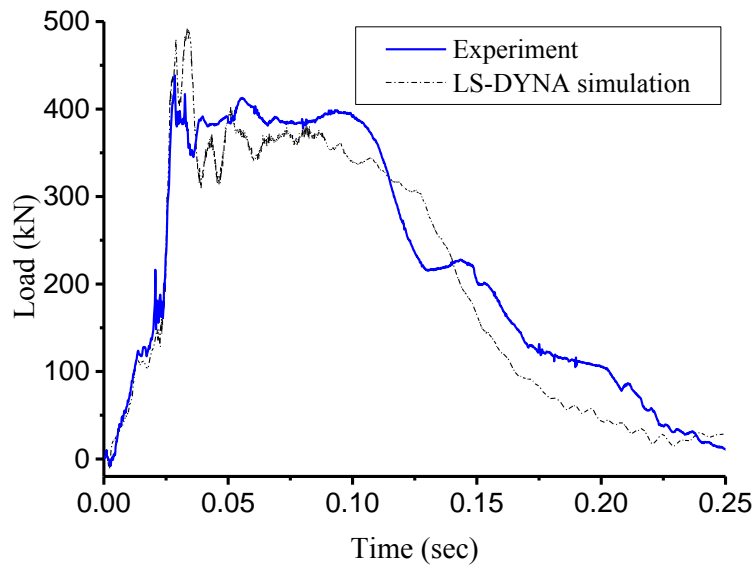


Figure 4-12: Equivalent impact load comparison between experiment and simulation

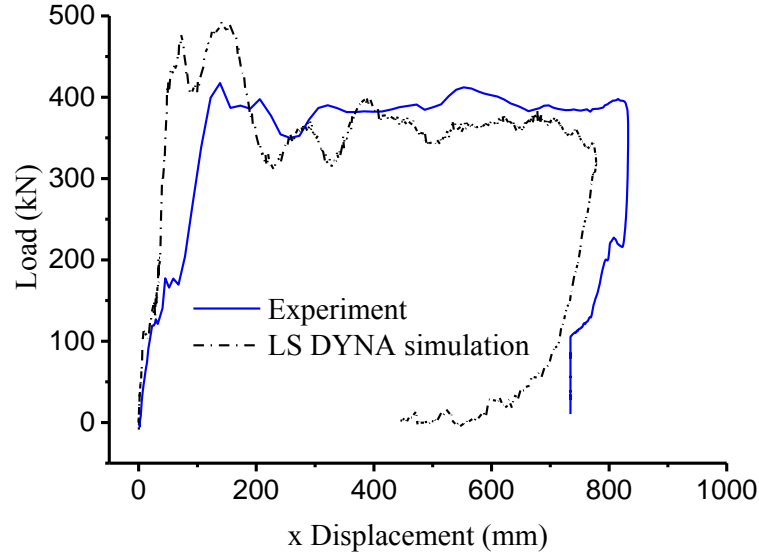


Figure 4-13: Load-Displacement comparison between experiment and simulation

M50 calibration

The M50 test was performed with medium duty truck with 50 mph (80 kph) on 3m embedded single pile in very dense crushed limestone. The test was a replica of the K-12 (M50) test in Lim’s (2011) study with an extension in height of the pile to capture the deformation. Several iterations were made in order to calibrate the numerical model (Figure 4-14). Because the shaft does not fail during the impact, the engine is stuck in its place (Figure 4-15) while in the experiment the shaft was broken and engine moved backward (Figure 4-16). The misbehavior of the elements in the numerical model causes a higher peak load on the pile due to the engine impact. As a result the pile deforms and bends extremely more in order to absorb the impact energy. A solution for this problem is to modify and re-mesh the truck model that was under developing by TTI Roadside Safety division meanwhile this study was ongoing. Another solution is to erode the failed

elements in the shaft part which did not work because of instability of the model after the eroding.

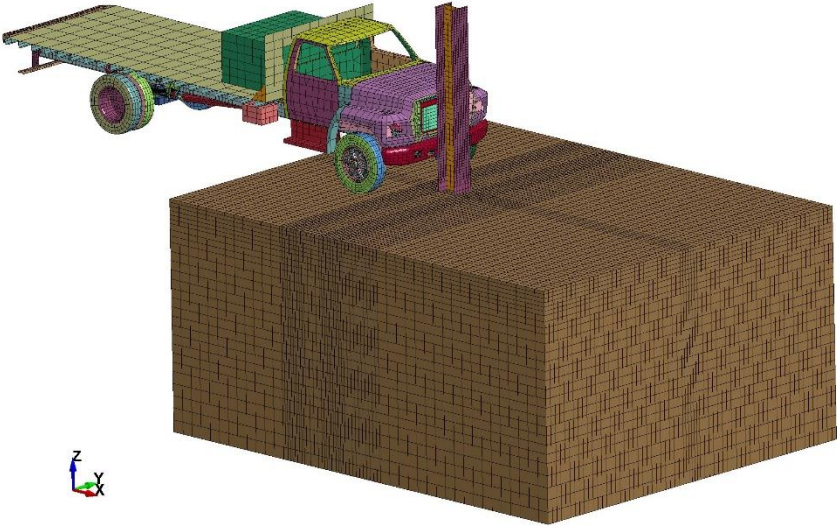


Figure 4-14: M50 test numerical model

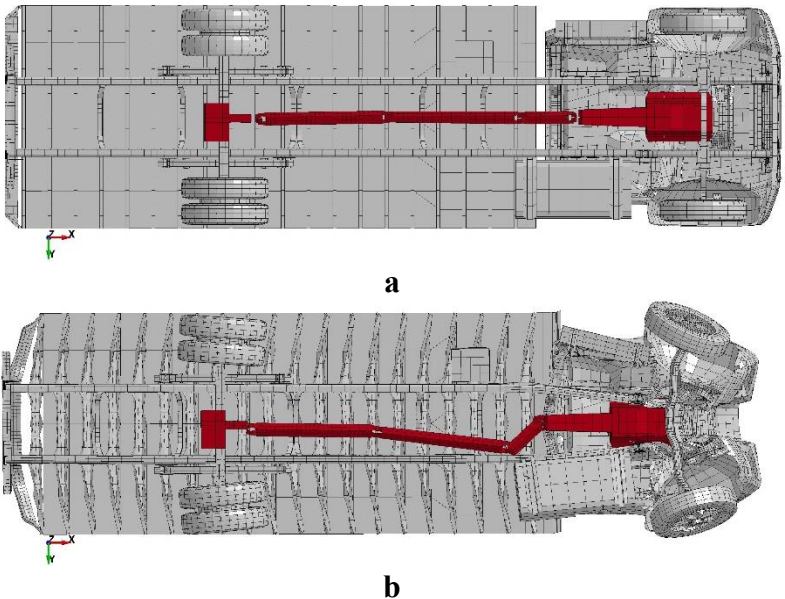


Figure 4-15: Shaft deformation during the impact in numerical model a) before the impact, b) after the impact



Figure 4-16: Broken shaft in the M50 test

Figure 4-17 and Figure 4-18 show the displacement and load comparison between experiment and LS-DYNA simulation. As it can be seen in these figures at $t=0.038$ sec a peak load happens that makes a yield point on the pile. After this time the slope of displacement changes significantly and maximum displacement reaches up to 1300 mm.

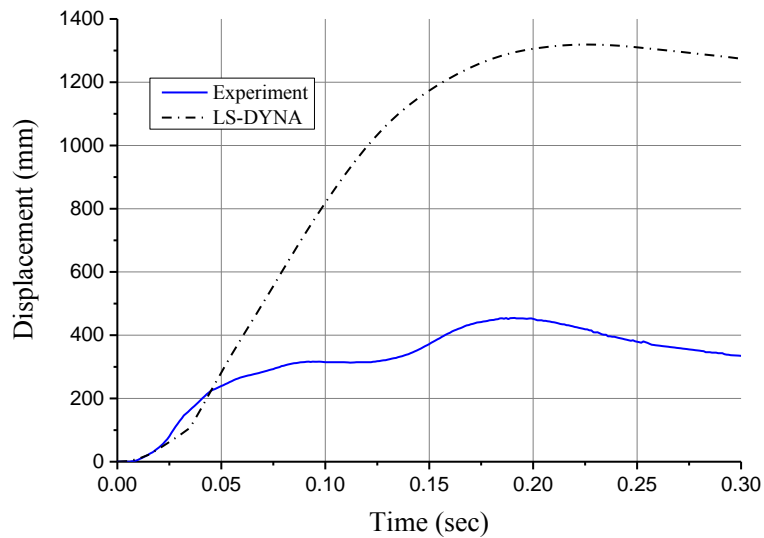


Figure 4-17: Displacement comparison between experiment and simulation for M50 test

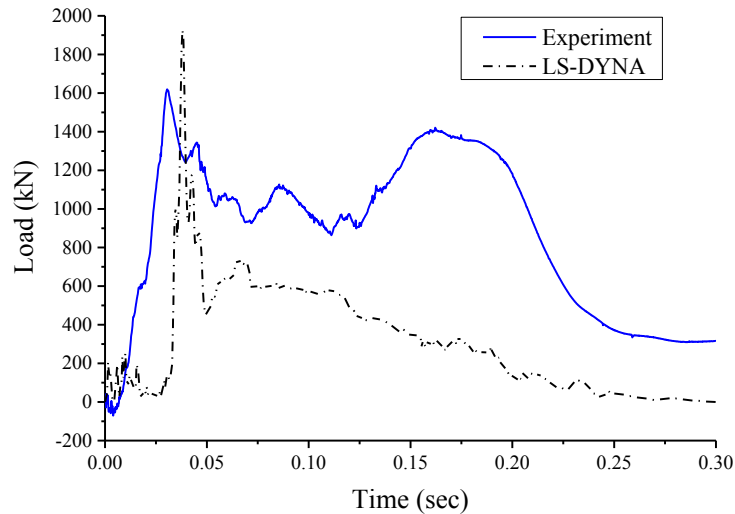


Figure 4-18: Load comparison between experiment and simulation for M50 test

Verifying simulations

In order to verify the simple model for pile analysis under lateral impact, we designed and performed a set of simulations. The simulation features were selected by using the experimental designed method to cover the parameters in the best way. The vehicles used in these simulations are very small passenger car (Geo Metro) and Pickup truck (Chevrolet C2500). The simulations were conducted in both granular (Drucker Prager material) and clayey (Von Mises material) soil with pile embedment range 2 to 3.5 meters.

Experimental design

An experimental design is a process that organizes and selects the suitable experiments' parameters to ensure that enough amount of data and proper type are produced to test a hypothesis. In this study the space filling technique with Stratified Latin Hypercube Sampling (SLHS) design type was used. Space-filling designs are used when there is few information about the factors effects on responses. The method does not

assume a particular model form and the aim of this technique is to spread the points randomly as evenly as possible.

Latin hypercube sampling is a statistical form of sampling developed by McKay et al. (1979, 239-245). The stratified option of this method was used to set the parameters in definite levels. The Points were selected in order to minimize the Root Mean Square (RMS) variation of the Cumulative Distribution Function (CDF) from the ideal CDF.

Table 4-9 lists the design parameter stratum used in the experimental design for LS-DYNA simulations. We categorized the soil into 5 classes according to soil strength for both sand and clay. Soil properties including undrained shear strength (s_u) for clay (Table 4-10), friction angle (ϕ), cohesion (c), dilation angle (ψ) for sand (Table 4-11) and modulus of elasticity (E) for both soil types were chosen based on strength level.

Table 4-9: Virtual experiment parameters used in experimental design

Property	Range	number of stratum
Soil strength	Clay: soft- very hard (Table 4 10) Sand: loose- very dense (Table 4-11)	5
Pile embedment depth	2m-3.5m	4 (0.5m step)
Vehicle mass	808 kg and 2013 kg	2
Vehicle speed	40 mph-60 mph	3 (10 mph step)

Table 4-10: Soil strength classification and properties of each class for clay

Clay type	p _L (kPa)	s _u (kPa)	E (Mpa)
Soft	300	50	5
Medium soft	800	100	10
Medium	1300	150	15
Hard	2000	200	20
Very hard	+2500	250	25

Table 4-11: Soil strength classification and properties of each class for sand

Sand type	p _L (kPa)	φ	ψ	c (kPa)	E (MPa)
Loose	400	35	0	5	5
Medium loose	700	35	10	10	10
Medium	1100	40	10	20	15
Dense	1700	40	12	30	20
Very dense	+2500	40	15	40	30

24 virtual experiments for clayey soil and 23 virtual experiments for granular soil were designed. All the simulations were done on a pile with circular section with two diameters of 0.2m and 0.35m. The diameter of the pile was selected relative to soil strength and pile size to have reasonable deformation in soil. The soil density for all the simulation was assumed to be 2100 kg/m³.

Virtual experiment data

Three major outputs were measured from designed simulations: Maximum displacement at impact point, Maximum rotation of pile at impact point, Maximum equivalent dynamic load applied at impact point. Table 4-12 presents the 47 designed virtual experiments and the results. The results are used for calibrating the simple model in the next section.

Table 4-12: Virtual experiments specifications and results

Soil type	Embedment depth (m)	Mass (kg)	V (Mph)	B (m)	Max displacement (m)	Max rotation (degree)	Max load (kN)	
Clay	Medium soft	2	808	50	0.35	0.49	13	190
	Medium	2	808	40	0.35	0.19	5	170
	Medium	2	2013	40	0.35	0.49	12.9	391
	Medium	2	808	50	0.35	0.27	7.2	200
	Medium	2	2013	50	0.35	0.68	17.6	400
	Medium	2	808	60	0.35	0.37	9.3	205
	Hard	2	808	50	0.2	0.33	8.9	200
	Medium soft	2.5	808	50	0.35	0.39	8	290
	Medium	2.5	2013	60	0.35	0.66	15.1	680
	Hard	2.5	808	60	0.35	0.17	3.9	420
	Very hard	2.5	808	40	0.2	0.11	3.2	214
	Very hard	2.5	2013	50	0.35	0.33	7.6	710
	Soft	3	808	60	0.35	0.63	12	414
	Medium	3	2013	40	0.35	0.28	6	610
	Medium	3	2013	50	0.35	0.42	8.8	668
	Medium	3	808	60	0.35	0.22	4.6	425
	Medium	3	808	40	0.2	0.17	4.1	180
	Medium	3	808	40	0.35	0.1	2.1	280
	Medium	3	2013	60	0.35	0.54	11.6	720
	Hard	3	808	50	0.2	0.19	4.8	240
	Soft	3.5	2013	60	0.35	1.2	21.7	630
	Medium soft	3.5	2013	40	0.35	0.4	7.2	665
	Medium	3.5	2013	40	0.35	0.27	5.1	690
	Very hard	3.5	2013	40	0.35	0.14	2.9	770
Sand	Medium Loose	2	808	50	0.35	0.58	14.9	182
	Medium	2	808	40	0.35	0.22	6	168
	Medium	2	2013	40	0.35	0.56	14.6	455
	Medium	2	808	50	0.35	0.32	8.6	240
	Medium	2	2013	50	0.35	0.75	19.6	426
	Medium	2	808	60	0.35	0.38	10.4	214
	Dense	2	808	50	0.2	0.34	9.3	210
	Medium Loose	2.5	808	50	0.35	0.41	9.3	257
	Medium	2.5	2013	60	0.35	0.72	16.3	666
	Very dense	2.5	808	60	0.35	0.28	6.3	357
	Very dense	2.5	808	40	0.2	0.13	3.5	200
	Very dense	2.5	2013	50	0.35	0.3	6.9	733
	Loose	3	808	60	0.35	0.6	11.7	425
	Medium	3	2013	40	0.35	0.35	7.2	600
	Dense	3	2013	50	0.35	0.35	7.2	660
	Medium	3	808	60	0.35	0.24	4.8	428
	Dense	2	808	40	0.2	0.3	9.6	170
	Medium	3	808	40	0.35	0.13	2.8	285
	Very dense	3	808	50	0.2	0.2	5	257
	Loose	3.5	2013	60	0.35	1.1	20	650
	Medium Loose	3.5	2013	40	0.35	0.43	7.6	640
	Medium	3.5	2013	40	0.35	0.29	5.5	610
	Very dense	3.5	2013	40	0.35	0.15	2.9	784

5. ANALYTICAL MODEL

The expensive current LS-DYNA simulation solution in terms of time, license cost, and complexity led us to develop a simple approach for analyzing single piles under lateral impact. The purpose of this part of the study is to develop a simple and fast computer program to analyze the behavior of a single post under a truck impact for any soil type, any truck mass, and velocity and any post size. The output contains the information needed for the user to design a single post under specific impact from a truck while showing the anticipated displacement and inclination of the post during impact.

Smith (1960, 35-61) introduced a simple solution for pile-driving analysis by using the wave equation and a simple model for the soil in order to estimate the pile drivability, the pile stresses, and the pile capacity. In the case of lateral dynamic loading, the modeling of the post and soil is more complicated. Ghazzaly et al (1976, 363-368) introduced an approximate, rational approach for the analysis of a vertical post subjected to low-amplitude, surface, lateral vibrations. The concept of a beam on elastic foundation in an elastic half-space was used in the development of the proposed method.

Plassiard & Donzé (2009, 759) used a discrete element model to reproduce both quasi-static and dynamic behavior of granular material under massive boulder falling impact. They showed that using the main quasi static properties of soil is not sufficient for modeling the behavior in dissipation of energy and a complementary dissipative laws should be considered into the contact model.

Maxwell and Kelvin-Voigt (Figure 5-1) are the most basic models that are being used for material behavior under dynamic loads as viscoelastic materials. The Maxwell model,

a combination of a dashpot (plasticity element) and a spring (elasticity element) in a row can be used to present effects of shear stress or strain on viscoelastic fluid materials occurring in nature, e.g. dispersions. Viscoelastic solids, which show a complete recovery have an analogous in a parallel combination of a dashpot and a spring (Kelvin Voigt model). Gels and soils with water contents and texture (clayey, silty) may be an example for this model. (Markgraf, Horn, and Peth 2006, 1-14)

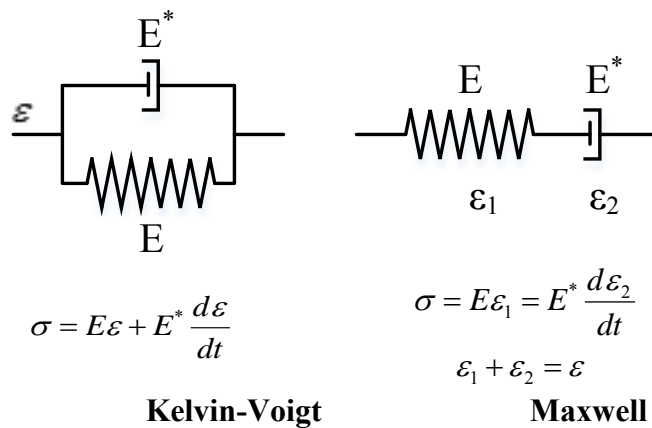


Figure 5-1: Kelvin-Voigt and Maxwell material models

After Smith other scholars have been made some modifications on the model by adding or relocating the springs and dashpots (Figure 5-2). As an example Randolph (2000, 3-11) made some modifications on the Smith's model by separating the viscous and inertia behavior of model (Figure 5-3).

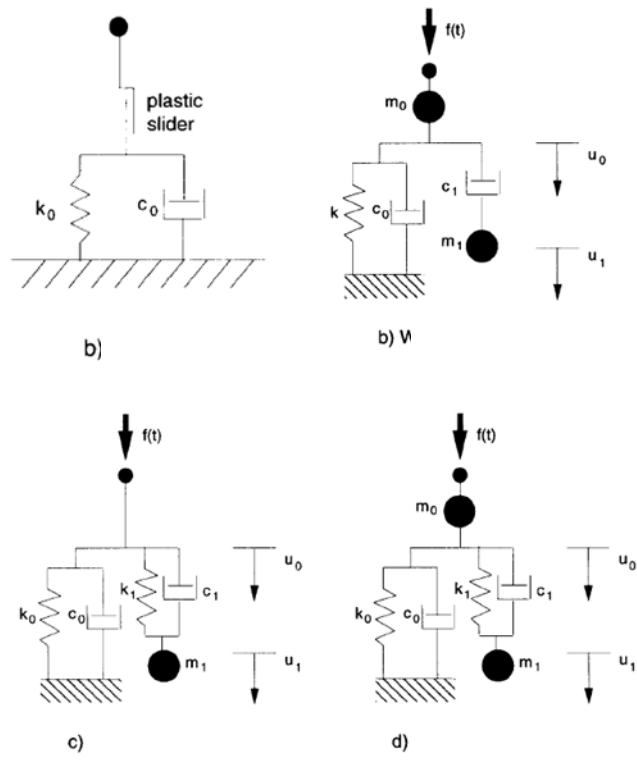


Figure 5-2: Material models for soil behavior under dynamic load (Deeks and Randolph 1995, 307-329)

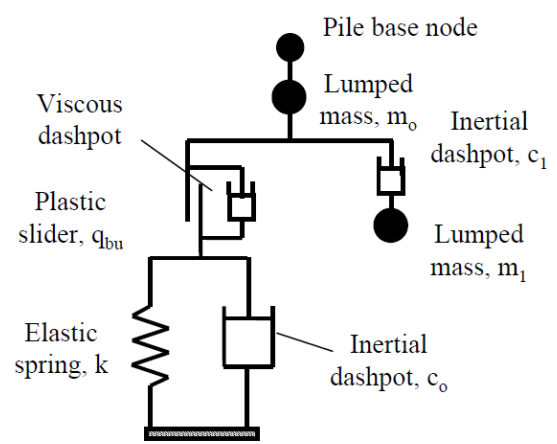


Figure 5-3: Soil model for pile-soil interaction (Randolph 2000, 3-11)

Even though these models can predict the behavior of the pile under dynamic load, the parameters calibration is difficult and improper calibrating causes more error in behavior estimation. Using simple models results in a limited number of parameters to be calibrated and less calculation effort in a system analysis. In this section the behavior of two basic simple models subjected to an impact are investigated and compared with one of the experiments then the theory of suggested pile-soil model is discussed. Then the parameters sensitivity analysis is studied. Finally, the parameters of the model are explained and calibrated against the experiments and simulations described in pervious sections.

Model theory

Soil material model

Two viscoelastic basic material models, Kelvin-Voigt and Maxwell, were selected for investigating a suitable model for soil under impact loading. For both of these models the inertia effect is added in the equations, which is shown by a lumped mass. In order to model soil failure, the soil in this study was assumed to be elastic-perfectly plastic.

Writing the governing equation for each model gives us Partial Differential Equations (PDE) that cannot be solved with ordinary methods. The Finite Difference method with the explicit approach is one of the simplest methods to solve this PDE. By using central difference formulas and applying boundary conditions (initial velocity of striking mass) we will have a step forward solution for the equation. This method is simple enough that it can be coded in Microsoft Office Excel (Mirdamadi et al. 2012, 2227-2233).

The result from single degree of freedom of two material models are compared with test P1 in Figure 5-4 and Figure 5-5. As can be seen from the outputs the Kelvin-Voigt model shows a better prediction than the Maxwell model. The Maxwell model cannot generate the peak in the acceleration; also the maximum load from this model is equal to the minimum resistance of the damper and the spring. Therefore this resistance is at most equal to the static resistance. For the Kelvin Voigt model on the other hand the resistance from the damper and the spring sum up, so the model gives us more resistance than static. Based on the SDOF model the modified Kelvin-Voigt model is selected for the soil material model (Mirdamadi et al. 2012, 2227-2233).

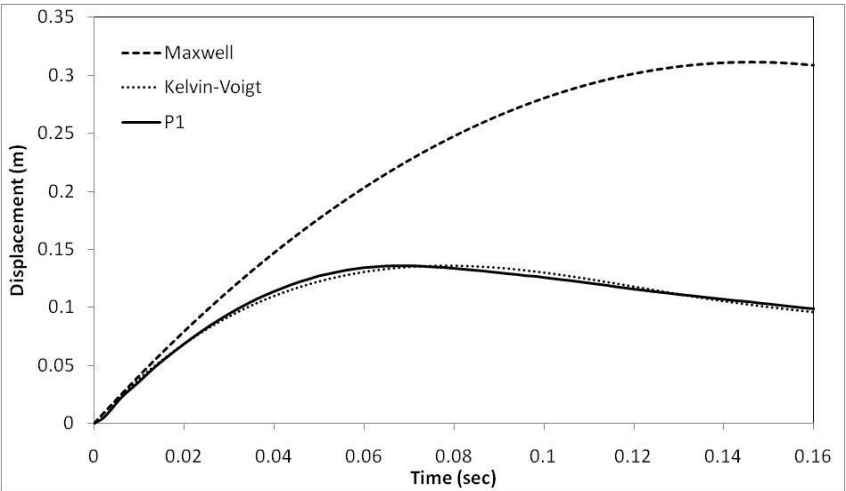


Figure 5-4: Displacement result from the Maxwell and the kelvin-Voigt model and comparison with P1 test (Mirdamadi et al. 2012, 2227-2233)

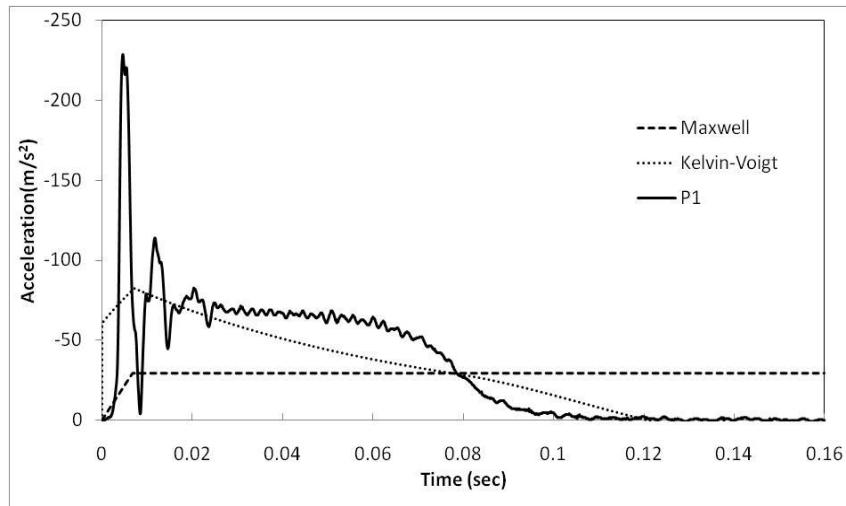


Figure 5-5: Acceleration result from the Maxwell and the kelvin-Voigt model and comparison with P1 test (Mirdamadi et al. 2012, 2227-2233)

Pile-soil model

An *Euler–Bernoulli* beam (Equation 5-1) supported by a simple soil model is used to model a vertical single pile embedded in soil. The beam model is perfectly elastic and the soil model is an extended version of the Kelvin-Voigt spring and dashpot model; it contains a spring with elastic perfectly plastic behavior, a parallel dashpot with linear viscosity behavior, and a mass for inertia effect (Figure 5-6). In the model the lumped masses attached to pile denote the both soil and pile inertia. The equation of motion of post is developed by considering the force equilibrium on each post's node (Equation 5-1).

Equation 5-1

$$\frac{d^2}{dz^2} \left(EI \frac{d^2 y}{dz^2} \right) = q$$

where:

E: Modulus of elasticity of post material

I: Moment of inertia of the post against bending around the horizontal axis perpendicular to the impact

y : The post horizontal displacement at a depth z and a time t

Equation 5-2

$$M \frac{\partial^2 y}{\partial t^2} + C \frac{\partial y}{\partial t} + Ky = F$$

where:

M : Mass per unit of length (post plus associated soil mass) in kg/m or N.s²/m²

C : Damping of the system per unit of length in kg/m.s or N.s/m²

K : Spring stiffness per unit of length kg/m.s² or N/m²

F : The force per unit length of post at a depth z and a time t

Combining Equation 5-1 and Equation 5-2 leads to the governing partial differential equation for the problem (PDE):

$$EI \frac{\partial^4 y}{\partial z^4} + M \frac{\partial^2 y}{\partial t^2} + C \frac{\partial y}{\partial t} + Ky = 0 \quad \text{or} \quad EIy'''' + M\ddot{y} + C\dot{y} + Ky = 0$$

Equation 5-3

In order to solve this PDE, the Central Finite Difference with an explicit method is selected as one of the simplest and most efficient approaches. The Explicit method calculates the state of a system at a later time from the state of the system at the current time. The post is divided in finite elements with a height h and the central difference formulas are chosen for stability. Then the PDE becomes:

$$EI \left(\frac{y_{i+2,j} - 4y_{i+1,j} + 6y_{i,j} - 4y_{i-1,j} + y_{i-2,j}}{h^4} \right) + M \left(\frac{\ddot{y}_{i,j+1} - 2\ddot{y}_{i,j} + \ddot{y}_{i,j-1}}{\Delta t^2} \right) + C \left(\frac{y_{i,j+1} - y_{i,j-1}}{2\Delta t} \right) + ky_{i,j} = 0$$

Equation 5-4

Where i is the location-depth index and j is the time index

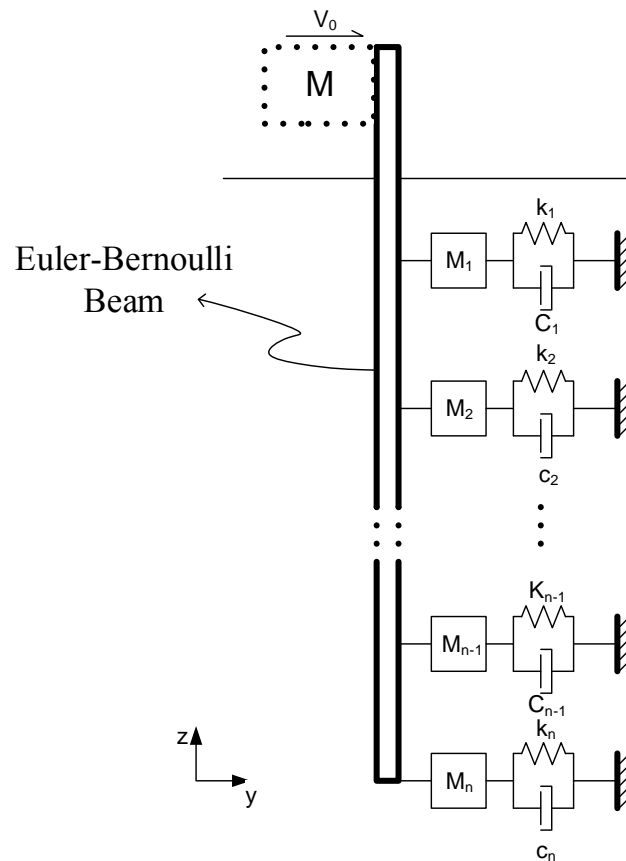


Figure 5-6: Pile-soil interaction model under lateral impact

If we rewrite Equation 5-4 as a function of node displacements including depth and time the result is:

$$(m + c)y_{i,j+1} = -ey_{i-2,j} + 4ey_{i-1,j} - (6e - 2m + k)y_{i,j} + 4ey_{i+1,j} - ey_{i+2,j} + (c - m)y_{i,j-1}$$

Equation 5-5

Where the e, c and m are:

$$e = \frac{EI}{h^4} \quad m = \frac{M}{\Delta t^2} \quad c = \frac{C}{2\Delta t}$$

The boundary conditions for this equation are:

$$V_0 = 0 \Rightarrow \frac{\partial^3 y}{\partial z^3} @ node 0 = 0 \Rightarrow y_{3,j} - 2y_{2,j} + 2y_{0,j} - y_{-1,j} = 0$$

$$M_0 = 0 \Rightarrow \frac{\partial^2 y}{\partial z^2} @ node 0 = 0 \Rightarrow y_{2,j} - 2y_{1,j} + y_{0,j} = 0$$

$$V_n = 0 \Rightarrow \frac{\partial^3 y}{\partial z^3} @ node n = 0 \Rightarrow y_{n+2,j} - 2y_{n+1,j} + 2y_{n-1,j} - y_{n-2,j} = 0$$

$$M_n = 0 \Rightarrow \frac{\partial^2 y}{\partial z^2} @ node n = 0 \Rightarrow y_{n+1,j} - 2y_{n,j} + y_{n-1,j} = 0$$

The initial conditions can be either a load-time history or displacement-time history on any nodes of the post. The impact condition can also be a lumped mass with a given initial velocity applied at the location of impact. In this case $y_{i,-1} = -\Delta t \cdot v_0$ is the initial condition (i is the location of impact node on post) without any other input time history.

Equation 5-5 is written at each node and the final matrix equation is:

$$\begin{pmatrix}
 (m_1+c_1)/2 & 0 & 0 & 0 & 0 & 0 & 0 & \dots \\
 0 & m_2+c_2 & 0 & 0 & 0 & 0 & 0 & \dots \\
 0 & 0 & m_3+c_3 & 0 & 0 & 0 & 0 & \dots \\
 0 & 0 & 0 & m_4+c_4 & 0 & 0 & 0 & \dots \\
 \vdots & \vdots & \vdots & \vdots & \vdots & \vdots & \vdots & \vdots \\
 \vdots & \vdots & \vdots & \vdots & \vdots & \vdots & \vdots & \vdots \\
 \dots & \dots & \dots & \dots & \dots & 0 & m_{n-2}+c_{n-2} & 0 & 0 \\
 \dots & \dots & \dots & \dots & \dots & 0 & 0 & m_{n-1}+c_{n-1} & 0 \\
 \dots & \dots & \dots & \dots & \dots & 0 & 0 & 0 & (m_n+c_n)/2
 \end{pmatrix}
 \begin{pmatrix}
 y_{1,j+1} \\
 y_{2,j+1} \\
 y_{3,j+1} \\
 y_{4,j+1} \\
 \vdots \\
 \vdots \\
 y_{n-2,j+1} \\
 y_{n-1,j+1} \\
 y_{n,j+1}
 \end{pmatrix}
 =$$

$$\begin{pmatrix}
 -e+m_1-k_1/2 & 2e & -e & 0 & 0 & 0 & \dots \\
 2e & -5e+2m_2-k_2 & 4e & -e & 0 & 0 & \dots \\
 -e & 4e & -6e+2m_3-k_3 & 4e & -e & 0 & \dots \\
 0 & -e & 4e & -6e+2m_4-k_4 & 4e & -e & \dots \\
 \vdots & \vdots & \vdots & \vdots & \vdots & \vdots & \vdots \\
 \vdots & \vdots & \vdots & \vdots & \vdots & \vdots & \vdots \\
 \dots & \dots & 0 & -e & 4e & -6e+2m_{n-2}-k_{n-2} & 4e & -e \\
 \dots & \dots & 0 & 0 & -e & 4e & -5e+2m_{n-1}-k_{n-1} & 2e \\
 \dots & \dots & 0 & 0 & 0 & -e & 2e & -e+m_n-k_n/2
 \end{pmatrix}
 \begin{pmatrix}
 y_{1,j} \\
 y_{2,j} \\
 y_{3,j} \\
 y_{4,j} \\
 \vdots \\
 \vdots \\
 y_{n-2,j} \\
 y_{n-1,j} \\
 y_{n,j}
 \end{pmatrix}
 +$$

$$\begin{pmatrix}
 (c_1-m_1)/2 & 0 & 0 & 0 & \dots \\
 0 & c_2-m_2 & 0 & 0 & \dots \\
 0 & 0 & c_3-m_3 & 0 & \dots \\
 0 & 0 & 0 & c_4-m_4 & \dots \\
 \vdots & \vdots & \vdots & \vdots & \vdots \\
 \vdots & \vdots & \vdots & \vdots & \vdots \\
 \dots & \dots & \dots & \dots & \dots \\
 \dots & \dots & 0 & c_{n-2}-m_{n-2} & 0 & 0 \\
 \dots & \dots & 0 & c_{n-1}-m_{n-1} & 0 & 0 \\
 \dots & \dots & 0 & 0 & (c_n-m_n)/2 & 0
 \end{pmatrix}
 \begin{pmatrix}
 y_{1,j-1} \\
 y_{2,j-1} \\
 y_{3,j-1} \\
 y_{4,j-1} \\
 \vdots \\
 \vdots \\
 y_{n-2,j-1} \\
 y_{n-1,j-1} \\
 y_{n,j-1}
 \end{pmatrix}$$

Figure 5-7: Matrix form for governing equations

The result of this method gives us a diagonal matrix for the unknown matrix coefficient which means that we do not need to invert the matrix and therefore the solving process will be very fast. This advantage is very important in the solution of this numerical problem because the solution will not take much computational time and the coding will be simplified (for example with Microsoft Excel). The only issue for this explicit method is that the convergence criterion requires very small time steps. The optimum value of the time step for speed and accuracy cannot be defined by the program, so it is a parameter which has to be input by the user.

Model parameters

The input parameters for each node are the load-displacement function (k), the viscous damping coefficient (C), the associated soil mass contributing to the inertia resistance (m), the bending stiffness (EI), the geometry (length and width) of the post, the number of nodes (n), and the time increment (Δt). The Mass of vehicle (M_T) and vehicle velocity (V_T) are boundary force parameters. Any of the soil or post constitutive parameters can be changed during the time of the impact; this means that nonlinear behavior is also possible with this method.

Soil stiffness

The recommended material model for the soil stiffness is an elastic perfectly plastic model (Figure 5-8). As shown on Figure 5-8, the unloading path is vertical with zero stiffness after that. This is because during the rebound of the post, there is no (or a very small) resistance due to the soil stiffness. In this study the purpose of the current model is

to predict the maximum displacement and load; therefore the behavior of pile until the second step in the Figure 5-8 is important.

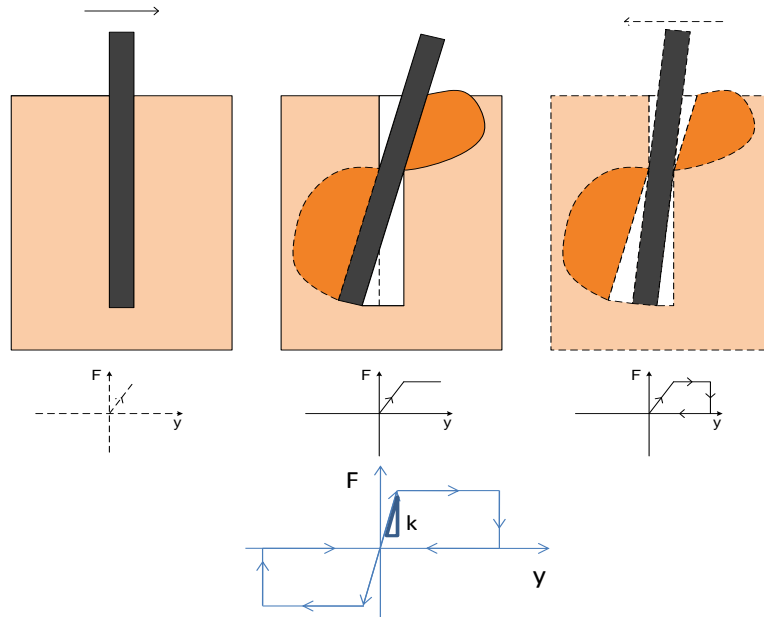


Figure 5-8: Load-displacement curve for spring element

One of the best soil tests to determine the k and F_{yield} is pressuremeter test because of the same loading nature in the test and the experiment. The model parameters are defined from PMT using Equation 5-6 and Equation 5-7. The Equation 5-6 is based on Briaud's (1997, 958-964) recommendation in SALLOP method. The unit of k is in pressure (e.g. MPa, kPa) and the unit of F_{yield} is load per length (e.g. kN/m).

Equation 5-6

$$k = 2.3E_s$$

Equation 5-7

$$F_{yield} = p_L \cdot B$$

where:

E_s : Soil modulus of elasticity from PMT

p_L : Limit pressure in PMT

B : Width of the pile perpendicular to impact direction

Soil damping

“Damping is the phenomenon by which mechanical energy is dissipated (usually converted into internal thermal energy) in a dynamic system. Some knowledge of the level of damping in dynamic system is important in the utilization, analysis, and testing of a system. For example in cases that impact or high velocity load apply on system, resistance of material cannot be shown with only elastoplastic behavior and damping effects of system must be considered in the analysis.” (De Silva 2007)

“In characterizing damping in a dynamic system, it is important, first, to understand the major mechanisms associated with the dissipation of mechanical energy in the system. Then, a suitable damping model should be chosen to represent the associated energy dissipation. Finally, damping values (model parameters) are determined, for example, by testing the system or representative physical model, by monitoring the system response under transient condition during normal operation, or by employing already available data.” (De Silva 2007)

Three primary mechanisms of damping are important in the study of mechanical system. They are

- 1- Internal damping (of material)
- 2- External Damping (at joint and interface or wave propagation)
- 3- Fluid damping (through fluid-structure interaction)

“Internal (material) damping results from mechanical-energy dissipation within the material because of various microscopic and macroscopic processes. External damping is caused by mechanical-energy dissipation resulting from relative motions between components in a mechanical structure that has common points of contacts, joint, or support” (De Silva 2007). In the media (e.g. soil layer) when we have wave transferring, another damping is generated due to wave propagation. This damping depends on geometry and material properties of the propagated zone. Fluid damping arises from the mechanical-energy dissipation resulting from drag forces and associated dynamic interactions when a mechanical system or its components move in a fluid.

The dominant damping type in soils under large deformation impact is Radiation (geometric) damping that is an external damping category. Energy is removed from the compliant system by the foundation medium during a dynamic disturbance due to the propagation of waves into this support medium and is commonly called geometric or radiation damping (Rainer 1975, 13-22). This type of damping occurs in dynamic foundation soil interaction and in addition to soil material properties, geometry of layer and foundation is important in amount of this damping.

Radiation or geometric damping is a fundamental concept in modern methods of analysis of dynamic soil-structure interaction. Whenever a foundation element moves against the surrounding soil, stress waves originate at the contact surface and spread outward. These waves carry away some of the energy transmitted by the foundation into the soil, a phenomenon reminiscent of the absorption of energy by viscous dampers, hence, it is called radiation damping. The magnitude of this damping depends mainly on the

frequency of excitation, the geometry of the soil-foundation system, the mode of oscillation, and the stress-strain characteristics of the soil. Its existence was first unveiled from Reissner's solution to the problem of an elastic halfspace dynamically excited by a uniformly loaded circular disk vibrating vertically. It has since been indirectly obtained as part of the elastodynamic (wave-propagation) solution to numerous soil-foundation interaction problems. (Gazetas and Dobry 1984b, 937-956; Reissner 1936, 381-396) Under high strain loading viscous behavior can also be observed in clayey soil.

The most difficult parameter to determine is the dashpot coefficient (C). Different equations have been published in literature but they were not developed for this specific problem and do not seem to match the results of the experiments. Some of the well-known equations for damping coefficient are:

– Smith (1960, 35-61) $R_t = R_s(1 + Jv)$ $0.05 < J < 0.5$

sec/m

R_t : Total resistance

R_s : Static resistance

J: damping constant

v: Velocity

– Briaud and Terry (1986, 387-405) $\frac{s_{u1}}{s_{u2}} = \left(\frac{t_1}{t_2}\right)^{-n}$ $0.01 < n < 0.1$

s_{u1}, s_{u2} : Undrained shear strength measured with time to failure t_1 and t_2

n: viscous exponent

– Wolf and Somaini (1986, 683-703) $c = \beta \frac{k_s}{V_s} \gamma$

β : Dimensionless frequency

k_s : Soil stiffness

V_s : Shear wave velocity of soil

γ : Dimensionless coefficient of the dampers

After investigating several damping estimator equations we came up with Wolf and Somaini (1986, 683-703) recommendation with some modification:

Equation 5-8

$$C = \alpha \frac{Bk_s}{V_s}$$

where:

C: Damping coefficient for soil material model

α : Dimensionless damping factor

k_s : Soil stiffness, $k_s=2.3E_s$

V_s : Shear wave velocity of soil (Equation 5-9)

B: Width of the pile perpendicular to impact direction

The soil shear wave velocity can be estimated from:

Equation 5-9

$$V_s = \sqrt{\frac{G_s}{\rho_s}}$$

where:

G_s : Soil shear modulus, $G_s = \frac{E_s}{2(1+\nu)}$

ρ_s : Soil density

ν : Soil poisson's ratio

In this study the dimensionless damping factor is estimated from the experiments and simulations. A constrained nonlinear optimization algorithm (Interior-Point Algorithm Option) was used to find the optimum value of α to minimize the error equation (Err) of simple model rotation prediction. The medium scale tests are not used in the error equation because in those experiments piles did not stop the impact and no maximum rotations were measured.

Equation 5-10

$$Err_R = \sum (Ln(R_i) - Ln(\hat{R}_i))^2$$

where:

R_i : Measured maximum rotation from i th real or virtual experiment

\hat{R}_i : Predicted maximum rotation of i th observation by simple method

The result shows that $\alpha=0.149$ is the optimum damping factor for Equation 5-8 based on 54 measured values (7 real experiments and 47 numerical simulation). The unit of soil damping in this model is pressure by time (e.g. kPa.sec)

Soil mass

In order to contribute inertia effect a lumped mass is used in the soil model. The mass is representative of both mass of pile and soil mass. The sensitivity analysis on the model

and observation of medium scale test for mass drop tests show that the mass of the soil does not have a significant effect on the results. After investigating different used for mass equations, an equation was recommended and calibrated (Equation 5-12). The equation was developed based on contributing important parameters in the soil mass including density and dimension.

Equation 5-11

$$m = m_{pile} + m_{soil}$$

Equation 5-12

$$m_{soil} = \eta \rho_s BL$$

where:

η : Dimensionless mass factor

ρ_s : Soil density

B: Width of the pile perpendicular to impact direction

L: Pile embedment

The same approach of the damping factor estimation was used to estimate the soil mass factor the only difference was that optimization was done on error function of maximum equivalent load (Equation 5-13).

Equation 5-13

$$Err_f = \sum (Ln(F_i) - Ln(\hat{F}_i))^2$$

where:

F_i : Measured maximum equivalent load from i th real or virtual experiment

\hat{F}_i : Predicted maximum equivalent load of i th observation by simple method

The result implies that $\eta=0.013$ is the optimum value for mass factor in this model based on 60 observations (13 experiments and 47 numerical simulations). The unit of soil mass in this model is mass over length (e.g. kg/m)

Vehicle mass and velocity

As mentioned before, different types of loading can be applied Load-time history, displacement-time history and impact parameters (mass and velocity of impact) are the loading conditions which can be used in the simulation, but for the problem addressed in this project, mass and velocity of the truck at impact are the only input parameters for external loading.

The energy of impact during the vehicle impact is spent in deforming the pile-soil system and vehicle itself. The impact in the proposed method is modeled as a rigid impact and there is no flexibility in the mass. One solution to match the imposed energy from the vehicle to the pile-soil system is to reduce the velocity of the vehicle by a factor. The factor value depends on different parameters for example stiffness of soil and pile geometry and the average number was selected based on simulations results.

The velocity factor is estimated from applied energy to the pile-soil system (Equation 5-14) or absorbed energy by vehicle (Equation 5-15) that obtained from LS-DYNA numerical simulations. The two methods of calculation may not result in a same number because of the energy loss during the analysis (e.g. contact, hourglass,...)

Equation 5-14

$$\kappa = \sqrt{\frac{E_T - E_V}{E_T}}$$

Equation 5-15

$$\kappa = \sqrt{\frac{E_S}{E_T}}$$

where:

E_T : Total initial kinetic energy of the vehicle ($\frac{1}{2}M_T V_T^2$)

E_V : Deformation energy of the vehicle

E_S : Deformation energy of soil-pile system

Table 5-1 lists the κ factor for all the simulations from both soil energy and vehicle energy. The average of κ from vehicle energy is 0.62 and from soil energy is 0.55. For simplicity a constant number $\kappa=0.6$ were selected as a reduction factor for vehicle velocity in the model. This means only about 36% of the total energy transfers to the pile-soil system and the remaining energy is spent by the vehicle deformation and the contact.

Table 5-1: Vehicle velocity reduction factor

	Soil type	Embedment depth	Mass	V	B	κ (from vehicle energy)	κ (from soil energy)
		(m)	(kg)	(Mph)	(m)		
Clay	Medium soft	2	808	50	0.35	0.70	0.59
	Medium	2	808	40	0.35	0.46	0.48
	Medium	2	2013	40	0.35	0.66	0.56
	Medium	2	808	50	0.35	0.55	0.50
	Medium	2	2013	50	0.35	0.71	0.57
	Medium	2	808	60	0.35	0.61	0.53
	Hard	2	808	50	0.2	0.61	0.52
	Medium soft	2.5	808	50	0.35	0.63	0.55
	Medium	2.5	2013	60	0.35	0.73	0.59
	Hard	2.5	808	60	0.35	0.47	0.44
	Very hard	2.5	808	40	0.2	0.43	0.41
	Very hard	2.5	2013	50	0.35	0.63	0.53
	Soft	3	808	60	0.35	0.69	0.57
	Medium	3	2013	40	0.35	0.59	0.55
	Medium	3	2013	50	0.35	0.64	0.60
	Medium	3	808	60	0.35	0.55	0.50
	Medium	3	808	40	0.2	0.48	0.48
	Medium	3	808	40	0.35	0.40	0.40
	Medium	3	2013	60	0.35	0.71	0.59
	Sand	Hard	3	808	50	0.2	0.50
Soft		3.5	2013	60	0.35	0.80	0.63
Medium soft		3.5	2013	40	0.35	0.62	0.59
Medium		3.5	2013	40	0.35	0.59	0.53
Very hard		3.5	2013	40	0.35	0.47	0.45
Medium Loose		2	808	50	0.35	0.71	0.64
Medium		2	808	40	0.35	0.47	0.48
Medium		2	2013	40	0.35	0.68	0.64
Medium		2	808	50	0.35	0.59	0.55
Medium		2	2013	50	0.35	0.72	0.63
Medium		2	808	60	0.35	0.64	0.56
Dense		2	808	50	0.2	0.67	0.61
Medium Loose		2.5	808	50	0.35	0.67	0.62
Medium		2.5	2013	60	0.35	0.75	0.65
Very dense		2.5	808	60	0.35	0.62	0.52
Very dense		2.5	808	40	0.2	0.65	0.50
Very dense		2.5	2013	50	0.35	0.68	0.56
Loose		3	808	60	0.35	0.69	0.68
Medium		3	2013	40	0.35	0.64	0.63
Dense		3	2013	50	0.35	0.70	0.60
Medium	3	808	60	0.35	0.64	0.54	
Dense	2	808	40	0.2	0.53	0.48	
Medium	3	808	40	0.35	0.71	0.59	
Very dense	3	808	50	0.2	0.59	0.55	
Loose	3.5	2013	60	0.35	0.78	0.69	
Medium Loose	3.5	2013	40	0.35	0.61	0.63	
Medium	3.5	2013	40	0.35	0.62	0.60	
Very dense	3.5	2013	40	0.35	0.59	0.48	

Output

The direct output of the analysis is the displacement of each node as a function of time. By using the central finite difference technique, velocity and acceleration can also be calculated for each node. In order to remove the noise on the acceleration curve a smoothing filter is applied on the acceleration results which performs a 50 msec average on the acceleration. At any time during the impact, the external force at the top of the post is the product of the impact point acceleration by the impacting mass. The internal moment and shear at any depth versus time can also be obtained as output. An example graphical output for an impact simulation is shown in Figure 5-9. In this example, a 6x6x3/8 HSS post section with a length of 1.25 m and an embedment of 1 m is impacted with a mass of 900 kg and a velocity of 4.7 m/s. The spring used is elastic-perfectly plastic. Other input parameters are as follows:

Number of nodes=10	$E=2 \times 10^{11} \text{ N/m}^2$	$k_s=1.4 \times 10^7 \text{ N/m}^2$	$\Delta t=10^{-5} \text{ s}$
$C=160000 \text{ N/s}$	$I=1.86 \times 10^{-5} \text{ m}^4$	Spring failure load=103500	N/m

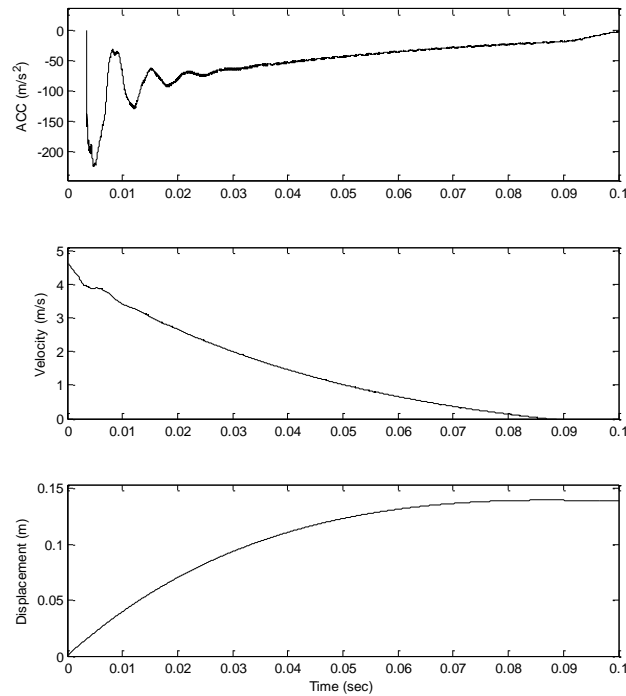


Figure 5-9: Example of output result for lateral impact at impacted node

Sensitivity analysis

Sensitivity analysis is the study of how the uncertainty in the output of a mathematical model or system (numerical or otherwise) can be apportioned to different sources of uncertainty in its inputs (Saltelli and others 2004). The technique is used to determine how variation in input parameters affects the output results. In this study a series of sensitivity analyses were performed on the proposed model to determine the importance of ranking input parameters. The analysis was performed on the PU40 impacting 2m embedment pile with 0.35m width in medium clay. The input and output parameters of the case are shown in Table 5-2 and Figure 5-10.

Table 5-2: Sensitivity analysis center case input parameters

Vehicle	Velocity of truck, V_0	40(17.9) mph(m/sec)
	Mass of Truck, M_T	2250 kg
Pile	Embedment depth, L	2 m
	Height of impact, H	0.75 m
	Width of the post, B	0.35 m
	Elastic modulus, E_{post}	210 MPa
	Moment of Inertia, I_{post}	18855.3 cm ⁴
	Mass of post per length, M_p	107
Soil	Limit pressure, P_L	1300 kPa
	Elastic modulus, E_s	20 MPa
	density	2058 kg/m ³
	Poisson's ratio	0.49
Numerical parameters	Time increment, Δt	1.00E-05
	number of elements, n	12

8 input parameters (Vehicle mass, Vehicle velocity, Soil damping, Soil stiffness, Soil mass, Soil limit pressure, Pile width, Pile embedment depth) were selected for sensitivity analysis. Two output results (rotation and load) were investigated in the analysis. The displacement has the same trend as rotation sensitivity curve. The normalized rotation and load results versus parameters factor are displayed in Figure 5-11 and Figure 5-12. According to the sensitivity analyses vehicle velocity has the most important contribution on both rotation and load. For the soil parameters the most effective input is soil limit pressure (p_L) and soil mass has the least contribution in the rotation and load output. The model is most sensitive to pile geometry specially embedment depth. The detail sensitivity analyses results for each parameter are presented in appendix 5.

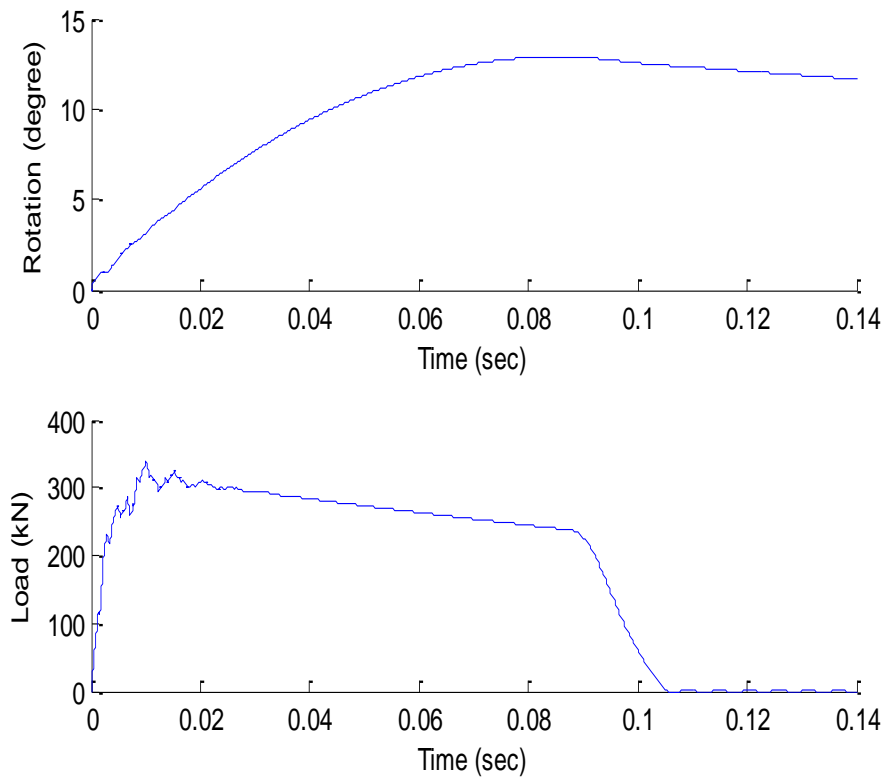


Figure 5-10: Sensitivity analysis center case output result

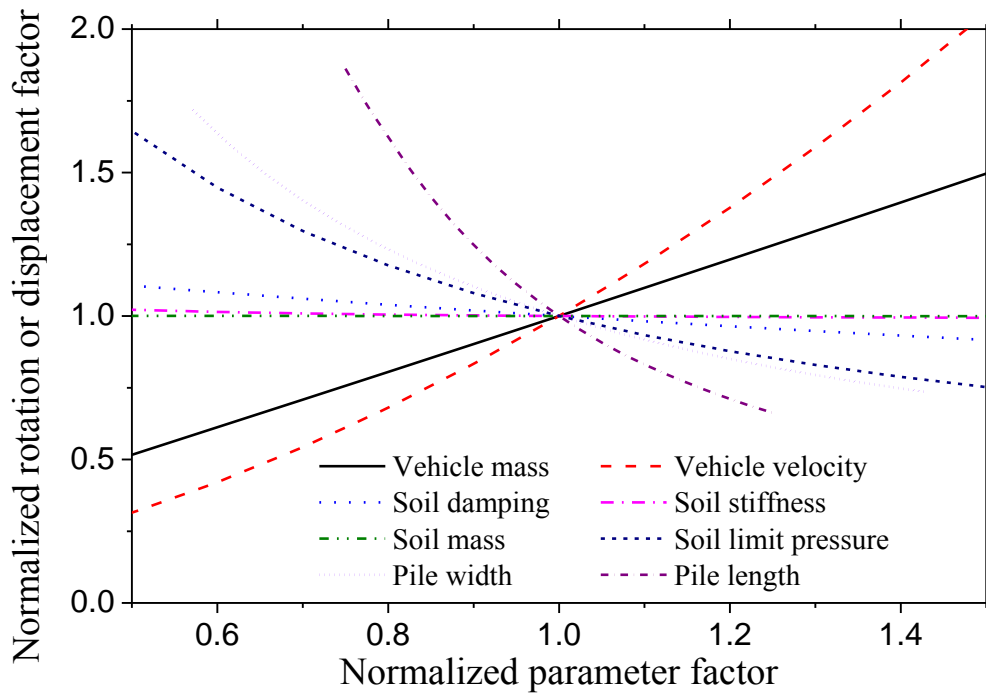


Figure 5-11: Sensitivity of normalized rotation results versus parameters factor

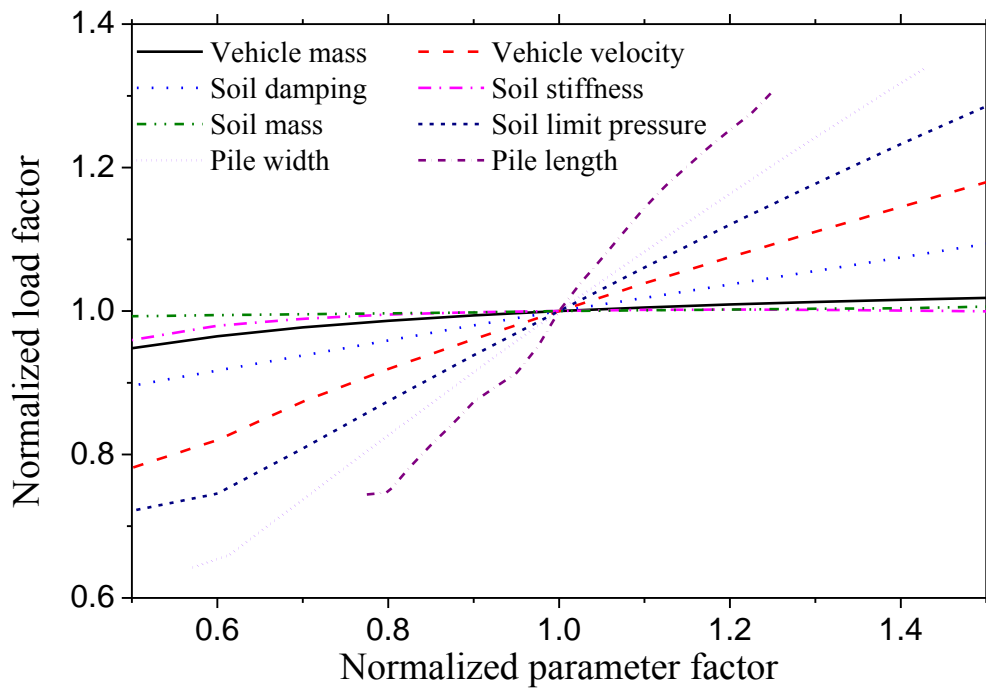


Figure 5-12: Sensitivity of normalized load results versus parameters factor

In order to select the proper time increment and node numbers in the finite difference solution of the proposed model two sensitivity analyses also were conducted. There is no significant change in the rotation and the load prediction by changing the time steps (Figure 5-13), however the solution would not converge for big Δt . In this study $\Delta t=10^{-5}$ sec was selected for calibration.

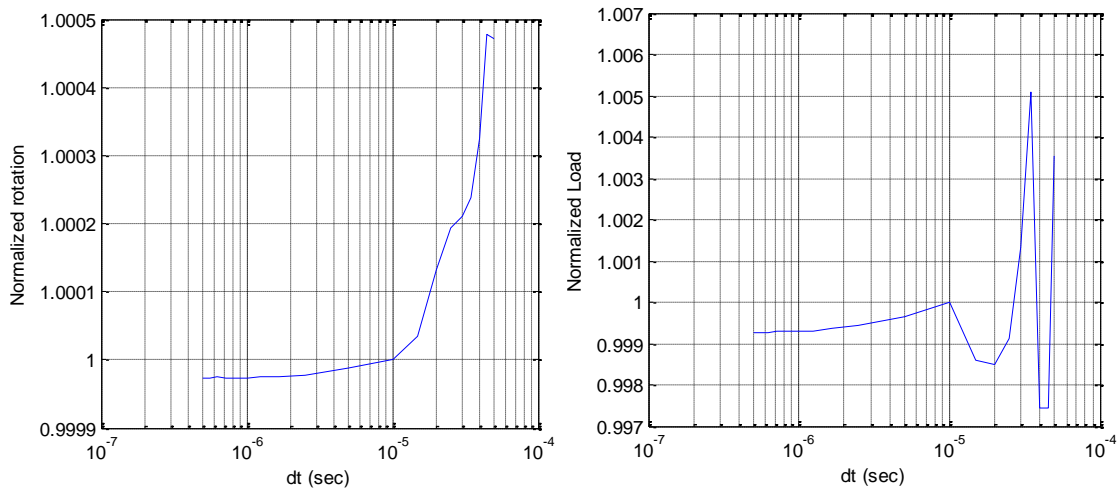


Figure 5-13: Model sensitivity for time increment

In the finite difference method using few elements causes inaccuracy in the results, but on the other hand increasing the number of elements forces a reduction in the time step for stability and to have convergence in the solution. The model sensitivity result for the number of nodes indicates that for the selected Δt , 10 to 15 nodes (9 to 14 elements) will give us a reasonable result for both rotation and load. In this study 12 nodes were selected

for calibration. Figure 5-14 shows the rotation and load variation by changing the number of nodes on the pile.

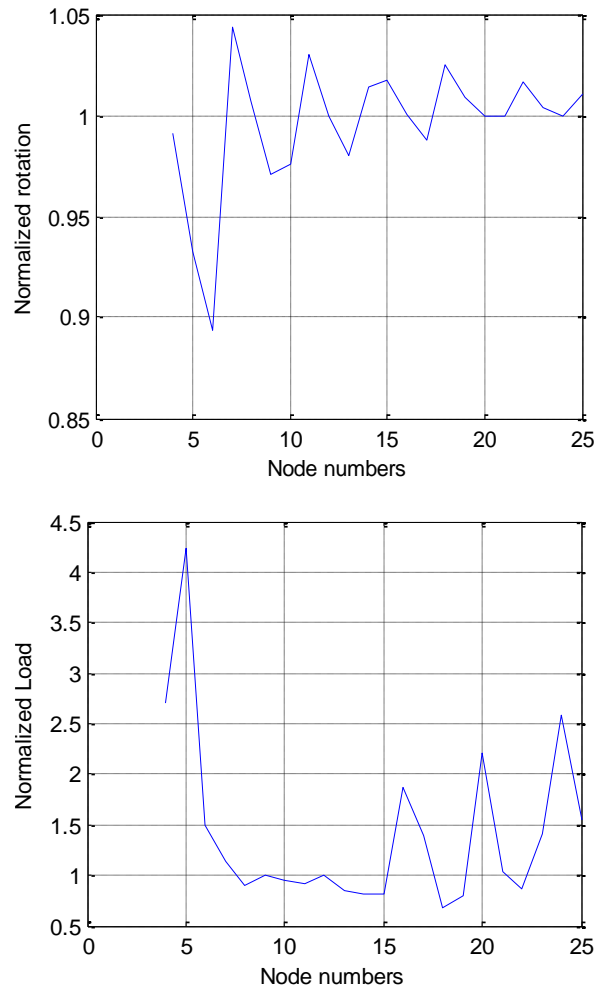


Figure 5-14: Model sensitivity for number of nodes

Model calibration

The proposed model was calibrated against the real and virtual experiments. A total number of 2 full scale tests, 11 medium scale tests and 47 numerical simulations were

used to calibrate and modify the simple model. Two outputs of rotation and equivalent impact load were calculated for calibration process. The load was made a dimensionless by dividing the corresponding impact moment at ground level by the elastic moment capacity of the pile (Equation 5-16).

Equation 5-16
$$DLM = \frac{M_{impact}}{M_{yield}}$$

The comparison between the predicted quantities and measured are shown in Figure 5-15 to Figure 5-18.

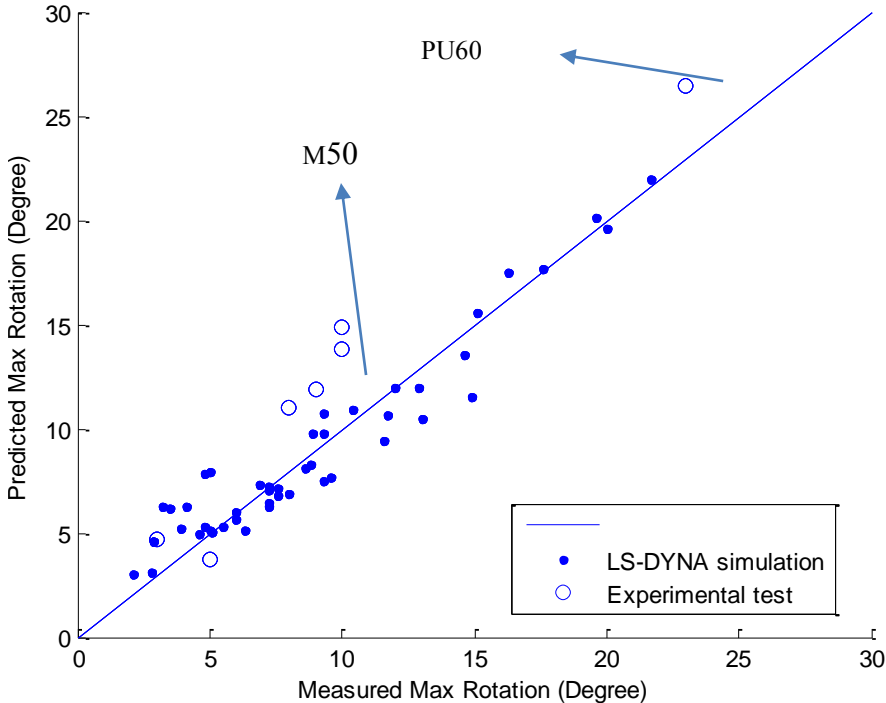


Figure 5-15: Rotation prediction vs measured of single pile under impact

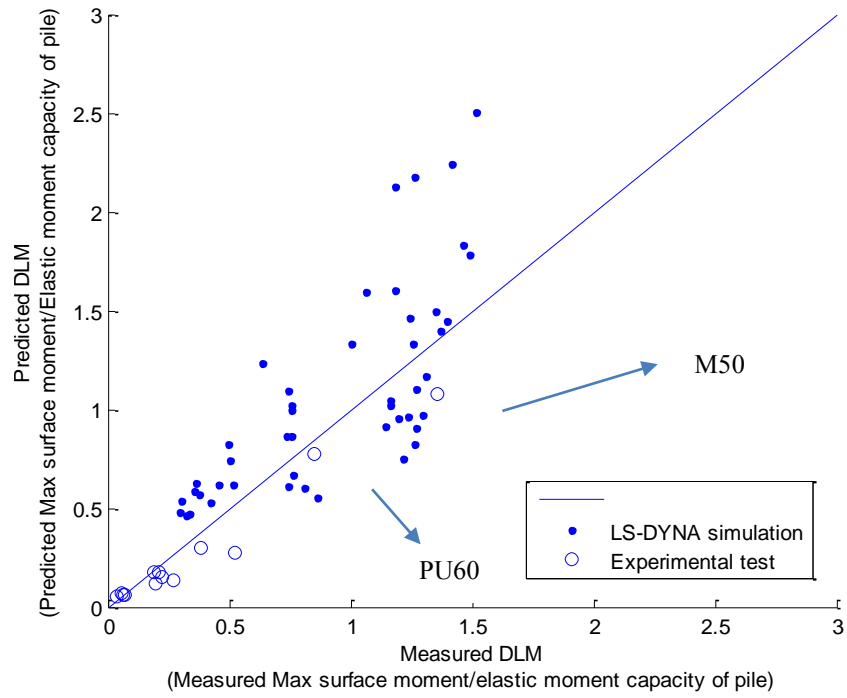


Figure 5-16: Dimensionless moment prediction vs measured of single pile under impact

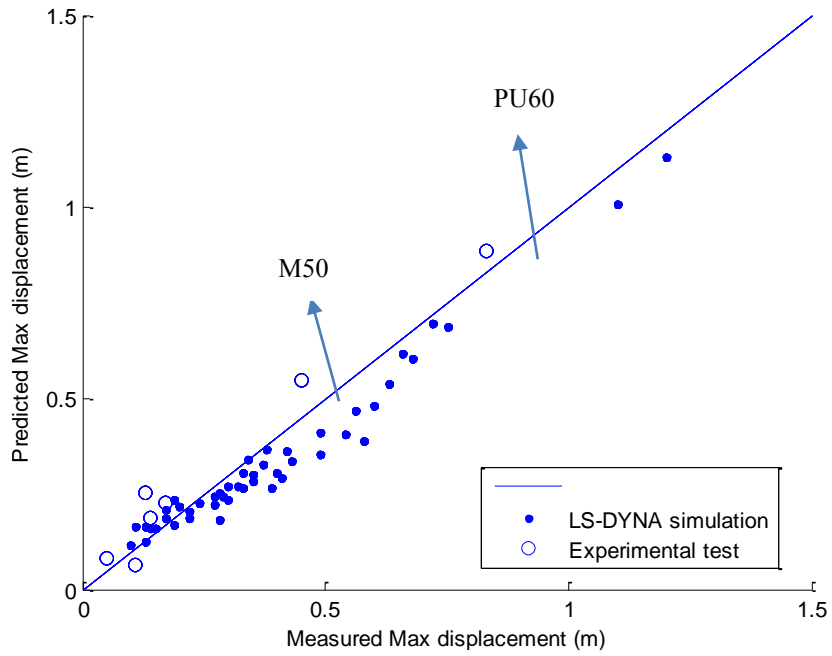


Figure 5-17: Displacement prediction vs measured of single pile under impact

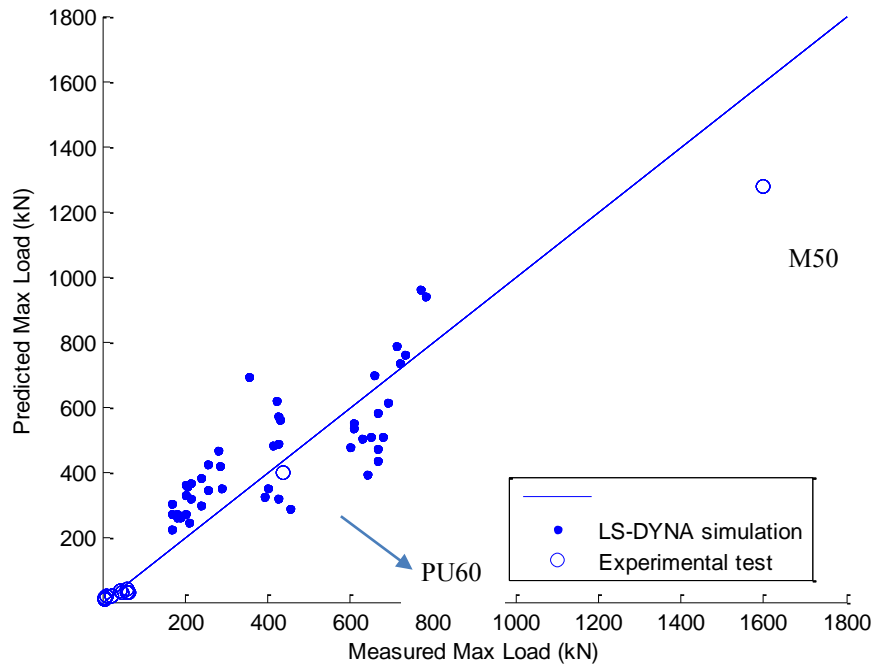


Figure 5-18: Equivalent impact load prediction vs measured of single pile under impact

The results show that the model predicts the displacement and rotation more accurately than the load. In the displacement and rotation the model usually predicts values larger than the simulations and smaller than the experiments while for the load prediction the opposite trend happens.

PU60

Figure 5-19 to Figure 5-21 presents the results among experimental, LS-DYNA simulation, and simple proposed model for PU60 test. The model parameters for these analyses were selected based on the site investigation and lab tests. The displacement vs. time results show that the model overpredicts the maximum displacement by 6.5% (884 mm by simple model and 830 mm from experiment), while LS-DYNA underpredicts the

maximum displacement by 6.3% (778 mm). The load vs. time predictions by the simple model show a sharp rise in load because the crushing of the truck at impact is not simulated leading to a rigid impact. In Figure 5-20 the predicted load by the simple model is shifted in order to match the peak loads on the curve. The simple code predicted the load with 10% error (400 kN by simple model and 440 kN from experiment), while LS-DYNA's error is 11% (490 kN). Maximum rotation from simple model is 26.4 degree compared to 23 degree in test and 23 in LS-DYNA simulation.

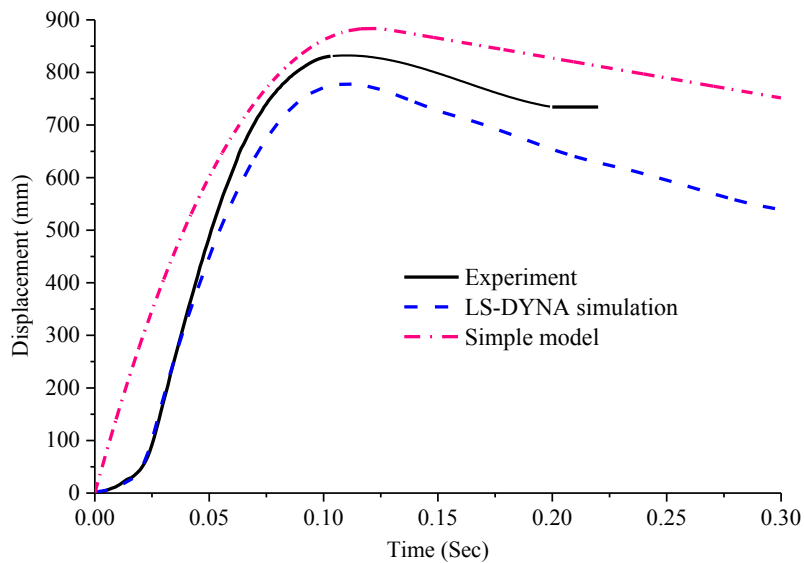


Figure 5-19: PU60 impact displacement-time results from experiment, LS-DYNA simulation, and simple model

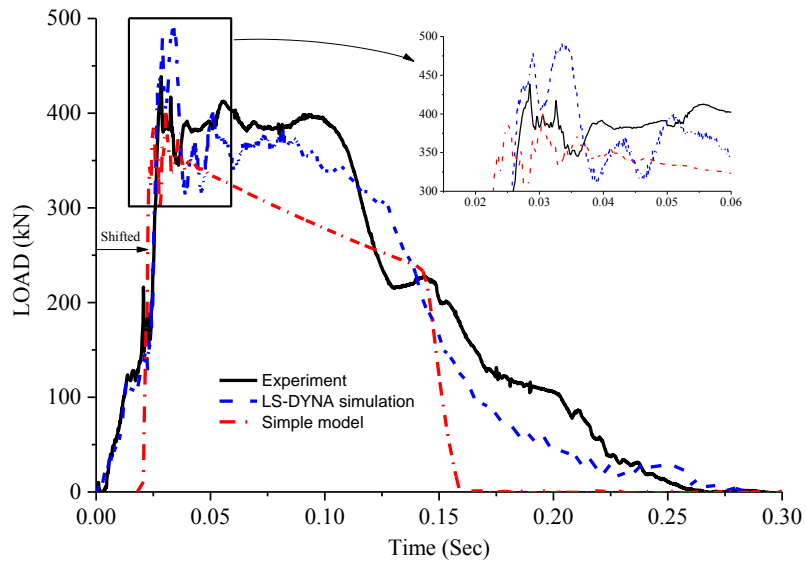


Figure 5-20: PU60 impact Load-time results from experiment, LS-DYNA simulation, and simple model

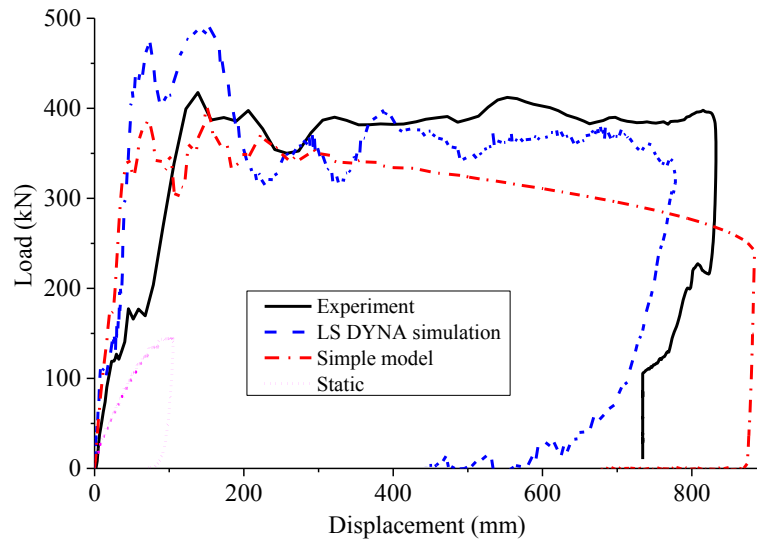


Figure 5-21: PU60 impact Load-displacement results from experiment, LS-DYNA simulation, simple model, and static

M50

Since the current numerical model of medium duty truck is not suitable for the large deformation and we cannot generate data bank from the LS-DYNA simulation. Technically the simple model was not calibrated for M type vehicles and the simple model results for M type vehicle are purely predictive. However the results from the model prediction show a reasonable match between displacement and load. Figure 5-22 to Figure 5-24 show the displacement and load results comparison between experiment and simple model prediction for M50 test. In displacement proposed model could predict the movement of pile at impact point with 22% error (550 mm by simple model vs 450 from experiment). For the load result the simple model underpredicts 20% less than experiment (1280 kN by simple model vs 1600 kN in experiment). The predicted rotation by simple model is 11.9° compared to 9° in the experiment.

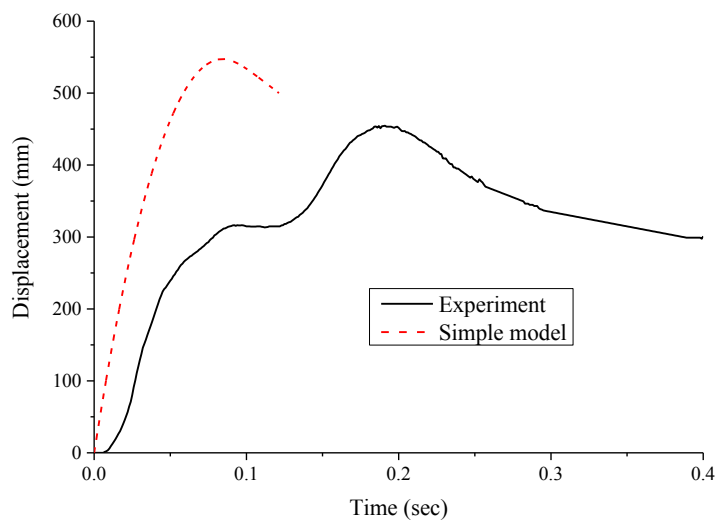


Figure 5-22: M50 displacement comparison between simple model and experiment

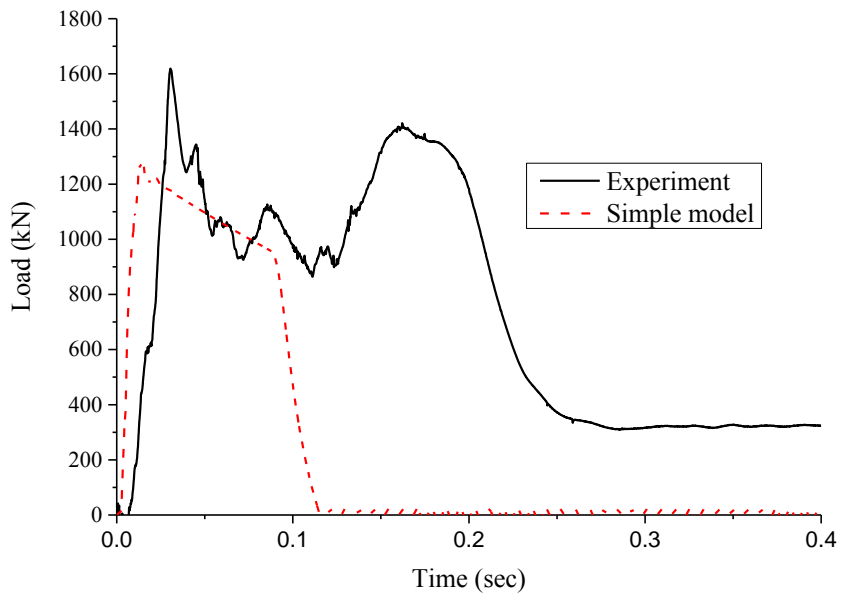


Figure 5-23: M50 load comparison between simple model and experiment

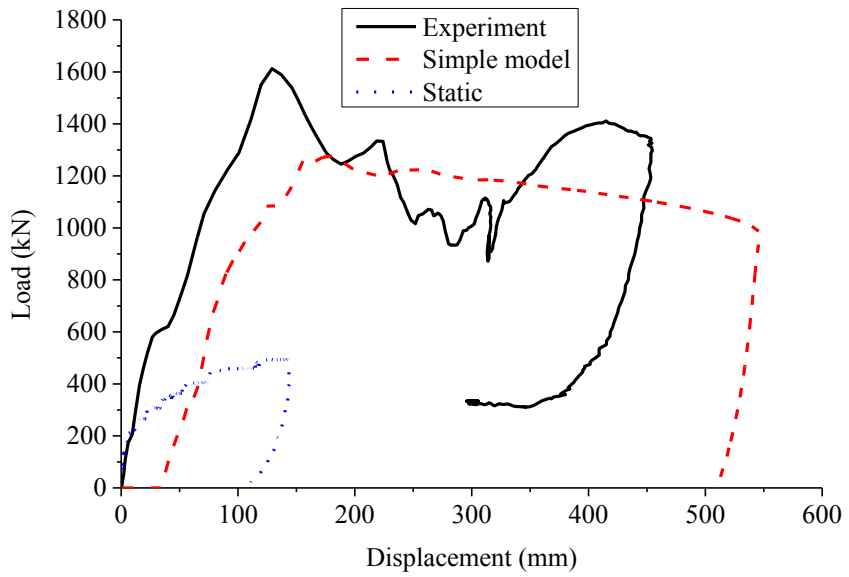


Figure 5-24: M50 load-displacement curve comparison between simple model and experiment

6. PROBABILISTIC DEMAND MODEL AND FRAGILITY ESTIMATE

The simple predictive demand model for the lateral behavior of single pile under truck impact is developed in section 5. The model is deterministic and based on the limited number of experimental and numerical data. As a result, the model does not include any terms to account for different kinds of uncertainties; therefore the estimation is biased. In this section we utilize a Bayesian framework developed by Gardoni (2002-a) to improve the simple deterministic model to a probabilistic demand model. This unbiased model accounts for both epistemic uncertainties (lack of knowledge, deliberate choice to simplify matters, errors in measuring, finite size of observation) and aleatory uncertainties (inherent in nature, uninfluenced by the observer or the manner of the observation) (Gardoni, et al, 2002-b). The approach considers the observations based on experimental and numerical results, physical laws, engineering judgment and experience. By using a series of explanatory functions, we correct the bias in the deterministic model. The outcome of this study are two types of probabilistic dimensionless demand models for rotation and impact load on pile for both types of soil (clay and sand).

The developed probabilistic demand model and the capacity described in ASTM F2656 are used in a limit-state function to construct the fragility (conditional failure probability of structure member given set of demand variables) of a pile under a vehicle impact. Since according experience and experimental field tests the dominant failure criterion is the displacement or the rotation of the pile, the system fragility is developed based on the rotation of the pile at impact point.

Probabilistic demand models

The definition of the model in this section is the numerical expression that relates the desirable demand quantities (e.g. rotation or load at the impact point) to input measurable parameters $\mathbf{x} = (x_1, x_2, \dots)$ (e.g., soil properties, geometry of the pile, and vehicle mass and velocity). The deterministic model generates set of results for a set of input parameters while the results of a probabilistic model are distributions of a quantities moreover the probabilistic model takes uncertainties into account. In this study deterministic the demand model is the simple model developed in the section 5.

According to Gardoni (2002) the two main uncertainties are aleatory and epistemic uncertainties. The aleatory uncertainties, also known as inherent variability or randomness, are irreducible and inherent in nature, so observation and model improvement may not influence these uncertainties. In the model formulation, these types of uncertainties exist in the input variables x and the error term ε . On the other hand epistemic uncertainties come from lack of knowledge, from deliberate choice to simplify the model, from errors that arise in measuring observations, and from the finite size of observation samples. These uncertainties can be reduced by some techniques including improving the model, measuring with more accuracy and gathering more results; In probability models formulation they are presented in the parameter Θ and partly in the error term ε .

In order to build a model based on rules of mechanics and physics, engineering judgment, and also considering uncertainties, following Gardoni et al. (2002 ,2003), I add

series of correction terms to the deterministic demand model. By using Gardoni, et al., (2003) framework, the proposed probabilistic demand model is:

Equation 6-1
$$D(\mathbf{x}, \Theta) = \hat{d}(\mathbf{x}) + \gamma(\mathbf{x}, \Theta) + \sigma \varepsilon$$

where:

D : Demand quantity, e.g., displacement or rotation of the impact point of the pile, or load applied at impact point on the pile. It is preferable to make this value dimensionless (e.g., transfer displacement to drift or rotation)

$\mathbf{x} = (\mathbf{r}, \mathbf{s})$: Input variables consist of measurable variables (\mathbf{r}) (e.g. geometry, material properties), and initial conditions (\mathbf{s}) (e.g., vehicle velocity and vehicle mass)

$\Theta = (\boldsymbol{\theta}, \sigma)$: Set of parameters to fit the model to observed data

$\boldsymbol{\theta} = \theta_j = (\theta_1, \theta_2, \dots)$: Set of unknown model parameters

$\hat{d}(\mathbf{x})$: Selected deterministic demand model as a function of input variables

$\gamma(\mathbf{x}, \boldsymbol{\theta})$: Correction term for the bias inherent in the deterministic model

$\sigma \varepsilon$: Model error

ε : Random variable with zero mean and unit variance and

σ : Standard deviation of the model error

Note that for given \mathbf{x} , $\boldsymbol{\theta}$ and σ , we have $\text{Var}[D(\mathbf{x}, \Theta)] = \sigma^2$ as the variance of the model. For this formulation sometimes we need to use a suitable transformation as a variance stabilizing transformation (like a natural logarithm) of the demand quantity to satisfy two assumptions: independency between model parameters \mathbf{x} and model variance σ^2 (homoscedasticity assumption), and normal distribution for ε (normality assumption).

The correction term $\gamma(\mathbf{x}, \boldsymbol{\theta})$ corrects the available bias in the deterministic model $\hat{d}(\mathbf{x})$ by exploiting a set explanatory functions $h_j(\mathbf{x})$ and express the bias correction term in the form of:

Equation 6-2
$$\gamma(\mathbf{x}, \boldsymbol{\theta}) = \sum_{j=1}^q \theta_j h_j(\mathbf{x})$$

where:

$h_j(\mathbf{x})$: j^{th} explanatory function ($j = 1, \dots, q$)

q: The total number of explanatory functions

The explanatory functions $h_j(\mathbf{x})$ should be selected in a way that improves the deterministic model prediction $\hat{d}(\mathbf{x})$. One approach is to use terms that do not exist in the $\hat{d}(\mathbf{x})$ and by exploiting the rules of mechanics. Using engineering judgment can also help selecting the suitable $h_j(\mathbf{x})$ to find the missing terms in $\hat{d}(\mathbf{x})$. It is desirable to select the explanatory function with the same unit of the deterministic model; as a result, θ_j becomes dimensionless. The typical choices for h_1 and h_2 are 1 and $\hat{d}(\mathbf{x})$ to detect potential constant bias and to capture under or overestimates of the $\hat{d}(\mathbf{x})$, respectively. By examining the unknown model parameters of θ_j , we are able to detect significant and desirable explanatory functions and describe the biases in the deterministic model (Gardoni, 2002).

The model parameters, $\Theta = (\theta, \sigma)$ are estimated using a Bayesian approach with the following well-known updating rules (Box and Tiao, 1992):

Equation 6-3 $f(\Theta|\mathbf{d}) = \kappa L(\Theta|\mathbf{d})p(\Theta)$

where:

$f(\Theta|\mathbf{d})$: Posterior distribution that represents the updated distribution of Θ , given information from a set of new observations $\mathbf{d}=(d_1, d_2, \dots)$, which can be real or virtual experiment results.

κ : Normalizing factor in order to ensure the integration of posterior equals to one.

$L(\Theta|\mathbf{d})$: Likelihood function that represents the information about Θ from new observations \mathbf{d} , formulation of which depends on the type and form of available information.

$p(\Theta)$: Prior distribution representing the information about Θ prior to obtaining the observations \mathbf{d} .

Prior distributions

For cases when there is no information and/or engineering judgment about the Θ , prior should not affect the posterior distribution. The general assumption is that θ and σ are approximately independent, so we have $p(\Theta) \approx p(\theta)p(\sigma)$. According to Jeffrey's rule (1961) and Box and Tiao (1992), for the cases without prior information $p(\theta)$ is locally uniform; therefore $p(\Theta) \approx p(\sigma)$. They also showed that noninformative prior for σ is

$$p(\sigma) \propto \frac{1}{\sigma}; \text{ therefore } p(\Theta) \propto \frac{1}{\sigma}.$$

The posterior distribution for current work becomes prior for model modification with future experiments results, and this process can be repeated any number of times. However, any change in the deterministic model requires the procedure from the beginning.

Equation 6-4
$$p(\Theta|d_1, d_2, \dots, d_{q+r}) \propto p(\Theta|d_1, d_2, \dots, d_q)L(\Theta|d_{q+1}, d_{q+2}, \dots, d_{q+r})$$

Likelihood functions

Information from observations is presented in the model through the likelihood function. Likelihood is proportional to the conditional probability of observation for given value of Θ (Gardoni et al., 2002). Three types of observations are possible:

- 1- Lower bound datum: demand is measured at the level that the system does not reach the desirable situation
- 2- Equality datum: demand is measured at the final situation of the system
- 3- Upper bound datum: demand is measured at the level that the system passes the desirable situation

For example, for the model of maximum displacement of a pile under vehicle impact, if the displacement of the pile is measured before the maximum displacement or because of any reason it is considered as less than real value then we would have lower-bound datum. In the case that displacement is detected more than real value, we would have upper-bound datum. For an exact measurement of the pile at the maximum displacement, the equality datum is captured. Following Gardoni et. Al., (2002), likelihood is written as:

$$\begin{aligned}
\text{Equation 6-5} \quad L(\boldsymbol{\theta}) &\propto \prod_{\text{Equality data}} P[\sigma\varepsilon_i = r_i(\boldsymbol{\theta})] \\
&\times \prod_{\text{Lower bound data}} P[\sigma\varepsilon_i > r_i(\boldsymbol{\theta})] \\
&\times \prod_{\text{Upper bound data}} P[\sigma\varepsilon_i < r_i(\boldsymbol{\theta})]
\end{aligned}$$

where:

$$\text{Equation 6-6} \quad r_i(\boldsymbol{\theta}) = d_i - \hat{d}(\mathbf{x}_i) - \gamma(\mathbf{x}_i, \boldsymbol{\theta})$$

d_i : Observed demand value for a \mathbf{x}_i

In order to satisfy the homoscedasticity assumption (independency between model variance σ^2 and \mathbf{x}), $r_i(\boldsymbol{\theta})$ may be defined in form of Equation 6-7 or Equation 6-8 (considering the non-negative nature of d value) depending rate of change in σ versus \mathbf{x} .

$$\text{Equation 6-7} \quad r_i(\boldsymbol{\theta}) = \ln(d_i) - \ln[\hat{d}(\mathbf{x}_i)] - \gamma(\mathbf{x}_i, \boldsymbol{\theta})$$

$$\text{Equation 6-8} \quad r_i(\boldsymbol{\theta}) = \sqrt{d_i} - \sqrt{\hat{d}(\mathbf{x}_i)} - \gamma(\mathbf{x}_i, \boldsymbol{\theta})$$

In this study, because we have maximum displacement for all the experimental tests and also assume the virtual experiments with LS-DYNA is accurate and exact; all the data are equality data, so we have:

$$\text{Equation 6-9} \quad L(\boldsymbol{\theta}) \propto \prod_{\text{Equality data}} P[\sigma\varepsilon_i = r_i(\boldsymbol{\theta})]$$

Since we assumed ε has normal distribution (normality assumption), likelihood can be written as:

$$\text{Equation 6-10} \quad L(\boldsymbol{\theta}) \propto \prod_{\text{Equality data}} \left\{ \frac{1}{\sigma} \varphi \left[\frac{r_i(\boldsymbol{\theta})}{\sigma} \right] \right\}$$

where:

φ : Probability Density Function (PDF) for the normal standard distribution

Observation (d_i) and measurable variables (\mathbf{x}_i) may contain errors due to measurement device or procedure. Error in measuring (for lab and controlled experiment results observations and variables), simulation error (for observation from simulations results) are the two main types of errors that exist in d_i and \mathbf{x}_i . The origin of this uncertainty arises from epistemic in nature, therefore improving in measurement method and device will reduce it. In order to model these errors we let $d_i = \tilde{d}_i + e_{d_i}$ and $\mathbf{x}_i = \tilde{\mathbf{x}}_i + \mathbf{e}_{x_i}$ be the measured values in the model, where \tilde{d}_i and $\tilde{\mathbf{x}}_i$ are the recorded value and e_{d_i} and \mathbf{e}_{x_i} are the errors in the result and input values for i th observation. The statistical error parameters usually obtained from calibration of measurement device and calibration of simulation or procedure. In most cases we can assume the e_{d_i} and \mathbf{e}_{x_i} are normally distributed and statistically independent. Assuming that, there is no systematic error in the data, the means of both e_{d_i} and \mathbf{e}_{x_i} are zero.

Considering recording error in the model for equality data we have:

$$\text{Equation 6-11} \quad \tilde{d}_i + e_{d_i} = \hat{d}(\tilde{\mathbf{x}}_i + \mathbf{e}_{x_i}) + \gamma(\tilde{\mathbf{x}}_i + \mathbf{e}_{x_i}, \boldsymbol{\theta}) + \sigma \varepsilon_i$$

$$\text{Equation 6-12} \quad r_i(\boldsymbol{\theta}, \mathbf{e}_{x_i}) = \tilde{d}_i - \hat{d}(\tilde{\mathbf{x}}_i + \mathbf{e}_{x_i}) - \gamma(\tilde{\mathbf{x}}_i + \mathbf{e}_{x_i}, \boldsymbol{\theta})$$

$$\text{Equation 6-13} \quad L(\boldsymbol{\Theta}) \propto \prod_{\text{Equality data}} P[\sigma \varepsilon_i - e_{d_i} = r_i(\boldsymbol{\theta}, \mathbf{e}_{x_i})]$$

For the cases that we use simulation results for observations, since the input parameters are exact and theoretically without error, the \mathbf{e}_{x_i} terms are zero and e_{d_i} terms are the only

measured error in the model. In this situation the likelihood function for equality data takes the form:

$$\text{Equation 6-14} \quad L(\boldsymbol{\theta}, \sigma) \propto \prod_{\text{Equality data}} \left\{ \frac{1}{\hat{\sigma}(\boldsymbol{\theta}, \sigma)} \varphi \left[\frac{\hat{r}_i(\boldsymbol{\theta})}{\hat{\sigma}(\boldsymbol{\theta}, \sigma)} \right] \right\}$$

where:

$$\text{Equation 6-15} \quad \hat{\sigma}^2(\boldsymbol{\theta}, \sigma) = \sigma^2 + s_i^2$$

s_i^2 : Variance of e_{di}

$$\text{Equation 6-16} \quad \hat{r}_i(\boldsymbol{\theta}) = \tilde{d}_i - \hat{d}(\mathbf{x}_i) - \gamma(\mathbf{x}_i, \boldsymbol{\theta})$$

Noticed that Equation 6-16 may be transferred in from of log or root square to satisfy homoscedasticity assumption.

Posterior distributions

As mentioned earlier, following Bayesian method, the estimation of parameters Θ based on prior (old knowledge) and likelihood (new knowledge) is reflected in the posterior distribution. Increasing sample numbers and improving the prior function produce a better estimation of $\boldsymbol{\theta}$ and lower mean value of σ . Once the final posterior is determined, the mean value of vector $\boldsymbol{\theta}$ will be used in the probabilistic demand model (Equation 6-1). Two methods based on the result data and the prior type are available to compute the posterior distribution.

Closed form solution

For a linear model of θ parameters if all the experimental results data are equality type without recording error and the prior distribution is noninformative, then the solution can be developed in a closed-form solution. For any other conditions, for example, when we

have upper bound data or a prior distribution based on previous studies, computation of the posterior and finding normalizing factor κ is complicated and needs numerical solutions.

In order to solve the represented demand model in Equation 6-1 in a closed-form solution by using equality observation, we can rewrite it as

$$\text{Equation 6-17} \quad \mathbf{d}_R = \mathbf{H}\boldsymbol{\theta} + \sigma\boldsymbol{\varepsilon} \quad \text{or} \quad (d_m)_R = H_{m,n} \cdot \theta_n + \sigma\varepsilon_t$$

where

$\mathbf{d}_R = \mathbf{d} - \hat{\mathbf{d}}(\mathbf{x})$: Vector of residual demand (or transformed with proper function like natural logarithm) with size of $M \times 1$, and $\mathbf{d} = (d_1, d_2, \dots, d_M)$ is equality observation from real or virtual experiments while M is the total number of observations.

\mathbf{H} : Matrix of explanatory function with size of $M \times N$, while N is the number of explanatory functions.

According to Box and Tiao (1997), assuming a noninformative prior and independency between $\boldsymbol{\theta}$ and σ (or $\log(\sigma)$ for the case where natural logarithm transformation function is used), the posterior of $\boldsymbol{\theta}$ and σ are as function of multivariate t-distribution (Equation 6-18) and inverse-chi-squared distribution (Equation 6-19), respectively.

$$\text{Equation 6-18} \quad f(\boldsymbol{\theta} | \mathbf{d}_R) = t_k \left[\hat{\boldsymbol{\theta}}, \Sigma, \nu \right] = \frac{\Gamma\left(\frac{\nu + N}{2}\right)}{\Gamma\left(\frac{\nu}{2}\right) \nu^{\frac{N}{2}} \pi^{\frac{N}{2}} \Sigma^{\frac{1}{2}} \left[1 + \frac{(\boldsymbol{\theta} - \hat{\boldsymbol{\theta}})^T (\boldsymbol{\theta} - \hat{\boldsymbol{\theta}})}{\nu \cdot \Sigma} \right]^{\frac{\nu + N}{2}}}$$

Equation 6-19 $f(\sigma^2 | \mathbf{d}_R) = \nu s^2 \cdot \text{inv } \chi^2(\nu) = \nu s^2 \cdot \frac{1}{2^{\frac{\nu}{2}} \Gamma\left(\frac{\nu}{2}\right) \sigma^{2\left(\frac{\nu}{2}+1\right)} e^{-\frac{1}{2\sigma^2}}}$

where

t_k : Multivariate t-distribution

$\text{inv } \chi^2$: Inverse-chi-squared distribution

$$\hat{\boldsymbol{\theta}} = (\mathbf{H}^T \mathbf{H})^{-1} \mathbf{H}^T \mathbf{d}_R$$

$$s^2 = \frac{1}{\nu} (\mathbf{d}_R - \hat{\mathbf{d}}_R)^T (\mathbf{d}_R - \hat{\mathbf{d}}_R)$$

$$\hat{\mathbf{d}}_R = \mathbf{H} \hat{\boldsymbol{\theta}}$$

$$\Sigma = s^2 (\mathbf{H}^T \mathbf{H})^{-1}$$

$$\nu = M - N$$

M: Number of observations

N: Number of explanatory functions

Noting that:

Mean and mode of $\boldsymbol{\theta} = \hat{\boldsymbol{\theta}}$

$$\text{Covariance of } \boldsymbol{\theta} = \frac{\nu}{\nu-2} \Sigma = \frac{\nu s^2}{(\nu-2)} (\mathbf{H}^T \mathbf{H})^{-1}$$

$$\text{Mean of } \sigma^2 = \frac{\nu}{(\nu-2)} s^2$$

$$\text{Variance of } \sigma^2 = \frac{2\nu^2}{(\nu-2)^2(\nu-4)} s^4$$

Importance sampling method

In the cases with non-equality data or error in the results measurement or when we have prior information from past experiences or engineering judgment, we cannot use the closed-form solution to compute the posterior. In this case, computing the posterior distribution as well as κ (normalizing factor in order to ensure the integration of posterior equals to one), is not easy and needs multifold integration over the Bayesian Kernel $L(\theta)p(\theta)$. Gardoni (2002) developed an algorithm for computing the posterior statistics in these cases, using importance sampling. Importance sampling is a general technique for estimating properties of a particular distribution, while only having samples generated from a different distribution rather than the distribution of interest.

Methodology for model selection

In order to build the described probabilistic demand model, $D(\mathbf{x}, \Theta)$ (Equation 6-1), according to Gardoni (2002), the following steps are required:

- 1- Define the deterministic demand function (simple method in section 5) and explanatory function (bases on the rules of mechanics and engineering judgment).
- 2- Gather experimental tests results and generate simulation tests results (section 3 and 4).
- 3- Perform the Bayesian method and to compute posterior function of Θ .

- 4- Do the stepwise deletion by examining the coefficient of variations of θ_i and omitting the $h_i(x)$ that has the largest value of c.o.v. Larger c.o.v means less informative of explanatory function.
- 5- Combine the correlated explanatory functions by checking the absolute value of correlation coefficients between $\theta_i, \left| \rho_{\theta_i, \theta_j} \right|$. $|\rho| > 0.7$ indicates that $h_i(x)$ and $h_j(x)$ are closely related, so the combination of them is enough. For the cases when $0.5 < |\rho| < 0.7$, one of the θ s can be replaced by

Equation 6-20

$$\theta_i = \mu_{\theta_i} + \rho_{\theta_i, \theta_j} \frac{\sigma_{\theta_i}}{\sigma_{\theta_j}} (\theta_j - \mu_{\theta_j})$$

Repeat steps 4 and 5 after each reduction or correction of explanatory function to reach a c.o.v of θ_i in the close range of value and have an absolute correlation coefficient less than 0.5. If the mean value of σ has increased by an unacceptable amount during the deletion process, the reduction is not desirable and the model before the deletion process is as efficient as possible.

Rotation and load demand models

Rotation demand model

The rotation demand model is defined as the rotation of single pile at impact point under the vehicle impact. The logarithmic transformation is used to satisfy the homoscedasticity and normality assumptions. Total number of 54 results (7 real and 47 virtual experiments) data are used in the model generation. Due to a lack of prior

information on the model parameters, a non-informative prior is used and $p(\Theta) \propto \frac{1}{\sigma}$ is selected for non-informative prior. The result error term in the simulations rotation results is defined based on the PU60 test simulation verification. The simulation maximum rotation was 20° while the real experiment resulted in 23° rotation on the post; therefore the error in the results (e_d) is assumed $Ln(\frac{23}{20}) = 0.14$ for all the numerical simulations and 0 for experimental tests. Primary 10 explanatory functions developed based on engineering judgment are:

$$h_1 = 1$$

$$h_2 = Ln(\hat{d}_r)$$

\hat{d}_r : Simple model rotation output

$$h_3 = \hat{d}_r$$

$$h_4 = \frac{\hat{F}_{impact}}{F_{static}}$$

\hat{F}_{impact} : Simple model Impact load output

F_{static} : Lateral static capacity of pile with SALLOP method (Briaud 1997, 958-

964)

$$h_5 = \frac{\frac{1}{2} M_T V_T^2}{F_{static} \hat{d}_d}$$

M_T : Vehicle mass

V_T : Vehicle velocity in simple model= $0.6 \times$ real vehicle velocity

\hat{d}_d : Simple model displacement output

$$h_6 = \frac{\frac{1}{2} M_T V_T^2}{C_s \cdot V_T \cdot L \cdot \hat{d}_d}$$

C_s : Soil damping

L: Pile embedment depth

$$h_7 = \frac{\frac{1}{2} M_T V_T^2}{(C_s \cdot V_T \cdot L + F_{static}) \hat{d}_d}$$

$$h_8 = \frac{\frac{1}{2} M_T V_T^2}{\hat{F}_{impact} \hat{d}_d}$$

$$h_9 = 1000 \frac{E_{soil}}{E_{pile}}$$

E_{soil} : Soil modulus of elasticity

E_{pile} : Pile modulus of elasticity

$$h_{10} = \frac{M_T}{(M_{soil} + M_{pile})L}$$

M_{soil} : Mass of soil per length in simple model

M_{pile} : Mass of pile per length

The stepwise deletion procedure according to section 0 is used to select the most informative explanatory function. Since the prior in this model is noninformative, the c.o.v of θ_s , performing maximum likelihood estimation (MLE), are in the same range of

posterior analysis. Therefore the stepwise deletion process is performed on the likelihood. Figure 6-1 summarizes the stepwise deletion process for rotation demand model. As it is shown in the figure at each step the maximum c.o.v of model parameters θ is detected and the explanatory function for that parameter is omitted. For example at step 4, θ_7 has the maximum c.o.v equal to 1.6 and for the next step the h_7 is removed from the model. The process continues until a jump is observed in the σ value. In this model between step 7 and 8 a significant increase happens in σ value (Figure 6-2); therefore we stop at step 7 and model is selected based on parameters in step 7. The final model at this step is presented in Equation 6-21 or in different presentation Equation 6-22.

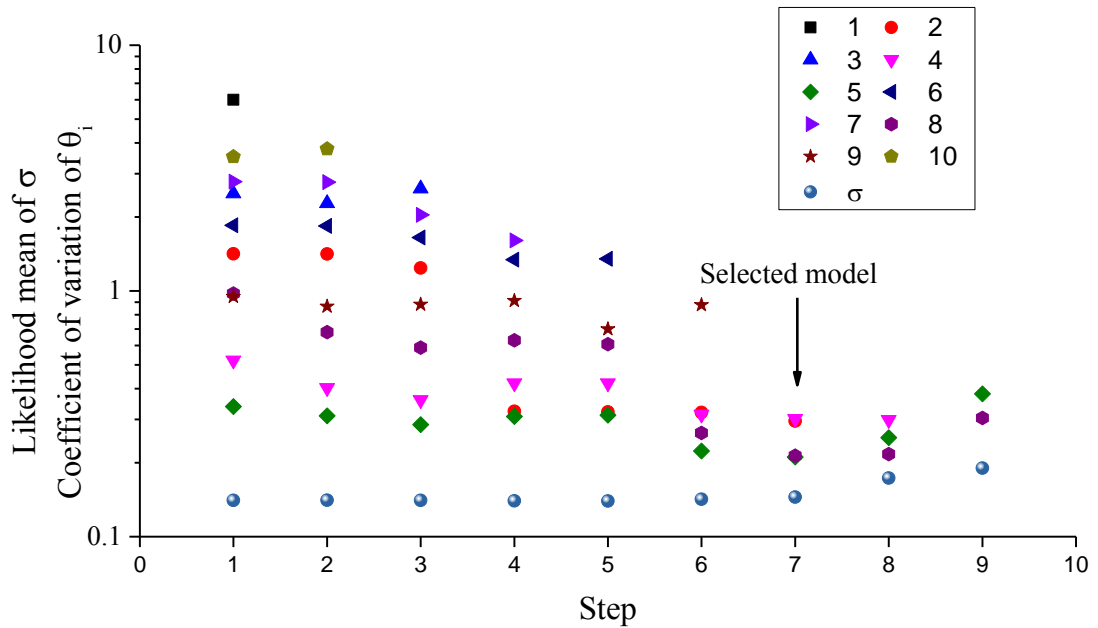


Figure 6-1: Stepwise deletion process for rotation demand model

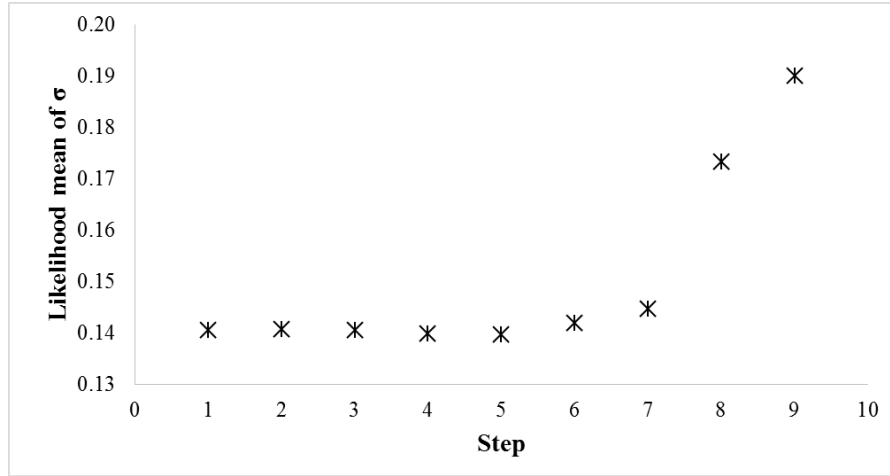


Figure 6-2: Likelihood mean of σ change in stepwise deletion process

Equation 6-21

$$\begin{aligned} \ln(D_r(\mathbf{x}, \Theta)) &= \ln(\hat{d}_r(\mathbf{x})) + \theta_{r2} \ln(\hat{d}_r(\mathbf{x})) \\ &+ \theta_{r4} \frac{\hat{F}_{impact}}{F_{static}} + \theta_{r5} \frac{M_T V_T^2}{2F_{static} \hat{d}_d} + \theta_{r8} \frac{M_T V_T^2}{2\hat{F}_{impact} \hat{d}_d} + \sigma_r \varepsilon_r \end{aligned}$$

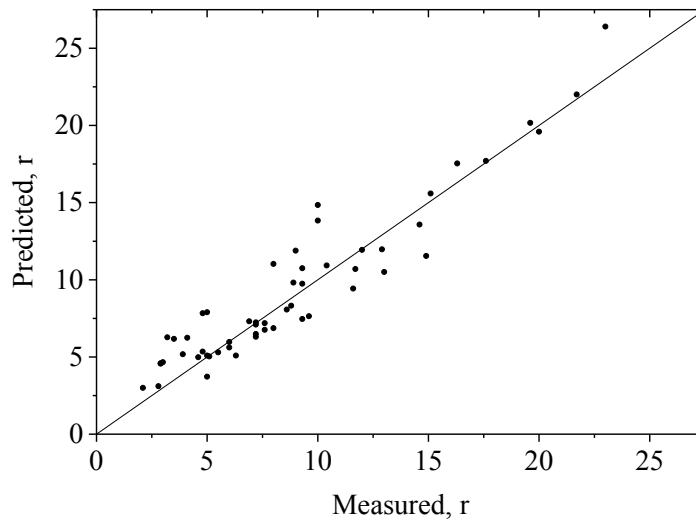
Equation 6-22

$$D_r(\mathbf{x}, \Theta) = \hat{d}_r(\mathbf{x}) \cdot e^{\theta_{r2} \ln(\hat{d}_r(\mathbf{x}))} \cdot e^{\theta_{r4} \frac{\hat{F}_{impact}}{F_{static}}} \cdot e^{\theta_{r5} \frac{M_T V_T^2}{2F_{static} \hat{d}_d}} \cdot e^{\theta_{r8} \frac{M_T V_T^2}{2\hat{F}_{impact} \hat{d}_d}} \cdot e^{\sigma_r \varepsilon_r}$$

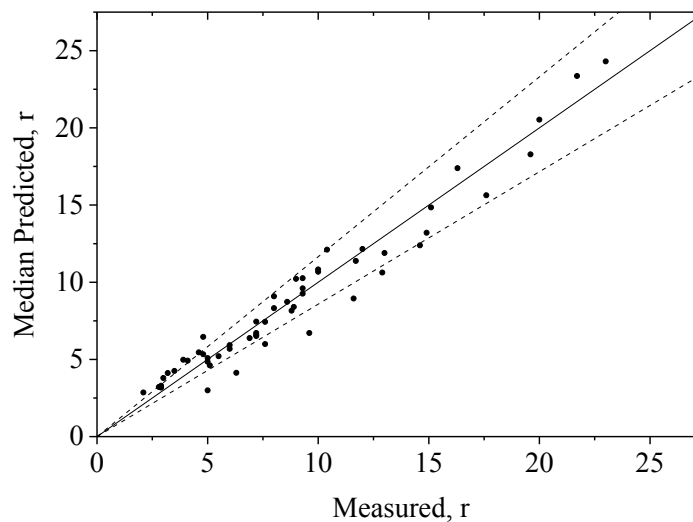
Table 6-1 presents the posterior statistics of the rotation model parameters. According to correlation coefficient there are a strong correlation between θ_{r4} and θ_{r5} with $|\rho|=0.929$ and between θ_{r4} and θ_{r8} with $|\rho|=0.836$ and θ_{r5} and θ_{r8} with $|\rho|=0.835$. Since the simple model is developed as a computational code there is no need to combine the parameters. Figure 6-3 shows the prediction versus measured rotation based on deterministic and probabilistic model. The dashed lines are the region with one standard deviation of the model.

Table 6-1: Posterior statistics of the parameters in the rotation demand model

Parameter	Mean	Standard deviation	Correlation Coefficient				
			θ_{r2}	θ_{r4}	θ_{r5}	θ_{r8}	σ_r
θ_{r2}	-0.233	0.064	1				
θ_{r4}	-0.228	0.063	0.075	1			
θ_{r5}	0.851	0.164	-0.344	-0.929	1		
θ_{r8}	-0.942	0.205	-0.158	0.836	-0.835	1	
σ_r	0.153	0.020	-0.067	0.016	0.009	0.041	1



(a)



(b)

Figure 6-3: Comparison between measured versus predicted rotation demands: (a) deterministic model and (b) median probabilistic model

For the perfect prediction results the solid points should be located on the 1:1 line. According to Figure 6-3 the solid dots line closer to the 1:1 line and the region becomes narrower in the probabilistic model which shows the model works well in modifying the deterministic model. For example, the M50 prediction in the probabilistic model is modified from 11.9° to 10.2° while the experiment maximum rotation was 9° this indicates 19% improvement in the prediction.

Load demand model

In order to make the load dimensionless, dimensionless moment (DLM) is defined as the ratio of impact moment at level ground over the elastic moment capacity of pile (Equation 6-23). DLM can also be estimated as the ratio of equivalent impact load over the load magnitude at the impact point to yield the pile at the surface. 60 results (13 real experiments and 47 simulations) are used for model parameter calculation. The 11 explanatory functions are selected for the Bayesian updating method. The functions are the same as the functions used in the rotation probabilistic model except $h_2 = \text{Ln}(\hat{d}_{DLM})$ and $h_{11} = \hat{d}_{DLM}$, where \hat{d}_{DLM} is the simple model dimensionless moment (DLM) output. The probabilistic model for load is also transformed by logarithmic transformation. The result error is based on PU60 simulation compared to experiment which equals to $\text{Ln}(\frac{490}{440}) = 0.11$ for all the simulations and 0 for experiments. The informative parameters are filtered with stepwise deletion method. As it is shown in Figure 6-4 and Figure 6-5 the deletion process is stopped in step 7 where the likelihood mean of σ changes significantly, and 5 final explanatory functions are selected. The final probabilistic demand model of

DLM is presented in Equation 6-24. Similar to the rotation demand because of lack of prior information on model parameters, we use a non-informative prior in computing the posterior statistics.

Equation 6-23

$$\hat{d}_{DLM} = \frac{\hat{M}_{impact}}{\hat{M}_{yield}}$$

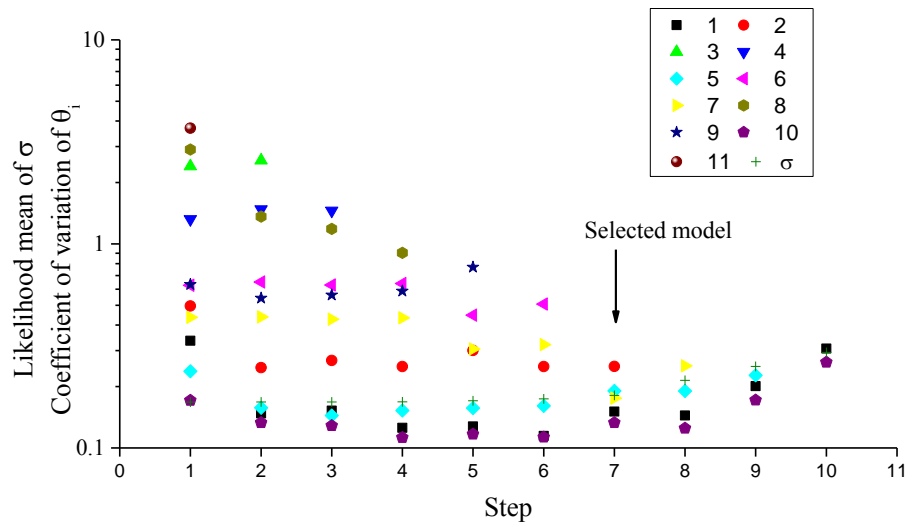


Figure 6-4: Stepwise deletion process for dimensionless moment demand model

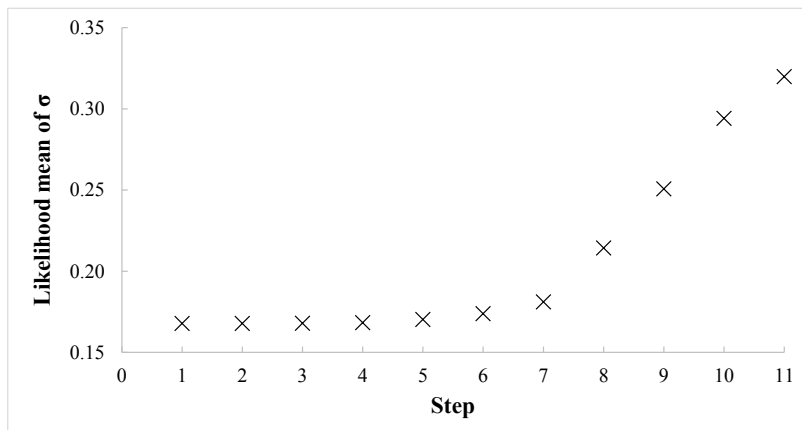


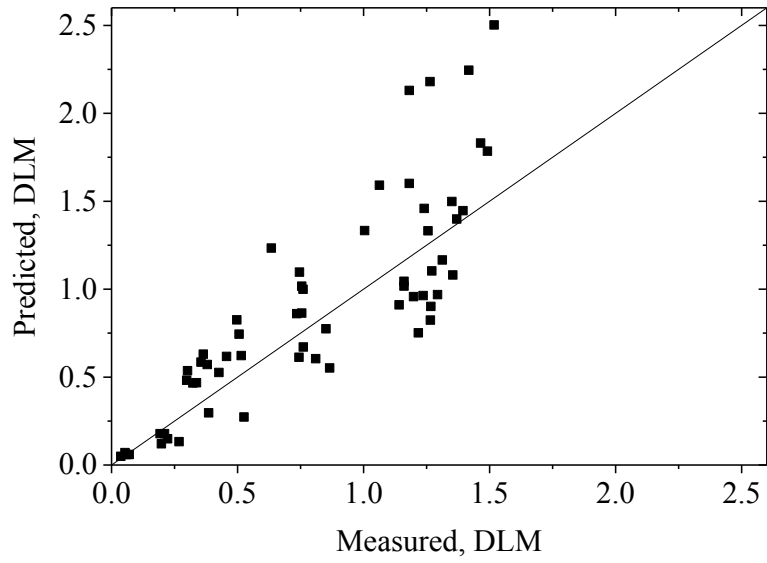
Figure 6-5: Likelihood mean of σ change in stepwise deletion process

$$\begin{aligned}
 \text{Equation 6-24} \quad & \text{Ln}(D_{DLM}(\mathbf{x}, \Theta)) = \text{Ln}(\hat{d}_{DLM}(\mathbf{x})) + \theta_{DLM1} + \theta_{DLM2} \text{Ln}(\hat{d}_{DLM}(\mathbf{x})) \\
 & + \theta_{DLM5} \frac{M_T V_T^2}{2F_{static} \hat{d}_d} + \theta_{DLM7} \frac{M_T V_T^2}{2(C_s \cdot V_T \cdot L + F_{static}) \hat{d}_d} \\
 & + \theta_{DLM10} \frac{M_T}{(M_{soil} + M_{pile})L} + \sigma_{DLM} \epsilon_{DLM}
 \end{aligned}$$

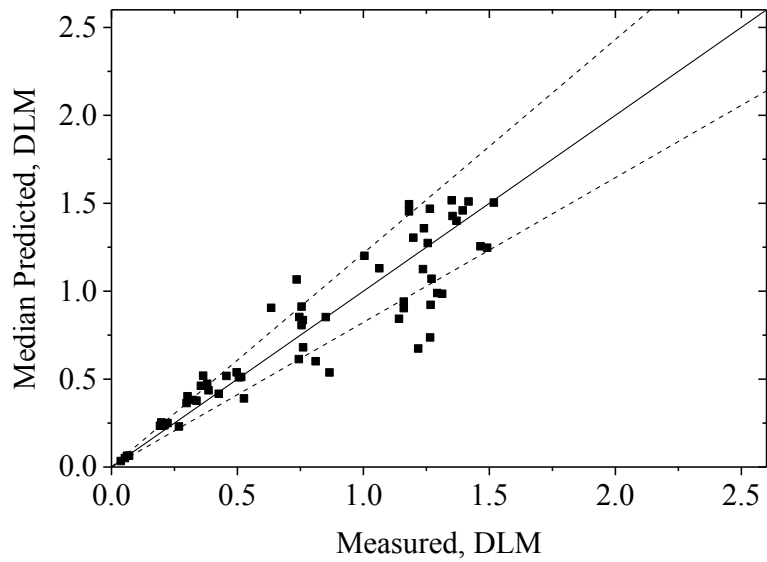
Table 6-2 gives the posterior statistics of the DLM demand model parameters and Figure 6-6 shows the comparison between the deterministic simple demand model (a) and the median probabilistic demand model for DLM. For example the predicted DLM from M50 test with DLM=1.354 ($F_{\text{impact}}=1600$ kN) by deterministic model is 1.08 ($F_{\text{impact}}=1276$ kN) while the median demand model predicts the DLM=1.427 ($F_{\text{impact}}=1686$) kN. The modification in the DLM (or load) demand model is more efficient than rotation one.

Table 6-2: Posterior statistics of the parameters in the Dimensionless moment demand model

Parameter	Mean	Standard deviation	Correlation Coefficient					
			θ_{DLM1}	θ_{DLM2}	θ_{DLM5}	θ_{DLM7}	θ_{DLM10}	σ_{DLM}
θ_{DLM1}	-1.806	0.215	1					
θ_{DLM2}	0.186	0.046	-0.557	1				
θ_{DLM5}	0.484	0.072	-0.904	0.442	1			
θ_{DLM7}	2.128	0.344	-0.705	0.606	0.387	1		
θ_{DLM10}	0.040	0.005	-0.921	0.735	0.806	0.698	1	
σ_{DLM}	0.195	0.026	-0.074	-0.025	0.129	-0.006	0.037	1



(a)



(b)

Figure 6-6: Comparison between measured versus predicted dimensionless moment demands: (a) deterministic model and (b) median probabilistic model

Fragility estimation

Fragility is defined as the probability failure of a system when the prescribed limit state is reached or passed for specific set of boundary variables. The fragility is sometimes called probability of failure (Gardoni, Der Kiureghian, and Mosalam 2002, 1024-1038). Let $g_k(\mathbf{x}, \Theta_k)$ be a mathematical model describes a k th condition that structure cannot fulfils the design criteria where \mathbf{x} and Θ_k are the input variables and model parameters, respectively. The criteria refer to the structural integrity, fitness for use, unsafe condition, durability or other design requirements. The limit state can be categorized in either ultimate limit or serviceability limit state and it is defined as $g_k(\mathbf{x}, \Theta_k) \leq 0$. Input variables can be classified in two variables \mathbf{r} and \mathbf{s} , $\mathbf{x} = (\mathbf{r}, \mathbf{s})$, where \mathbf{r} is measurable variables (e.g. geometry, material properties), and \mathbf{s} is initial conditions (e.g., vehicle velocity and vehicle mass).

Following Gardoni et al. (2002, 1024-1038) a predictive estimation of fragility of a system is formulated as:

Equation 6-25
$$F(\mathbf{s}, \Theta) = P \left[\bigcup_k \{g_k(\mathbf{r}, \mathbf{s}, \Theta_k) \leq 0\} \mid \mathbf{s}, \Theta \right]$$

where:

$P[A|s]$: Conditional probability of event A for given variables s

$g_k(\mathbf{r}, \mathbf{s}, \Theta_k) = C_k(\mathbf{r}, \mathbf{s}, \Theta_k) - D_k(\mathbf{r}, \mathbf{s}, \Theta_k)$: Limit state function as a function of $C_k(\mathbf{r}, \mathbf{s}, \Theta_k)$ (capacity model) and $D_k(\mathbf{r}, \mathbf{s}, \Theta_k)$ (demand model) of k th failure criterion.

Capacity and demand models

One failure mode is considered for building the fragility in this study. Based on the experience at Roadside Safety and Physical Security at Texas Transportation Institute (TTI) and real and virtual experiments the capacity of single pile to stop a vehicle from passing the post is 20° rotation of the pile at impact point. Considering no failure due to bending on the pile, the capacity can also be estimated from a simple assumption that vehicle slide over the pile. Figure 6-7 shows schematic diagram for capacity of single pile under impact.

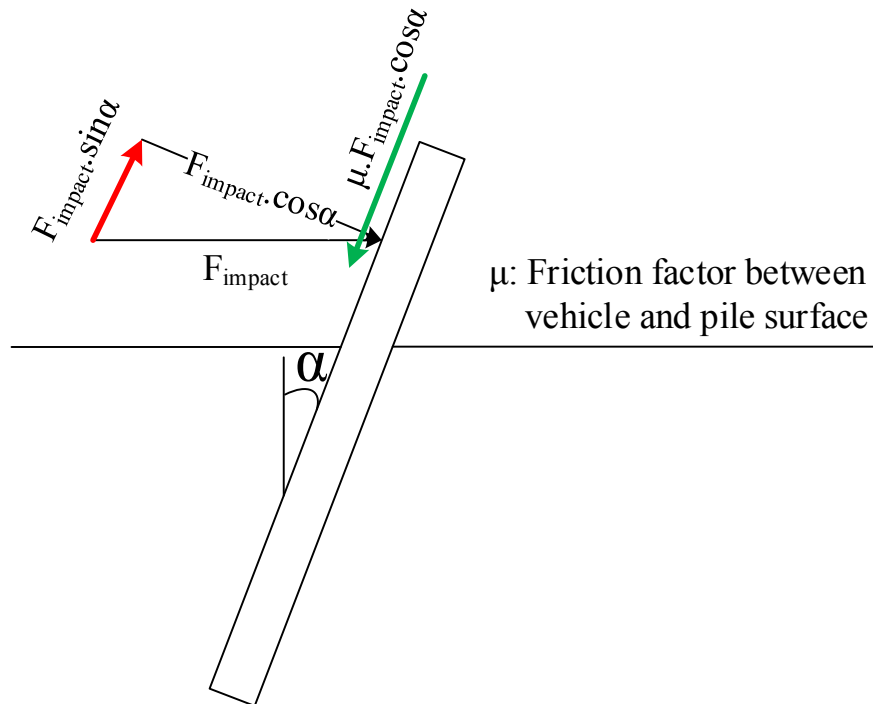


Figure 6-7: Capacity estimation of pile under lateral impact

Taking 0.4 for steel friction factor gives us capacity of pile equals to 21° . A constant number (20 degree) for failure rotation is selected as the capacity in fragility computation. Demand probabilistic model is described in Equation 6-22. Therefore, the limit state function is formulated as Equation 6-26:

Equation 6-26

$$g_r(\mathbf{x}, \Theta_r) = 20^\circ - D_r(\mathbf{x}, \Theta_r)$$

where $D_r(\mathbf{x}, \Theta_r)$ is described in Equation 6-22.

Fragility calculation

Two methods of point and predictive estimation are available to calculate the fragility. In the point estimation the uncertainty of model parameters is ignored and fragility is obtained from point estimation of parameters mean value ($\hat{\Theta}$). The uncertainty in this method arises only from input variables \mathbf{r} and random model correction ε . The numerical computation method of point estimation of fragility is developed by Ditlevsen and Madsen (1996). The predictive estimation of fragility considers Θ parameters as random variables and it takes both aleatory and epistemic uncertainties into account. The distribution can be obtained from the posterior derived with Bayesian approach (Gardoni 2002).

In this study the fragility estimates are based on passing a vehicle from single pile which is corresponding to 20° rotation of single post under impact of vehicle in specific soil with specific pile embedment depth and width. In developing the fragility curve soil properties, pressure limit (p_L) and soil modulus (E) are considered lognormal random variables, respectively with mean of 1300 kPa and 20 MPa (Medium strength), and standard deviation of 130 kPa (c.o.v=10%) and 6 MPa (c.o.v=30%). Soil unit weight mean

is selected 21 kN/m^3 with standard deviation of 1.05 kN/m^3 (c.o.v=5%) and lognormal distribution. Finally, the mean of lognormal distribution of impact height is considered 0.75m with standard deviation of 0.075m (c.o.v=10%).

Monte Carlo simulations are used to produce the fragility curves. Figure 6-8 and Figure 6-9 present the 2D and 3D predictive fragility surface in terms of mass and velocity of the vehicle. The pile-soil system in the fragility estimation is a 0.35m diameter tube section (HSS $14 \times 1/2$) single pile with 2m embedment in medium strength clay. The Figure 6-8 shows the contour line in level of fragility in the range of 10% to 90% addition to 1% probability of failure line. 4 passed experiments simulated with LS-DYNA and a failed experiment related to PU60 test are shown on the fragility curve. The PU60 impact condition on this pile has 87% estimated possibility of failure.

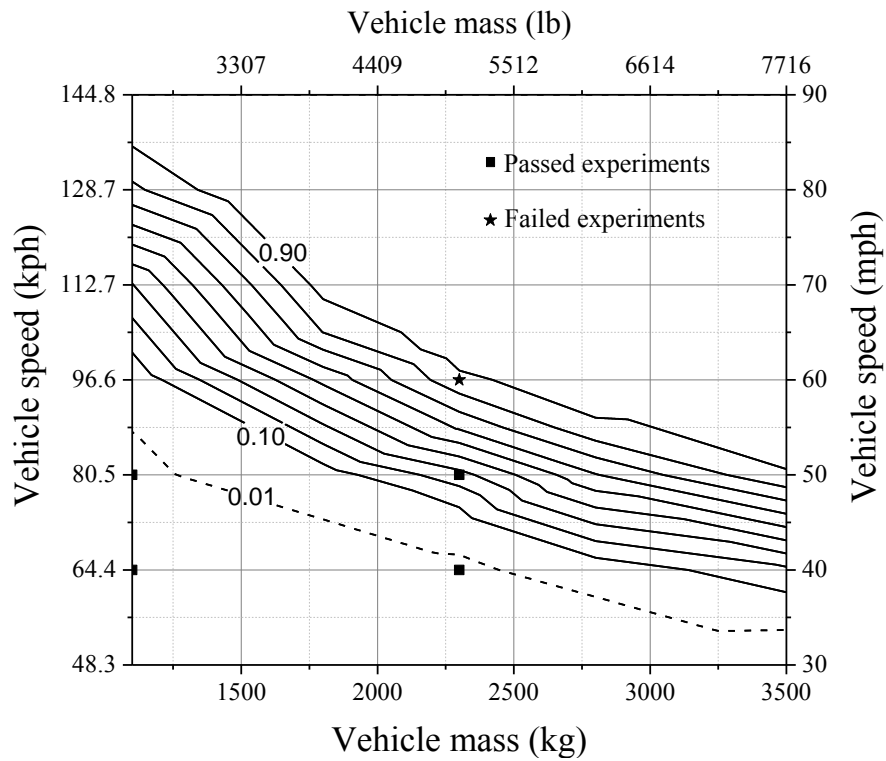


Figure 6-8: Fragility estimation for HSS 14×1/2 single pile with 2m embedment depth in medium clay under vehicle impact

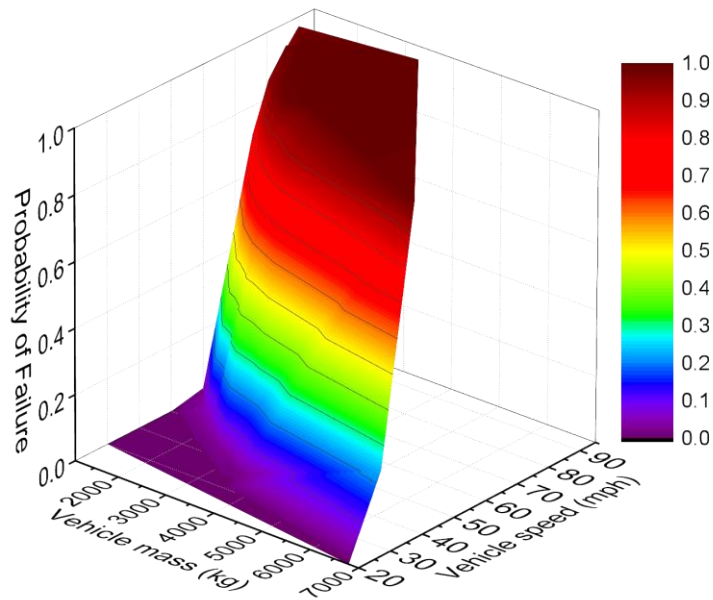


Figure 6-9: 3D fragility surface for HSS 14×1/2 single pile with 2m embedment depth in medium clay under vehicle impact

Figure 6-10 shows the univariate fragility curve associated with pickup truck (PU Designation according to ASTM-F2656) as function truck velocity. The solid line represents the predictive estimate and dashed line indicates the 15% and 85% confidence bounds. Bounds of fragility is evaluated by first-order analysis on the limit state function described by Gardoni, et al (2002, 1024-1038). The slope of curve is effected by aleatory uncertainties (uncertainties in soil properties and impact height and ϵ) and the boundary width is related to epistemic uncertainties (probabilistic parameters, Θ).

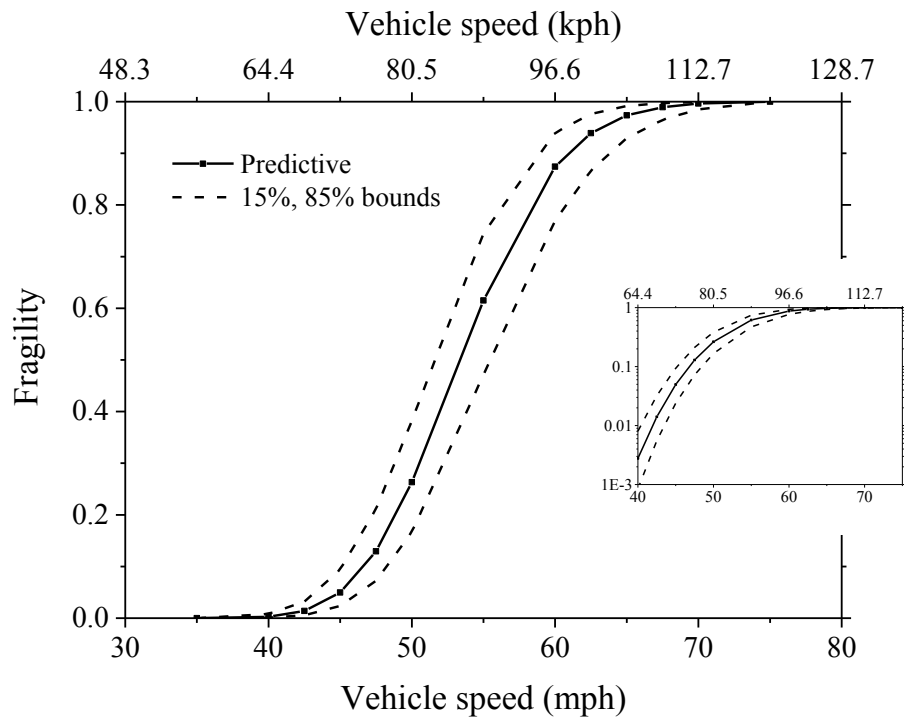


Figure 6-10: Fragility estimate of Pickup truck impact on HSS 14×1/2 single pile with 2m embedment depth in medium clay

7. CONCLUSION

The main goal of this research is to develop a deterministic and probabilistic simple model of single pile behavior under lateral vehicle impact. In order to reach the goal a simple method and computational code to analyze the behavior of a single pile subjected to a truck impact for any soil type, any truck mass, any truck velocity and any pile size is developed and modified with Bayesian approach.

The four major components in the research are:

1. Experimental tests: design and performance of scaled and full scale tests as well as soil testing
2. Numerical simulations: perform enough numerical simulation cases with LS-DYNA to calibrate the simple and probabilistic model
3. Analytical solution: design of a simple model and derivation of associated equations and solution
4. Probabilistic model: build a probabilistic capacity model and estimate the system fragility.

Experimental tests

A set of 12 impact tests were performed and form a very valuable database from which to evaluate design recommendations. Only 2 of these 12 tests are full scale tests: one single pile test in medium clay with pickup truck with 60 miles per hours speed (PU60) and one single pile test in very dense crushed limestone with 50 miles per hours speed (M50). In order to investigate the soft soil behavior 6 medium scale tests for the purpose of constant

velocity in soft clay and loose sand with a heavy bogie were conducted. 4 medium scale tests with dropping mass for the purpose of constant acceleration were also performed in the soft clay and loose sand. For each soil type static and creep lateral behavior of single piles were also tested. All the tests were instrumented with accelerations, strain gauges, and high speed cameras for dynamic and string-pot, load cell, and inclinometer for static tests. An extensive site investigation and lab tests were used to obtain the soil properties. In the field, more than 10 different types of in-situ and lab test were conducted. The main field test used in the simple code is the pressuremeter test because of the lateral loading analogy. The outcomes of this part are a data set for simulation and simple model calibration in addition to observation leads us to identify the soil important parameters.

LS-DYNA Simulation

Series of numerical simulations (LS-DYNA) to fill the gap in the database of experiments were done. This is advantageous because numerical simulations are much less costly than full scale experiments. A total number of 49 impact simulations (2 calibrating and 47 database simulations) were performed to calibrate the simple model parameters. Two soil models, von Mises and Drucker Prager, and two vehicle types, very small passenger car and pickup truck, were used in the simulations. The quantities of displacement, rotation, and equivalent impact load were obtained from the simulation to be used in the simple model calibration.

Simple analytical model

The outcome of this part is a simple code (in Matlab or Microsoft Office Excel) to analyze the behavior of a single pile subjected to a vehicle impact based on in-situ or laboratory based soil parameters. The simple code is calibrated with a set of full-scale and model scale experiments and a number of LS-DYNA numerical simulations.

A beam on elastic foundation theory has been expanded to solve the dynamic impact problem. A simple Matlab program called TAMU-POST has been developed. The input to the program makes use of common properties for the soil, the post, and the beam. For the soil, the damping factor and the associated mass during impact have been theoretically and empirically correlated and predictive equations have been developed. The output of the program gives the displacement, slope, deceleration, and force vs. time as well as the envelope of the maximum bending moments in the post vs. depth. The program has been verified by comparing predicted and measured displacement and deceleration vs. time signals.

Probabilistic model and fragility estimate

All the work done for the first part has been deterministic in nature and there are uncertainties associated with each one of the input parameters including the type of truck that will impact the barrier and the heterogeneity of the soil deposit. There are also uncertainties associated with the theoretical model developed to predict the system behavior.

In order to quantify the uncertainties in the parameters and the simple model, a set of probabilistic models were designed, and fragility estimation was developed by using one of the models. For the risk and reliability analysis, a Bayesian framework was chosen to expand the simple deterministic model to probabilistic demand models. The probabilistic demand model and the required capacity were used in a limit-state function to construct the fragility (conditional probability of failure of the structural member given a set of demand variables) of the pile under a vehicle impact.

REFERENCES

- AASHTO (Ed.). (2012). *LRFD Bridge design specifications* (6th Edition ed.). Washington, DC: American Association of State Highway and Transportation Officials.
- Abou-matar, H., Rausche, F., Thendean, G., Likins, G., & Goble, G. (1996). Wave equation soil constants from dynamic measurements on SPT. Paper presented at the *Proc. 5th Int. Conf. App. Stresswave Theory to Piles, Orlando, Florida*, 163-175.
- Alberson, D. C., Buth, C. E., Briaud, J. L., & Menhes, W. L. (2007). *DOS K12 testing and evaluation of direct embedded pier*. (). College Station, TX.: Texas Transportation Institute.
- Alejano, L. R., & Bobet, A. (2012). Drucker–Prager criterion. *Rock Mechanics and Rock Engineering*, 45(6), 995-999. doi:10.1007/s00603-012-0278-2
- API, R. (2007). 2A-WSD, 2007,“ *Recommended Practice for Planning, Designing and Constructing Fixed Offshore Platforms–Working Stress Design*, ” American Petroleum Institute,
- Applied Foundation Testing, I. (2012). *Final report of lateral STATNAMIC load testing*. ().Applied Foundation Testing, Inc.
- ASTM Standard D1586. (2011). *Standard test method for standard penetration test (SPT) and split-barrel sampling of soils*. West Conshohocken, PA: ASTM International. doi:10.1520/D1586-11
- ASTM Standard D2166. (2013). *Standard test method for unconfined compressive strength of cohesive soil*. West Conshohocken, PA: ASTM International. doi:10.1520/D2166_D2166M
- ASTM Standard D2850. (2003a (2007)). *Standard test method for unconsolidated-undrained triaxial compression test on cohesive soils*. West Conshohocken, PA: ASTM International. doi:10.1520/D2850-03AR07
- ASTM Standard D3080. (2004). *Standard test method for direct shear test of soils under consolidated drained conditions*. West Conshohocken, PA: ASTM International. doi:10.1520/D3080-04

- ASTM Standard D3966. (2007(2013)). *Standard test methods for deep foundations under lateral load*. West Conshohocken, PA: ASTM International. doi:10.1520/D3966_D3966M
- ASTM Standard D4648. (2013). *Standard test method for laboratory miniature vane shear test for saturated fine-grained clayey soil*. West Conshohocken, PA: ASTM International. doi:10.1520/D4648_D4648M-13
- ASTM Standard D4719. (2007). *Standard test methods for prebored pressuremeter testing in soils*. West Conshohocken, PA: ASTM International. doi:10.1520/D4719-07
- ASTM Standard D4945. (2012). *Standard test method for high-strain dynamic testing of deep foundations*. West Conshohocken, PA: ASTM International. doi:10.1520/D4945-12
- ASTM Standard D6951. (2009). *Standard test method for use of the dynamic cone penetrometer in shallow pavement applications*. West Conshohocken, PA: ASTM International. doi:10.1520/D6951_D6951M-09
- ASTM Standard D7383. (2010). *Standard test methods for axial compressive force pulse (rapid) testing of deep foundations*. West Conshohocken, PA: ASTM International. doi:10.1520/D7383-10
- ASTM Standard F2656. (2007). *Standard test method for vehicle crash testing of perimeter barriers*. West Conshohocken, PA: ASTM International. doi:10.1520/F2656-07
- Babu, K., & Sridhar, K. (2010). *Design of machine elements* McGraw-Hill Education (India) Pvt Limited. Retrieved from <http://books.google.com/books?id=Px9kbvsG3WYC>
- Boulanger, R. W., Curras, C. J., Kutter, B. L., Wilson, D. W., & Abghari, A. (1999). Seismic soil-pile-structure interaction experiments and analyses. *Journal of Geotechnical and Geoenvironmental Engineering*, 125(9), 750-759.
- Briaud, J. (1992). *The pressuremeter* Taylor & Francis/A.A. Balkema.

- Briaud, J. (1997). SALLOP: Simple approach for lateral loads on piles. *Journal of Geotechnical and Geoenvironmental Engineering*, 123(10), 958-964.
- Briaud, J. (2013). *Geotechnical engineering: Unsaturated and saturated soils* John Wiley & Sons.
- Briaud, J., Lim, S. G., & Mirdamadi, A. (2012). Testing of piles subjected to truck impact. *The 9th International Conference on Testing and Design Methods for Deep Foundations*, Kanazawa, Ishikawa, Japan.
- Briaud, J., & Terry, T. (1986). Rate effect for vertical and horizontal pile response. Paper presented at the *Numerical Methods in Offshore Piling International Conference*, Nantes, France. 387-405.
- Broms, B. B. (1964a). Lateral resistance of piles in cohesive soils. *Journal of Soil Mechanics and Foundations Division, ASCE90 (SM2)*, 90(2), 27-63.
- Broms, B. B. (1964b). Lateral resistance of piles in cohesionless soils. *Journal of Soil Mechanics and Foundations Division, ASCE90 (SM3)*, 90(3), 123-156.
- Broms, B. B. (1965). Design of laterally loaded piles. *Journal of Soil Mechanics and Foundations Division, ASCE91 (SM3)*, 91(3), 77-99.
- Brown, D. A. (1998). STATNAMIC lateral load response of two deep foundations. Paper presented at the *Statnamic Loading Test 1998: Proceedings of the Second International Statnamic Seminar*, 28-30.
- Brown, D. A. (1999). An experiment with statnamic lateral loading of a drilled shaft. Paper presented at the *Analysis, Design, Construction, and Testing of Deep Foundations (OTRC '99 Conference)*, Austin, Texas, United States. (88) 309-318.
- Brown, D. A. (2007). Rapid lateral load testing of deep foundations. *DFI Journal*, 1(1), 54-62.
- De Silva, C. W. (2007). *Vibration: Fundamentals and practice*. CRC Press.
- Deeks, A. J., & Randolph, M. F. (1995). A simple model for inelastic footing response to transient loading. *International Journal for Numerical & Analytical Methods in Geomechanics*, 19(5), 307-329.

- Dewoolkar, M. M., Hwang, J., & Ko, H. (2008). Physical and finite element modeling of lateral stability of offshore skirted gravity structures subjected to iceberg impact load. *Ocean Engineering*, 35(16), 1615-1626.
- Ditlevsen, O., & Madsen, H. O. (1996). *Structural reliability methods* Wiley New York.
- Dobry, R., Vicente, E., O'Rourke, M. J., & Roesset, J. M. (1982). Horizontal stiffness and damping of single piles. *Journal of Geotechnical and Geoenvironmental Engineering*, 108(GT3), 439-459.
- Duncan, J. M., Evans Jr, L. T., & Ooi, P. S. (1994). Lateral load analysis of single piles and drilled shafts. *Journal of Geotechnical Engineering*, 120(6), 1018-1033.
- Evans, L. T., & Duncan, J. M. (1982). *Simplified analysis of laterally loaded piles* University of California, Department of Civil Engineering.
- Gardoni, P. (2002). *Probabilistic models and fragility estimates for structural components and systems*. (Ph. D., Univ. of California, Berkeley, Berkeley, Calif.).
- Gardoni, P., Der Kiureghian, A., & Mosalam, K. M. (2002). Probabilistic capacity models and fragility estimates for reinforced concrete columns based on experimental observations. *Journal of Engineering Mechanics*, 128(10), 1024-1038. doi:10.1061/(ASCE)0733-9399(2002)128:10(1024)
- Gazetas, G., & Dobry, R. (1984a). Horizontal response of piles in layered soils. *Journal of Geotechnical Engineering*, 110(1), 20-40.
- Gazetas, G., & Dobry, R. (1984b). Simple radiation damping model for piles and footings. *Journal of Engineering Mechanics*, 110(6), 937-956.
- Ghazzaly, O. I., Hwong, S. T., & O'neil, M. W. (1976). Approximate analysis of a pile under dynamic, lateral loading. *Computers & Structures*, 6(4-5), 363-368. doi:[http://dx.doi.org/10.1016/0045-7949\(76\)90013-4](http://dx.doi.org/10.1016/0045-7949(76)90013-4)
- Grundhoff, T. (1997). Horizontal impact loads on large bored single piles in sand. Paper presented at the *Proceedings of the 1997 7th International Offshore and Polar Engineering Conference. Part 3 (of 4)*, Honolulu, HI, USA. , 1 753-760.

- Guo, W. D. (2008). Laterally loaded rigid piles in cohesionless soil. *Canadian Geotechnical Journal*, 45(5), 676-697.
- IABSE. (1983). *Ship collision with bridges and offshore structures*. (No. 3 vols). Copenhagen, Denmark: International Association of Bridge and Structural Engineers Colloquium.
- Ishihara, K. (1996). *Soil behaviour in earthquake geotechnics* Clarendon Press; Oxford University Press.
- Kitiyodom, P., Matsumoto, T., Kojima, E., Kumagai, H., & Tomisawa, K. (2006). Analysis of static and dynamic horizontal load tests on steel pipe piles. Paper presented at the *Proc. 10th International Conference on Piling and Deep Foundations*, 690-699.
- Kitiyodom, P., Matsumoto, T., Tomisawa, K., Kojima, E., & Kumagai, H. (2007). Dynamic and static horizontal load tests on steel pipe piles and their analyses. Paper presented at the *Proc. of Int. Workshop on Recent Advance of Deep Foundations (IWDPF 07)*,
- Lee, S., Chow, Y., Karunaratne, G., & Wong, K. (1988). Rational wave equation model for pile-driving analysis. *Journal of Geotechnical Engineering*, 114(3), 306-325.
- Liang, R., & Sheng, Y. (1992). Interpretation of smith model parameters based on cavity expansion theory. Paper presented at the *Proc., 4th Int. Conf. on Appl. of Stress-Wave Theory to Piles*, 111-116.
- Lim, S. G. (2011). *Development of design guidelines for soil embedded post systems using wide-flange I- beams to contain truck impact* Texas A&M University.
- Livermore Software Technology Corporation (LSTC). (2006). *LS-DYNA theory manual*. Livermore, CA:
- Livermore Software Technology Corporation (LSTC). (2013). *LS-DYNA R7.0 keyword manual vol II*. Livermore, CA:
- LS-DYNA support. (2013). Hourglass. Retrieved Feb, 2014, Retrieved from <http://www.dynasupport.com/howtos/element/hourglass>

- Lysmer, J., & Richart, F. E. (1966). Dynamic response of footings to vertical loading. *Journal of Soil Mechanics & Foundations Div*,
- Malkawi, A., & Khalid, M. (1996). Estimating damping constant of the pile soil system directly from measured displacement using hilbert transform technique. *Application of Stress-Wave Theory to Piles*, University of Florida , Gainesville, FL. , 5th 37-54.
- Markgraf, W., Horn, R., & Peth, S. (2006). An approach to rheometry in soil mechanics—Structural changes in bentonite, clayey and silty soils. *Soil and Tillage Research*, 91(1), 1-14.
- Martin, C. M., & Randolph, M. F. (2006). Upper-bound analysis of lateral pile capacity in cohesive soil. *Géotechnique*, 56(2), 141-145. doi:10.1680/geot.2006.56.2.141
- Matlock, H. (1970). Correlations for design of laterally loaded piles in soft clay. Paper presented at the *Offshore Technology in Civil Engineering@ sHall of Fame Papers from the Early Years*, 77-94.
- McKay, M. D., Beckman, R. J., & Conover, W. J. (1979). A comparison of three methods for selecting values of input variables in the analysis of output from a computer code. *Technometrics*, 21(2), 239-245.
- McVay, M. C., & Kuo, C. L. (1999). *Estimate damping and quake by using traditional soil testings*. ().University of Florida, Department of Civil Engineering.
- McVay, M. C., Wasman, S. J., Consolazio, G. R., Bullock, P. J., Cowan, D. G., & Bollmann, H. T. (2009). Dynamic Soil–Structure interaction of bridge substructure subject to vessel impact. *Journal of Bridge Engineering*, 14(1), 7-16.
- Mirdamadi, A., Lim, S. -, Briaud, J. L., Roesset, J., & Alberson, D. (2012). Single degree of freedom modeling and testing of a pile under lateral impact load. Paper presented at the *GeoCongress 2012: State of the Art and Practice in Geotechnical Engineering*, Oakland, CA. (225 GSP) 2227-2233. doi:10.1061/9780784412121.228
- Mitwally, H. M., & Novak, M. (1988). *Pile driving analysis using shaft models and FEM* London: Geotechnical Research Centre, University of Western Ontario.

- Mohammadi, S. D., Nikoudeh, M. R., Rahimi, H., & Khamsehchiyan, M. (2008). Application of the dynamic cone penetrometer (DCP) for determination of the engineering parameters of sandy soils. *Engineering Geology*, 101(3–4), 195-203. doi:<http://dx.doi.org/10.1016/j.enggeo.2008.05.006>
- Motta, E. (2012). Lateral deflection of horizontally loaded rigid piles in elastoplastic medium. *Journal of Geotechnical and Geoenvironmental Engineering*, 139(3), 501-506.
- Murff, J. D., & Hamilton, J. M. (1993). P-ultimate for undrained analysis of laterally loaded piles. *Journal of Geotechnical Engineering*, 119(1), 91-107.
- Nguyen, T., Berggren, B., & Hansbo, S. (1988). A new soil model for pile driving and driveability analysis. Paper presented at the *3rd International Conference on Application of Stress-Wave Theory to Piles, Canada*,
- Novak, M. (1974). Dynamic stiffness and damping of piles. *Canadian Geotechnical Journal*, 11(4), 574-598.
- Novak, M., Nogami, T., & Aboulella, F. (1978). DYNAMIC SOIL REACTIONS FOR PLANE STRAIN CASE. *Journal of the Engineering Mechanics Division*, 104(4), 953-959.
- Paikowsky, S., & Chernauskas, L. (1996). Soil inertia and the use of pseudo viscous damping parameters. Paper presented at the *5th International Conference on the Application of Stress-Wave Theory to Piles*, 203-216.
- Plassiard, J., & Donzé, F. (2009). From static response to impact loading in soils: A discrete element method analysis. Paper presented at the *AIP Conference Proceedings*, , 1145 759.
- Poepsel, P. H., & Dowd, W. M. (1995). Elasto-plastic response of deep foundations and soil for ship impact loading; apalachicola river bridge, florida. Paper presented at the *7th Triennial Conference, Ports '95*, 1227-1238.
- Potts, D., M., & Zdravkovic, L. (1999). *Finite element analysis in geotechnical engineering: Theory* Thomas Telford.

- Poulos, H. G., & Hull, T. S. (1989). The role of analytical geomechanics in foundation engineering. Paper presented at the *Foundation Engineering: Current Principles and Practices*, 1578-1606.
- Poulos, H. G., & Davis, E. H. (1980). *Pile foundation analysis and design*
- Poulos, H. G. (1971). Behavior of laterally loaded piles: I-single piles. *Journal of the Geotechnical Engineering Division*, 97(5), 711.
- Rainer, J. (1975). Damping in dynamic structure-foundation interaction. *Canadian Geotechnical Journal*, 12(1), 13-22.
- Randolph, M. F. (2000). Pile-soil interaction for dynamic and static loading. *Application of Stress-Wave Theory to Piles, Appendix*, Sao Paulo, Brazil. 3-11.
- Randolph, M. F. (1981). The response of flexible piles to lateral loading. *Geotechnique*, 31(2), 247-259.
- Randolph, M. F., & Houlsby, G. (1984). The limiting pressure on a circular pile loaded laterally in cohesive soil. *Geotechnique*, 34(4), 613-623.
- Reese, L. C. (1984). *Handbook on design of piles and drilled shafts under lateral load*. (No. FHWA-IP-84-11). University of Texas, Austin: Federal Highway Administration.
- Reese, L. C., & Van Impe, W. F. (2001). *Single piles and pile groups under lateral loading* CRC Press.
- Reissner, E. (1936). Stationäre, axialsymmetrische, durch eine schüttelnde masse erregte schwingungen eines homogenen elastischen halbraumes. *Archive of Applied Mechanics*, 7(6), 381-396.
- Saez Barrios, D. O. (2010). *Determination of soil properties for sandy soils and road base at riverside campus using laboratory testing and numerical simulation*. (Master of science, Texas A&M University).
- Saltelli, A., Tarantola, S., Campolongo, F., & Ratto, M. (2004). *Sensitivity analysis in practice: A guide to assessing scientific models* John Wiley & Sons.

- SD-STD-02.01, R. A. (2003). *Test method for vehicle crash testing of perimeter barriers and gates*. Washington, D.C: Physical Security Division Office of Physical Security Programs Bureau of Diplomatic Security U.S. Department of State.
- Smith, E. A. (1960). Pile-driving analysis by the wave equation. *Journal of the Engineering Mechanics Division, Proceedings of the American Society of Civil Engineers*, 86(SM 4), 35-61.
- Sterndorff, M., Waegter, J., & Eilersen, C. (1992). Design of fixed offshore platforms to dynamic ship impact loads. *Journal of Offshore Mechanics and Arctic Engineering*, 114, 149-153.
- Struck, W., & Voggenreiter, W. (1975). Examples of impact and impulsive loading in the field of civil engineering. *Materials and Structures*, 8(2), 81-87.
- Svinkin, M., & Abe, S. (1992). Relationship between case and hysteretic damping. Paper presented at the *Proceedings of the 4th International Conference on the Application of Stress-Wave Theory to Piles*, Edited by FBJ Barends. AA Balkema, the Netherlands, 175-182.
- Tacioglu, E., Rha, C., & Wallace, J. W. (2006). A robust macroelement model for Soil–Pile interaction under cyclic loads. *Journal of Geotechnical & Geoenvironmental Engineering*, 132(10), 1304-1314. doi:10.1061/(ASCE)1090-0241(2006)132:10(1304)
- Terzaghi, K. (1955). Evaluation of coefficients of subgrade reaction. *Geotechnique*, 5(4), 297-326.
- Texas A&M Supercomputing Facility. (2014). Retrieved Feb, 2014, Retrieved from <http://sc.tamu.edu/>
- U.S. Department of Defense. (January 2014). *DoD barrier anti-ram vehicle barrier list*. ().United States Army Corps of Engineering.
- Wellington, A. M., & Hering, R. (1893). *Piles and pile-driving* Engineering News Publishing Co.
- Wikipedia. (2014). Von mises yield criterion. Retrieved 1 March, 2014, Retrieved from http://en.wikipedia.org/wiki/Von_Mises_yield_criterion

- Woisin, G. (1976). Die killisionsversuche der GKSS. *Jahrbuch Der Schiffbautechnischen Gesellschaft*, 70, 465.
- Wolf, J. P., & Somaini, D. R. (1986). Approximate dynamic model of embedded foundation in time domain. *Earthquake Engineering & Structural Dynamics*, 14(5), 683-703. doi:10.1002/eqe.4290140502
- Wu, W., & Thomson, R. (2007). A study of the interaction between a guardrail post and soil during quasi-static and dynamic loading. *International Journal of Impact Engineering*, 34(5), 883-898. doi:10.1016/j.ijimpeng.2006.04.004
- Zhu, B., Chen, R. -, Chen, Y. -, & Zhang, Z. -. (2012). Impact model tests and simplified analysis for flexible pile-supported protective structures withstanding vessel collisions. *Journal of Waterway, Port, Coastal and Ocean Engineering*, 138(2), 86-96. doi:10.1061/(ASCE)WW.1943-5460.0000110
- Zhu, B., Chen, R. -, Guo, J. -, Kong, L. -, & Chen, Y. -. (2012). Large-scale modeling and theoretical investigation of lateral collisions on elevated piles. *Journal of Geotechnical and Geoenvironmental Engineering*, 138(4), 461-471. doi:10.1061/(ASCE)GT.1943-5606.0000623

BORING LOG NO. B-3

CLIENT: **Texas A&M University
College Station, Texas** PROJECT: **Pick Up Truck Impact on Single Pile**

BORING LOCATION: **See Boring Location Plan, Exhibit A-2** SITE: **Riverside Campus
Bryan, Texas**

Graphic Log	DESCRIPTION	DEPTH, FEET	SAMPLES				TESTS										
			USCS SYMBOL	TYPE	SPT, BLOWS/FT	CALIBRATED HAND PENETROM., TSF	MOISTURE CONTENT, %	DRY DENSITY, PCF	LIQUID LIMIT, %	PLASTIC LIMIT, %	PLASTICITY INDEX	MINIUS #200 SIEVE, %	COMPRESSIVE STRENGTH, TSF	FAILURE STRAIN, %	CONFINING PRESSURE, PSI		
	Approx. Surface Elevation: Existing Grade																
	FILL: SANDY LEAN CLAY dark gray	1.0		ST	4.5												
	SANDY LEAN CLAY dark gray and light tan, very stiff			CL	4.5												
				ST	4.5												
				ST	4.5												
				ST	4.5												
				ST	4.5												
	- reddish brown and light tan, with calcareous nodules below 5 feet	5		ST	4.5												
				ST	4.5												
		7.0		ST	4.5												
	Boring terminated at 7 feet.																

STRATIFICATION LINES REPRESENT APPROXIMATE BOUNDARIES BETWEEN SOIL TYPES. IN SITU, THE TRANSITION BETWEEN STRATA MAY BE MORE GRADUAL. REMARKS: Dry augered to 7 feet.

WATER LEVEL OBSERVATIONS ↓ ↓ ↓ ↓ FREE WATER WAS NOT OBSERVED DURING DRY DRILLING OPERATIONS		DATE DRILLED 12/3/2012 PROJECT NUMBER A1125038	Page 1 of 1 EXHIBIT A-5
--	--	---	---

APPENDIX 2

Boring log and for fresh very dense crushed limestone

BORING LOG NO. B-71												Page 1 of 1	
PROJECT: Pick-up Impact on Single Pile						CLIENT: Texas A&M University College Station, Texas							
SITE: Riverside Campus Bryan, Texas													
GRAPHIC LOG	LOCATION	DEPTH (FL)		FIELD TEST RESULTS	STRENGTH TEST			WATER CONTENT (%)	DRY UNIT WEIGHT (pcf)	ATTERBERG LIMITS			
	See Exhibit A-2	WATER LEVEL OBSERVATIONS	SAMPLE TYPE		TEST TYPE	COMPRESSIVE STRENGTH	STRAIN (%)			LL-PL-PI	PERCENT FINES		
	DEPTH												
	FILL - LIMESTONE BASE MATERIAL												
			5	X	5-8-8 N=16			9					
			5	X	4-5-5 N=10			10					
		7.5	X	5-7-1 N=8			9						
	LEAN CLAY WITH SAND (CL), tan and reddish brown, soft												
		10.0	X	1-1-2 N=3			21		37-15-22	72			
Boring Terminated at 10 Feet													
Stratification lines are approximate. In-situ, the transition may be gradual.												Hammer Type: Automatic	
Advancement Method: Dry auger to 10 feet.				See Exhibit A-3 for description of field procedures. See Appendix B for description of laboratory procedures and additional data (if any). See Appendix C for explanation of symbols and abbreviations.				Notes:					
Abandonment Method: Borings backfilled with soil cuttings upon completion.													
WATER LEVEL OBSERVATIONS No free water observed								Boring Started: 7/30/2013		Boring Completed: 7/30/2013			
								Drill Rig: Truck		Driller: Total Support Services			
								Project No.: A1125038		Exhibit: A-1			

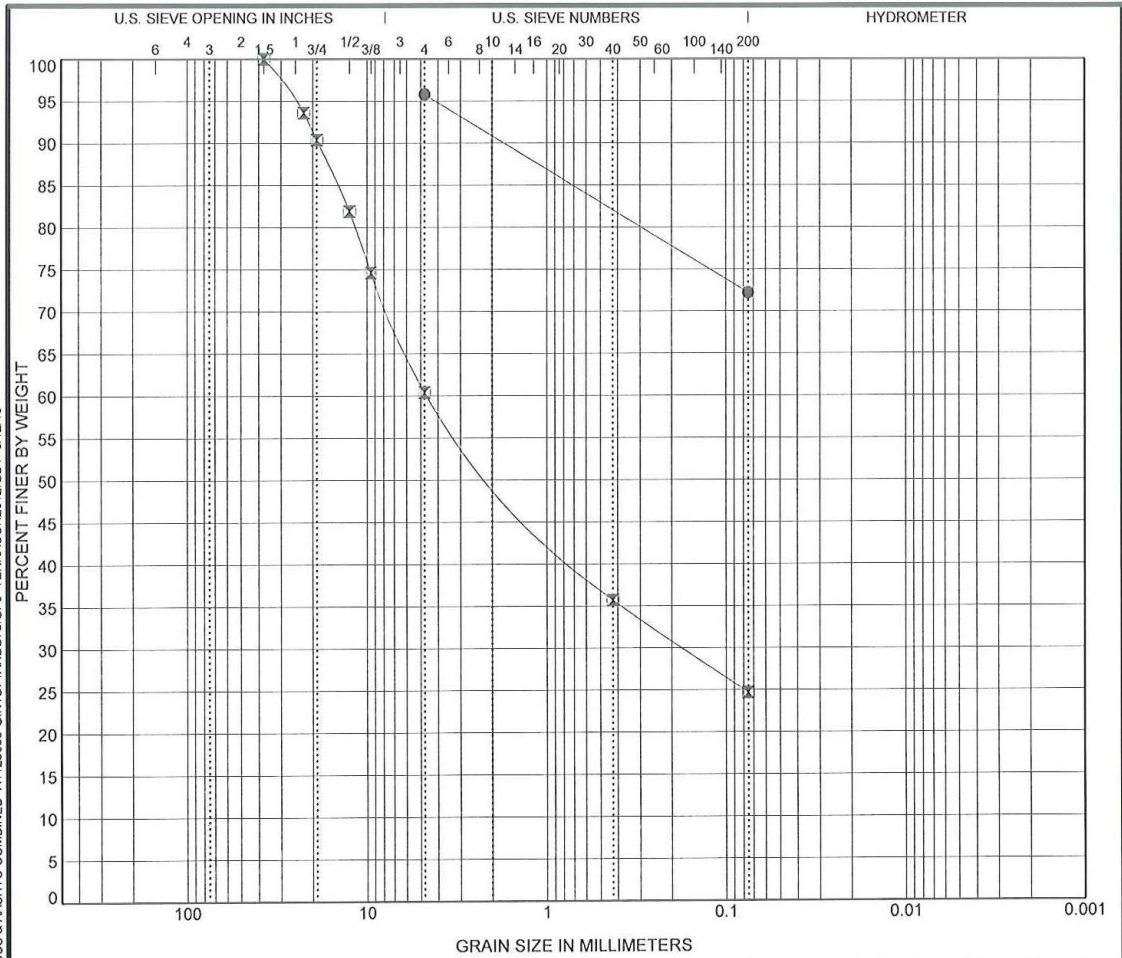
THIS BORING LOG IS NOT VALID IF SEPARATED FROM ORIGINAL REPORT. GEO SMART LOG-NO WELL A1125038-GINTB77ANDB75.GPJ

BORING LOG NO. B-75

PROJECT: Pick-up Impact on Single Pile				CLIENT: Texas A&M University College Station, Texas								
SITE: Riverside Campus Bryan, Texas												
GRAPHIC LOG	LOCATION See Exhibit A-2	DEPTH (Ft.)	WATER LEVEL OBSERVATIONS	SAMPLE TYPE	FIELD TEST RESULTS	STRENGTH TEST			WATER CONTENT (%)	DRY UNIT WEIGHT (pcf)	ATTERBERG LIMITS	PERCENT FINES
	DEPTH					TEST TYPE	COMPRESSIVE STRENGTH	STRAIN (%)			LL-PL-PI	
	FILL - LIMESTONE BASE MATERIAL	5			6-7-6 N=13			8				
		5			5-5-4 N=9			8				
		7.5			5-7-5 N=12			9				
	LEAN CLAY WITH SAND (CL), tan and reddish brown, medium stiff	10.0			1-2-3 N=5			19				
	<i>Boring Terminated at 10 Feet</i>	10										
Stratification lines are approximate. In-situ, the transition may be gradual.				Hammer Type: Automatic								
Advancement Method: Dry auger to 10 feet.				See Exhibit A-3 for description of field procedures. See Appendix B for description of laboratory procedures and additional data (if any).				Notes:				
Abandonment Method: Borings backfilled with soil cuttings upon completion.				See Appendix C for explanation of symbols and abbreviations.								
WATER LEVEL OBSERVATIONS								Boring Started: 7/30/2013		Boring Completed: 7/30/2013		
No free water observed								Drill Rig: Truck		Driller: Total Support Services		
								Project No.: A1125038		Exhibit: A-2		

THIS BORING LOG IS NOT VALID IF SEPARATED FROM ORIGINAL REPORT. GEO SMART LOG-NO WELL A1125038-GINTB7-ANDB75.GPJ

GRAIN SIZE DISTRIBUTION ASTM D422



COBBLES	GRAVEL		SAND			SILT OR CLAY
	coarse	fine	coarse	medium	fine	

Boring ID	Depth	USCS Classification	AASHTO Classification			LL	PL	PI	Cc	Cu
● B-71	8.5	LEAN CLAY with SAND(CL)	14(A-6)			37	15	22		
⊗ Bulk	0.0	SILTY GRAVEL with SAND(GM)	0(A-1-b)			18	17	1		

Boring ID	Depth	D ₁₀₀	D ₆₀	D ₃₀	D ₁₀	%Gravel	%Sand	%Silt	%Clay
● B-71	8.5	4.75				0.0	23.6	72.2	
⊗ Bulk	0.0	37.5	4.568	0.173		39.6	35.7	24.7	

PROJECT: Pick-up Impact on Single Pile

SITE: Riverside Campus
Bryan, Texas



PROJECT NUMBER: A1125038

CLIENT: Texas A&M University
College Station, Texas

EXHIBIT: B-1

LABORATORY TESTS ARE NOT VALID IF SEPARATED FROM ORIGINAL REPORT. GRAIN SIZE: USCS & AASHTO COMBINED A1125038-GINTB71-AND875.GPJ TERRACON2012.GDT 8/12/13

Boring log and for aged very dense crushed limestone

BORING LOG NO. B-1 (10 years old)											
Page 1 of 1											
PROJECT: Pick-up Impact on Single Pile						CLIENT: Texas A&M University College Station, Texas					
SITE: Riverside Campus Bryan, Texas											
GRAPHIC LOG	LOCATION	DEPTH (FL)	WATER LEVEL OBSERVATIONS	SAMPLE TYPE	FIELD TEST RESULTS	STRENGTH TEST			ATTERBERG LIMITS	PERCENT FINES	
	See Exhibit A-2					TEST TYPE	COMPRESSIVE STRENGTH	STRAIN (%)	WATER CONTENT (%)	DRY UNIT WEIGHT (pcf)	LL-PL-PI
	FILL - LIMESTONE BASE MATERIAL	5		X	5-10-15 N=25						
				X	17-31-50 N=18						
				X	N=50/5*						
	LEAN CLAY WITH SAND (CL) , tan and reddish brown	8.0		X	4-7-10 N=17						
	Boring Terminated at 8 Feet										
Stratification lines are approximate. In-situ, the transition may be gradual. Hammer Type: Automatic											
Advancement Method: Dry auger to 10 feet.				See Exhibit A-3 for description of field procedures. See Appendix B for description of laboratory procedures and additional data (if any). See Appendix C for explanation of symbols and abbreviations.				Notes:			
Abandonment Method: Borings backfilled with soil cuttings upon completion.											
WATER LEVEL OBSERVATIONS No free water observed								Boring Started:		Boring Completed:	
								Drill Rig: Truck		Driller: Total Support Services	
								Project No.: A1125038		Exhibit: A-1	

THIS BORING LOG IS NOT VALID IF SEPARATED FROM ORIGINAL REPORT. GEO SMART LOG-NO WELL. A1125038-GINTB71ANDB75.GPJ




BORING LOG NO. B-2 (80 days old)

Page 1 of 1

PROJECT: Pick-up Impact on Single Pile

CLIENT: Texas A&M University
College Station, Texas

SITE: Riverside Campus
Bryan, Texas

GRAPHIC LOG	LOCATION See Exhibit A-2	DEPTH (FL)	WATER LEVEL OBSERVATIONS	SAMPLE TYPE	FIELD TEST RESULTS	STRENGTH TEST			WATER CONTENT (%)	DRY UNIT WEIGHT (pcf)	ATTERBERG LIMITS	PERCENT FINES
	DEPTH					TEST TYPE	COMPRESSIVE STRENGTH	STRAIN (%)			LL-PL-PI	
	FILL - LIMESTONE BASE MATERIAL	5		X	9-10-9 N=19							
				X	5-5-6 N=11							
				X	4-5-7 N=12							
	LEAN CLAY WITH SAND (CL) , tan and reddish brown	6.0		X	3-5-8 N=13							
	<i>Boring Terminated at 8 Feet</i>	8.0										
Stratification lines are approximate. In-situ, the transition may be gradual.												
Hammer Type: Automatic												
Advancement Method: Dry auger to 10 feet.				See Exhibit A-3 for description of field procedures. See Appendix B for description of laboratory procedures and additional data (if any). See Appendix C for explanation of symbols and abbreviations.				Notes:				
Abandonment Method: Borings backfilled with soil cuttings upon completion.												
WATER LEVEL OBSERVATIONS <i>No free water observed</i>								Boring Started:		Boring Completed:		
								Drill Rig: Truck		Driller: Total Support Services		
								Project No.: A1125038		Exhibit: A-2		

THIS BORING LOG IS NOT VALID IF SEPARATED FROM ORIGINAL REPORT. GEO SMART LOG-NO WELL A1125038-SINTE71ANDB75.GPJ

BORING LOG NO. B-3(10 years old)

PROJECT: Pick-up Impact on Single Pile	CLIENT: Texas A&M University College Station, Texas
SITE: Riverside Campus Bryan, Texas	

GRAPHIC LOG	LOCATION See Exhibit A-2	DEPTH (Ft.)	WATER LEVEL OBSERVATIONS	SAMPLE TYPE	FIELD TEST RESULTS	STRENGTH TEST			ATTERBERG LIMITS		
						TEST TYPE	COMPRESSIVE STRENGTH	STRAIN (%)	WATER CONTENT (%)	DRY UNIT WEIGHT (pcf)	LL-PL-PI
DEPTH											
8.0	FILL - LIMESTONE BASE MATERIAL	5		X	9-9-9 N=18						
				X	4-7-5 N=12						
				X	5-6-6 N=12						
8.0	LEAN CLAY WITH SAND (CL) , tan and reddish brown			X	2-4-9 N=13						
	<i>Boring Terminated at 8 Feet</i>										

Stratification lines are approximate. In-situ, the transition may be gradual.

Hammer Type: Automatic

Advancement Method: Dry auger to 10 feet.	See Exhibit A-3 for description of field procedures. See Appendix B for description of laboratory procedures and additional data (if any). See Appendix C for explanation of symbols and abbreviations.	Notes:
Abandonment Method: Borings backfilled with soil cuttings upon completion.		
WATER LEVEL OBSERVATIONS <i>No free water observed</i>		Boring Started: Drill Rig: Truck Project No.: A1125038
		Boring Completed: Driller: Total Support Services Exhibit: A-3

THIS BORING LOG IS NOT VALID IF SEPARATED FROM ORIGINAL REPORT. GEO SMART LOG-NO WELL. A1125038-GINTB71-ANDB75.GPJ

APPENDIX 3

Vehicle Parameter for PU (Pick-up truck)

Date: 2012-11-30 Test No.: 478260-USD14

Year: 2000 Make: Chevrolet

Tire Inflation Pressure: 60 PSI Odometer: 190363

Describe any damage to the vehicle prior to test:

● Denotes accelerometer location.

NOTES: _____

Engine Type: V8

Engine CID: 5.7 liter

Transmission Type:

Auto

Manual

Optional Equipment:

Dummy Data:

Type: No dummy

Mass: _____

Seat Position: _____

Geometry (inches)

A	<u>74.00</u>	E	<u>50.00</u>	J	<u>43.00</u>	N	<u>63.00</u>	R	<u>28.75</u>
B	<u>34.00</u>	F	<u>216.00</u>	K	<u>26.00</u>	O	<u>64.50</u>	S	<u>34.50</u>
C	<u>132.00</u>	G	<u>60.46</u>	L	<u>3.50</u>	P	<u>29.50</u>	T	<u>57.50</u>
D	<u>72.25</u>	H	<u>----</u>	M	<u>17.00</u>	Q	<u>17.50</u>	U	<u>132.00</u>

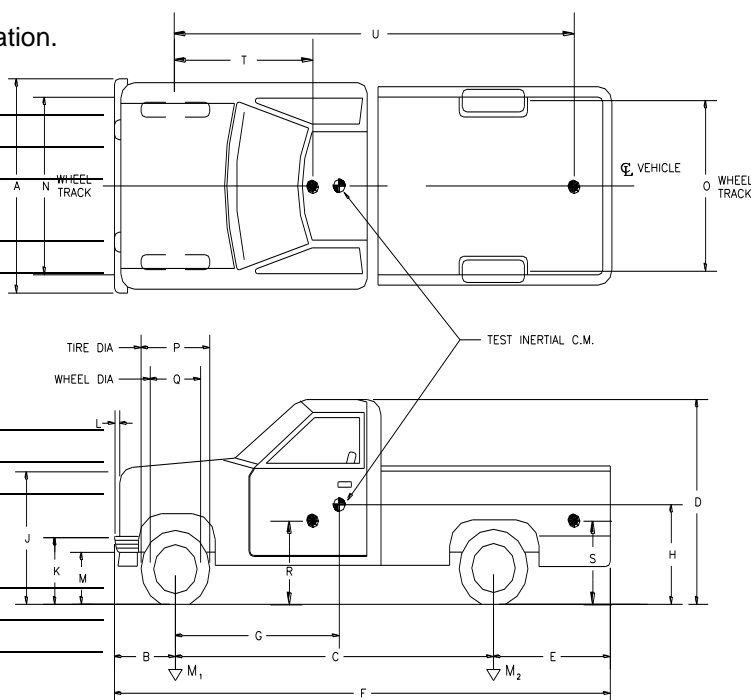
Mass

(lb)

	<u>Curb</u>	<u>Test Inertial</u>	<u>Gross Static</u>
M ₁	<u>2674</u>	<u>2745</u>	<u>2745</u>
M ₂	<u>1951</u>	<u>2320</u>	<u>2320</u>
M _{Total}	<u>4625</u>	<u>5065</u>	<u>5065</u>

Mass Distribution

(lb): LF: 1433 RF: 1312 LR: 1145



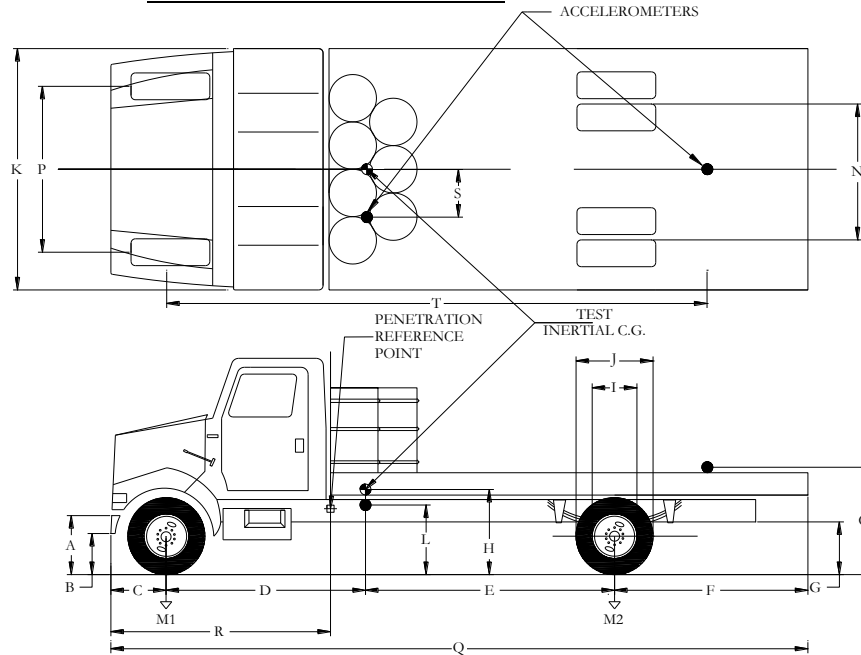
APPENDIX 4

Vehicle Parameter for M (Medium-duty truck)

DATE: 2013-09-25 TEST NO.: 478260-USD21

YEAR: 2000 MAKE: International

TIRE SIZE: 275/80R22.5



GEOMETRY (inches)

A 31.00 B 20.00 C 30.50 D 104.58 E 101.42 F 86.00
 H 39.90 I 23.50 J 39.50 K 95.75 L 27.00 N 73.00
 P 80.50 Q 322.50 R 106.00 S 18.50 T 188.00 D+E 206.00

Allowed Range for Wheelbase (D+E) = 208 ±20 inches;
 Allowable Flatbed Length = 18 ft ±24 inches; Allowable U-bolt Spacing = 3 ft ±8 inches

MASS DISTRIBUTION (lb)

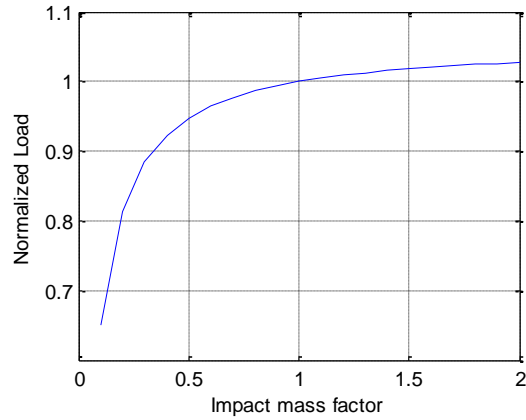
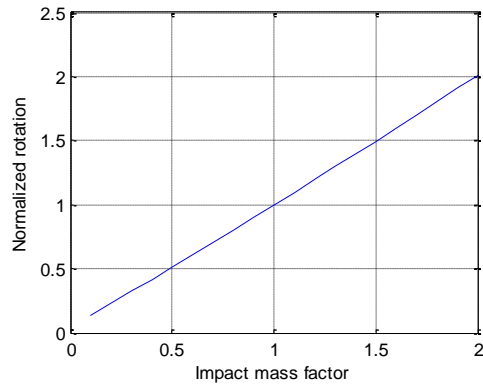
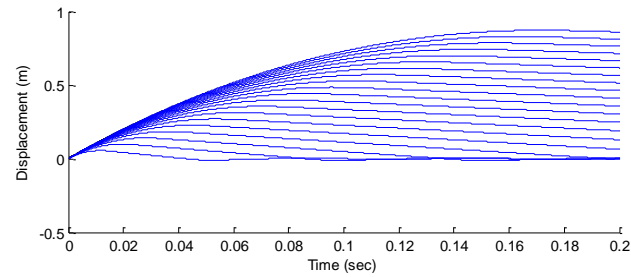
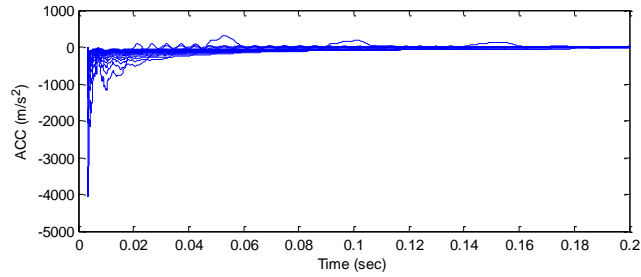
LF 3610 RF 3780 LR 3810 RR 3810

<u>MASS (lb)</u>	<u>CURB</u>	<u>TEST INERTIAL</u>
M ₁	<u>6460</u>	<u>7390</u>
M ₂	<u>6590</u>	<u>7620</u>
M _{Total}	<u>13050</u>	<u>15010</u>

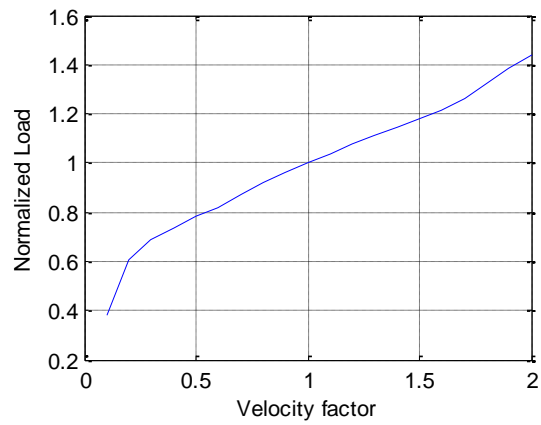
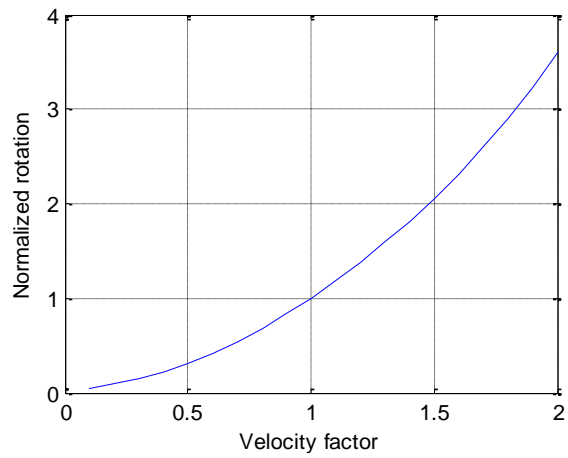
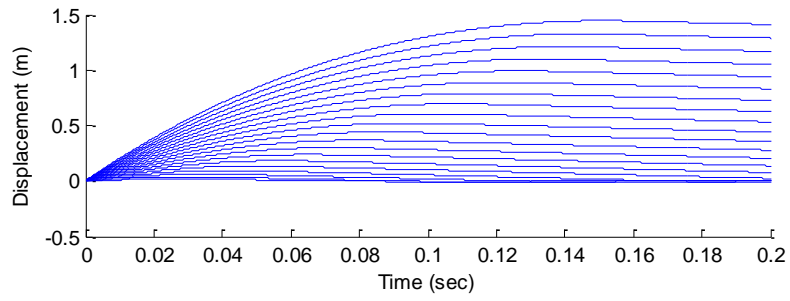
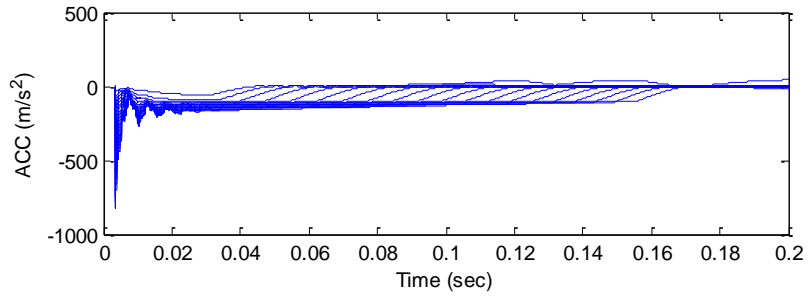
APPENDIX 5

Sensitivity Analyses

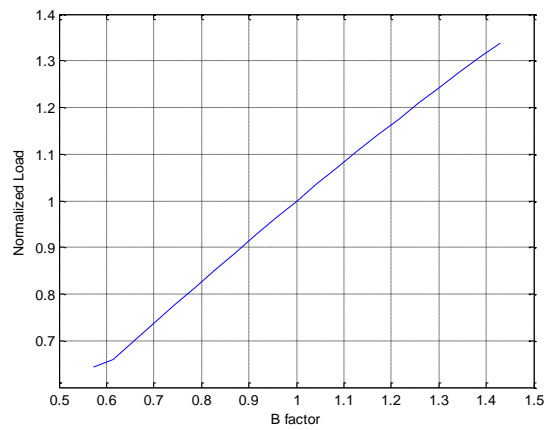
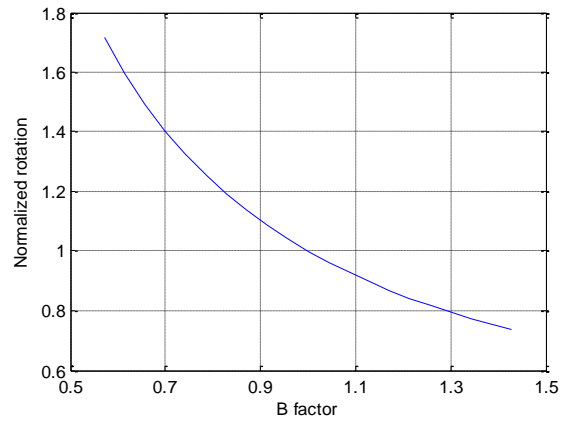
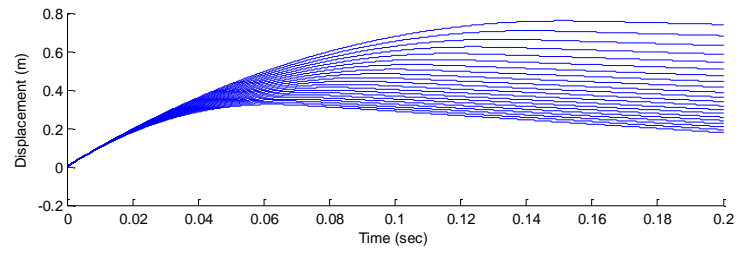
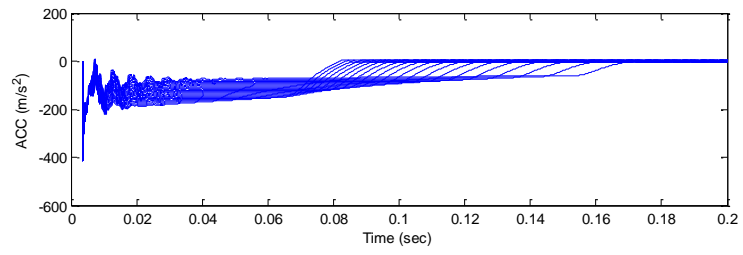
Vehicle mass



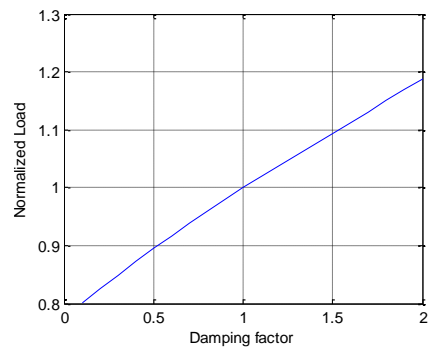
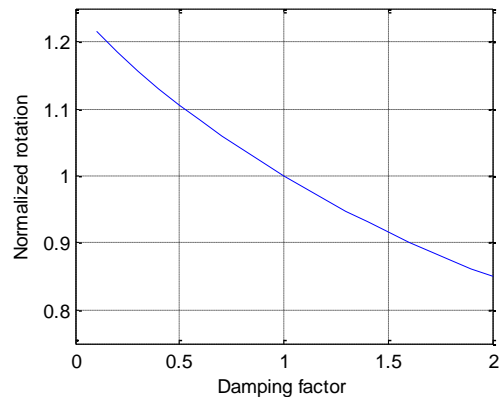
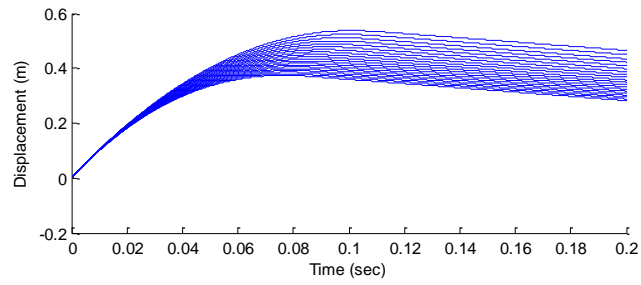
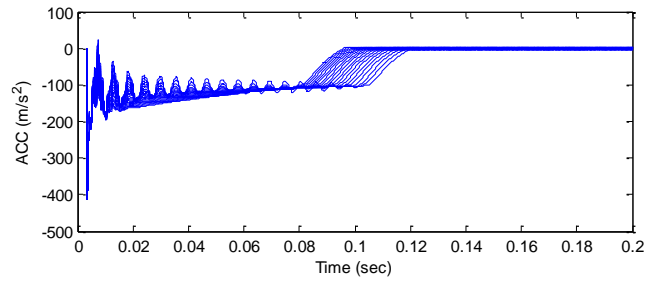
Vehicle velocity



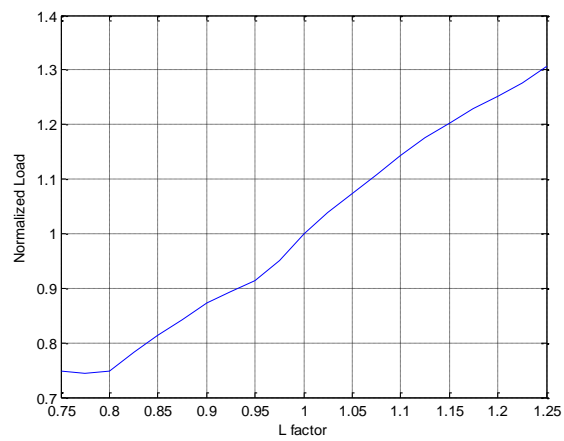
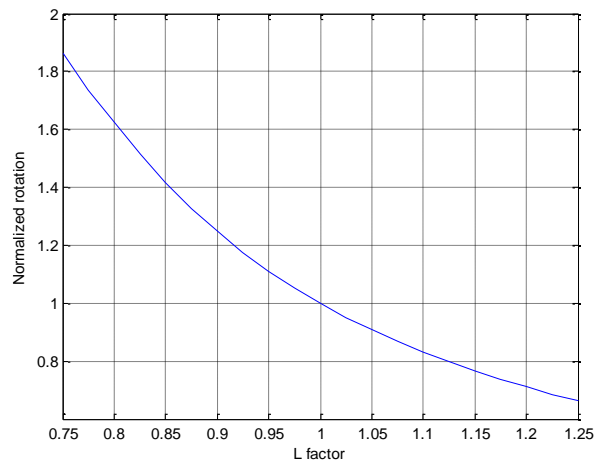
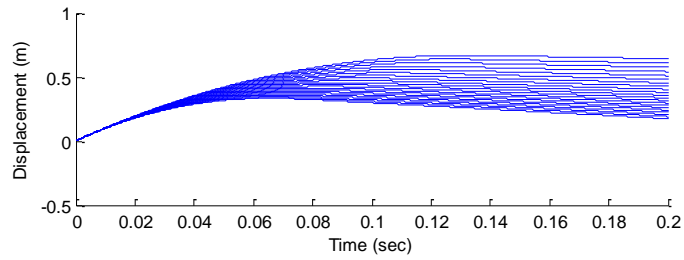
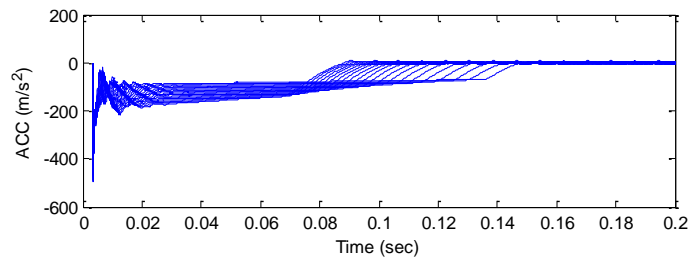
Pile width (B)



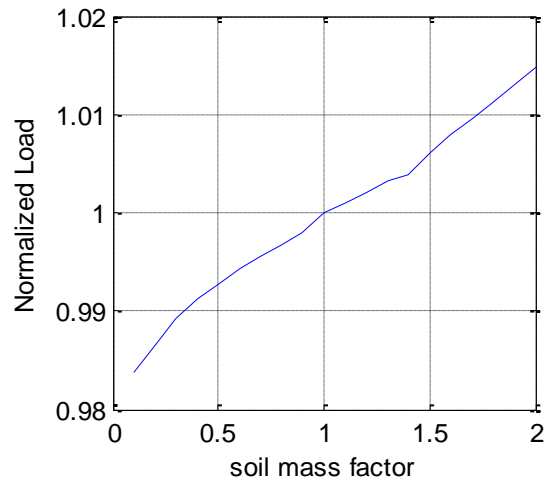
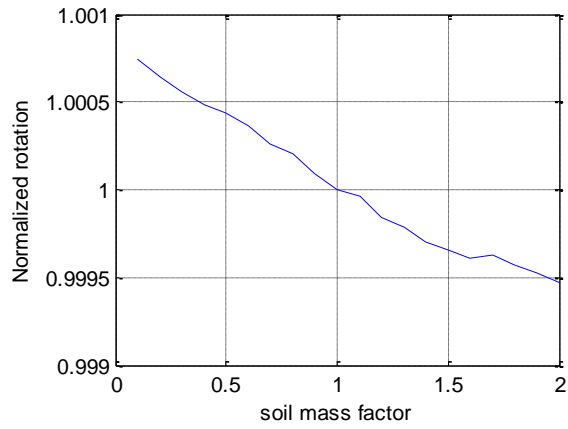
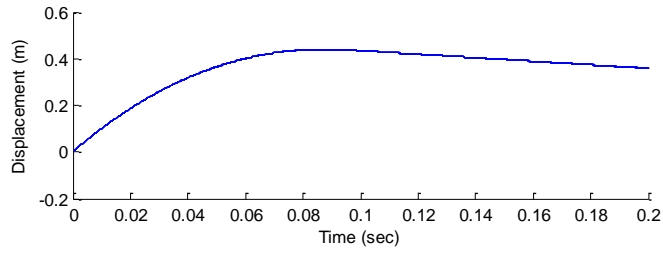
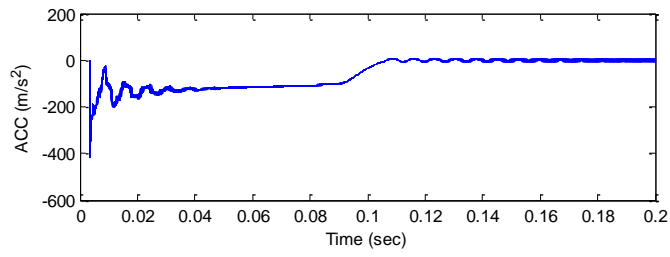
Soil damping



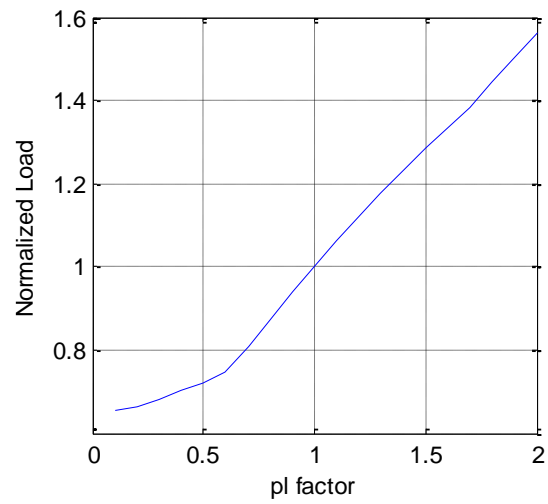
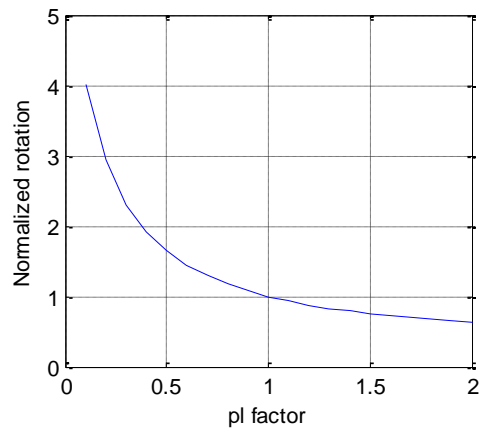
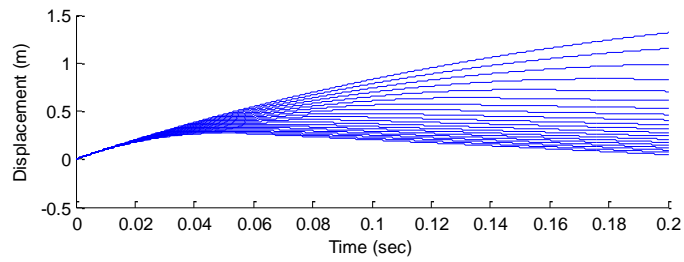
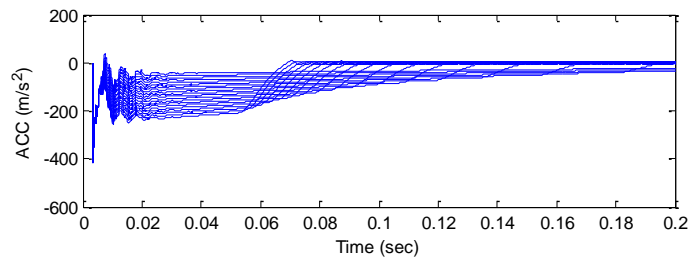
Pile embedment (L)



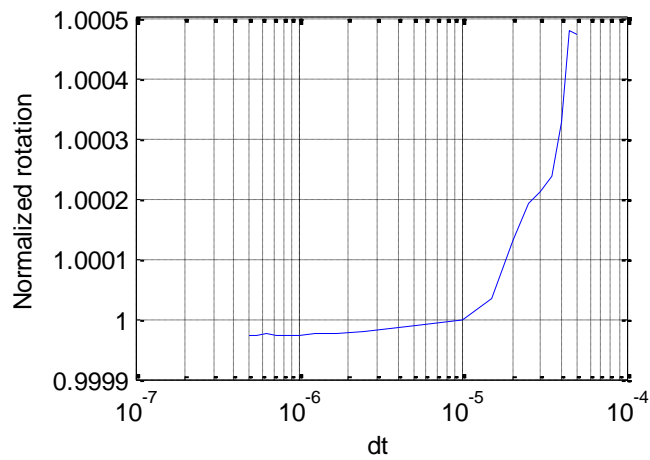
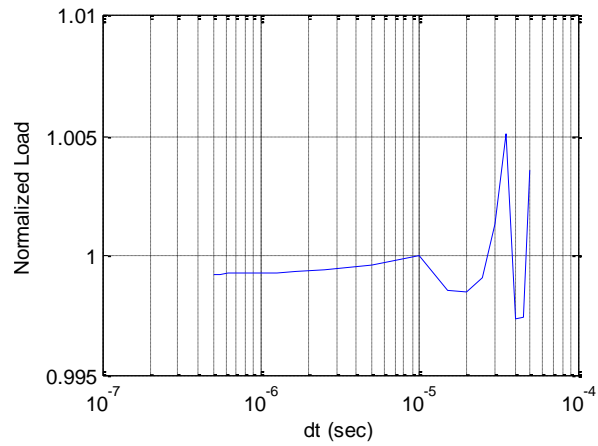
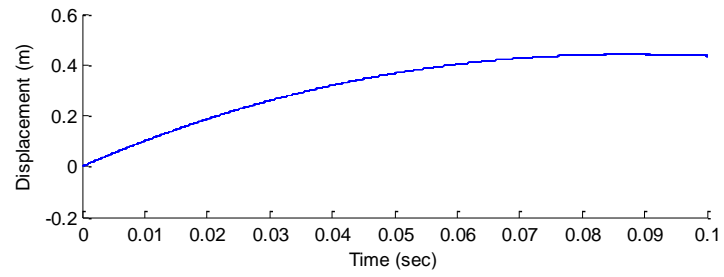
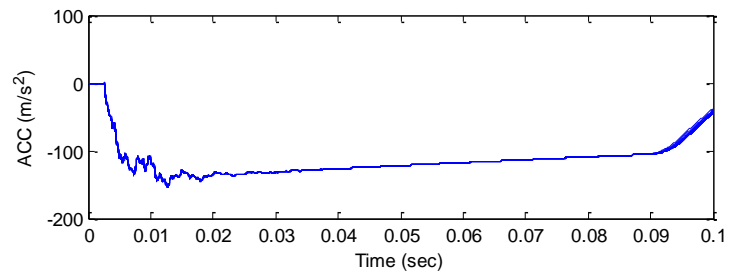
Soil mass



Soil limit pressure



Delta t



Node number

